REPORT DOCUMENTATION PAGE

Form Approved
OMB No. 0704-0188

Public reporting burden for this collection of information is estimated to average ... hour per response, including the time for reviewing instructions, searching existing data sources, gathering and maintaining the data needed, and completing and reviewing the collection of information. Send comments regarding this burden estimate or any other aspect of this collection of information, including suggestions for reducing this burden, to Washington Headquarters Services, Directorate for information Operations and Reports, 1215 Jefferson Davis Highway, Suite 1204, Arlington, VA 22202-4302, and to the Office of Management and Budget, Paperwork Reduction Project (0704-0188), Washington, DC 20503.

REPORT DATE	REPORT TYPE AND DATES COVERED
February 1, 1992	Final Report

4. TITLE AND SUBTITLE
Mechanistic Studies of Superplasticity of Structural Ceramics

FUNDING NUMBERS
AFOSR-87-0289

(2)

6. AUTHOR(S)
I-Wei Chen

7. PERFORMING ORGANIZATION NAME(S) AND ADDRESS(ES)
University of Michigan
Department of Materials Science & Engineering
2300 Hayward St.
Ann Arbor, MI 48109-2136

PERFORMING ORGANIZATION REPORT NUMBER
AFOSR-TR- 92 0087

9. SPONSORING/MONITORING AGENCY NAME(S) AND ADDRESS(ES)
AFOSR
AFOSR/NE
Bldg. 410
Bolling AFB, Washington D.C. 20332-6448

SPONSORING/MONITORING AGENCY REPORT NUMBER

11. SUPPLEMENTARY NOTES

12a. DISTRIBUTION/AVAILABILITY STATEMENT
Unrestricted

13. ABSTRACT (Maximum 200 words)

A comprehensive methodology for developing superplastic ceramics, evaluating superplastic formability, and understanding microstructural evolution and flow mechanisms during large deformation has been developed in the present project. A summary of these accomplishments, which focuses on two important classes of structural ceramics, zirconia and silicon nitride, is provided here in the form of nine published journal papers, conference contributions and general reviews.

14. SUBJECT TERMS
Ceramics, Superplasticity, Forming, Zirconia, Silicon Nitride

15. NUMBER OF PAGES
127

I. INTRODUCTION

The search for an alternative yet reliable near net-shape forming method for structural ceramics has naturally led to superplastic forming following the discovery in 1986 of ceramic superplasticity in zirconia. In the research supported under AFOSR Grant No. 87-0289, the first goal was to develop a mechanistic understanding of the central microstructural requirement for facilitating deformation and forming. The limited state-of-the-art available at the beginning of the project (3Y-TZP and its composite with alumina was the only family of superplastic ceramics known) dictated that a second goal was to explore other phase fields of potential new superplastic structural ceramics. The third goal was to develop methods that would allow pressure used in superplastic forming to suppress cavitation. The first two goals were successfully met through a combination of experimental research and mechanical modelling. The third goal of pressure forming was not completed in time before the termination of the project.

The research falls into the following major categories:

(a) Fundamental alloy development to define the scope and the strategy for formulating ceramic composition, processing pathway, and microstructural development for optimal formability;

(b) Investigation of grain boundary interactions with microstructure/deformation controlling dopants;

(c) Investigation of liquid additives and their role in deformation processes;

(d) The development of a new biaxial forming test to assess ceramic formability.

In this report, we will give an account of this research by presenting the results of the major investigations in the form of published journal papers, conference contributions, and general reviews. The format consists of a series of short introductions, followed by the relevant publications in that area that will furnish the mechanistic details in both modelling and experimental observations.

2.1 "Development of Superplastic Structural Ceramics"

I-W. Chen and L.A. Xue, *Journal of the American Ceramic Society*

journal

J. Am. Ceram. Soc., 73 [9] 2585-2609 (1990)

Development of Superplastic Structural Ceramics

I-Wei Chen* and Liang An Xue*

Department of Materials Science and Engineering, University of Michigan, Ann Arbor, Michigan 48109-2136

Superplastic structural ceramics (Y-TZP, Al_2O_3, Si_3N_4, and their composites) that can withstand biaxial stretching to large strains have been developed recently. Microstructural design of these ceramics first requires an ultrafine grain size that is stable against coarsening during sintering and deformation. A low sintering temperature is a necessary, but not a sufficient, condition for achieving the required microstructure. In many cases, the selection of an appropriate phase, such as tetragonal phase in zirconia or α phase in silicon nitride, which is resistant to grain growth, is crucial. The use of sintering aids and grain-growth inhibitors, particularly those that segregate to the grain boundaries, can be beneficial. Second-phase particles are especially effective in suppressing static and dynamic grain growth. Another major concern is to maintain an adequate grain-boundary cohesive strength, relative to the flow stress, to mitigate cavitation or grain-boundary cracking during large strain deformation. Existing evidence suggests that a lower grain-boundary energy is instrumental in achieving this objective. The selection of an appropriate phase and the tailoring of the grain boundary or liquid-phase composition can sometimes drastically alter the cavitation resistance. Related observations on forming methods, forming characteristics, and sheet formability are also reviewed. The basic deformation characteristics are similar to diffusional creep and are dominated by grain-boundary diffusion. However, deformation characteristics are frequently altered by interface reactions, second-phase hardening/softening, and dynamic grain-growth-induced strain hardening. Ductility and formability, on the other hand, are controlled by the flow stress and flaw distribution, not by deformation instability as in superplastic metals. Analytical models and empirical correlations are presented to describe various constitutive relations pertaining to superplastic ceramics. [Key words: structural materials, superplastics, models, grain boundaries, microstructure.]

I. Introduction

SUPERPLASTICITY is phenomenologically defined as the ability of a material to exhibit exceptionally large tensile elongation during stretching.[1,2] It is a property commonly found in many metals and alloys when the grain size is refined below several micrometers and the deformation temperature is above two-thirds of the melting point.[2] At such small sizes micrograins can flow, much like sand particles in a water-saturated slip, by way of atomic diffusion along grain boundaries. Models of diffusional creep and grain-boundary sliding, which predict a nearly Newtonian flow rate inversely proportional to the grain size to a certain power, have been advanced to explain such a phenomenon.[1,3-7] The details of these mechanistic models, however, have received only limited experimental corroboration, and the exact mechanisms of superplasticity are still controversial to this date. Despite such uncertainties, these materials intrinsically embody a high resistance to strain localization, or necking, in tensile deformation because necking necessarily entails a higher local strain rate and thus a higher local flow stress, which will be resisted by the rest of the body.[3,8] Several commercial processes in metal industries have taken advantage of these

R. E. Newnham—contributing editor

Manuscript No. 197477. Received June 18, 1990, approved June 26, 1990.

Supported by U.S. Air Force Office of Scientific Research under Grant No. 87-0289, U.S. Department of Energy under Grant No. DE-FG02-87ER45302, and U.S. Army Research Office under Contract No. DAAL03-89-K0133.

*Member, American Ceramic Society

high ductilities to form intricate, large-scale components directly into their net shape.[7,9,10]

Following the report in 1986 of superplasticity in 3Y-TZP,[11] a fine-grained tetragonal zirconia partially stabilized by 3 mol% yttria, considerable research has been conducted to explore the generality of this phenomenon in other ceramics.[12] Existing evidence indicates that the polycrystalline ceramics with a grain size below 500 nm are potentially superplastic at high homologous temperatures. Single-phase ceramics which have been found to be superplastic, i.e., which exhibit large ductility in uniaxial or biaxial stretching, include Y-TZP,[11] alumina,[13] and hydroxyapatite.[14] Polyphase ceramics which have been found to be superplastic include zirconia/alumina,[13,15,16] zirconia/mullite,[17-19] silicon nitride,[20] and silicon nitride/silicon carbide with other mixed phases.[21,22] This list is expected to expand in the future.

Several biaxially punch-stretched samples made of various structural ceramics, i.e., zirconia, alumina, silicon nitride, and their composites, are shown in Fig. 1. The broad forming conditions, in terms of forming temperature and forming time, are indicated. The quality of the as-formed surfaces is excellent. These demonstrations suggest the possibility of deformation processing of dense ceramics at high temperatures (using methods commonly reserved for metals, plastics, and glasses). These processes could include sheet forming, blowing, extrusion, stamping, and forging. Compared with the conventional forming processes of crystalline ceramics, which are conducted at low temperature before firing, these processes have the advantages of greater shape flexibility and better dimensional accuracy. The latter are especially important considerations for net-shape forming.[9]

This paper describes various materials considerations which have guided the development of superplastic structural ceramics. The scope of this paper is shown in Fig. 2, which outlines the major factors involved in ceramic superplasticity and their interrelationships. Within this context, we have attempted to critically assess the most significant results in the literature of ceramic superplasticity, and to provide an overview of the highlights of our own effort in this area. The intimate and complicated structure-property-processing relationships in this class of ceramics, which must have an ultrafine microstruc-

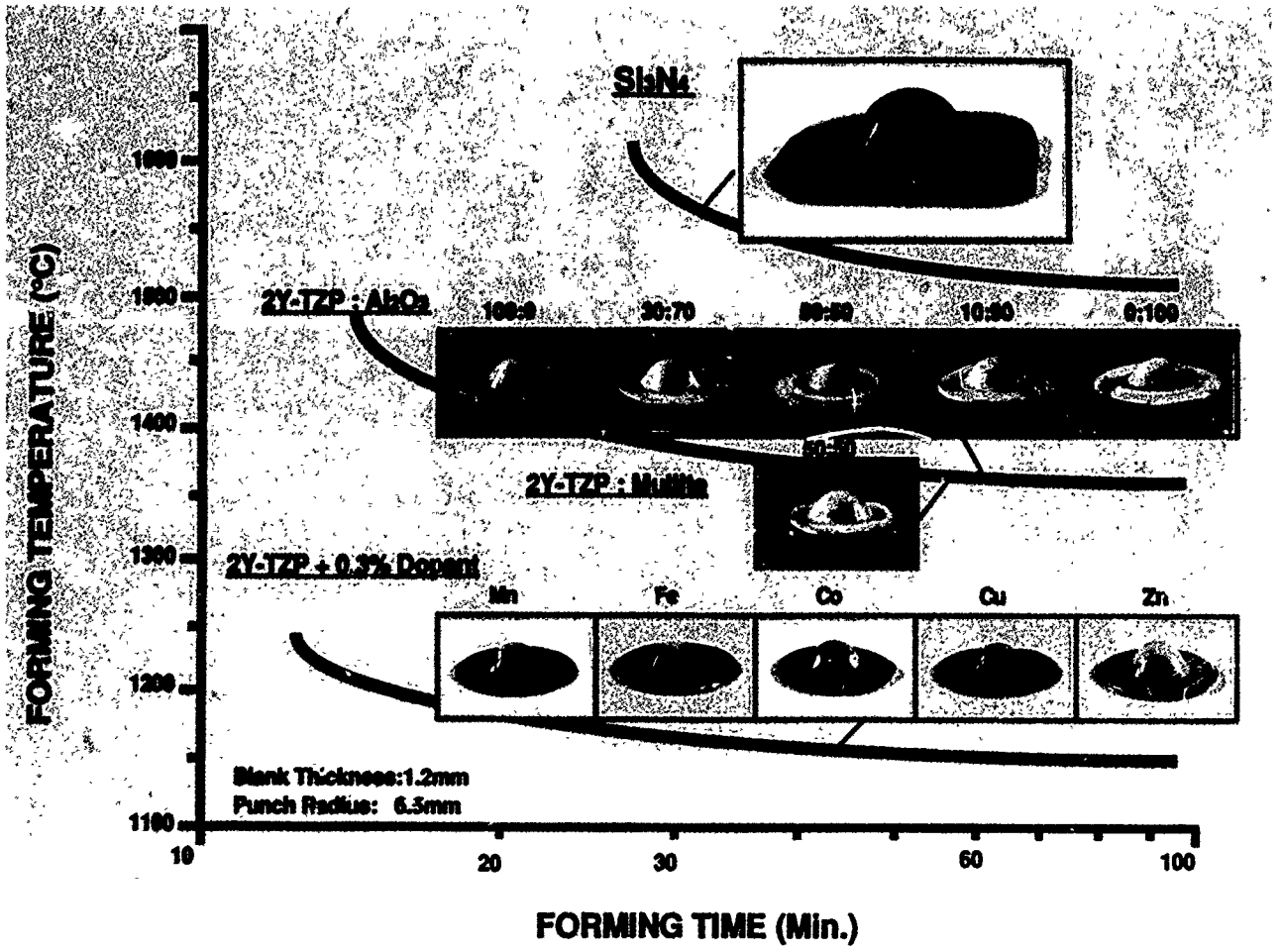

Fig. 1. Superplastic forming temperatures and times of structural ceramics. Hemispherical punch with a 6.5-mm radius was used to stretch the initially flat, 1-mm-thick disks into the shape shown. Surface finish was excellent and glossy for silicon nitride, zirconia, and zirconia-rich composites. Surface of alumina, although free of visible defects, appeared dull. Under optimal conditions, forming operation can be completed at even lower temperatures and shorter times.

ture achievable through a judicious crystal structure selection or a second-phase addition, form the subject of Section II of this paper. Deformation characteristics and methods for evaluating formability are described in Sections III and IV to provide further insight into this active research field.

II. Materials Considerations

In developing superplastic ceramics, high deformation rate and high ductility are the primary objectives. Practical considerations further dictate that these properties should be achievable at the lowest temperature possible. The basis of materials considerations concerning a high deformation rate and a low deformation temperature lie in the constitutive equation of superplastic flow, which can be expressed in the following form:[2]

$$\dot{\varepsilon} = A\sigma^n/d^p \qquad (1)$$

where $\dot{\varepsilon}$ is the strain rate, σ is the stress, d is the grain size, n and p are stress and grain-size exponents, respectively, and A is a temperature-dependent, diffusion-related coefficient which can be expressed in an Arrhenius form. For superplastic ceramics, n and p are typically between 1 and 3. Therefore, a high deformation rate and a low deformation temperature can be achieved by the following steps.

(i) *Lowering grain size:* Grain-growth control can be achieved through low-temperature sintering and the use of additives;[23] present practice has found a lower limit of approximately 200 nm for the grain size in bulk ceramics such as TZP, alumina, silicon nitride, and their composites. Microstructures of some selected superplastic ceramics are shown in Fig. 3.

(ii) *Increasing lattice diffusivity, grain-boundary diffusivity, or introducing a grain-boundary liquid phase as a fast diffusion path:* The forming temperature of Y-TZP has been lowered from 1350° to below 1200°C with the addition of a small amount of transition-metal oxides which segregate to grain boundaries.[24] In silicon nitride, a liquid phase is also present which facilitates deformation.[20,21]

Although these two steps are necessary, they are not sufficient for achieving superplasticity in a given ceramic for the following reasons. First, in many instances the fine-grained microstructure proves to be unstable under superplastic deformation; i.e., dynamic grain growth may take place. Thus, a fine initial microstructure provides little assurance of the formability of a ceramic. Second, failures of superplastic ceramics appear to be of a brittle intergranular type which is not preceded by extensive necking, unlike most superplastic metals and alloys. Thus, a high cohesive strength at grain boundaries is crucial for achieving high ductility without fracture. Additives for grain refinement or a grain-boundary liquid must be carefully selected so that a high grain-boundary strength is not compromised

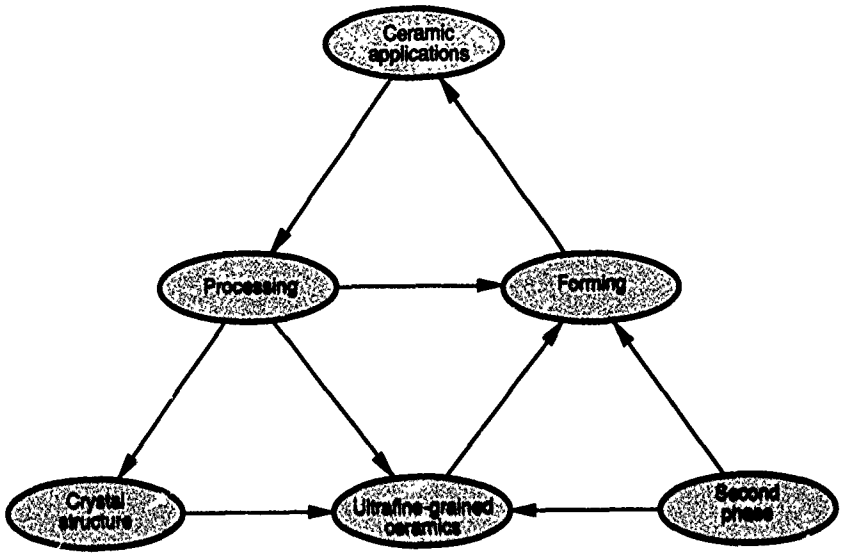

Fig. 2. Structure–property–processing relationships in superplastic ceramics for structural applications.

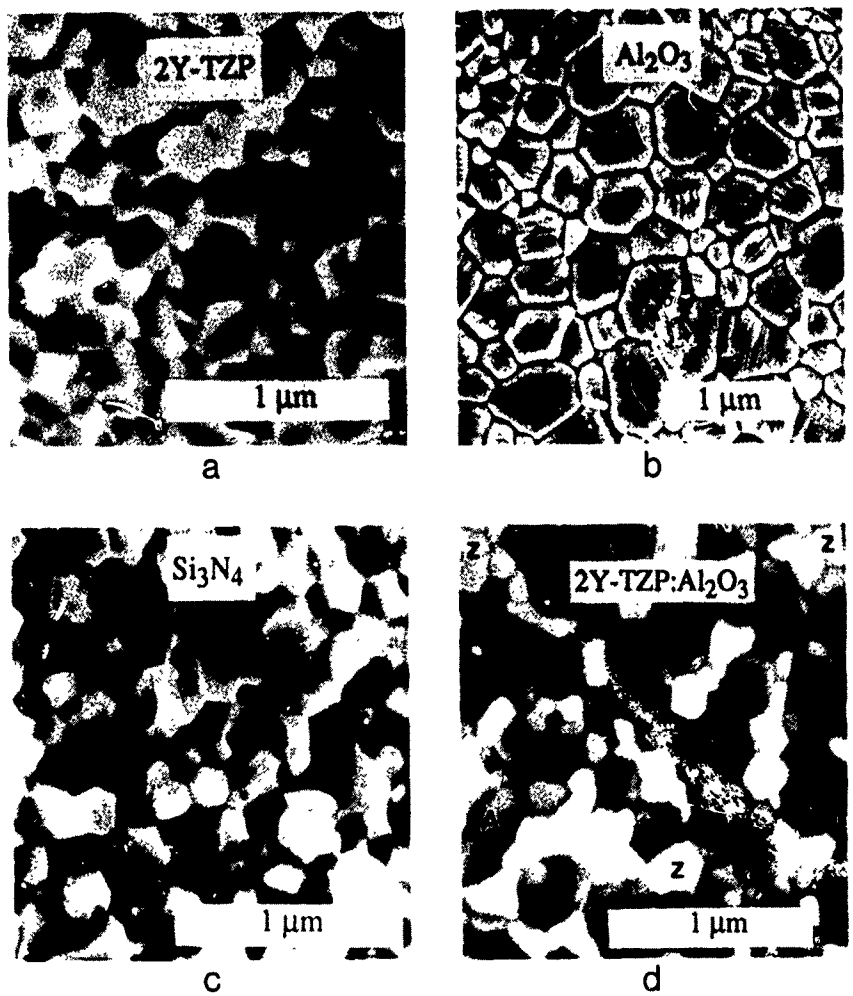

Fig. 3. Scanning electron microscopy micrographs of ultrafine grains of superplastic ceramics (a) 2Y-TZP (b) alumina, (c) silicon nitride, and (d) 2Y-TZP/alumina at equal volume fraction

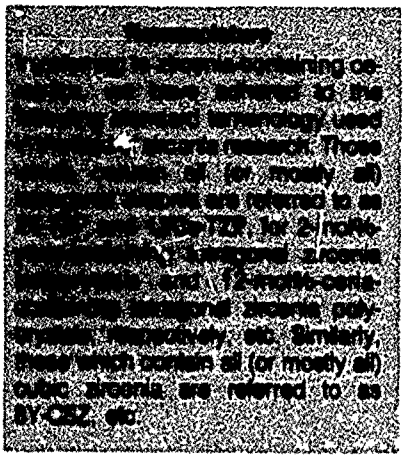

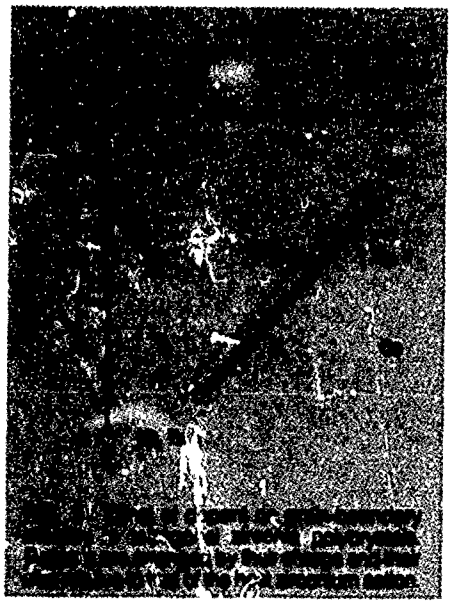

Prior to the recent discovery of ceramic superplasticity, there was little appreciation or understanding of these aspects in the ceramic field. Therefore, the initial attempts at microstructural and microchemical tailoring of superplastic structural ceramics demanded considerable empiricism. Over the last two years, however, intensive studies on superplastic zirconia and the development of superplastic alumina and silicon nitride collectively provided an extensive body of knowledge on the problems of dynamic grain growth and grain-boundary cohesive strength. They also shed some light on related aspects, such as grain-boundary chemistry, grain-boundary mobility, grain-boundary energy, and their relation to deformation and fracture of ultra-fine-grained ceramics.

This knowledge can now be used to formulate some useful and self-consistent guidelines to direct future materials design for superplastic applications. In the following sections, overviews of this knowledge, and the insights derived thereby, are summarized for each class of ceramics to better elucidate the processing–structure–forming relationships outlined in Fig. 2.

(1) Zirconia Ceramics

Tetragonal zirconia polycrystals, containing 2 to 4 mol% yttria, have been reported to be superplastic at temperatures above 1300°C,[12] beginning with the work of Wakai *et al.* on 3Y-TZP.[11,25-28] For more than a decade, we have known that yttria-stabilized tetragonal zirconia has a characteristically fine-grained microstructure[29] (see Fig. 3(a)), which is relatively uncommon among ceramics. The need for maintaining a submicrometer grain size was initially motivated by the pursuit of transformation toughening.[29-31] Ultrafine grains are required to avoid spontaneous tetragonal-to-monoclinic transformation, for which nucleation statistics are grain-size dependent.[32] The subsequent use of this material as a tough and strong ceramic (K_{IC} above 5 MPa·m$^{1/2}$ and strength exceeding 1200 MPa)[33] has stimulated the industry to provide powders of an excellent sinterability. These commercially available powders can be readily processed to obtain dense ceramics with a grain size ranging from 0.3 to 0.5 μm, sufficiently fine to allow superplasticity above 1350°C. It is for this reason that 3Y-TZP has become almost the universal choice for demonstrating ceramic superplasticity in the last few years.

The relatively good characteristics of zirconia powders contribute to their excellent sinterability and microstructure. The question then becomes, "Is there an intrinsic explanation, if any exists, for the very fine grain size observed?"[34] A related question is whether there is an intrinsic cause for the emergence of Y-TZP as an excellent superplastic ceramic. We believe that the answers to both questions have now been given. The primary attributes of Y-TZP as a fine-grained superplastic ceramic are closely related to the strong segregation of solute cations to the grain boundary, which lowers the grain-boundary mobility and the grain-boundary energy.[35] A secondary advantage of TZP appears to be its ability to contain a glassy grain-boundary phase, which facilitates sintering and deformation without compromising microstructural stability and grain-boundary strength.

Direct evidence for Y^{3+} segregation at TZP grain boundaries has been provided by X-ray photoelectron spectroscopy (XPS) of intergranularly fractured specimens.[36] Similar segregation and grain-growth studies on the effects of other cations have revealed a general trend: divalent and trivalent cations are enriched at the grain boundary, whereas tetravalent and pentavalent ones are not. Only the former can suppress grain growth. The effectiveness of the dopants Ca^{2+}, Mg^{2+}, Y^{3+}, Yb^{3+}, In^{3+}, Sc^{3+}, Ce^{4+}, Ti^{4+}, Ta^{5+}, and Nb^{5+} in suppressing grain growth ranks in the order listed from most to least effective. This sequence can be rationalized if it is recognized that the grain boundary in TZP is positively charged[36] and that larger cations diffuse more slowly.[37] A schematic diagram illustrating the trend for grain-boundary mobility is shown in Fig. 4. Essentially, from the charge consideration, cations of a valence lower than 4+ are expected to form a space charge cloud[38] around the grain boundary, more so for Ca^{2+} and Mg^{2+} than for Y^{3+} and other trivalent cations. Tetravalent and pentavalent cations are not expected to segregate for the same reason. From the size–diffusivity consideration, the solute drag of the larger cation is expected to be more effective, i.e., Ca^{2+} more than Mg^{2+}, and Y^{3+} more than Yb^{3+}, In^{3+}, and Sc^{3+}, in that order. Yttrium cations, being trivalent and oversized, with a relatively large (2.5 mol%) solubility in zirconia, thus serve as a rather effective solute in suppressing grain growth during sintering. It is for this reason that fine-grained Y-TZP is readily obtainable under nearly all processing conditions.

A comparison of the grain-boundary mobility of 2Y-TZP, 12Ce-TZP, 12Ce-TZP with 0.3 and 1 mol% calcia, and 8Y-CSZ is made in Fig. 5. Compared with Y-TZP, both Ce-TZP and CSZ have a much faster rate of grain growth. Microanalysis of the near grain-boundary region reveals little solute segregation in Ce-TZP and 8Y-CSZ. In the case of Ce-TZP, the mobility of the grain boundary can be lowered progressively by adding calcia, which segregates strongly.[36] Calcium, as noted, is the most potent dopant for suppressing grain growth in TZP. Therefore, the observed effects are in accordance with the space charge model.

Rapid grain growth has been observed in a number of materials that have been superplastically deformed.[12,39-43] Accord-

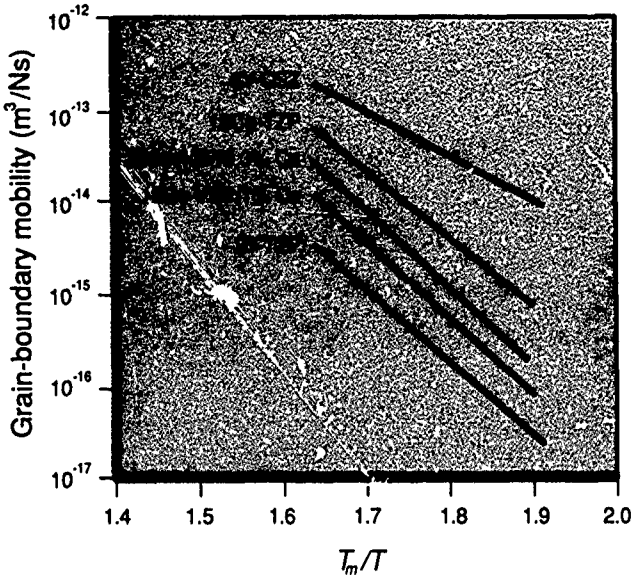

Fig. 5. Grain-boundary mobility of TZP and CSZ plotted versus reciprocal homologous temperature (T_m is melting point).

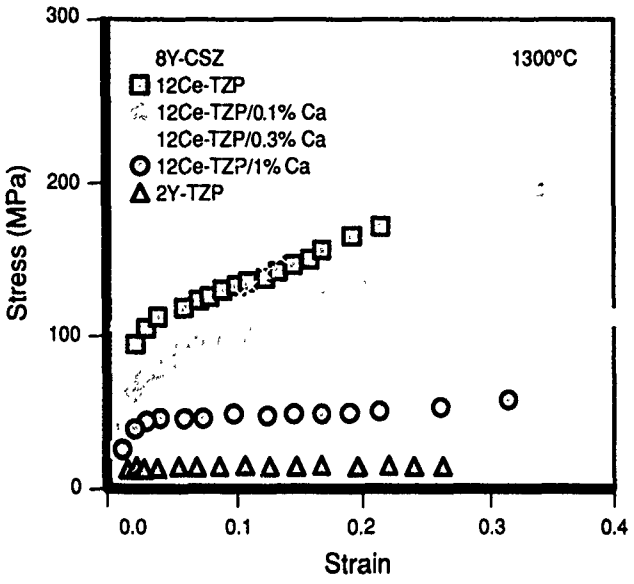

Fig. 6. Stress–strain curves of TZP and CSZ. Initial grain sizes are 0.48 μm (8Y-CSZ), 0.56 μm (12 Ce-TZP with 0%, 0.1%, and 0.3% Ca), 0.3 μm (12Ce-TZP with 1% Ca), and 0.21 μm (2Y-TZP). Tendency for strain hardening directly corresponds to the magnitude of grain-boundary mobility shown in Fig. 5. (Strain rate is 10^{-4} s^{-1} except in the case of 8Y-CSZ and 12Ce-TZP with 1% Ca where 3×10^{-4} s^{-1} is used.)

ing to Eq. (1), grain coarsening during deformation causes an increase of the flow stress. The resultant strain hardening is very pronounced, and it unmistakably signals the occurrence of dynamic grain growth. To illustrate this, stress–strain curves of 2Y-TZP, 12Ce-TZP, 12Ce-TZP with 0.3 and 1 mol% calcia, and 8Y-CSZ are shown in Fig. 6. Among them, 12Ce-TZP and 8Y-CSZ exhibit pronounced strain hardening and grain growth, but 2Y-TZP and Ce-TZP with 1 mol% calcia do not. (These tests were performed in compression to minimize the effect of cavitation or grain-boundary cracking, which is quite severe in 8Y-CSZ.) Comparing these results with Fig. 5, we further note that, even though the addition of 0.3 mol% calcia is enough to largely suppress static grain growth, it is inadequate for suppressing dynamic grain growth. It seems likely that, under superplastic deformation, grain boundaries are able to break away from the solute cloud[44] when only 0.3 mol% calcia is present. Thus, although solute segregation may still slow down dynamic grain growth, in general, it does so less effectively than that for static grain growth.

In addition to being susceptible to dynamic grain growth, 12Ce-TZP and especially 8Y-CSZ seem to cavitate easily, even when deformed in compression. This observation suggests that they have a lower grain-boundary strength than that of Y-TZP. A higher grain-boundary energy in 8Y-CSZ than that of Y-TZP has been reported based on dihedral angle measurements in the two-phase tetragonal/cubic zirconia ceramics[35] (see Table I and Fig. 7). Because the dihedral angle is determined by the ratio of the interfacial energies, these data allow the calculation of the relative energies of the tetragonal grain boundary (γ_{tt}), cubic grain boundary (γ_{cc}), and tetragonal/cubic phase boundary (γ_{tc}). This gives $\gamma_{tt}:\gamma_{tc}:\gamma_{cc} = 1:1.3:1.6$. (Similar correlations have also been observed in alumina and its phase boundaries with zirconia, as will be discussed in the next section.) This correlation suggests that an added benefit of solute segregation in Y-TZP is the lowering of the grain-boundary energy, which could, in turn, have the effect of increasing the cohesive strength of the grain boundary. If this correlation extends to other zirconia ceramics, it also follows that, because they lack solute segregation, both 8Y-CSZ and 12Ce-TZP have higher grain-boundary energies and thus lower cohesive strengths.

To enhance the diffusivity and lower the deformation resistance of zirconia ceramics, additives which segregate to the grain boundary and which possibly form a grain-boundary low-melting phase can be quite effective. Transition-metal oxides

Table I. Dihedral Angles and Interfacial Energies of Zirconia and Alumina

		Dihedral angle, θ (deg)		Interfacial energy, γ	
Ceramic	Stabilizer	$\theta_{c,\,tt}$	$\theta_{t,\,cc}$	γ_{cc}/γ_{tt}	γ_{tc}/γ_{cc}
TZP/CSZ	4 mol% Y_2O_3	134	97	1.7	1.3
	6 mol% Y_2O_3	131	105	1.5	1.2
	6 mol% Y_2O_3*	134	107	1.5	1.3
	5.5 mol% In_2O_3	136	95	1.8	1.3
	5 mol% Sc_2O_3	140	113	1.6	1.5
		$\theta_{a,\,tt}$	$\theta_{t,\,aa}$	γ_{aa}/γ_{tt}	γ_{at}/γ_{tt}
Alumina/zirconia	Alumina/2Y-TZP	130	90	1.67	1.18
		$\theta_{a,\,cc}$	$\theta_{c,\,aa}$	γ_{aa}/γ_{cc}	γ_{aa}/γ_{ac}
Alumina/zirconia	Alumina/8Y-CSZ	114	96	1.23	1.34

*0.1 mol% Mn_3O_4 also added

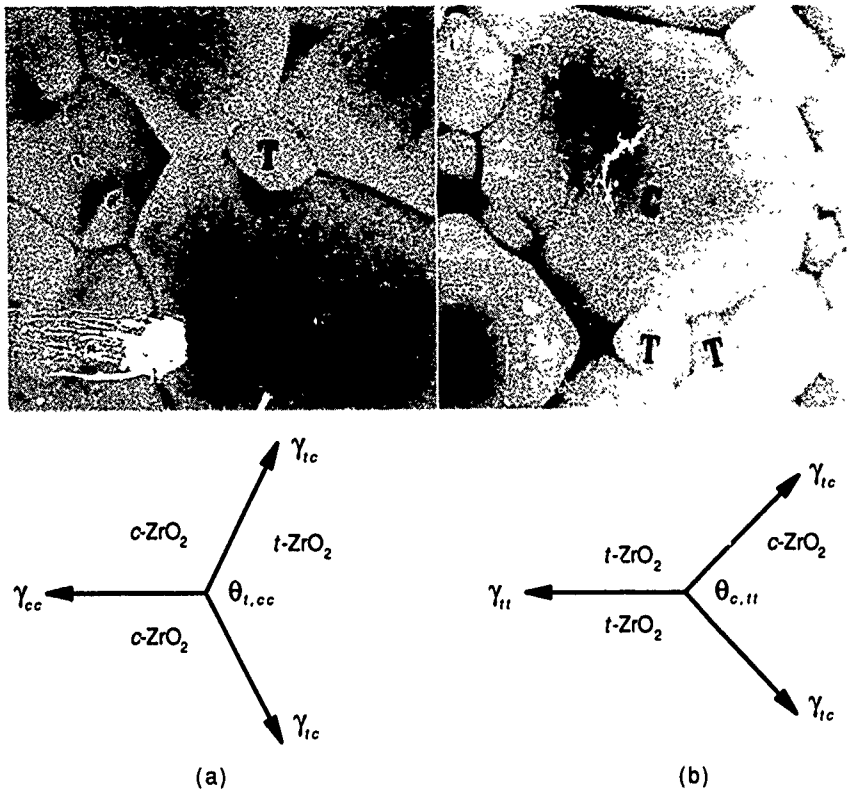

Fig. 7. Relationship between dihedral angles and interfacial energies (a) tetragonal grain (T) surrounded by cubic grains (C) in 6 mol% yttria/zirconia, indicating $\gamma_{cc}>\gamma_{tc}$ and (b) cubic grain (C) surrounded by tetragonal grains (T) in 4 mol% yttria/zirconia, indicating $\gamma_{tt}<\gamma_{tc}$

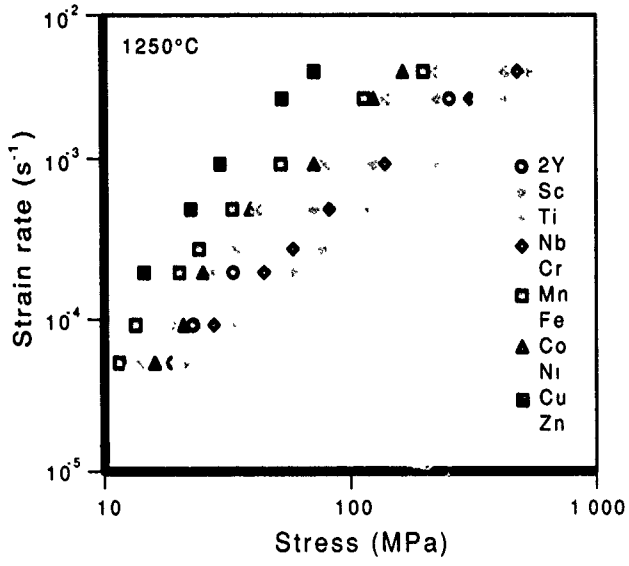

Fig. 8. Strain rate versus stress of TZP with 0 3 mol% of cation additive as shown. Base composition contains 2 mol% yttria and is denoted by 2Y

(Sc, Ti, Nb, Cr, Mn, Fe, Co, Ni, Cu, and Zn) at 0.3 mol% have been investigated for this purpose.[45] Of the above, Mn, Co, Ni, and Zn were found to lower the sintering temperature and lower the grain size; Cu was found to lower the sintering temperature but slightly increase the grain size; and Sc, Ti, Nb. and Cr did not aid sintering. Deformation data for 2Y-TZP with various dopants, sintered and tested at 1250°C, are shown in Fig. 8. Figure 8 shows that Mn, Fe, Co, Cu, and Zn lower the flow stress, with Cu being the most effective. Segregation of these latter elements to the grain boundary was confirmed by XPS. Additional studies of the Cu-doped 2Y-TZP further established the formation of a grain-boundary liquid phase around 1130°C, although, even before melting, the grain-boundary phase had already facilitated deformation by enhancing diffusivity.[24] In all cases, ductility of the ceramics, as well as other important mechanical properties (strength, toughness, hardness, and stability against moisture), was not impaired by the small amount of additives.

Note that zirconia ceramics usually contain a certain amount of Si impurity, which is localized at the grain boundaries.[46] A ternary eutectic between zirconia, yttria, and silica exists at 1350°C. Most likely the addition of Mn, Fe, and Zn has lowered the eutectic temperature. In the case of Cu, it is reported that a binary eutectic of copper(II) oxide (or copper(I) oxide) and zirconia lies between 1100° and 1150°C, depending on the oxygen potential.[47] This report is consistent with the better sinterability and superplastic formability of this class of ceramics; namely, "undoped" Y-TZP becomes superplastic above 1350°C, doped Y-TZPs are superplastic at 1250°C, whereas Cu doping lowers the forming temperature further to 1150°C.

It is remarkable that all Y-TZP ceramics are superplastically formable, as demonstrated in Fig. 1 (Formability will be discussed in more detail in Section IV.) Apparently, there is no loss of grain-boundary strength despite a thin grain-boundary layer of amorphous or even liquid phase, which is the result of unintended source/process contamination or deliberate doping. In this context, note that the characteristic dihedral angles measured at triple points between various zirconia phases are always quite distinct (Fig. 7). This distinction indicates that their respective interfacial energies are well-defined. We then conclude that the presence of a thin grain-boundary phase in Y-TZP ceramics does not dispel the classical notion of interfacial and like energies,[36] and that even "contaminated" grain boundaries can have excellent strength and cavitation resistance.

Thus, the following major conclusions concerning superplastic material development can be made from zirconia studies

(i) The selection of an appropriate crystalline phase is often important for achieving an ultrafine grain size in single-phase ceramics. Tetragonal zirconia is a superior superplastic ceramic whereas cubic zirconia is not.

(ii) Both static grain growth and dynamic grain growth are closely related to the grain-boundary mobility. In tetragonal zirconia, segregating dopants are much more effective in suppressing static grain growth than dynamic grain growth.

(iii) Solute segregation has an added benefit in lowering grain-boundary energy and, correspondingly, strengthening the grain boundary.

(iv) The grain-boundary amorphous second phase, containing Si, Zr, Y, O, and most of the heavier transition-metal cations of the third row, is very effective in lowering the superplastic flow stress and increasing the deformation rate without lowering the grain-boundary cohesive strength.

(2) Alumina

There have been several unsuccessful attempts in the past to develop superplastic alumina.[16,48-52] However, the tensile ductilities reported in these studies were all much lower than that found in zirconia. Recently, we have succeeded in superplastically stretching alumina (doped with 200 ppm magnesia) to large strains.[3] A disk so formed is shown in Fig. 1, and its microstructure is illustrated in Fig. 3(b).

Although large-strain superplasticity is now possible, difficulties encountered in the course of developing superplastic alumina did provide valuable lessons to our current thinking about superplasticity in ceramics. These difficulties are related to processing, the use of additives, and their consequences on microstructural development and superplastic characteristics.

Unlike the case of Y-TZP, special attention must be paid to alumina powder processing. Because sintering alumina below 1300°C requires considerable skill and effort,[53] and grain growth above 1300°C is rather fast, only a very narrow processing window is available for this ceramic. The window may be widened somewhat by the use of additives that suppress grain growth, by hot-pressing, and by improving powder processing to allow densification at lower temperatures. Unfortunately, we have found magnesia ineffective in further lowering of the grain-growth rate in very-fine-grained alumina sintered below 1300°C. As for hot-pressing, results of previous studies seem to place a lower bound of about 1 μm for the grain size of alumina,[43,50,54] which is not fine enough for superplastic applications. Thus, low-temperature sintering is the only alternative.

From a processing viewpoint, the main obstacles for low-temperature sintering of ceramic powders are hard agglomerates in the powders and poor packing in the green body.[53,55,56] Powders often contain hard agglomerates which later sinter at different rates and inhibit shrinkage of the matrix by exerting a mechanical constraint. Poor packing of powders lowers the green density, which often delays sintering and leaves behind flaws.[56] These problems can largely be avoided by meticulous handling of powders. This entails breaking up hard agglomerates in the starting powders, manipulating and controlling interparticle forces in the colloidal powder suspension, and direct consolidation of the slurry into a green body using colloidal pressing or pressure filtration techniques.[56] The resultant homogeneous green compact, with a higher density and fewer defects and agglomerates, has a markedly improved sinterability. This can facilitate low-temperature sintering and the attainment of very fine microstructures.

Low-temperature sintering of pure alumina at 1150°C has been reported using special classified powders of a very fine particle size.[53] In this case, the grain size at 99% of theoretical density is 0.25 μm. The yield of this type of processing, however, is too low for the purpose of laboratory testing of superplastic formability. Using unclassified powders and colloidal processing techniques, we have been able to sinter pure alumina at a temperature of 1250°C. The microstructure of a sintered pure alumina is shown in Fig. 9(a). The grain size is as fine as 0.5 μm and remains relatively stable during annealing at temperatures below 1300°C.

Pure alumina of such a grain size has a very low initial flow stress. However, it fails to deform superplastically because of rapid dynamic grain growth, which causes strain hardening (see Fig. 9(b) for the deformed microstructure and Fig. 10 for the stress–strain curve). Note that grains of a larger size in the deformed microstructure tend to be elongated. This is a general feature of grain growth in alumina and may be attributed to the anisotropy in grain-boundary energy.[57] Large grains of this type serve as stress concentrators and potent nucleation sites for cavitation, thus degrading the ductility. A higher deformation temperature only exacerbates the problems, as shown in Fig. 9(c).

A fundamental problem associated with pure alumina is its relatively high grain-boundary energy. In addition to providing a higher driving force for grain growth, the high energy may also cause the grain boundary to have a relatively low cohesive strength, according to the argument advanced in the previous section. The direct evidence for a higher grain-boundary energy is once again provided by dihedral angle measurements, and the results are illustrated in Table I and Fig. 11. In this case, an alumina/zirconia two-phase microstructure is used to establish the ratio of the

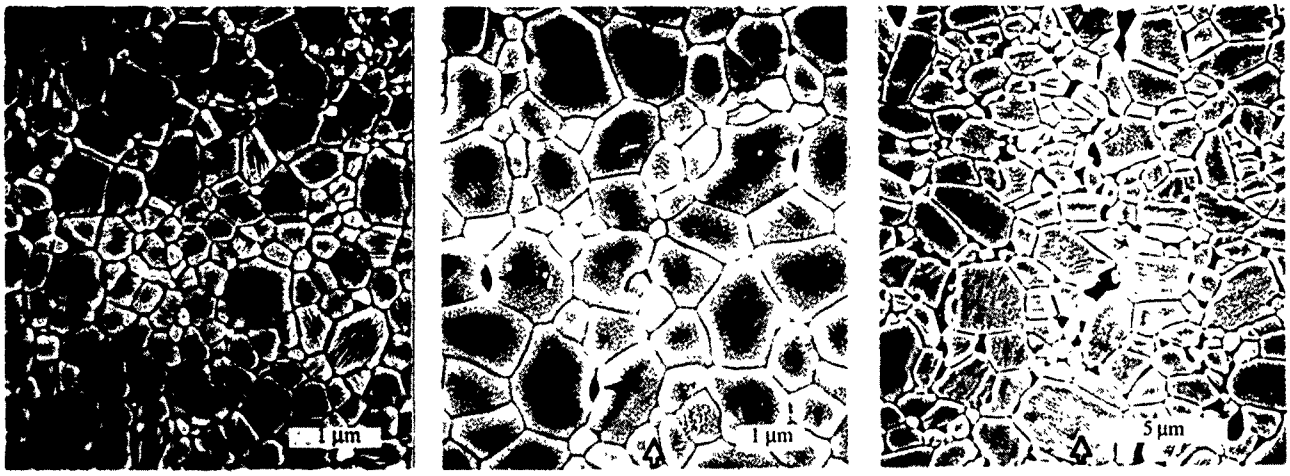

Fig. 9. Microstructure of pure alumina (a) as sintered at 1250°C, (b) deformed in compression at 1250°C (strain rate of 1.5×10^{-5} s^{-1}, total strain of 0.3) with compression axis shown by hollow arrows and cavities by solid arrows, and (c) same as (b) but deformed at 1400°C (strain rate of 2.4×10^{-4} s^{-1}; total strain of 0.68)

grain-boundary energies of alumina (γ_{aa}) and zirconia (γ_{tt} and γ_{cc}) to the interfacial energy between the two (γ_{at} and γ_{ac}). The ratio reveals that the grain-boundary energy of alumina is even higher than that of cubic zirconia, which is higher than that of 2Y-TZP, as noted previously. The interfacial energies follow the sequence γ_{aa}, γ_{cc}, γ_{ac}, γ_{at}, γ_{tt}, from highest to lowest. As expected, pure alumina has a high propensity for cavitation, even in compression (see Figs 9(b) and (c)).

We have already mentioned magnesia as an additive for grain-growth control. Segregation of magnesia and other additives in alumina is fairly well established and has been attributed to the elastic energy due to a size misfit.[58] Unlike zirconia, however, alumina has very little solubility for most aliovalent cations. For example, the solubility of magnesia at 1500°C is only 200 ppm.[59] At such a low concentration and at low temperatures (below 1300°C), magnesia has an unnoticeable effect on static grain growth. However, dynamic grain growth can be brought under control by the same amount of magnesia. This can be appreciated by comparing the stress–strain curve of pure alumina and 200 ppm-magnesia-doped alumina in Fig 10. The relatively mild strain hardening of the latter is a direct consequence of the slower dynamic grain growth in this material. As demonstrated in Fig. 1, magnesia-doped alumina can be superplastically stretched to large strains.

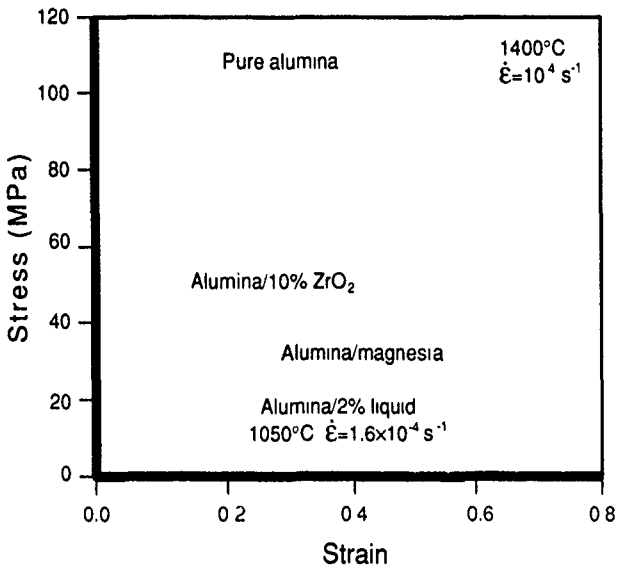

Fig. 10. Stress–strain curves for alumina. Strain hardening in pure alumina and magnesia-doped alumina is due to dynamic grain growth. The eventual decrease in stress in pure alumina is a result of cavitation. Note that alumina with 2% liquid was tested at a lower temperature

Attempts have also been made to introduce a low-melting liquid phase (such as boron oxide and copper(II) oxide) and various charge-compensating dopant pairs (such as Cu^{2+} and Ti^{4+}) to alumina to lower the sintering and superplastic forming temperatures. These ceramics have very fine grains and they can be sintered and deformed at temperatures around 1050°C. The resultant stress–strain curve is shown in Fig 10. However, deformation is accompanied by abnormal growth of some grains. The cause for abnormal grain growth in this case is probably again associated with the anisotropy of grain–liquid interfaces. Moreover, the tensile ductilities are disappointing for these specimens, reaching only 15%. These low ductilities indicate a severely degraded grain-boundary cohesive strength, which is further compounded by the stress concentrations around abnormally large and elongated grains.

Thus, the following major conclusions are made from the above data for superplastic alumina:

(i) Because of its high and anisotropic

grain-boundary energy, pure alumina is weak along the grain boundary and is prone to rapid, abnormal grain growth, making it an inherently difficult choice for ceramic superplasticity.

(ii) The use of additives is less effective for alumina than that for zirconia because of the limited solubilities of nearly all the cations. This results in the relatively weak grain-boundary cohesion observed in most cases to date.

(iii) Although magnesia is not necessarily needed for effecting low-temperature sintering, it does lower the grain-boundary mobility in dynamic grain growth. This has made large-strain superplastic stretching possible.

(iv) As the liquid phase lowers the flow stress of alumina, it also facilitates abnormal grain growth and probably lowers the interfacial strength. Superplasticity of alumina at low temperatures (below 1350°C) thus appears unlikely, except in composites.

(3) Silicon Nitride

Two superplastic silicon nitrides have been reported recently. A fine-grained silicon nitride/silicon carbide composite (20 wt% silicon carbide) containing a variety of other mixed phases was deformed in tension to 150% at 1600°C and a strain rate of 4×10^{-5}/s.[21] Another silicon nitride,[20] shown in Fig. 1, was punch-stretched at 1500°C. The microstructure of the latter is shown in Fig. 3(c).

In ceramic alloy design, there is a close analogy between silicon nitride and the two other ceramics discussed in the previous sections. Like zirconia, two polymorphs, α- and β-silicon nitride, exist which transform from one to the other by reconstruction. Both phases have a large range of solubility. The α-phase solid solution can be represented as $M_{z/n}Si_{6-x-z}Al_{x+z}O_xN_{8-x}$ and is commonly referred to as α'-sialon in this form.[60] Here M is a cation of a valence n and of an appropriate ionic radius. The β-phase solid solution can be represented at $Si_{6-x}Al_xO_xN_{8-x}$ and is referred to as β'-sialon in this form.[61] Both phases are derived from the respective α- or β-silicon nitride unit cell by partial replacement of Si^{4+} by Al^{3+}. Valence compensation is by substitution of N^{3-} or O^{2-} and, in the case of α'-sialon, by additional modifier cations occupying the interstices of the (Si–Al)–(N,O) network similar to that of the stuffed derivatives of silica.[62] Similar to alumina, β'-silicon grains have a strong tendency for anisotropic grain growth at higher temperatures. They typically assume a needlelike morphology, and the growth mechanism involved has been identified previously.[63] In contrast, α'-sialon grains tend to be small and equiaxed over a wide range of temperature, even though its crystal structure is highly anisotropic.[60]

To sinter both sialons, metal oxides are often added as liquid-phase sintering aids.[64] This enhances densification and facilitates the conversion of the starting powders to the final, alloyed phases of the intended compositions. The amount and the composition of the liquid, as well as those of other phases, undergo continuous changes as sintering and annealing proceed.[64] Because metal cations can be incorporated into the α'-sialon, it is theoretically possible to obtain a single-phase α'-sialon without any remaining liquid phase. This is not the case for β'-sialon, which has no solubility for any cations other than Si^{4+} and Al^{3+}.

The superplastic silicon nitride shown in Figs. 1 and 3(c) was designed to form α'-sialon.[20] A small amount of crystalline yttrium aluminum garnet and α-silicon nitride also exist in the final phase assemblage at 1500°C. The amount of the liquid phase that exists during forming is relatively small. This ceramic maintains an equiaxed grain shape during superplastic forming. Because of the very fine and stable microstructure, this ceramic can be

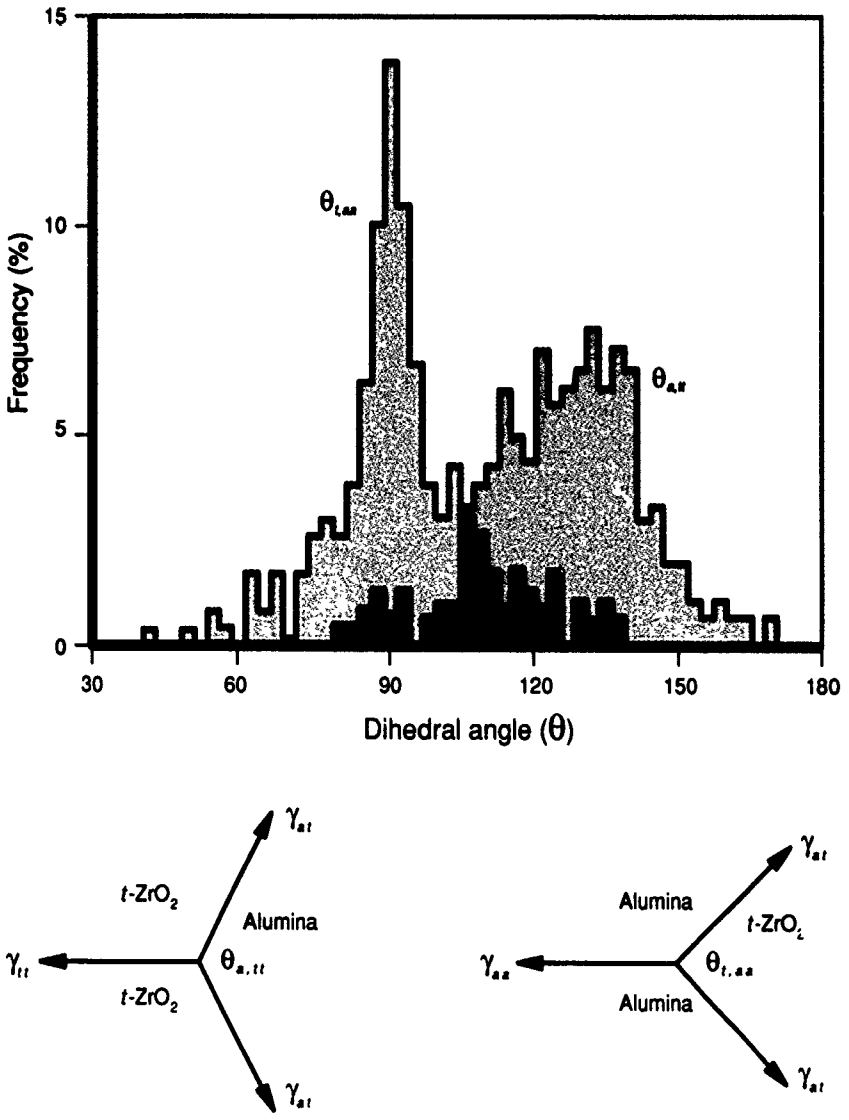

Fig. 11. Examples of distributions of dihedral angles between alumina and tetragonal zirconia The peak values are given in Table I Also shown schematically is the relationship between dihedral angles and interfacial energies

deformed at a relatively low temperatures. The presence of the liquid phase lowers the flow stress still further. As shown in Fig. 12, only a mild strain hardening is apparent in superplastic deformation. The deformed microstructure, containing mostly equiaxed, fine grains, is shown in Fig. 13(a).

Wakai *et al.* took a different approach to developing a superplastic silicon nitride.[21,22] They added silicon carbide to silicon nitride in the hope that grain growth would be suppressed. In addition, they used an amorphous Si-C-N powder to fabricate a hot-pressed composite in the hope that the initial grain size would be minimized. However, the composition of this silicon nitride was such that β'-silicon nitride was the predominant phase, which began to develop an elongated grain shape in fabrication.[22] The sintering aids added (yttria and alumina) provided a considerable amount of liquid-phase and other phase mixtures which evolved with time. Although this silicon nitride can be deformed above 1600°C, strain hardening is prominent, possibly because of the anisotropic grain growth of β'-sialon.[21,22] The higher deformation temperature also dictates that a severe weight loss occurs because of vaporization of silica from the liquid phase, and from nitrogen decomposition. Despite these problems, a large tensile ductility exceeding 150% was achieved, although the weight loss has caused deterioration of the surface finish.[21] A comparison of the stress-strain curves and deformed microstructures of the above two superplastic silicon nitrides is shown in Figs. 12 and 13. It is evident that the flow stress of α'-sialon is much lower than that of β'-sialon/silicon carbide and that the microstructure of the former is much finer.

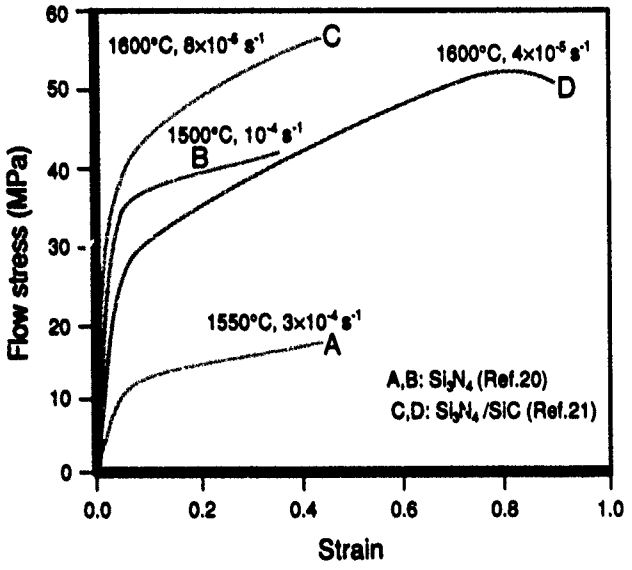

Fig. 12. Stress-strain curves of silicon nitrides, where, A and B are mostly α'-sialon deformed in compression,[20] and C and D are mostly β'-sialon with 30 vol% silicon carbide deformed in tension.[21] Note that A and B have much less strain hardening than C and D.

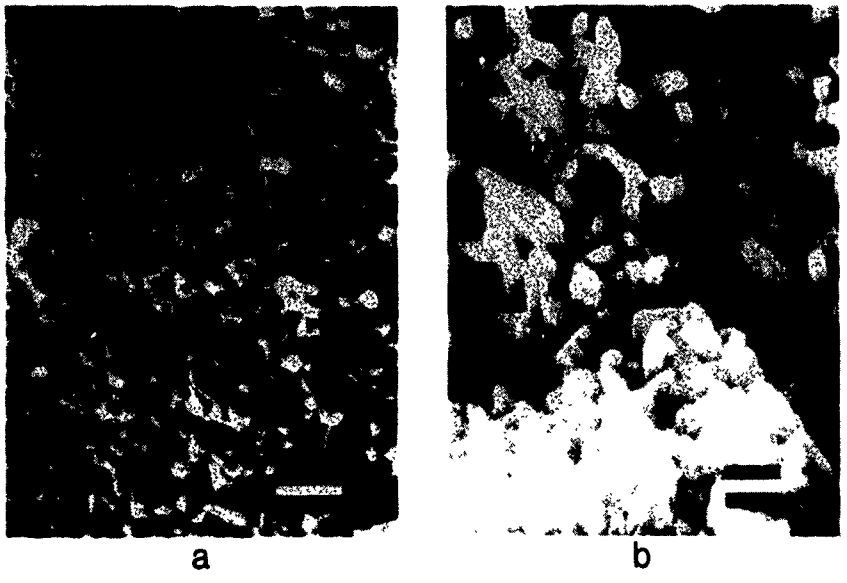

Fig. 13. (a) Microstructure of a deformed silicon nitride containing mostly α'-sialon (bar = 1 μm) Note similarity with Fig. 3(c) due to the absence of anisotropic grain growth (b) Microstructure of a deformed silicon nitride containing mostly β'-sialon and 30 vol% silicon carbide (bar = 1 μm), showing much grain growth during deformation.

Thus, despite the substantially different phase compositions, amounts of the liquid, strain-hardening rates, microstructures, and deformation characteristics, large ductilities seem obtainable in several families of fine-grained silicon nitrides. This suggests that the (Si, Al, O, N) liquid present, partially modified by yttrium and possibly other cations, is available for superplastic stretching in that the liquid provides an adequate plastic deformation stability and cavitation resistance to prevent strain localization and fracture. Although further research is required to establish the optimum composition of the liquid and the lower limit of its amount for superplastic forming, these initial findings and their implications are indeed encouraging.

The following major conclusions regarding the development of superplastic silicon nitride are made.

(i) Obtainable through judicious phase and compositional control, equiaxed fine-grained silicon nitride in the form of α-silicon nitride and α'-sialon are resistant to static and dynamic grain growth. In contrast, β-silicon nitride and β'-sialon are prone to anisotropic grain growth during forming, particularly at higher temperatures, which causes severe strain hardening.

(ii) The liquid phase in silicon nitride, containing Si, Al, O, N, Y, and possibly additional cations, has adequate cohesive strength to resist cavitation in superplastic forming.

(iii) Silicon nitrides are excellent candidates for superplastic forming at intermediate temperatures, around 1500°C. At higher temperatures, weight loss from liquid vaporization becomes severe and the surface quality deteriorates.

(4) Composites

Composites of zirconia/alumina[16,65] and zirconia/mullite[17,18] have been investigated throughout the entire range of composition. Y-TZP with up to 80 vol% of alumina or mullite are superplastic and have very good formability.[19] Pure alumina is also superplastic, under optimal conditions. Pure mullite has not been made superplastic as of this date.

Compared with monolithic ceramics, composites have the distinct advantage of superior microstructural stability against both static and dynamic grain growth. The as-sintered composites usually have a smaller grain size, even though they may require a higher sintering temperature than those of the monolithic ceramics made of either constituent. In particular, a duplex microstructure can be obtained, i.e., one in which two phases are of nearly equal volume fraction and are both multiply connected. Known for its fine grain sizes and excellent resistance against coarsening, many such microstructures have figured prominently in the historical development of superplastic metallic alloys (e.g., Pb–Sn and Zn–Al alloys, α-β brass, α-β Ti alloys, and α-γ stainless steel).[2] Duplex microstructures have also been obtained for zirconia/mullite and zirconia/alumina composites. An example of the latter is shown in Fig. 3(d) with a grain size of about 0.2 μm. Sintered in the temperature range of 1370° to 1480°C, these duplex composites can maintain their very fine microstructures even after large superplastic deformation, provided that the deformation temperature does not exceed the sintering temperature.

Considerable microstructural stability is already evident when the second phase is present at a smaller volume fraction, typically no more than 20%. This improvement is especially important for dynamic grain growth. A striking example is encountered in alumina with zirconia inclusions. Although fine-grained pure alumina is subject to rapid dynamic grain growth, its grain size remains largely stable during superplastic deformation when 10 vol% zirconia is added. This addition of zirconia also suppresses (or eliminates) strain-hardening behavior, as shown in Fig. 10, thus improving the superplastic formability of this material.

From a microstructural control view point, there is an important relationship between the matrix grain size and the size or amount of the second-phase particles. Since the early work of Zener,[66] the particle-pinning effect has been of continuing interest. Superplastic ceramic composites offer an opportunity to reexamine this effect in ultra-fine-grained ceramics. According to the analysis of Hellman and Hillert,[67] the matrix grain size, d, is 1.8 times that of the particle size, r, normalized by the cube root of the volume fraction, v. This is equivalent to having 6 pinning particles, on average, for every grain. In this model, grains are pinned in three dimensions by particles residing on grain corners.

Data from fine-grained zirconia/mullite and zirconia/alumina, for a volume fraction of the second phase between 1% and 15%, are plotted in Fig. 14 to evaluate this prediction. Although some scattering does exist, these data can be reasonably correlated by the following equation:

$$d = \alpha r/v^{1/3} \qquad (2)$$

where α is about 0.75. This is equivalent to having 0.4 of a pinning particle for every grain. Since Hellman and Hillert's model assumes equilibrium and the prediction is for the limiting grain size, it is expected that the model has severely underestimated the pinning effect. This is especially so when low-mobility grain boundaries dominate, as should be the case in the best superplastic ceramics. From a practical point of view, the indication of a much stronger pinning effect than their model has suggested is certainly encouraging.

The beneficial effect of a second phase on coarsening stability is largely lost when a significant amount of liquid phase is present. For example, adding silicon carbide to silicon nitride appears to have little effect on the growth of β'-sialon grains (Fig. 13(b)), which assume a characteristically elongated shape.[21] Growth of β'-sialon grains probably proceeds via a solution–reprecipitation mechanism through the liquid phase aided by phase conversion in these ceramics.[63,64] Because particle coarsening is only weakly

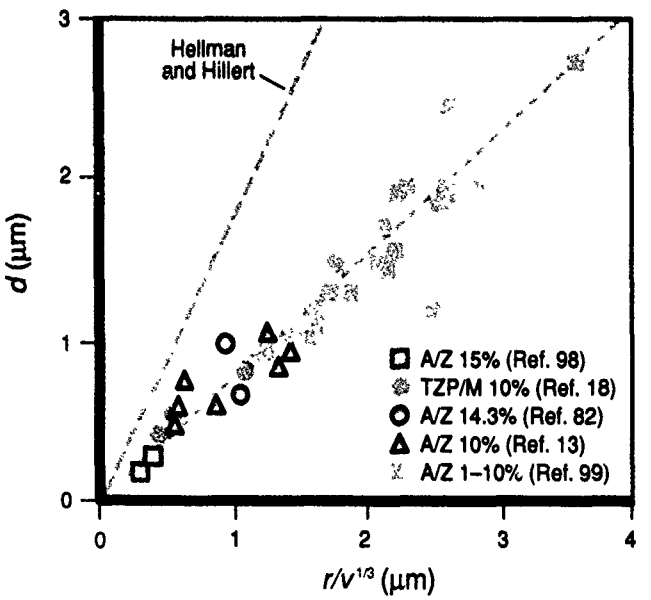

Fig. 14. Grain size d as a function of inclusion size r and volume fraction of inclusions v. The matrices are alumina (A) and TZP. Inclusions are zirconia (Z) and mullite (M), with their volume fractions indicated

dependent on the volume fraction of the particulate phase itself,[68] the presence of another inert inclusion phase (silicon carbide) is not expected to have a major effect on the coarsening of silicon nitride. Experimental observations of considerable strain hardening in this material (see Figs. 12(c) and (d)), as well as the deformed microstructure reported (Fig. 13(b)), are consistent with the above expectation.

The following major conclusions regarding the development of superplastic ceramic composites are made.

(i) As in metals, ceramic composites with a duplex microstructure are essentially stable against static and dynamic coarsening at temperatures below that for sintering. These composites are excellent superplastic ceramics.

(ii) Composites with a modest amount of second phase gain considerable stability against static and dynamic grain growth. Thus, the grain size remains small after sintering and during forming and the material becomes superplastic. In alumina, for example, particle pinning renders the composite superplastic whereas pure alumina is not.

(iii) When grain growth occurs by Ostwald ripening via solution, diffusion, and reprecipitation through a liquid phase, static and dynamic grain growth cannot be suppressed merely by the introduction of second-phase inclusions. Unless the primary phase is itself stable against coarsening, these composites have only a limited capacity for superplastic deformation.

III. Deformation Characteristics

Although there is general agreement that deformation mechanisms in superplasticity are similar to diffusional creep,[3] definitive identification of specific mechanisms has not been successful. Reviews of data from superplastic metals reveal that, in several important aspects, superplasticity[2,4-7] differs from diffusional creep.[38] First, the grain shape change after large deformation is remarkably small, contrary to that envisioned in diffusional creep models. Second, the contribution from grain-boundary sliding is unusually large, compared with diffusional creep. Third, the stress and grain-size exponents are often substantially different from the prediction of simple diffusional creep models. These discrepancies have motivated several models which modify the conventional descriptions of diffusional creep for superplastic applications. In particular, concepts such as grain switching,[4] grain rotation,[5] and grain-shape transformation[6] have been introduced, and the enhanced roles of grain-boundary sliding and grain-boundary migration have been proposed. Some also envision an interplay of diffusional processes and (grain-boundary or lattice) dislocation processes.[69,70] Despite these efforts, such models are largely qualitative and fail to quantitatively account for the observed deformation rate of superplasticity.

This state of the art dictates that the present discussion of deformation characteristics should be confined to comparisons based on the phenomenological constitutive equation (Eq. (1)). In the following, an analysis of the stress, grain size, and temperature dependence of deformation for several superplastic ceramics is first presented. The effect of a second phase is then rationalized based on continuum mechanics models and on interface-related considerations. Finally, the origin and the effect of dynamic grain growth on deformation characteristics are explored. We postpone the discussion of fracture to Section IV where superplastic formability is assessed.

(1) Stress, Grain Size, and Temperature Dependence

Our discussion of the stress, grain size, and temperature dependence in ceramic superplasticity is concentrated on 2Y-TZP and alumina, where the best and most complete data are available. Although 3Y-TZP has been widely studied, it contains some cubic grains which tend to grow larger in size over time, making a definitive analysis of the deformation characteristics more difficult. For comparison, diffusional creep data of Y-CSZ will also be reviewed.[71-74]

In the absence of any intentionally added liquid phase, data for 2Y-TZP from different studies[12,17,24,75] are in reasonable agreement with each other when experiments conducted under similar deformation conditions are compared (see Fig. 15(a)). No significant grain growth is evident in 2Y-TZP at lower test temperatures. The stress exponent ranges from 1.5 to 2, and is independent of temperature. Wakai has also reported an increasing stress exponent with decreasing grain size,[12,75] a trend similar to the one observed in alumina.[54] Data illustrating this trend, commonly associated with interface-controlled diffusional creep,[54] are compiled in Fig. 16 and are discussed later. This trend is less obvious at higher stresses and strain rates. The grain-size exponent of 2Y-TZP ranges between 1 and 3, according to the various reports in the literature. However, because the stress exponent can itself be a strong function of the grain size, the grain-size exponent may appear higher at higher stresses.

The above observations are analogous to fine-grained superplasticity in metals and alloys and are generally incompatible with dislocation creep. The following considerations further rule out dislocation creep as a major mechanism in ceramic superplasticity. Flow stress for dislocation motion is strongly dependent on the solute content in zirconia ceramics.[76] If the available flow stress data of Y-CSZ[76] are extrapolated to lower yttrium content, as

appropriate for Y-TZP, they are still much higher, by 1 or 2 orders of magnitude, than the superplastic flow stress shown in Fig 15(a). This argument is also reinforced by the independent observation[17] that the anticipated dislocation spacing λ, which should follow a universal scaling law,[77] $\lambda = 2bG/\sigma$, much exceeds that of the zirconia grain size in most cases, especially at higher temperatures. In this scaling law, G is the shear modulus and b is the Burgers vector. The size of subgrains, if they do exist from regrouping of dislocations, would be even larger.[77] Thus, lattice dislocation activities are not likely to be significant in superplastic zirconia, except at very high strain rates.

In the literature of superplastic metals and alloys, transitions between deformation regimes signified by a change of the stress exponent are well documented.[2] In contrast, the transition from the superplastic regime (referred to as regime II in the superplasticity literature)[2] to a dislocation regime (regime III) is rarely seen in ceramics. This is primarily due to the fact that most ceramics do not have sufficient strength to resist fracture before the high flow stresses required for the transition can be reached. Moreover, no threshold stress (regime I) is evident in ceramics, at least over the stress range thus far investigated. Thus, ceramic superplasticity, as typified by the data shown in Fig. 15(a) for 2Y-TZP, apparently lies entirely in regime II.

The temperature dependence of Y-TZP follows an Arrhenius behavior, characterized by an activation energy ranging from 530 to 630 kJ/mol.[12,17,24,75] This value is somewhat higher than the activation energy of cation lattice diffusion in cubic zirconia.[37] However, no diffusion data are currently available for any tetragonal zirconia. Note that activation energies for grain-boundary mobility of a variety of TZP, shown in Fig. 5, which is probably rate limited by lattice diffusion of cations in the space charge cloud, are also higher than the activation energy of ca-

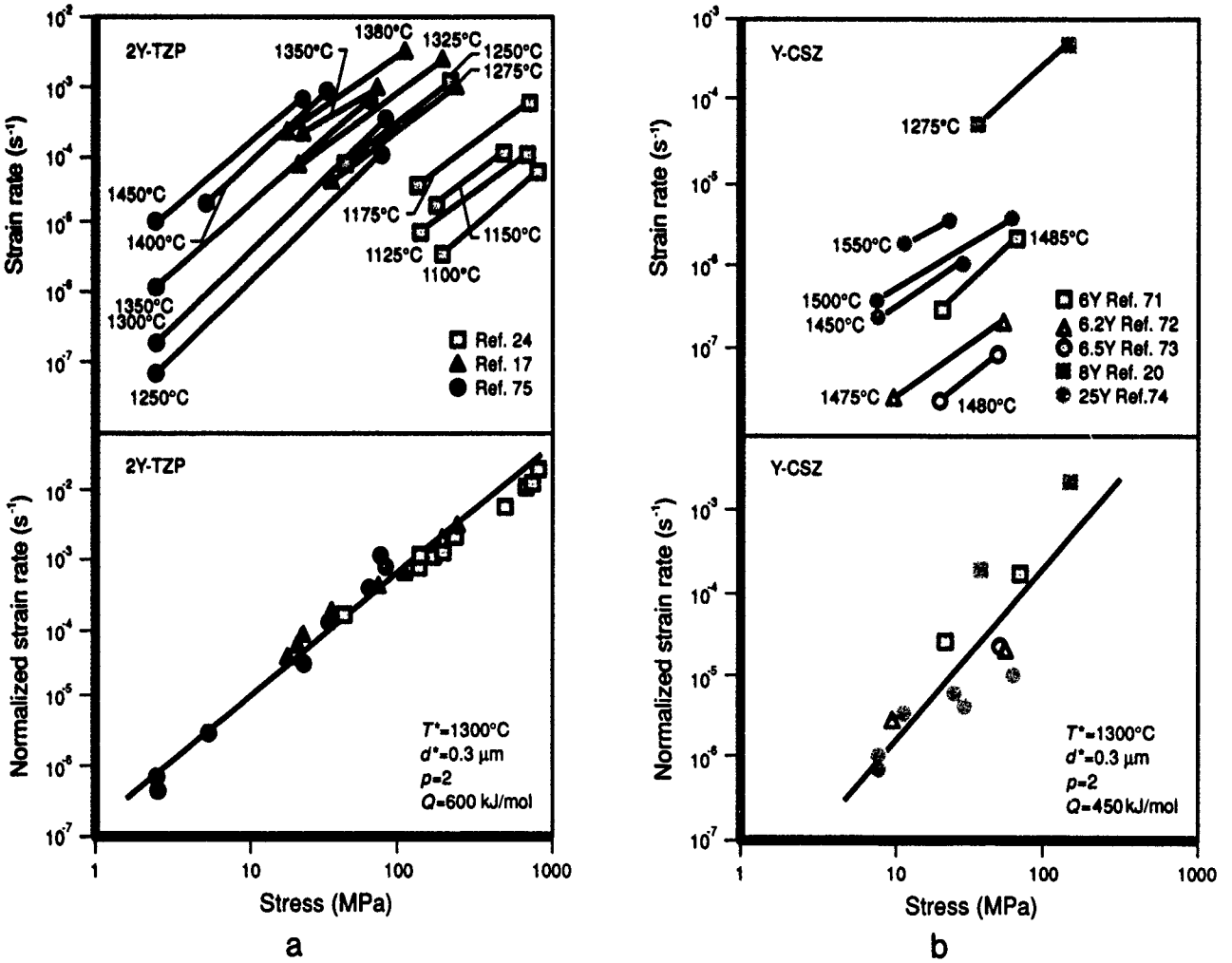

Fig. 15. (a) Relationship between strain rate and stress for 2Y-TZP Grain size is 0.21 μm for Ref. 24, 0.39 μm for Ref. 17, and 0.48 μm for Ref. 75. Grain sizes cited here are 1.56 times the average linear intercept distance between grain boundaries. Range of data for different forming conditions is indicated in the upper figure by symbols at the two ends of each line. Data are replotted in the lower figure after normalization to a reference temperature T^* and a reference grain size d^* using values of grain-size exponent p and activation energy Q, as shown. Very good agreement between different data sets is apparent. (b) Relationship between strain rate and stress for Y-CSZ Grain size for Ref. 71 is 17 μm, Ref 72 is 17.5 μm, Ref. 73 is 29 μm, Ref 20 is 0.48 μm, and Ref 74 is 2.6 μm, 3 5 μm, and 4 2 μm for 1450°, 1500°, and 1550°C, respectively. Compositions of yttria are indicated as well. When the data are normalized, as in Fig 15(a), they fall on a single line Data of the fine-grained Y-CSZ are comparable to those of 2Y-TZP, shown in Fig. 15(a).

tion lattice diffusion in cubic zirconia.[36] However, a nonlinear stress dependence and the possibility of interface-controlled creep preclude a definitive interpretation of the activation energy.

Although deformation mechanisms of superplasticity are similar to diffusional creep, circumstances for interface-controlled deformation may arise when grain boundaries do not act as perfect sources and sinks for vacancies or they do not slide or migrate freely.[78] In this case, the strain rate may increase nonlinearly with stress, and sometimes the materials may even exhibit a threshold deformation stress. For example, interface reactions involving dislocation glide or climb result in a quadratic dependence of strain rate on stress,[79] whereas those involving nucleation may show an exponential dependence on stress.[80] At smaller grain sizes, when diffusional creep is too fast to be equaled by interface reactions, the nonlinear stress dependence should be accentuated. Solute segregation or particle pinning may also hinder diffusional creep by restricting grain-boundary sliding or migration, which is generally necessary for grain-to-grain accommodation. Similar circumstances for interface-controlled deformation may arise when a grain-boundary liquid is present.[81]

A detailed study of 2Y-TZP containing a copper-rich grain-boundary phase has demonstrated the transition behavior between various mechanisms.[24] The stress exponent, grain-size exponent, activation energy, and the effect of the amount of copper(II) oxide, have been determined. From these data, it has been concluded that, in undoped 2Y-TZP, deformation is controlled by grain-boundary diffusion. In doped 2Y-TZP, below the eutectic temperature, deformation is controlled by diffusion along the copper-rich grain-boundary phase and is dependent on the amount of copper(II) oxide. Above the eutectic temperature, deformation is still enhanced by the liquid present, although the strain rate is now limited by interface reactions and independent of the amount of the liquid phase. The stress exponent increases and the grain-size exponent decreases when grain-boundary melting occurs. As shown in Fig. 17, this transition is rather abrupt and serves as a good indicator of the presence of a liquid-phase effect in superplastic ceramics, whereas the more gradual rise above the melting point can be attributed to interface reactions. A similar increase of the stress exponent with temperature occurs when a liquid phase is present in alumina. For example, when 2% liquid is added to pure alumina, n increases from 1.1 at 1050°C to 1.5 at 1150°C, as shown in Fig. 17. The deformation rate is enhanced greatly by the liquid (Fig. 10). Once again, interface reactions are suggested as the rate-limiting deformation mechanisms.

Substantially similar deformation characteristics have been observed for 3Y-TZP, although data from various reports are slightly more scattered.[12,25-28] This is not surprising because of the compositional variations of commercial powders from different sources. Carry has documented such compositional effects[28] on deformation behavior in two batches of 3Y-TZP, although further studies are still required to identify the critical elements (probably aluminum and silicon) which influence the flow stress and ductility. More interestingly, even 8Y-CSZ appears to deform at rates similar to those of 2Y-TZP at a comparable grain size and flow stress despite the difference in solute concentration and crystal structure.[20] However, in this case, superplastic deformation is

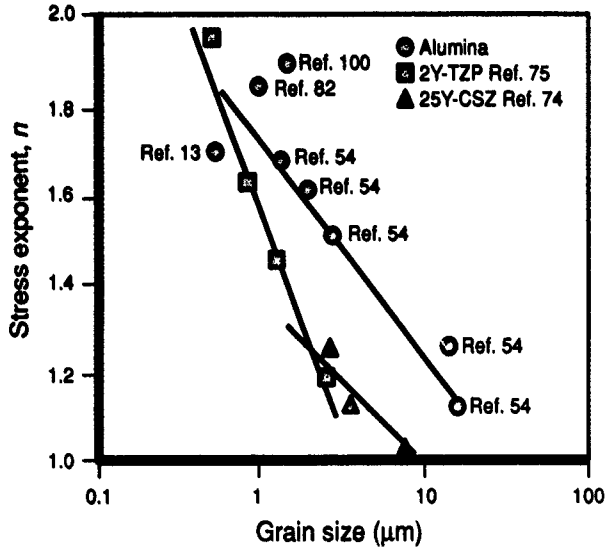

Fig. 16. Stress exponent versus grain size for three ceramics

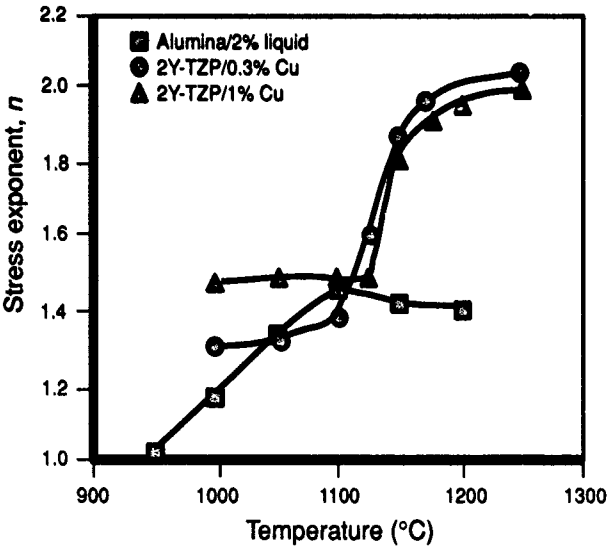

Fig. 17. Variation of stress exponent with test temperature. Abrupt increase in 2Y-TZP at 1130°C is due to melting of the grain-boundary phase. Melting temperature of the liquid in alumina is considerably lower. Gradual rise above the melting temperature is attributed to interface reactions in both cases

quickly overtaken by rapid static and dynamic grain growth and cavitation. The available data for other yttrium-stabilized cubic zirconia of much larger grain sizes and various compositions[71-74] are also reasonably similar to that for 2Y-TZP when extrapolated to comparable grain sizes. These data are compiled in Fig. 15(b). Note also the tendency for the stress exponents to decrease with increasing grain size, as shown in Fig. 16.

The analysis of stress, grain size, and temperature dependence of the deformation data for fine-grained pure alumina, except perhaps at the lowest testing temperature, is complicated by dynamic grain growth. At higher temperatures, static grain growth also becomes prominent and adds to the complexity. However, if the initial strain rate values of fine-grained alumina[13] are compared with the extrapolated values from larger-grained alumina reported in the literature,[54,82] then the values are generally in reasonable agreement as shown in Fig. 18. It may also be concluded from Fig. 18 that, when magnesia is intentionally added, it enhances the strain rate by a factor of 3 to 4 at most. Fortuitously, the flow stress of alumina happens to be of the same order of magnitude as that of Y-TZP and Y-CSZ of a comparable grain size. The activation energy ranges from 450 to 530 kJ/mol.[13,54,82]

At a grain size of 0.5 μm and temperatures between 1250° and 1400°C, deformation of alumina at low flow stresses is probably controlled by cation diffusion along the grain boundary, limited by interface reactions.[54] As evidence, the stress exponent is around 2 and decreases with increasing grain size as shown in Fig. 16, which is consistent with the interpretation of interface reaction-controlled mechanisms. The interpretation of interface control in alumina is given further credence by the effect of a small amount of grain-boundary precipitates. When 1000 ppm of insoluble zirconia is added to an otherwise pure alumina, the creep rate is severely suppressed by a factor of about 20.[82] Zirconia inclusions/particulates also raise the activation energy to around 750 kJ/mol, which is comparable with that found in alumina/zirconia composites.[65,82] Thus, although pure alumina deforms at about the same rate as 2Y-TZP of a comparable grain size, alumina may be considerably hardened in a zirconia/alumina composite. This is indeed the case, as discussed in the next section.

(2) Effect of a Second Phase

The effect of a second phase on superplastic deformation has been investigated using 2Y-TZP/mullite[17,18] and 3Y-TZP/alumina[16,65] as model systems. Mullite composition in these studies is off-stoichiometry, being rich in Al^{3+}, to maintain an equiaxed grain/inclusion shape. In both cases, there is little mutual solubility between constituent phases at the sintering and deformation temperatures. These composites are all superplastic, and may serve as model systems of a soft matrix (TZP) containing equiaxed, and presumably harder, inclusions (mullite and alumina). The particle shape effect of nonequiaxed hard inclusions on superplastic flow has also been considered in the literature[17] but will not be further pursued here.

An essentially insoluble second phase can have two effects on deformation resistance of a fine-grained ceramic: (a) a modification of continuum deformation mechanics and (b) a change in interface-related deformation characteristics. The first effect can be understood by continuum mechanics, in that the deformation resistance of a composite may be determined entirely by knowing the deformation resistance of the constituent phases, after computing the appropriate

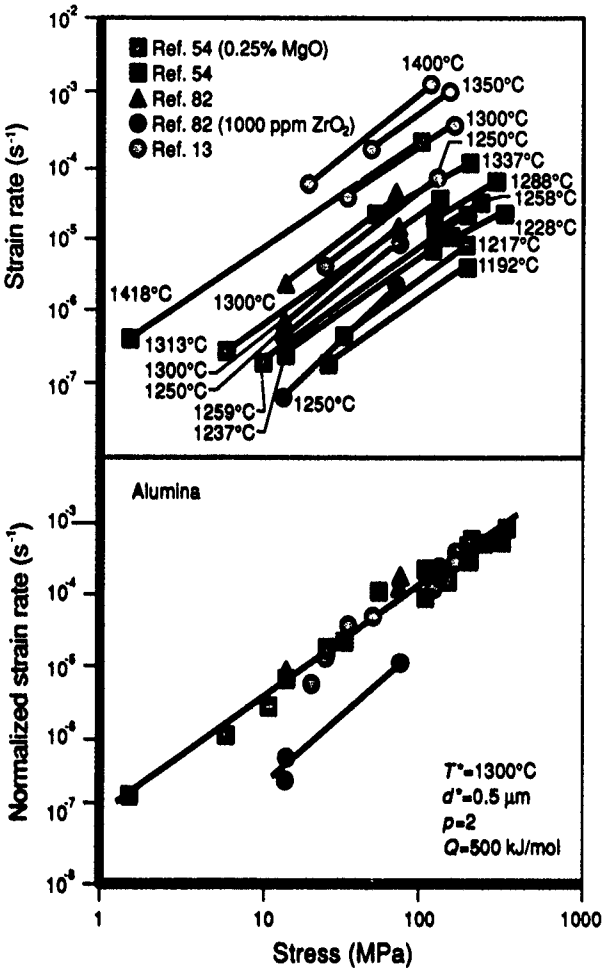

Fig. 18. Strain rate versus stress of alumina. Grain size for Ref. 54 is 1.25 μm for both pure and magnesia-doped material, Ref. 82 is 0.96 μm without zirconia and 0.59 μm with zirconia, Ref. 13 is 0.51 μm. Range of data for different forming conditions is indicated in the upper figure by the symbols at the two ends of each line. Grain sizes cited here are 1.56 times the average linear intercept distance between grain boundaries. Data are replotted in the lower figure after normalization to a reference temperature T^* and a reference grain size d^* using values of grain-size exponent p and activation energy Q, as shown. Very good agreement between different data sets is apparent.

stress and strain distributions in the two-phase composite.[6] The second effect is entirely microscopic, usually localized to grain boundaries and interfaces between phases, and arises from the alteration of the diffusion path, diffusion rate, and interface reactions due to chemical or structural modifications of the interface itself or of interfacial phases. Although the continuum effect becomes significant only at a substantial volume fraction—for example, 20%[83] of the second phase—the microscopic effect can be very pronounced with only a trace amount of additives. Both effects have been observed in superplastic ceramics, and in some cases concurrently, as will be discussed later in this section.

At 1350°C, the flow stress of mullite is 2 orders of magnitude higher than that of 2Y-TZP of a comparable grain size,[17,18,84] Hence, mullite inclusions in 2Y-TZP can be considered rigid. For such a composite, a continuum model, which pictures the composite flow as a non-Newtonian fluid containing rigid particulates, is appropriate.[6,17] The prediction of this rheological model is

$$\dot{\varepsilon} = \dot{\varepsilon}_0(1 - V)^{2+n/2} \quad (3)$$

where V is the volume fraction of the rigid inclusions, $\dot{\varepsilon}_0$ is the strain rate of the reference matrix (taken as the one with an identical grain size but without inclusions), and $\dot{\varepsilon}$ is the strain rate of the composite. Experimental data for 2Y-TZP containing up to 80 vol% mullite, shown in Fig. 19, are in very good agreement with this model if mullite is considered to be a rigid, included phase.

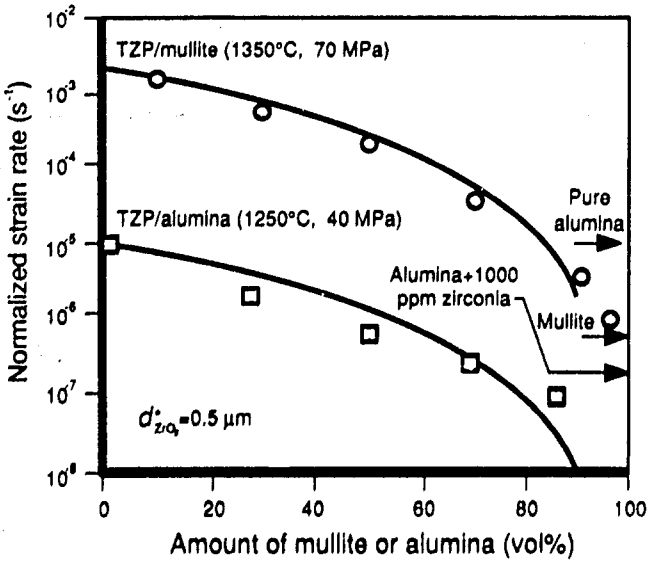

Fig. 19. Strain rate as a function of volume fraction of mullite or alumina in two TZP matrices deformed at the same flow stress. Strain rate data have been normalized, using the matrix grain size, to d^*. Also indicated on the right are the strain rate of pure alumina, mullite, and alumina with 1000 ppm zirconia, all at a comparable grain size. Two solid curves are predictions of the rheological model, assuming that mullite and alumina form rigid, equiaxed inclusions. Data for TZP/mullite are from Ref. 18, and for TZP/alumina from Refs. 40 and 65.

Deformation data for 3Y-TZP containing up to 70 vol% alumina, shown in Fig. 19, are also well described by the rigid inclusion model. This is surprising, however, because pure alumina has a deformation resistance comparable with that of 3Y-TZP, as noted previously. This apparent contradiction becomes explicable if we also recall that even a little zirconia impurity (1000 ppm) can severely reduce the deformation rate of alumina. Therefore, although pure alumina is no harder than 3Y-TZP, alumina in a zirconia matrix should behave similar to rigid inclusions, consistent with the data in Fig. 19. The continuum rheological model with rigid, equiaxed inclusions has thus been verified in superplastic flow of Y-TZP with both mullite and alumina as a second phase.

The effect of a second phase on the microscopic level is already exemplified by the dramatic hardening of pure alumina with a small addition of zirconia.[82] This is most likely due to the suppression of interface reactions or hindrance of grain-boundry movement by intergranular zirconia precipitates. Unlike alumina, mullite does not experience such an anomalous hardening effect caused by zirconia additions. On the other hand, small additions of zirconia progressively and substantially reduce the deformation resistance of mullite,[18] as evident from the data shown in Fig. 19, at near 100% mullite compositions. This softening effect is much larger than that expected from a continuum model that envisions, in this case, zirconia as fluidlike but equiaxed inclusions. Therefore, some microscopic chemical or structrual effect on the grain boundary which facilitates diffusion or sliding is again implied.

(3) Dynamic Grain Growth

A perhaps unique mechanism predominant in superplasticity is dynamic grain growth.[85] Strong strain hardening is evident whenever grain growth occurs during superplastic deformation. This becomes significant in Y-TZP above 1450°C[12,39,40] and in pure alumina above 1250°C.[41-43] Strong strain hardening was also observed in 12Ce-TZP and 8Y-CSZ at temperatures as low as 1200°C.[20] The mechanistic origin of dynamic grain growth is probably related to grain-boundary migration.[85] These mechanisms are central features of superplasticity and are necessary for maintaining an equiaxed grain shape to large deformation strains. If grain-boundary migration is stochastic, which is usual in grain-boundary sliding,[86] and is not overdamped by solute drag or particle pinning, then it can lead to stochastic grain growth by chance elimination of certain grains in the process.[87] Experimental data confirming this interpretation can be sought by writing the grain growth kinetics in the following form:

$$\dot{d} = B\dot{\varepsilon} \quad (4)$$

where $\dot{d}$ is the rate of grain growth and B is a proportionality constant that couples the strain rate through grain-boundary migration to the grain-growth rate. Thus, dynamic grain growth follows the equation

$$d = d_0 \exp(B\varepsilon) \quad (5)$$

where d_0 is the initial grain size before deformation.

Experiments deliberately conducted in a temperatrue regime in which static grain growth is negligible (but dynamic grain growth is significant) have verified the above prediction.[20] Figure 20 illustrates this behavior for several Ce-TZP ceramics tested in compression under various conditions. A linear correlation between $\ln (d/d_0)$ and ε is evident, giving a value of B of the order of unity. These data eventually deviate from the predicted linear relationship between $\ln d$ and ε. A review of the flow stress at the point of deviation suggests that it is probably high enough for yielding by slip to occur. When the latter becomes the dominant deformation mechanism, grain-boundary sliding, grain-boundary migration, and, hence, dynamic grain growth diminish in importance, and Eq. (4) is no longer valid because $\dot{\varepsilon}$ is no longer solely due to the boundary phenomena.

Note that dynamic grain growth never has been observed in coarse-grained (cubic) zirconia[71-74] and alumina[54] that were deformed in the diffusional creep regime. This strongly suggests that, although diffusional creep also necessarily entails grain-boundary sliding and perhaps grain-boundary migration, the extent of these activities is not as significant as in superplasticity. Indeed, the sliding and migration could be qualitatively quite different in nature in that grain switching,[41] grain rotation,[5] and grain-shape transformation,[6] occurring in superplasticity, do not seem important for diffusional creep. Both considerations may dictate that deformation-stimulated stochastic grain growth is less likely in diffusional creep than that in superplasticity.

Dynamic grain growth introduces several complications to the stress–strain curves and the parameters in the constitutive equation (Eq. (1)). Using the relation between grain size and strain it is possible to recast the standard constitutive equation (Eq. (1)) into the following form:

$$\ln \sigma = (Bp/n)\varepsilon + \ln [(d_0 p\dot{\varepsilon}/A)^{1/n}] \quad (6)$$

From Fig. 20 we find that B approaches unity. If we let p be 2 to 3 and n be 1.5 to 2, then Bp/n is between 1 and 2. Using this form, stress–strain curves of Ce-TZP and pure alumina (1250°C), which all suffer from severe dynamic grain growth but no static grain growth, are replotted in Fig. 21. Except for initial transients related to the elastic portions of the stress–strain curves, data in each branch appear to have a slope of 2, as expected from the above interpretation. For 8Y-CSZ[20] and alumina at higher temperatures, static grain growth is also prominent. This causes a higher strain hardening initially. At the later stage, as static grain growth decreases with increasing grain size, the terminal slope then approaches 2 again. These features are evident from their respective stress–strain curves, as shown in Fig. 21. The later leveling-off and the eventual drop of the flow stress in alumina (1400°C) is due to cavitation (see Fig. 9(c)).

Temperature dependence of deforma-

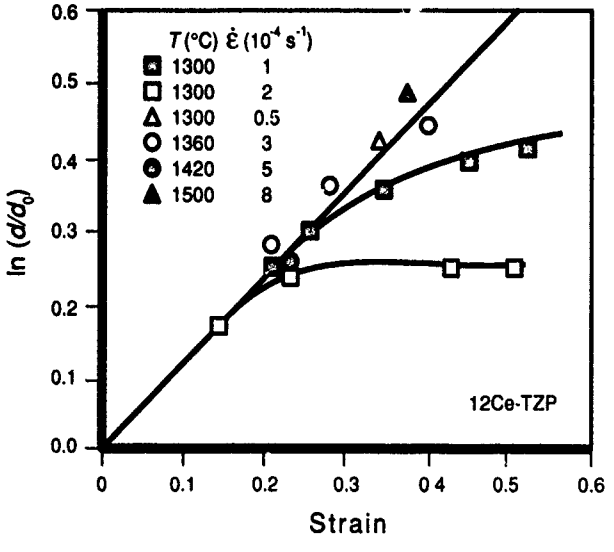

Fig. 20. Change in normalized grain size with strain of 12Ce-TZP, indicating dynamic grain growth. Data for various deformation conditions initially fall on a single line Later deviation from the straight line is probably due to plastic yielding

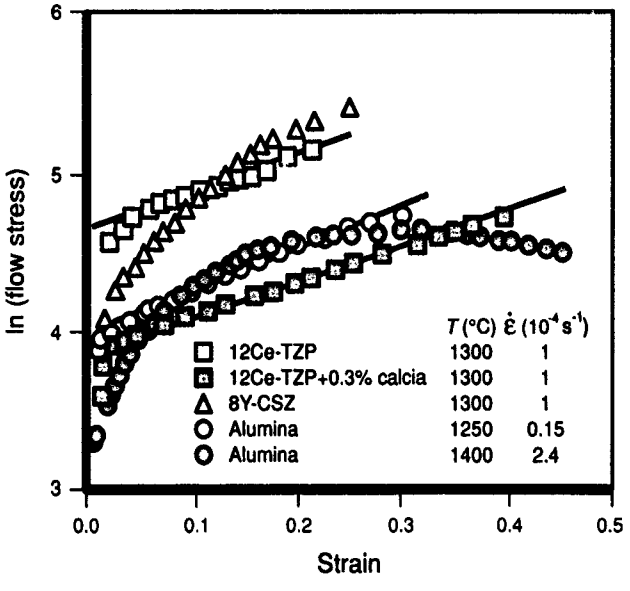

Fig. 21. Stress–strain curves of ceramics undergoing dynamic grain growth (Ce-TZP and alumina at 1250°C) and others undergoing both dynamic and static grain growth Note that stress is in logarithmic scale (see text)

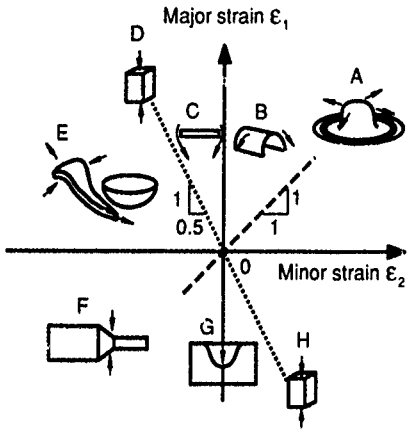

Fig. 22. Dominant strain states of various superplastic forming processes (see text for references).

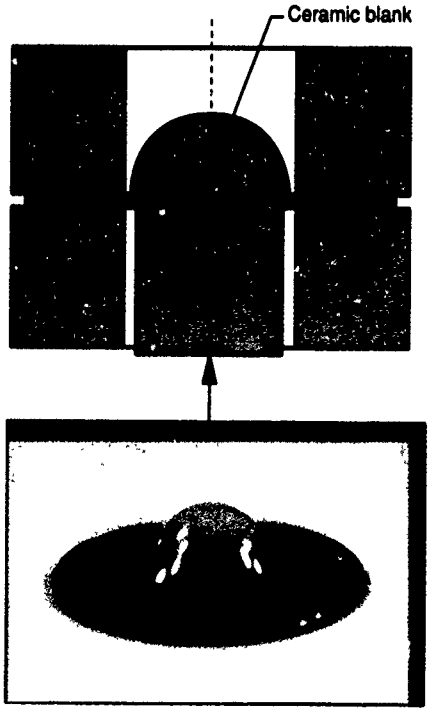

Fig. 23. (a) Schematic of punch-stretching test used to evaluate sheet formability in biaxial tension (b) Punch-stretched 2Y-TZP with 0.3 mol% copper(II) oxide Note the excellent surface finish and the groove around the dome Formed in air at 1150°C in 10 min

tion may also be altered by dynamic grain growth. At higher temperatures, dynamic grain growth is faster because of a higher grain-boundary mobility. This causes increasing strain hardening and lowering of the apparent activation energy.

(4) Summary

In summary, deformation mechanisms controlling superplasticity in fine-grained ceramics are similar to diffusional creep and are dominated by grain-boundary diffusion. Very fine grain sizes and the frequent presence of a grain-boundary phase seem to cause interface reactions to become the rate-limiting step in many instances. The basic deformation characteristics of a material can be altered by the addition of a second phase, which causes hardening or softening, and by dynamic grain growth, which causes strain hardening. Semiempirical models are available to describe the various constitutive behaviors observed experimentally.

IV. Superplastic Forming

(1) Formability Test

Many attempts have been made to form zirconia and other ceramics into shapes in the superplastic regime. The following forming methods have been attempted: uniaxial tension, uniaxial compression, bending, extrusion, inverse extrusion, and shell forming. These are shown schematically in Fig. 22, which indicates the dominant strain states of each method. Some methods involve tensile strain in one direction, such as uniaxial tension and bending (D^{11} and C^{88} in Fig. 22). Others are dominated by compression, such as extrusion and inverse extrusion (F^{89} and G^{89} in Fig. 22). In the shell-forming experiment (E in Fig. 22) of Mocellin *et al.*,[89] a balanced tension–compression path was used. In bending of a wide plate (B^{88} in Fig. 22) plane strain tension is encountered. Forming methods dominated by compression can also use powder preforms to achieve densification and shaping in one step, for example, in sinter forging and extrusion.

To evaluate formability of superplastic ceramics, a punch-stretching test (A in Fig. 22) has been developed.[90] This test was initially developed by metallurgists for evaluating sheet formability of metals at room temperature.[3,91] Both mechanical and practical considerations have established that such a test is more severe and informative than the conventional tensile test for the above purpose, at least for sheet-forming processes [3,91] In this test, an initially flat ceramic disk was punched at high temperature into a hat shape. The forming conditions—i.e., forming stress, strain rate, and temperature required to successfully complete the operation—then provide an indication of the formability of the ceramic. During forming, the disk was supported at the rim and was stretched over a hemispherical punch of a radius of 6.5 mm. In some experiments, to ensure that there was no drawing-in of the material during subsequent stretching, a groove was first formed between matching dies, and the disk was clamped firmly, as shown in Fig. 23(a). The punch was advanced at a programmed displacement rate until a bulged dome of a height equal to the punch radius was formed. At this point, the surface area of the dome is approximately twice that of the base, corresponding to a biaxial engineering strain of 100%.

Figure 1 shows a number of superplastically punch-stretched ceramics, with their approximate forming temperatures and times indicated. Generally, the required forming time increases with lower forming temperatures. This trend is shown by the three curves, which broadly outline the forming conditions for the three groups of ceramics. Among them, the zirconia ceramics with grain-boundary additives have the lowest forming temperature. Other oxide ceramics, especially ones with higher alumina content, required a higher forming temperature. Zirconia/mullite composites behave similarly, altough mullite has not yet been made superplastic. In the case of silicon nitride, 1500°C was necessary for successful punch stretching. Under the optimal forming conditions, 2Y-TZP with 0.3 mol% copper(II) oxide additive can be formed at 1150°C in 10 min.[90] A specimen so formed is shown in Fig. 23(b). Excellent surface finish is obtained in all cases, except alumina, by punch stretching.

The strain distribution of the punch-stretched object has been measured using markers inscribed onto the surface of the disk before forming.[90] This is shown in Fig. 24, in which strains are expressed as true strain. The slight depression around the pole is due to friction between the punch and the disk. A detailed analysis of the forming mechanics, which correctly predicts the strain distribution and the forming load–displacement curve measured experimentally, has been performed elsewhere.[19,90] To understand these results and for an order of magnitude estimation, we may approximate the punch-stretching test as pressure bulging from a circular disk to a hemispherical shell of the same radius. Because the total engineering strain is 100%, the average strain rate is simply τ^{-1}, where τ is the total forming time. The forming pressure f on the shell must satisfy the yield criterion.

$$f = 2Yt/R \qquad (7)$$

where Y is the flow stress in uniaxial tension at the appropriate strain rate, t is the thickness, and R is the punch/disk radius This bulge pressure is related to the punch load P through

$$P = R^2 f \sin^2 \beta \quad (8)$$

where β is the half angle subtended by the edge of the punch contact to the center line. At the end of punch stretching, when the height of the dome is equal to the radius, β is 90° to 69° for t/R varying from 0 to 0.1. Using Eqs. (7) and (8), forming pressure, flow stress, and average strain rate can be easily estimated. For example, a typical forming stress for doped zirconia was 20 MPa at 1200°C and a strain rate of 3×10^{-4} s^{-1}. For silicon nitride, a forming stress of 10 MPa was recorded at 1560°C and a strain rate of 3×10^{-4} s^{-1}. For alumina, successful punch stretching was achieved at 1450°C with 25 MPa and a strain rate of 3×10^{-4} s^{-1}.

Forming curves in terms of P/t_0R and h/R, as a function of time, with t_0 being the initial thickness and h the punch displacement, are shown in Figs. 25(a) and (b) for several materials formed under various loading/displacement conditions. During forming under a constant displacement rate, the average strain rate of the stretched material increases monotonically with time, reaching a maximum at the end. This causes a corresponding increase of forming stress. Using a variable displacement rate, which is faster initially but slower near the end, an approximate constant strain rate path can be achieved. This has the advantage of lowering the peak stress without necessarily increasing the total forming time so that failure probability is reduced.[90] A series of forming curves for a number of superplastic ceramics formed under this more favorable condition are shown in Fig. 25(b). Another alternative strategy used to lower the forming stress is to use a variable temperature ramp, which starts forming at a lower temperature and ends

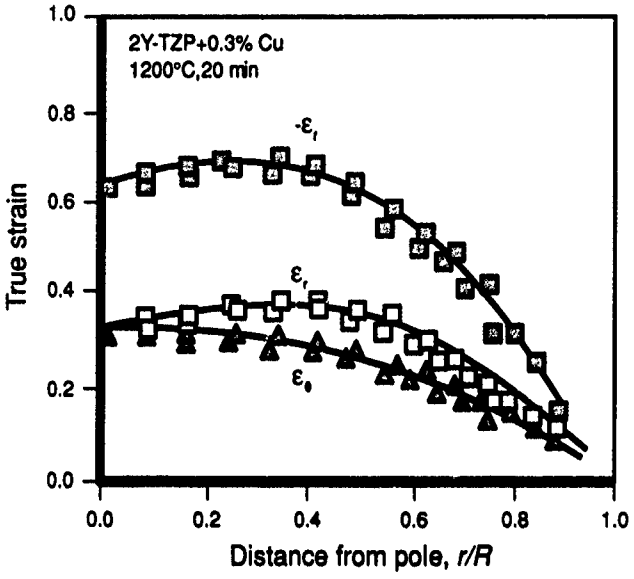

Fig. 24. Strain distribution on a punch-stretched 2Y-TZP. Radial strain (ε_r) and hoop strain (ε_θ) are measured by markers inscribed on the surface, and the thickness strain (ε_t) is computed from $\varepsilon_r + \varepsilon_\theta + \varepsilon_t = 0$.

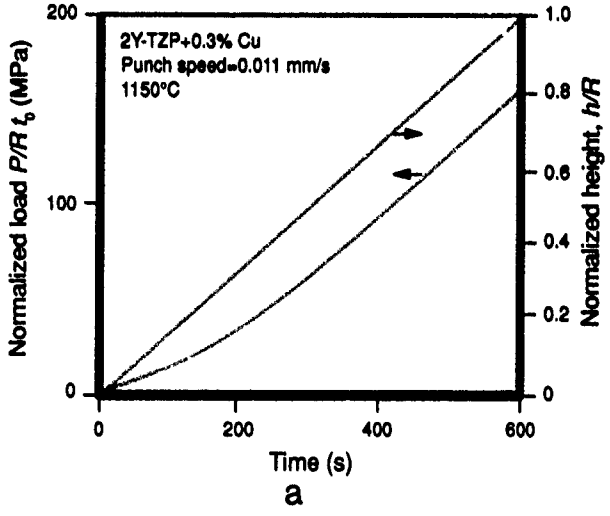

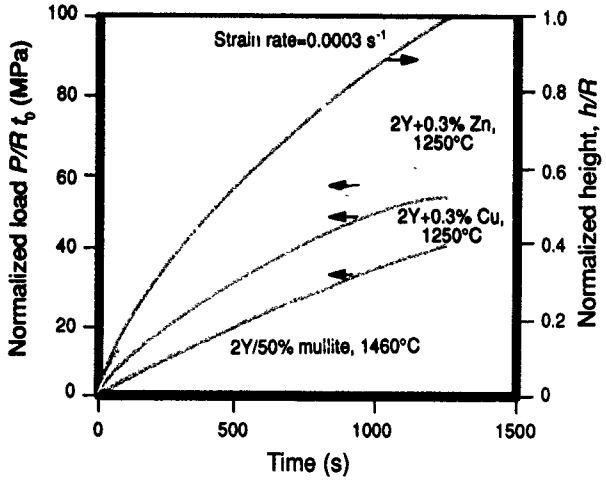

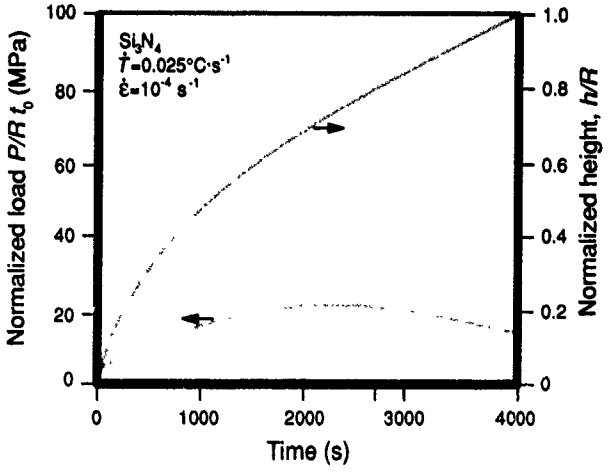

Fig. 25. (a) Forming load (normalized by punch radius R and initial thickness t_0) and dome height (normalized by R) versus forming time in a punch-stretching test. Note the sharp increase of forming load with time under the constant punch speed condition. (b) Normalized forming load and normalized dome height versus time for 2Y-TZP with 0.3 mol% zinc oxide, 2Y-TZP with 0.3 mol% copper(II) oxide, and 2Y-TZP with 50 mol% mullite. Forming schedule is programmed to achieve a constant strain rate. Note that the load increase is gradual and mild. (c) Normalized forming load and normalized dome height versus time for silicon nitride. A constant heating rate and a constant strain rate are used, starting at 1480°C.

at a higher temperature. An example of the latter, using a constant heating rate, is shown in Fig. 25(c). We have successfully formed silicon nitride and alumina using the latter schedule.

(2) Fracture Control

Formability is dictated by the strain to failure along the appropriate strain path representative of the forming route. Tensile ductilities of superplastic metals and alloys are known to correlate well with strain-rate sensitivity, m (i.e., the reciprocal stress exponent).[2] The higher the strain-rate sensitivity, the higher the tensile ductility. Such a correlation does not hold for superplastic ceramics, as shown in Fig. 26(a). To understand this, we recall that the physical basis of the ductility–m correlation is in the stability against necking, which increases with m for a strain-rate-sensitivity material.[3,8] The failure of this correlation, therefore, implies that, for superplastic ceramics, deformation stability is still essential, but is rarely the limiting factor for tensile ductility. Indeed, ductilities of superplastic ceramics should be much higher than those actually observed under most circumstances if necking were responsible for failure.

As a practical matter, grain-boundary decohesion always limits tensile ductility in superplastic ceramics. Although the exact mechanisms remain to be established, existing evidence supports the opinion that cavitation or grain-boundary cracking precedes fracture. Thus, cavitation resistance must figure prominently in evaluating formability. The central importance of grain-boundary cohesive strength, which controls the cavitation resistance, can thus be understood. On the other hand, for a given material, cavity and crack nucleation at grain boundaries under creep conditions is relatively insensitive to the temperature but extremely sensitive to the flow stress.[86,92-94] The latter is, in turn, controlled by deformation temperature, strain rate, and strain hardening. This would suggest that a better correlation for formability may be one relating ductility to flow stress rather than to strain-rate sensitivity. The available data for tensile ductilities of all superplastic ceramics thus far reported, plotted in Fig. 26(b), seem to support such a proposition in that a reasonably good correlation exists between increasing tensile elongation and decreasing flow stress for each group of materials. Indeed, after normalizing the flow stress by the reference stress that causes failure at 100% elongation for

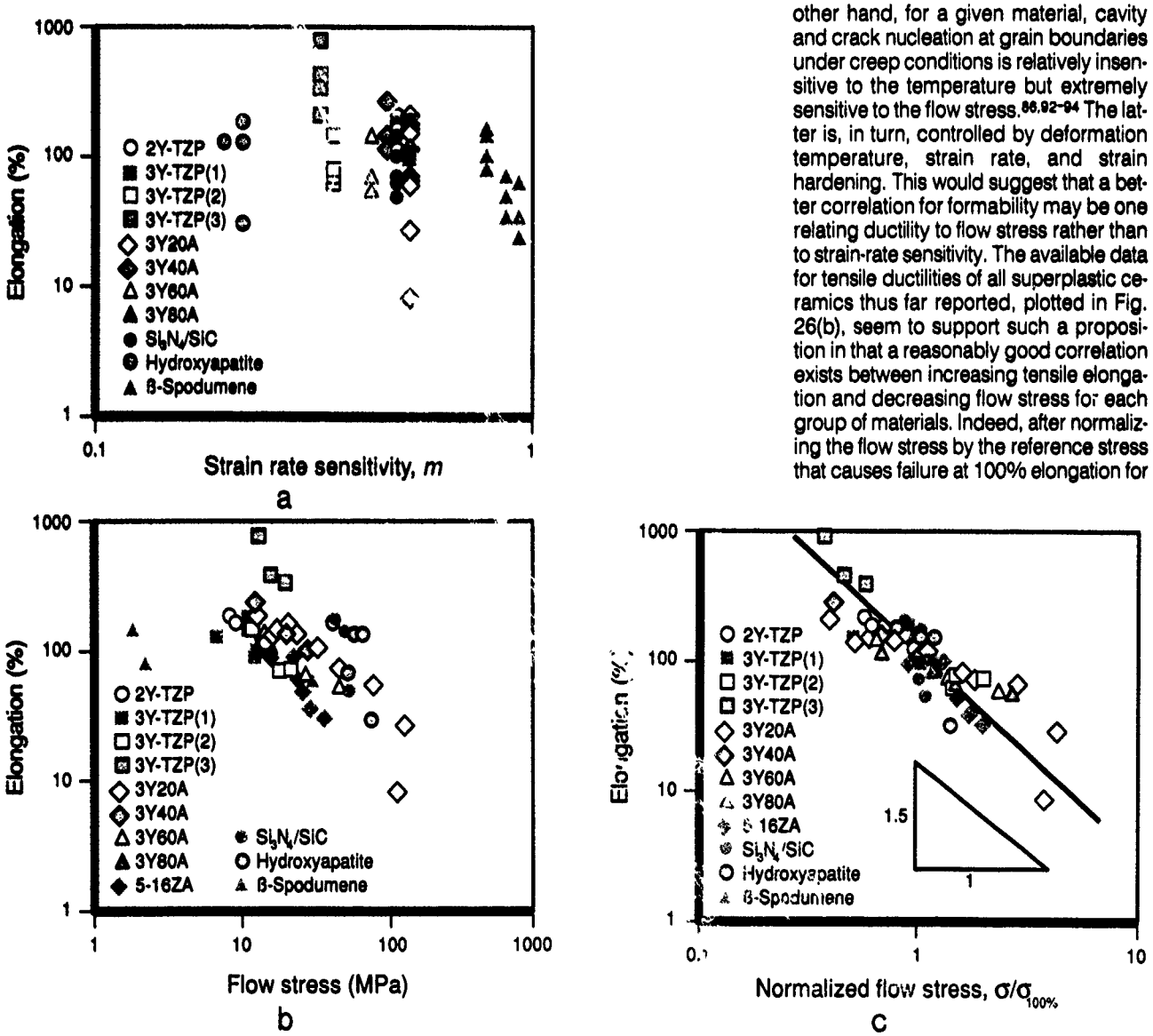

Fig. 26. (a) Lack of correlation between tensile elongation and strain rate sensitivity m. References are 12 for 2Y-TZP; 40 for 3Y-TZP(1); 28 for 3Y-TZP(2); 26 and 101 for 3Y-TZP(3); 40 for 3Y20A, 3Y40A, 3Y60A, and 3Y80A, 22 for silicon nitride/silicon carbide; 14 for hydroxyapatite, and 102 for β-spodumene. An example of the notation for the composites is that 3Y20A means 3Y-TZP with 20 wt% alumina. (b) Close correlation between tensile elongation and flow stress (5–16ZA means 5 to 16 vol% of 3Y-TZP in alumina matrix) (data from Ref. 48, otherwise the references and notations are the same as for Fig. 26(a)). (c) Close correlation between tensile elongation and normalized flow stress. The flow stress of each material is normalized by $\sigma_{100\%}$, which is the flow stress in Fig. 26(b) at an elongation of 100% for each material.

each group of ceramics, a clear trend common to all superplastic ceramics emerges, as shown in Fig. 26(c). This may be contrasted with the common observation, for superplastic metals and alloys, of a ductility maximum at an intermediate flow stress, which coincides with the maximum of strain-rate sensitivity.[2,3] Because the strain rate sensitivity is largely independent of elongation in Fig. 26(a), the strong correlation between elongation and flow stress in Figs. 26(b) and (c) must be regarded as a manifestation of the stress-controlled failure process unique to ceramics.

In the case of alumina/3Y-TZP composites, Wakai *et al.* have previously noted that the average alumina grain size correlates poorly with ductility, but that the size of the largest alumina grains in the composites correlates well.[48] This observation seems particularly explicable for alumina, which is prone to anisotropic, abnormal grain growth. The few large grains in an otherwise fine-grained matrix have a relatively minor influence on the average flow stress (see Eq. (3)) but cause considerable stress concentrations because of their poorer diffusional accommodation as a result of the longer diffusion distances in their vicinity. Therefore, these grains can cause enhanced cavitation, which is detrimental to tensile ductility. Other stress-concentrating heterogeneities will have a similar effect. Likewise, the deleterious effect of strain hardening on ceramic superplasticity is understandable, despite its supposedly beneficial influence on deformation stability.[8] Lowering the flow stress and increasing the grain-boundary strength thus provide the most effective methods for improving superplastic formability.

For ceramics, the superplastic punch-stretching test described above is a much more severe formability test than the uniaxial tension test favored by most investigators to characterize superplasticity. Generally speaking, fractures in ceramics are initiated at preexisting flaws introduced by preparation steps such as powder packing, sintering, and machining. In uniaxial tension, only preexisting cracks perpendicular to the stress axis may cause fracture. In biaxial stretching, cracks of all orientations are being stressed and may be fatal. Although the flaw tolerance at the forming temperature has been dramatically improved in superplastic ceramics, most of our failures that occurred were brittle in nature, especially at higher forming rates.[19] This also supports the conclusion that grain-boundary decohesion rather than necking is the failure-controlling event. Because variously oriented cracks are stressed and failure is brittle in nature, biaxial stretching experiments are much needed demonstration tests which should be routinely performed for superplastic ceramics to ensure their suitability for practical sheet-forming in applications

For reliable, flaw-free forming, the current practice in the superplastic metal industry is to use pressure forming in a configuration where the differential pressure effects shape deformation while the mean pressure suppresses cavitation.[7,9,10] In theory, a pressure on the order of the flow stress should be sufficient for suppression of cavity growth,[95,96] thus avoiding failure. Such an approach has been found to be successful for glass-ceramics, which can be stretched to 100% once cavitation is suppressed.[97] Because of the propensity for cavitation in many ceramics and the paramount importance of reliability to ceramic applications, we predict that a similar practice will eventually be adoped if superplastic sheet forming of structural ceramics should become a commercial endeavor.

V. Conclusions

Since the discovery of ceramic superplasticity in 1986, considerable progress in zirconia and other superplastic ceramics has been achieved. In this paper, we have attempted to provide instructive examples from this experience. Through these examples, we have emphasized the importance of structural and processing controls in achieving a superior microstructure and formability, the central role of static and dynamic characteristics of grain boundaries and phase boundaries, and the major differences between superplastic ceramics and their counterparts in metals and alloys. With powders of ever-improving sinterability and finer particle size becoming increasingly available, a lower sintering temperature, which is synonymous to a more uniform and finer microstructure, has been achieved for several major structural ceramics during the last few years. Complementary research on physical ceramics has further elucidated some of the basic principles of microchemical and microstructural control and directed the way of alloy development for better deformability and ductility. These interrelated materials considerations, previously outlined in Fig. 2, have now been addressed in some detail in this paper. The key issues discovered here are summarized in a block diagram in Fig. 27 for various structure–property–processing relationships. Although the implementation and specifics may vary from ceramic to ceramic, and further basic and applied research is still desirable, it is our hope that Fig. 27 will nevertheless provide a sketchy but useful "road map" to guide future superplastic ceramic development.

Looking forward, it is our opinion that most, if not all, ceramics can be rendered superplastic at reasonable forming temperatures and forming times no higher or longer than those currently used in commercial practice for ceramic sintering. We believe that our optimism is well based, judging from the experience in zirconia, alumina, silicon nitride, and their compos-

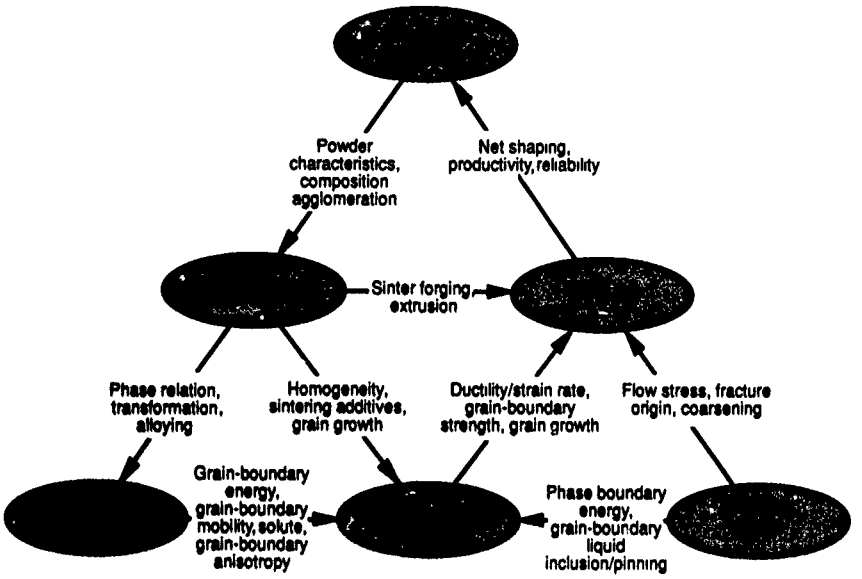

Fig. 27. Major issues in the structure-property-processing relationships in superplastic ceramics for structural applications.

ites. More broadly speaking, however, we must be reminded that, although a sound technical concept such as superplastic forming of ceramics may appear attractive and feasible, its eventual utilization, if at all, is largely decided upon by the market force. We are cautiously confident that, as the demand for structural ceramics grows in future years, superplastic ceramics will be further developed and that this unique net-shape manufacturing method will be applied to industrial processes.

Acknowledgment: The authors are grateful for the stimulating discussions with S. L Hwang, D. Jacobs, and X Wu. Unpublished data and figures have been provided by C. M. J. Hwang, S. L. Hwang, and X. Wu. Dr. F. Wakai kindly provided Fig. 13(b).

References

[1]C E. Pearson, "The Viscous Properties of Extruded Eutectic Alloys of Lead-Tin and Bismuth-Tin," *J Inst Met*, **54** [1] 111 (1934)

[2]J W. Edington, K N. Melton, and C P Cutler, "Superplasticity," *Prog. Mater Sci*, **21** [2] 61-170 (1976)

[3]W A. Backofen, Deformation Processing, Ch 10, pp 199-226 Addison-Wesley, Reading, MA, 1972

[4]M F Ashby and R A Verrall, "Diffusion-Accommodated Flow and Superplasticity," *Acta Metall*, **21**, 149-63 (1973)

[5]R C Gifkin, "Grain Boundary Sliding and Its Accommodation During Creep and Superplasticity," *Metall Trans A*, **7A** [8] 1225-32 (1976)

[6]I-W Chen, "Superplastic Flow of Two-Phase Alloys", Ch 5, pp. 5 1-5.20 in Superplasticity Edited by B Baudelet and M Suery Centre National de la Recherche Scientifique, Paris, France, 1985

[7]J Pilling and N Ridley, Superplasticity in Crystalline Solids Institute of Metals, London, U K , 1989

[8]E W. Hart, "Theory of the Tensile Test," *Acta Metall*, **15** [2] 351-55 (1967)

[9]N. E Paton and C H. Hamilton (editors), Superplastic Forming of Structural Alloys, pp. 257-71 The Metallurgical Society of AIME, Warrendale, PA, 1982

[10]M Doyama, S. S Sōmiya, R P. H Chang, M. Kobayashi, and F. Wakai, Superplasticity, MRS Conference Proceedings, International Meeting on Advanced Materials, Vol 7 Materials Research Society, Pittsburgh, PA, 1989

[11]F Wakai, S. Sakaguchi, and Y Matsuno, "Superplasticity of Yttria-Stabilized Tetragonal ZrO_2 Polycrystals," *Adv. Ceram. Mater.*, **1** [3] 259-63 (1986)

[12]F. Wakai, Y Kodama, and T Nagano, "Superplasticity of ZrO_2 Polycrystals," *Jpn J. Appl. Phys*, **28**, 69-79 (1989).

[13]L A Xue and I-W Chen; unpublished research presented at the 92nd Annual Meeting of the American Ceramic Society, Dallas, TX, April 22-26, 1990 (Paper No. 5-JV-90).

[14]F. Wakai, Y Kodama, S Sakaguchi, and T. Nonami, "Superplasticity of Hot Isostatically Pressed Hydroxyapatite," *J. Am. Ceram Soc.*, **73**, 457-60 (1990)

[15]F. Wakai and H Kato, "Superplasticity of TZP/Al_2O_3 Composite," *Adv Ceram. Mater.*, **3** [1] 71-76 (1988)

[16]F. Wakai, Y Kodama, S Sakaguchi, N Murayama, H Kato, and T Nagano, "Superplastic Deformation of ZrO_2/Al_2O_3 Duplex Composites"; pp. 259-66 in Superplasticity, MRS Conference Proceedings, International Meeting on Advanced Materials, Vol 7. Edited by M. Doyama, S. S. Sōmiya, R. P. H. Chang, M. Kobayashi, and F Wakai. Materials Research Society, Pittsburgh, PA, 1989.

[17]C. K. Yoon and I-W. Chen, "Superplastic Flow of Two-Phase Ceramics Containing Rigid Inclusions—Zirconia/Mullite Composites," *J. Am. Ceram Soc*, **73** [6] 1555-65 (1990)

[18]C K. Yoon, "Superplastic Flow of Mullite/2Y-TZP Composites"; Ph.D Thesis Department of Materials Science and Engineering, University of Michigan, Ann Arbor, MI, 1990

[19]X Wu, "Deformation Processing of Ceramics"; Ph.D Thesis Department of Materials Science and Engineering, University of Michigan, Ann Arbor, MI, 1990

[20]I-W Chen and S. L Hwang; unpublished research presented at the 91st Annual Meeting of the American Ceramic Society, Indianapolis, IN, April 23-27, 1989 (Basic Science Division, Paper No 120-B-89), and 92nd Annual Meeting of the American Ceramic Society, Dallas, TX, April 22-26, 1990 (Basic Science Division, Paper Nos 25-B-90 and 26-B-90)

[21]F Wakai, Y Kodama, S. Sakaguchi, N. Murayama, K Izaki, and K Nihara, "A Superplastic Covalent Crystal Composite," *Nature (London)*, **344**, 421-23 (1990)

[22]F Wakai, Y Kodama, S Sakaguchi, N Murayama, K Izaki, and K Nihara, "Superplasticity of Non-Oxide Ceramics", to be published in MRS Symposium Proceedings on Superplasticity in Metals, Ceramics, and Intermetallics Edited by M I Mayo, J Wadsworth, A K Mukherjee, and M Kobayashi Materials Research Society, Pittsburgh, PA, 1990

[23]R J Brook, "Controlled Grain Growth", pp 331-64 in Treatise on Materials Science and Technology, Vol. 9. Edited by F F Wang Academic Press, New York, 1976

[24]C-M J Hwang and I-W Chen, "Effect of a Liquid Phase on Superplasticity of 2-mol% Y_2O_3-Stabilized Tetragonal Zirconia Polycrystals," *J Am Ceram Soc*, **73** [6] 1626-32 (1990)

[25]T Hermansson, K P D Lagerlof, and G L Dunlop, Superplasticity and Superplastic Forming, p 631 Edited by C H Hamilton and N E Paton The Metallurgical Society of AIME, Warrendale, PA, 1988

[26]T G Nieh, C M McNally and J Wadsworth, "Superplastic Properties of a Fine-Grained Yttria-

Stabilized Tetragonal Polycrystal of Zirconia," *Scripta Metall.*, **22**, 1297–300 (1988).

[27]R. Duclos, J. Crampon, and B. Amana, "Structural and Topological Study of Superplasticity in Zirconia Polycrystals," *Acta Metall.*, **37** [3] 877–83 (1989).

[28]C. Carry, "High Ductilities, Superplastic Behavior, and Associated Mechanisms in Fine-Grained Ceramics"; in Superplasticity, MRS Conference Proceedings, International Meeting on Advanced Materials, Vol. 7. Edited by M. Doyama, S. S. Sōmiya, R. P. H. Chang, M. Kobayashi, and F. Wakai. Materials Research Society, Pittsburgh, PA, 1989.

[29]T. K. Gupta, J. H. Bechtold, R. C. Kuznicki, L. H. Cadoff, and B. R. Rossing, "Stabilization of Tetragonal Phase in Polycrystalline Zirconia," *J. Mater. Sci.*, **12**, 2421–26 (1977).

[30]T. K. Gupta, "Sintering of Tetragonal Zirconia and Its Characteristics," *Sci. Sintering*, **10** [3] 205–16 (1978).

[31]T. K. Gupta, F. F. Lange, and J. H. Bechtold, "Effect of Stress-Induced Phase Transformation on the Properties of Polycrystalline Zirconia Containing Metastable Tetragonal Phase," *J. Mater. Sci*, **13**, 1464–70 (1978).

[32]I-W. Chen, Y. H. Chiao, and K. Tsuzaki, "Statistics of Martensitic Nucleation," *Acta Metall.*, **33** [10] 1847–59 (1985).

[33]K. Tsukuma, Y. Kubota, and T. Tsukidate, "Thermal and Mechanical Properties of Y_2O_3-Stabilized Tetragonal Zirconia Polycrystals"; pp. 382–90 in Advances in Ceramics, Vol. 12, Science and Technology of Zirconia II. Edited by N. Claussen, M. Rühle, and A. H. Heuer. American Ceramic Society, Columbus, OH, 1983.

[34]F. F. Lange, "Transformation-Toughened ZrO_2: Correlations between Grain-Size Control and Composition in the ZrO_2–Y_2O_3 System," *J. Am. Ceram. Soc.*, **66** [3] 240–42 (1986).

[35]I. G. Lee and I-W. Chen, "Sintering and Grain Growth in Tetragonal and Cubic Zirconia"; pp. 340–45 in Sintering '87, Proceedings of the 4th International Symposium on Science and Technology of Sintering, Vol. 2, Nov. 4–7, 1987, Tokyo, Japan. Edited by S. S. Sōmiya, M. Shimada, M. Yoshimura, and R. Watanabe. Elsevier Applied Science, London, U.K., 1988.

[36]S. L. Hwang and I-W. Chen, "Grain-Size Control of Tetragonal Zirconia Polycrystals Using the Space Charge Concept", to be published in *J Am. Ceram. Soc.*, (1990)

[37]Y. Oishi, K. Ando, and Y Sakka, "Lattice and Grain-Boundary Diffusion Coefficients of Cations in Stabilized Zirconias", pp. 208–19 in Advances in Ceramics, Vol. 7, Characterization of Grain Boundaries Edited by M. F. Yan and A H Heuer. American Ceramic Society, Columbus, OH, 1983.

[38]W. D. Kingery, H K Bowen, and D. R. Uhlmann, Introduction to Ceramics; p. 240 Wiley, New York, 1976

[39]F. Wakai, S. Sakaguchi, and H. Kato, "Compressive Deformation Properties and Microstructures in the Superplastic Y-TZP," *J Ceram. Soc Jpn.*, **94** [8] 721–25 (1986)

[40]F. Wakai, "Superplasticity of Zirconia-Toughened Ceramics", Ph D. Thesis Kyoto University, Kyoto, Japan, 1988.

[41]J. D. Fridez, C Carry, and A Mocellin, "Effects of Temperature and Stress on Grain-Boundary Behavior in Fine-Grained Alumina", pp. 720–40 in Advances in Ceramics, Vol 10, Structure and Properties of MgO and Al_2O_3 Ceramics Edited by W D Kingery American Ceramic Society, Columbus, OH, 1984

[42]C Carry and A Mocellin, "Structural Superplasticity in Single-Phase Crystalline Ceramics," *Ceram. Int*, **13**, 89–98 (1987)

[43]K R Venkatachari and R Raj, "Superplastic Flow in Fine-Grained Alumina," *J Am Ceram Soc*, **69** [2] 135–38 (1986)

[44]J. W. Cahn, "The Impurity Drag Effect in Grain-Boundary Motion," *Acta Metall.*, **10** [9] 789–98 (1962).

[45]I-W. Chen and C-M J Hwang; unpublished research.

[46]M. Rühle, N. Claussen, and A. H. Heuer, "Microstructural Studies of Y_2O_3-Containing Tetragonal ZrO_2 Particles"; pp 352–70 in Advances in Ceramics, Vol 12, Science and Technology of Zirconia II. Edited by N. Claussen, M. Rühle, and A H. Heuer. American Ceramic Society, Columbus, OH, 1984

[47]E. M. Levin, C. R. Robbins, and H. F. McMurdie, Phase Diagrams for Ceramists, 1969. Edited by M. K. Reser. American Ceramic Society, Columbus, OH; Figs. 2145 and 2146.

[48]T. Kuroishi, K. Uno, and F. Wakai, "Characterization of Superplastic ZrO_2-Toughened Al_2O_3 Prepared by Slip Casting"; pp. 267–74 in Superplasticity, MRS Conference Proceedings, International Meeting on Advanced Materials, Vol. 7. Edited by M. Doyama, S. S. Sōmiya, R. P. H Chang, M. Kobayashi, and F. Wakai. Materials Research Society, Pittsburgh, PA, 1989.

[49]P. Gruffel, C. Carry, and A. Mocellin, "Effect of Testing Conditions and Doping on Superplastic Creep of Alumina," *Rev. Phys Appl.*, **23** [4] 716 (1988)

[50]P. Gruffel, C. Carry, and A. Mocellin, "Effect of Testing Conditions and Doping on Superplastic Creep of Alumina," *Sci. Ceram*, **14**, 587–92 (1988).

[51]W. R. Cannon, "High Ductility in Alumina Containing Compensating Additives", pp. 741–49 in Advances in Ceramics, Vol. 10, Structure and Properties of MgO and Al_2O_3 Ceramics. Edited by W. D. Kingery. American Ceramic Society, Columbus, OH, 1984.

[52]C. Carry and A. Mocellin, "High Ductilities in Fine-Grained Ceramic", Ch. 16, pp. 16.1–16.19 in Superplasticity. Edited by B. Baudelet and M. Suery Centre National de la Recherche Scientifique, Paris, France, 1985.

[53]T-S. Yeh and M. D. Sacks, "Low-Temperature Sintering of Aluminum Oxide," *J Am. Ceram Soc.*, **71** [10] 841–44 (1988).

[54]R. M. Cannon, W. H. Rhodes, and A. H. Heuer, "Plastic Deformation of Fine-Grained Alumina (Al_2O_3): I, Interface-Controlled Diffusional Creep," *J. Am. Ceram. Soc*, **63** [1–2] 48–53 (1980)

[55]W. H Rhodes, "Agglomerate and Particle-Size Effects on Sintering Yttria-Stabilized Zirconia," *J. Am. Ceram. Soc.*, **64** [1] 19–22 (1981)

[56]F. F. Lange, "Powder Processing Science and Technology for Increased Reliability," *J Am Ceram. Soc*, **72** [1] 3–15 (1989)

[57]W. A. Kaysser, M. Sprissler, C A. Handwerker, and J. Blendell, "Effect of a Liquid Phase on the Morphology of Grain Growth in Alumina," *J. Am Ceram. Soc.*, **70** [5] 339–43 (1987)

[58]C-W Li and W. D Kingery, "Solute Segregation at Grain Boundaries in Polycrystalline Al_2O_3", pp 368–78 in Advances in Ceramics, Vol. 10, Structure and Properties of MgO and Al_2O_3 Ceramics Edited by W D. Kingery American Ceramic Society, Columbus, OH, 1984

[59]S K Roy and R L Coble, "Solubilities of Magnesia, Titania, and Magnesium Titanate in Aluminum Oxide," *J. Am Ceram Soc*, **51** [1] 1–6 (1968)

[60]S Hampshire, H K. Park, D P Thompson, and K H. Jack, "α'-sialon Ceramics," *Nature (London)*, **274** [5674] 880–82 (1978)

[61]L J Gauckler, H L Lukas, and T Y Tien, "Crystal Chemistry of β-Si_3N_4 Solid Solutions Containing Metal Oxides," *Mater Res Bull*, **11** [5] 503–12 (1976)

[62]L. J. Gauckler, J Weiss, T Y Tien, and G Petzow, "Insolubility of Mg in β-Si_3N_4 in the System Al-Mg-Si-O-N," *J Am Ceram Soc*, **61** [9–10] 397–98 (1978)

[63]C M Hwang, T Y Tien and I W Chen, "Anisotropic Grain Growth in Final Stage Sintering

of Silicon Nitride Ceramics"; pp 1034–39 in Sintering '87, Proceedings of 4th International Symposium on Science and Technology of Sintering, Vol 2, Nov. 4–7, 1987, Tokyo, Japan. Edited by S S Sōmiya, M. Shimada, M. Yoshimura, and R Watanabe. Elsevier Applied Science, London, U K, 1988

[64]C. M. Hwang and T. Y. Tien, "Densification and Phase Transformation During Sintering of Silicon Nitride Ceramics", pp. 1028–33 in Sintering '87, Proceedings of 4th International Symposium on Science and Technology of Sintering, Vol 2, Nov 4–7, 1987, Tokyo, Japan. Edited by S S Sōmiya. M. Shimada, M. Yoshimura, and R. Watanabe. Elsevier Applied Science, London, U.K., 1988

[65]F. Wakai, "A Review of Superplasticity in ZrO_2-Toughened Ceramics," *Br Ceram. Trans J*, **88** [6] 205–208 (1989).

[66]C. Zener; private communication to the author See C. S. Smith, "Grains, Phases, and Interfaces: An Interpretation of Microstructure," *Trans AIME*, **175**, 15–51 (1948).

[67]P. Hellman and M. Hillert, "On the Effect of Second-Phase Particles on Grain Growth," *Scand. J. Metall.*, **4** [5] 211–19 (1975).

[68]I. N. Bransford and P. Wynblatt, "The Dependence of Ostwald Ripening Kinetics on Particle Volume Fraction," *Acta Metall.*, **27** [3] 489–97 (1979)

[69]A. Ball and M. M. Hutchinson, "Superplasticity in the Aluminum–Zinc Eutectoid," *Met. Sci. J*, **3** [1] 1–7 (1969)

[70]A. K. Mukherjee, "The Rate-Controlling Mechanism in Superplasticity," *Mater Sci. Eng.*, **8** [2] 83–89 (1971).

[71]P. E. Evans, "Creep in Yttria- and Scadia-Stabilized Zirconia," *J. Am Ceram. Soc.*, **53** [7] 365–69 (1970).

[72]L. L Fehrenbecher, F. P. Bailey, and N. A. McKinnon, "Compressive Creep of Yttria–Rare-Earth-Stabilized Zirconia Storage Heater Refractories," *SAMPE Q*, **2** [4] 18–30 (1971).

[73]M. S. Seltzer and P K. Talty, "High-Temperature Creep of Y_2O_3-Stabilized ZrO_2," *J. Am. Ceram Soc*, **58** [3–4] 124–30 (1975)

[74]D. Dimos and D C Kohlstedt, "Diffusional Creep and Kinetic Demixing in Yttria-Stabilized Zirconia," *J. Am Ceram. Soc.*, **70** [8] 531–36 (1987).

[75]F. Wakai and T Nagona, "The Role of Interface-Controlled Diffusion Creep on Superplasticity of Yttria-Stabilized Tetragonal ZrO_2 Polycrystals," *J. Mater. Sci. Lett.*, **7**, 607–609 (1988)

[76]A. Dominguez-Rodriguez, K. P. D Lagerlof, and A. H. Heuer, "Plastic Deformation and Solid-Solution Hardening of Y_2O_3-Stabilized ZrO_2," *J Am Ceram Soc.*, **69** [3] 281–84 (1986)

[77]S Takeuchi and A S Argon, "Review—Steady-State Creep of Single-Phase Crystalline Matter at High Temperature," *J Mater Sci.*, **11**, 1542–66 (1976)

[78]E. Arzt, M. F. Ashby, and R A Verrall, "Interface-Controlled Diffusional Creep," *Acta Metall*, **31** [12] 1977–89 (1983)

[79]B Burton, "Interface-Reacton-Controlled Diffusional Creep, A Consideration of Grain-Boundary Dislocation Climb Sources," *Mater Sci. Eng.*, **10** [1] 9–14 (1972)

[80]J W Cahn, "Theory of Crystal Growth and Interface Motion in Crystalline Materials," *Acta Metall*, **8** [8] 554–62 (1960)

[81]R Raj and C K Chyung, "Solution-Precipitation Creep in Glass Ceramics," *Acta Metall*, **29** [1] 159–66 (1981)

[82]F Wakai, T Iga, and T Nagano, "Effect of Dispersion of ZrO_2 Particles on Creep of Fine-Grained Al_2O_3," *J Ceram Soc Jpn*, **96** [12] 1206–209 (1988)

[83]I-W. Chen and A S. Argon, "Steady-State Power-Law Creep in Heterogeneous Alloys with Coarse Microstructures," *Acta Metall.*, **27**, 785–91 (1979)

[84]P. C. Dokko, J A Pask, and K S Mazdiyasni, "High-Temperature Mechanical Properties of Mullite Under Compression," *J. Am. Ceram. Soc.*, **60** [3–4] 150–55 (1977).

[85]D. S. Wilkinson, "Grain-Size Effects in Superplasticity"; Ch. 6, pp 6.1–6.6 in Superplasticity. Edited by B. Baudelet and M. Suery. Centre National de la Recherche Scientifique, Paris, France, 1985.

[86]I-W Chen and A. S Argon, "Creep Cavitation in 304 Stainless Steel," *Acta Metall.*, **29**, 1321–33 (1981).

[87]I-W. Chen, "A Stochastic Theory of Grain Growth," *Acta Metall.*, **35**, 1723–33 (1987).

[88]F. Wakai, S Sakaguchi, K. Kanayama, H. Kato, and H. Onishi, "Hot Work of Yttria-Stabilized Tetragonal ZrO_2 Polycrystals", pp. 315–22 in Ceramic Materials and Components for Engines. Edited by W. Bunk and H Hausner. Deutsch Keramische Gesellschaft, FRG, 1986.

[89]C. Carry and A. Mocellin, "Examples of Superplastic-Forming Fine-Grained Al_2O_3 and ZrO_2 Ceramics"; High Tech Ceramics, Materials Science Monograph 38A. Edited by P. Vincenzini. Elsevier Applied Science, Amsterdam, Netherlands, 1987.

[90]X Wu and I-W. Chen, "Superplastic Bulging of Fine-Grained Zirconia," *J. Am Ceram. Soc.*, **73** [3] 746–49 (1990).

[91]S. S. Hecker and A. K. Ghosh, "The Forming of Sheet Metal," *Sci Am*, [Nov] 100–109 (1976).

[92]A. S. Argon, I-W. Chen, and C. W. Lau, "Intergranular Cavitation in Creep"; pp. 46–85 in Creep-Fatigue-Environment Interactions. Edited by R. M Pelloux and N. S. Stoloff. The Metallurgical Society of AIME, Warrendale, PA, 1980.

[93]R. Raj and M. F Ashby, "Intergranular Fracture at Elevated Temperature," *Acta Metall.*, **23** [6] 653–66 (1975)

[94]A. G Evans, J R Rice, and J P Hirth, "Suppression of Cavity Formation in Ceramics' Prospects for Superplasticity," *J. Am. Ceram. Soc.*, **63** [7–8] 368–75 (1980)

[95]N Ridley and J. Pilling, "Cavitation in Superplastic Alloys—Experimental"; Ch 8, pp. 8 1–8.17 in Superplasticity Edited by B. Baudelet and M. Suery. Centre National de la Recherche Scientifique, Paris, France, 1985.

[96]M. Suery, "Cavitation in Superplastic Alloys—Theoretical"; Ch 9, pp. 9 1–9 19 in Superplasticity. Edited by B Baudelet and M Suery. Centre National de la Recherche Scientifique, Paris, France, 1985

[97]J-G Wang and R. Raj, "Influence of Hydrostatic Pressure and Humidity on Superplastic Ductility of Two β-Spodumene Glass-Ceramics," *J Am Ceram Soc*, **67** [6] 385–90 (1984)

[98]B Kibbel and A H Heuer, "Exaggerated Grain Growth in ZrO_2-Toughened Al_2O_3," *J Am Ceram Soc*, **69** [3] 231–36 (1986)

[99]F F Lange and M Hirlinger, "Hindrance of Grain Growth in Al_2O_3 by ZrO_2 Inclusions," *J Am Ceram Soc*, **67** [3] 164–68 (1984)

[100]A H Chokshi and J R. Porter, "High-Temperature Mechanical Properties of Single-Phase Ceramic," *J Mater Sci*, **21**, 705–10 (1986)

[101]T G Nieh, C M McNally, and J Wadsworth, "Superplasticity in Intermetallics. Alloys, and Ceramics," *J Met*, **41** [9] 31–35 (1989)

[102]J-G Wang and R Raj, "Mechanism of Superplastic Flow in Fine-Grained Ceramics Containing Some Liquid Phase." *J Am Ceram Soc*, **67** [6] 399–409 (1984) □

I-Wei Chen is Professor of Materials Science and Engineering at the University of Michigan at Ann Arbor. A native of Taiwan, he graduated from Tsinghua University (B.S.) and University of Pennsylvania (M.S.) majoring in physics. He received his Ph.D. in metallurgy from Massachusetts Institute of Technology in 1980. Prior to joining the University of Michigan in 1986, he was a joint Assistant Professor in the Department of Nuclear Engineering and the Department of Materials Science and Engineering at MIT. He has served the American Ceramic Society as Program Chair of the Basic Science Division (1989–1990) and as an Associate Editor of the *Journal* (since 1990). His major publications in ceramics are on zirconia phase transformation, microstructural modeling, and mechanical properties.

Liang An Xue is a Senior Research Fellow in the Department of Materials Science and Engineering at the University of Michigan. He received a B.S. in building materials in 1982 from Tongji University, Shanghai, China. He earned his Ph.D. in ceramics in 1987 from Leeds University, England, where he studied additives and grain-growth control of barium titanate ceramics under the supervision of Richard Brook. Prior to joining the University of Michigan in 1989, he was a Postdoctoral Associate in the Materials Science Department at Cornell University, working with Rishi Raj on the development of novel infrared window materials such as zinc sulfide/diamond composites. His main research interests include ceramic processing, superplasticity, and microstructural/property relationships in ceramics and ceramic composites. Dr. Xue is the author or coauthor of 20 scientific papers and 1 patent. He is a member of the Institute of Ceramics, U.K., and a member of the American Ceramic Society.

journal

J. Am. Ceram. Soc., 73 [9] 2610-14 (1990)

Microstructure and Composition of Alumina/Aluminum Composites Made by Directed Oxidation of Aluminum

Else Breval*

Materials Research Laboratory, The Pennsylvania State University, University Park, Pennsylvania 16802

Michael K. Aghajanian* and Stan J. Luszcz*

Lanxide Corporation, Newark, Delaware 19714

Two Al_2O_3/Al composites, grown by the directed oxidation of molten Al alloys at 1400 and 1600 K, were investigated by X-ray diffraction, optical microscopy, scanning electron microscopy, transmission electron microscopy, and wet chemical analysis. The materials were found to contain a continuous network of Al_2O_3, which was predominantly free of grain-boundary phases and was made up of nanometer- to micrometer-sized crystallites, a continuous network of Al alloy, and isolated inclusions of Al alloy. No crystallographic orientation was observed in the metallic phase, whereas the Al_2O_3 was oriented with its *c* axis parallel to the growth direction. The higher process temperature yielded a lower metal content and less connectivity of the metallic constituent. [Key words: alumina, aluminum, microstructure, composites, oxidation.]

I. Introduction

Reinforced ceramic composite bodies have been produced by the directed oxidation of Al alloys through preforms of reinforcing material.*,[1] The Al_2O_3/Al oxidation reaction product matrix grows at the interface of the oxidant and the reaction product, and thus is able to incorporate the reinforcement without disturbance or rearrangement. Composites with favorable structural properties containing particulate[2,3] and fiber[4,5] reinforcement have been fabricated.

To more fully understand the family of Al_2O_3/Al matrix composites that can be produced by this process, it is first necessary to obtain basic information about the matrix itself. To this end, the formation,[6] physical properties,[7] and failure mechanisms[8] of unreinforced Al_2O_3/Al reaction products have been studied. The present paper provides a detailed description of the microstructure and composition of selected Al_2O_3/Al materials. It should be noted that the microstructure of the reaction product is altered by the presence of a reinforcement during the growth process. However, the unreinforced matrix materials represent an appropriate starting point for the study of these composites.

II. Experimental Procedure

Two Al_2O_3/Al materials, designated A and C,[7] were investigated. Each was produced (grown) by oxidizing an Al alloy in air.[6] Material A was fabricated at 1400 K with Al alloy 5052 (nominally Al–2.5Mg) that was externally doped (coated) with 120 mesh SiO_2 particles. Material C was similarly produced at 1600 K with Al alloy 6061 (nominally Al–1Mg–0.6Si). In both cases, the process was stopped prior to converting all of the metal to oxide.

The microstructures of the materials were observed at three levels using optical microscopes, a scanning electron microscope (SEM),† and a transmission electron microscope (TEM),‡ operated at 120 kV, with an energy dispersive spectrometer (EDS).§ Polished sections were observed in the optical microscope, using reflected light, and in the SEM. Thin sections (30 ± 10 μm), which were leached in a 10% HCl solution to remove the interconnected metal, were observed optically in transmitted polarized light between crossed nicols to determine the optical orientation of the Al_2O_3 phase. Ion-beam-thinned specimens of the composites were examined in the TEM.

The phase composition was investigated by the use of ceramography, X-ray diffraction (XRD), wet chemistry, and EDS in conjunction with both the SEM and the TEM. The XRD was performed on powdered (400 mesh) specimens to detect the major phases present, and on smooth surfaces (both parallel and perpendicular to the growth direction) to determine possible preferred orientation of the constituents. A semiquantitative determination was conducted based on the intensities of the X-ray peaks after background subtraction, providing results of both nominal composition and orientation.

Two separate chemical analyses were performed, one examining the composite as a bulk and the second individually examining the ceramic and metallic constituents. The bulk analysis was accomplished by melting a powdered (400 mesh) specimen in lithium metaborate and then dissolving the specimen in a 4% HNO_3 solution, followed by a spectrochemical analysis. The individual analyses were performed by leaching a powdered (400 mesh) specimen in a boiling 10% HCl solution and subsequently analyzing the solution and the residue. It was assumed that the metallic constituent was completely dissolved and the ceramic constituent was completely retained. All solutions were analyzed.¶

III. Results and Discussion

(1) *Material A*

A low-magnification optical micrograph of an HCl-leached thin section oriented parallel to the growth direction, observed between crossed nicols and a gypsum red I plate oriented 45° to the nicols, is shown in Fig. 1. It reveals a structure with two distinct layers. The lower layer (i.e., first layer to grow), which accounts for only a small portion of the sample, measures 2 to 5 mm in thickness and appears

V. Chowdhry—contributing editor

Manuscript No. 197779. Received February 7, 1990; approved May 9, 1990.

*Member, American Ceramic Society.

*Process technology patented by Lanxide Corporation and given the trade name DIMOX™ directed metal oxidation process.

†Model DS-130, ISI, Santa Clara, CA

‡Model EM-420, Philips Electronic Instruments, Inc., Mahwah, NJ

§Model 860, Link Analytical, Inc., Palo Alto, CA.

¶Spectraspan III, Spectrametrics, Andover, MA

2.2 "Superplastic Ceramics"

I-W. Chen, in Ceramic Powder III: Ceramic Transactions, V. 12, Proceedings of 3rd International Symposium on the Science of Processing

SUPERPLASTIC CERAMICS

I-Wei Chen
Department of Materials Science & Engineering
University of Michigan
Ann Arbor, Michigan 48109-2136

Large strain superplastic bulge forming of zirconia was recently achieved at 1150°C at a strain rate of close to $10^{-3}s^{-1}$. In this way, it has been demonstrated to be a feasible forming technique for oxide ceramics. The key to the success of the tetragonal zirconia polycrystal as a superplastic ceramic lies partially in its relatively good powder characteristics, but more importantly in its incorporation of aliovalent stabilizers which additionally provide solute drag to suppress grain growth. Its forming characteristics can be further improved by a judicious addition of a grain boundary liquid phase, at a thickness of no more than 5nm. An overview of these advances and the parallel development in superplastic alumina is provided here.

I. INTRODUCTION

Forming of crystalline ceramics is usually carried out at low temperatures, before firing. The common forming practice in other materials industries (e.g. metals, plastics and glass), however, is via deformation processing of dense materials at higher temperatures. The main advantage of the latter process lies in its greater flexibility for shape and greater accuracy for dimension, which are especially important considerations for net-shape forming. Usually, because of the very limited ductility and the very high flow stress of most crystalline ceramics, such a method is not feasible.

In the last few years, considerable progress has been made on fine grain superplasticity which promises to fundamentally change the outlook for deformation processing of some crystalline ceramics. Several oxides, most notably some partially-stabilized tetragonal zirconia, have been found to have considerable tensile ductilities, in some cases well over 100%.[1-5] The flow stresses are relatively low, of the order of several tens of MPa. The basic phenomena observed in these ceramics are in accordance with the major findings in fine grain metals and alloys deformed in the superplastic regime.[6] Notably,

the strain rate varies with the second or third power of the reciprocal grain size, and with the flow stress almost linearly.

For practical reasons, it is desirable to achieve a high strain rate at as low a temperature as possible. This can be achieved by a combination of better powder processing, sintering and the attainment of microchemical and microstructural parameters beneficial for ceramic superplasticity. A basic understanding of these interrelated aspects is particularly helpful for the on-going effort in developing future superplastic ceramics. These issues are addressed in the present review.

In the following sections, we first provide a best-case example of the present practice of superplastic forming. We then review several superplasitcity studies of fine-grained zirconia to make evident main attributes responsible for its remarkable flow properties. Lastly, the outlook of superplastic forming for other ceramics is assessed in view of the state of the art.

II. SUPERPLASTIC FORMING

Many attempts have been made to form zirconia and other ceramics into shapes in the superplastic regime. In terms of forming methods, the following have been tried: uniaxial tension,[1-5] uniaxial compression,[7-8] bending,[9] extrusion,[10] inverse extrusion[10] and shell forming.[10] These are shown schematically in Fig. 1.

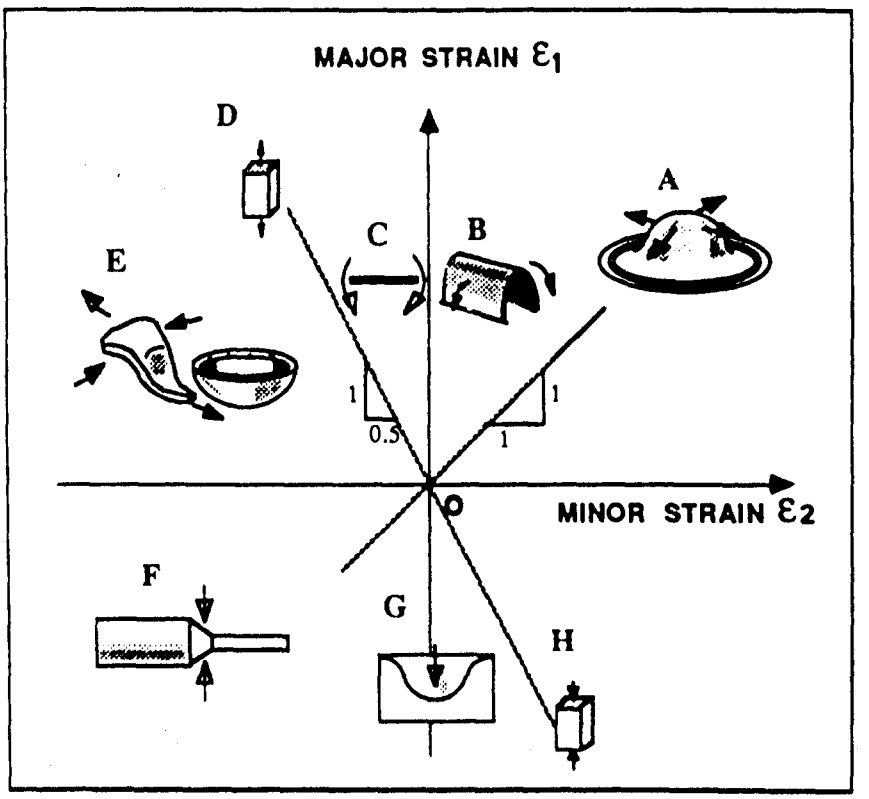

Fig. 1 Dominant strain states of various deformation processes. (See Table 1 for references.)

TABLE 1: Various Types of Superplastic Deformation Processing

	PROCESS	EXAMPLE	
A	Bulging	Wu and Chen	[11]
B	Plane Strain Bending	Wakai et al.	[9]
C	Simple Bending	Wakai et al.	[9]
D	Uniaxial Tension	Wakai et al.	[1]
E	Shell Forming	Carry and Mocellin	[10]
F	Extrusion	Carry and Mocellin	[10]
G	Inverse Extrusion	Carry and Mocellin	[10]
H	Uniaxial Compression	Venkatachari and Raj	[7]

Some of these methods involve tensile strain in one direction, such as uniaxial tension (see D in Fig. 1) and bending (C). Others are dominated by compression, such as extrusion (F) and inverse extrusion (G). In the shell-forming (E) experiment of Mocellin et al., a balanced tension-compression was used. In bending of a wide plate (B), plane strain tension is encountered. The tensile strains in bending are usually quite small.

Recently, biaxial tensile stretching has been demonstrated in our laboratory.[11] As shown in Fig. 2, a hemispherical dome can be formed by bulging a constrained disk using a punch. The biaxial tensile strain at the pole is a function of the disk thickness, punch radius and dome height. When the disk is clamped at the edge, a biaxial tensile strain of 30~40%, or an effective strain of 70%, is reached with a hemispherical shell, if the initial thickness of the disk is 1mm. The surface of the workpiece has an excellent finish after forming,

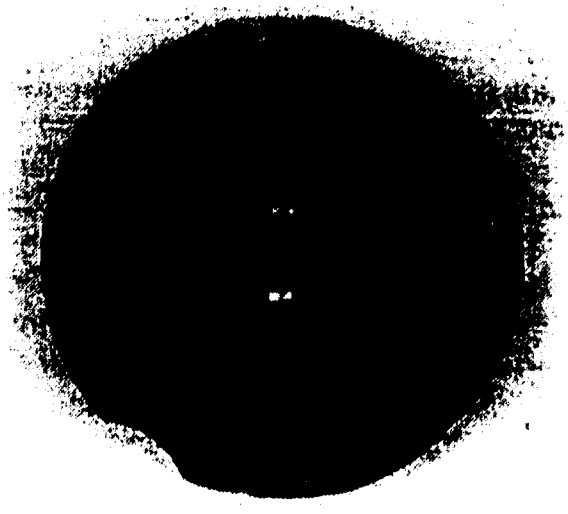

Fig. 2. A ZrO_2 sample after forming at 1150°C for 10 minutes, with a constant punch velocity of 0.6 mm/min.
(Disc diameter = 32 mm, thickness = 1 mm.)

and the ceramic is damage-tolerant, up to a critical strain rate of c.a. 10^{-3}/s. The significance of this demonstration is that it closely simulates the most severe sheet forming processes in practice where biaxial tension is encountered. Hence, its success lends considerable confidence to the application of superplastic forming for the industrial environment.

From a practical standpoint, the forming parameters which are of the most importance are the strain rate and the forming temperature. A high strain rate is required to ensure reasonable productivity, and a low forming temperature is desired to lower the capital cost and reduce tool wear. In the above example of biaxial tensile stretching, a strain rate of 10^{-3}/s and a forming temperature of 1150°C have been achieved. This means that the forming operation can be completed in about 10 minutes and that a conventional electric furnace can be used.

III. MICOSTRUCTURAL AND MICROCHEMICAL ASPECTS OF SUPERPLASTIC ZIRCONIA

Superplasticity is a process dominated by diffusional flow. Thus, the ability to obtain and maintain a very fine grain size and to enhance diffusion is crucial. Because of their lower melting temperatures, the deformation temperature of most metals can be raised without practical difficulty to 0.8 of the melting temperature. At high homologous temperatures, when the grain size is lowered to several microns, fast diffusion enhances superplastic flow enough to dominate. In oxide ceramics, a more reasonable working temperature is probably limited to between 1000 and 1500°C. By calculating the diffusional creep rate using the available diffusivity data[12] one can easily demonstrate that a submicron grain size is probably required to achieve a strain rate of 10^{-4}/s at these temperatures. Since very few ceramics have submicron grain sizes, ceramic superplasticity did not materialize until Wakai reported on 3Y-TZP in 1986.[1]

For more than a decade now, we have known that yttria-stabilized tetragonal zirconia has a characteristically fine-grained microstructure, which is uncommon among ceramics.[13] The need for maintaining a submicron grain size in this material was initially motivated by studies of transformation toughening.[13-15] These studies sought to avoid spontaneous tetragonal-to-monoclinic transformation for which the statistics of nucleation is grain size dependent.[16] The popular use of this material as a tough and strong ceramic (K_{IC} above 5 MPa $m^{1/2}$ and strength exceeding 1200 MPa)[17] has stimulated industry to provide commercial powders of excellent sinterability. These powders can be readily processed to obtain sintered ceramics of grain sizes from 0.3 to 0.5 microns, sufficiently fine to allow superplasticity above 1300°C.[1] It is for this reason that 3Y-TZP has become almost the universal choice for demonstrating ceramic superplasticity in the last few years.

Although the relatively good characteristics of zirconia powders have contributed to their excellent sinterability, the intrinsic cause of the very fine grain size is not clear.[18] Recently, through a detailed study of grain growth

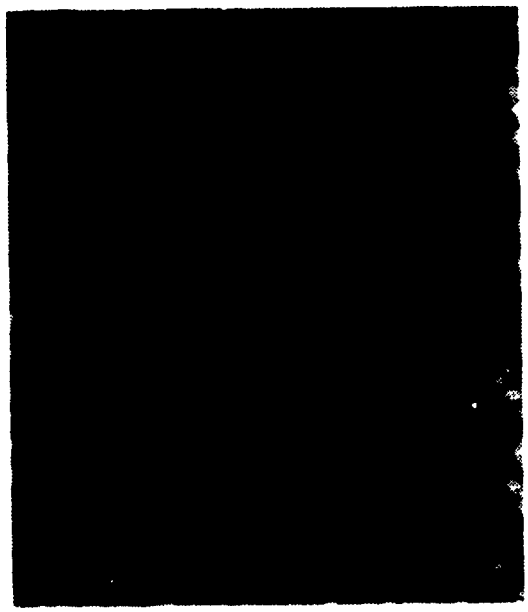

(a) 2Y-TZP

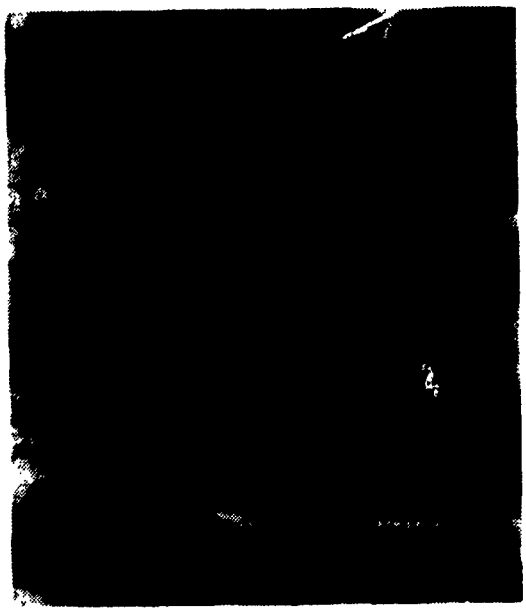

(b) 2Y-TZP/50 v/o Mullite

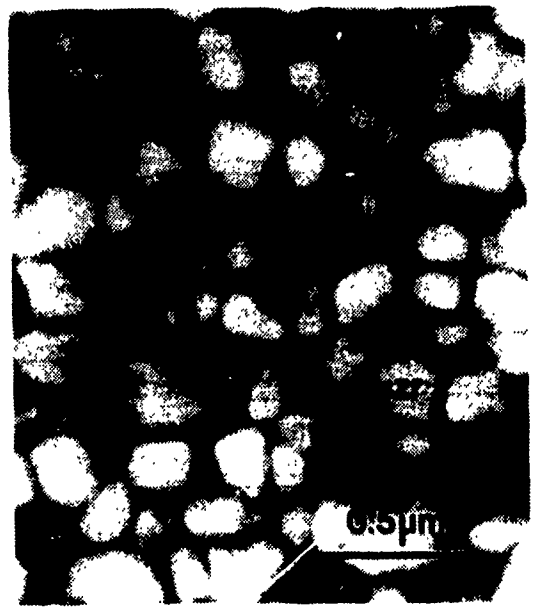

(c) 2Y-TZP/30 v/o Alumina

Fig. 3 Microstructures of (a) single-phase 2Y-TZP and two-phase composites containing (b) mullite and (c) alumina.

kinetics guided by crystal chemistry, we have identified the mechanism of grain-size stabilization in this class of ceramics.[19] Essentially, aliovalent solutes, such as Y^{+3}, segregate to the grain boundary of zirconia by the so-called space charge effect. The mobility of grain boundary is lowered because the solute cloud must be dragged along as the grain boundary migrates. This also has the effect of increasing the activation energy of grain growth from that of grain boundary diffusion to that of lattice diffusion. Among various solutes, the larger the effective charge, the stronger the segregation and the slower the grain growth. Furthermore, since the lattice diffusion of larger solutes is slower, larger solutes are more effective than smaller ones in suppressing grain growth. In this respect, Y^{+3}, being an aliovalent and oversized ion in the host matrix of ZrO_2, and having a relatively large (2.5 mole%) solubility among ceramics, serves as an effective solute in suppressing grain growth during sintering and superplastic deformation of partially-stabilized zirconia. An added benefit of solute segregation to grain boundary is the lowering of grain boundary energy[20] and, correspondingly, the enhancement of grain boundary cohesion. For these reasons, Y-TZP has emerged as an excellent superplastic ceramic.

As in metals, second phase particles are very effective in suppressing grain growth in ceramics. However, for superplastic applications, second phase particles have to be dispersed uniformly on a submicron scale to be effective. Furthermore, a suitable choice has to be found in order to maintain reasonable sinterability in the presence of second phase particles. This poses some processing problems. At the present time, some two-phase, zirconia-based superplastic ceramics such as zirconia-mullite and zirconia-alumina composites have been developed. When properly processed, they can achieve a grain size of the order of 0.2 micron (see Fig. 3). Nevertheless, they tend to have a higher flow stress because both mullite and alumina are best considered as hard inclusions in a soft zirconia matrix.[3,21] Therefore, their superplastic characteristics are not yet as good as Y-TZP.

The other approach to enhance superplasticity is to increase the diffusivity in fine grain ceramics. Some systematic attempts have been made in our laboratory in this direction.[22] In particular, we have investigated the effect of transition metal dopants on the superplasticity of Y-TZP. Many of the transition metal dopants, including Mn, Fe, Co, Ni, Cu and Zn, form a low-melting liquid phase residing on the zirconia boundaries. When the amount of the additive is properly controlled, it is possible to have a very thin, wetting amorphous phase along the grain boundary which aids diffusional flow but has little effect on grain boundary cohesion and other mechanical properties. For example, when 2Y-TZP is doped with 0.3 mol% CuO, strain rate can be increased by almost two orders of magnitude (as shown in Fig. 4), rendering superplastic deformation below 1200°C feasible. More detailed mechanistic studies have established the chemical composition of the grain boundary phase as Cu^{+1}, Zr^{+4}, Y^{+3}, Si^{+4} and O^{-2}, with a melting temperature around 1130°C. Deformation below the melting temperature is apparently diffusion-controlled; it becomes interface-controlled above the melting temperature.[22]

IV. PROSPECTS FOR SUPERPLASTIC FORMING OF OTHER CERAMICS

As illustrated in Section II, superplastic forming of zirconia ceramics looks promising in light of its low deformation temperature, high strain rates and excellent formability. Prospects for repeating the success of zirconia in other engineering ceramics, notably alumina, are assessed here.

Unlike zirconia, alumina is much more susceptible to grain growth both in sintering and deformation. It has a relatively low solubility for nearly all aliovalent dopants, and is strongly anisotropic in its grain boundary characteristics. These inherent features of alumina make it somewhat difficult to apply the same microchemical approach developed for zirconia ceramics. For example, the introduction of a liquid phase is known to

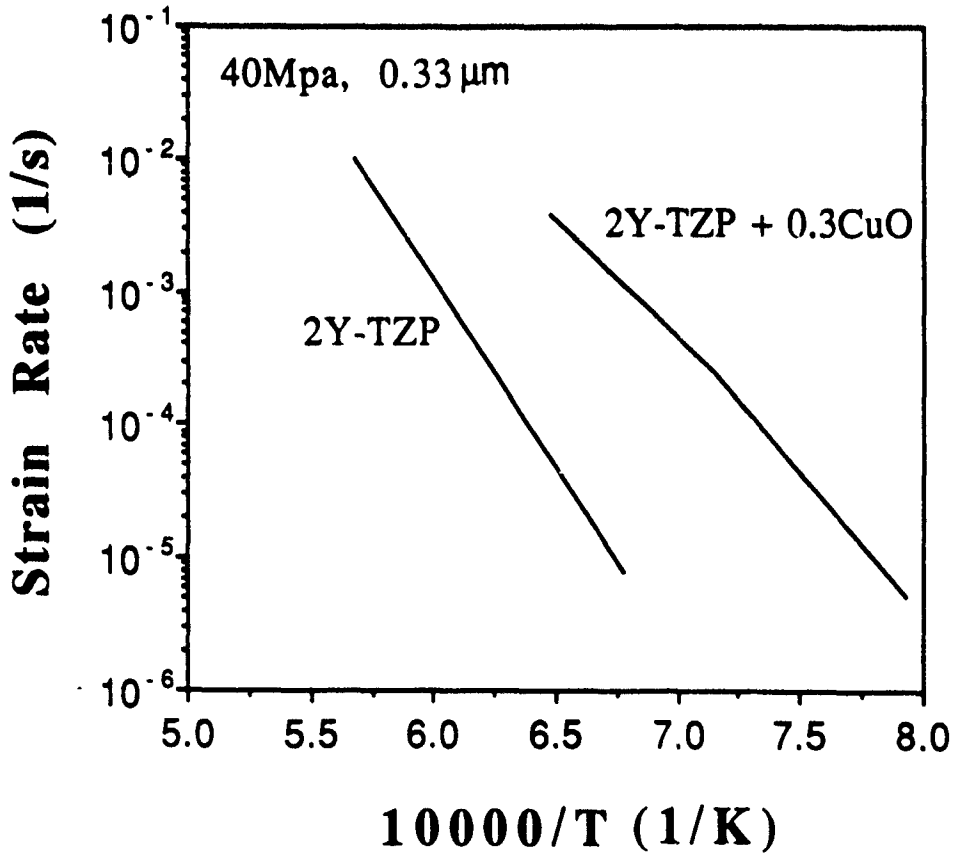

Fig. 4 Strain rate versus reciprocal temperature for 2Y-TZP with and without 0.3 mol% CuO. (stress = 40 MPa, grain size = 0.33 μm)

drastically enhance abnormal grain growth in alumina[23] and must be used judiciously. As another example, the space charge concept is difficult to verify in alumina because of the very low solubilities of most solutes.[24]

To establish base-line data for comparing alumina and zirconia, we have processed a high-purity alumina and evaluated its deformation characteristics. A

commercial powder was used as the starting material, followed by milling and slip casting in the presence of a surfactant. Sintering was conducted at 1250°C to reach 99% of the theoretical density. (Although the above temperature is somewhat higher than that used by Sacks et al.,[25] unlike their process, we did not further classify particles of the as-received powder. Therefore, the yield of this process is 100%). As shown in Fig. 5, alumina grains are equiaxed and have an average size of 0.6 micron. Deformation data of this alumina and, for comparison, of zirconia, are shown in Fig. 6. Essentially, we find that the deformation temperature of alumina needs to be 50°C above that of pure 2Y-TZP at a comparable grain size. However, since the sintered grain size of alumina is about a factor of 2.5 times higher than that of zirconia, another 50°C is probably required to compensate for this disadvantage. Thus, we are hopeful that pure alumina can be superplastically formed at slightly above 1300°C, and at a lower temperature if additives are used.

Fig. 5. Microstructure of alumina sintered at 1250°C

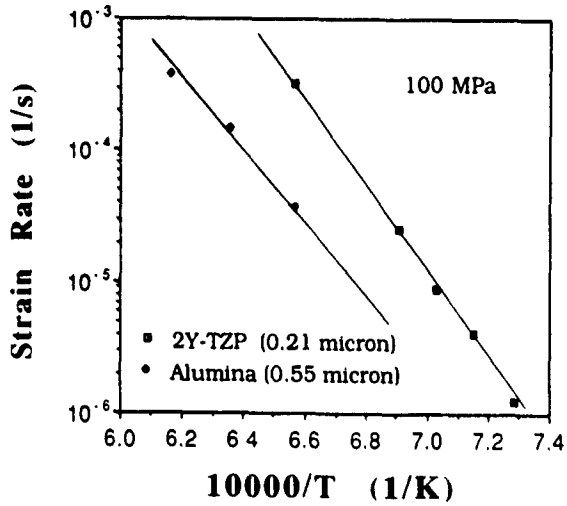

Fig. 6. Strain rate versus reciprocal temperature of 2Y-TZP and alumina

V. CONCLUSION

The recent progress in ceramic powder processing has resulted in much lower sintering temperatures for several commercial ceramics. A lower sintering temperature is synonymous to a more uniform and finer microstructure, which

coincides with the need of superplastic ceramics. With powders of ever-improving sinterability and finer particle size becoming increasingly available, further progress in developing superplastic ceramics looks promising. Complementary research on physical ceramics will elucidate the principles of microchemical and microstructural control and guide the way toward deformation and ductility enhancement.

More broadly, we must be reminded that while a novel processing concept, such as superplastic forming of ceramics, appears attractive and even technically feasible, whether it will be realized or not is largely decided upon by the market force. We are cautiously confident that, as the demand for advanced ceramics grows larger in future years, this unique net-shape processing method will be drawn upon and developed into an industrial process.

ACKNOWLEDGEMENT

Superplasticity research of I-Wei Chen at the University of Michigan is supported by U.S. DOE under Grant No. DE-FG02-87ER45302, U.S. AFOSR under Grant No. 87-0289, and U.S. ARO under Contract No. DAAL03-89 K0133.

REFERENCES

1. F. Wakai, S. Sakaguchi and Y. Matsuno, "Superplasticity of Yttria-Stabilized Tetragonal ZrO_2 Polycrystals," *Advanced Ceramic Materials*, **1** [3] 259-63 (1986).

2. F. Wakai and H. Kato, "Superplasticity of TZP/Al_2O_3 Composite," *Advanced Ceramic Materials*, **3** [1] 71-5 (1988).

3. F. Wakai, Y. Koidama, S. Sakaguchi, N. Murayama, H. Kato and T. Nagano, "Superplastic Deformation of ZrO_2/Al_2O_3 Duplex Composites," pp. 259-266, in Vol. 7, Superplasticity, Eds. M. Doyama, S.S. Somiya, R.P.H. Chang, M. Kobayashi and F. Wakai, Materials Research Society, Pittsburgh, Pa (1989).

4. T. Kuroishi, K. Uno and F. Wakai, "Characterization of Superplastic ZrO_2-Toughened Al_2O_3 Prepared by Slip Casting," pp. 267-74, in *MRS Int'l Mtg. on Adv. Mats.* Vol. 7, Superplasticity, Eds. M. Doyama, S.S. Somiya, R.P.H. Chang, M. Kobayashi and F. Wakai, Materials Research Society, Pittsburgh, Pa (1989).

5. T.G. Nieh, C.M. McNally and J. Wadsworth, "Superplastic Properties of a Fine Grained Yttria-Stabilized Tetragonal Polycrystal of Zirconia," *Scripta Metall.* **22**, 1297-1300 (1988).

6. J.W. Edington, K.N. Melton and C.P. Cutler, "Superplasticity," *Progress in Materials Science*, **21** [2] 61-170 (1976).

7. K.R. Venkatachari and R. Raj, "Superplastic Flow in Fine-Grained Alumina," *J. Am. Ceram Soc.*, **69** [2], 135-8 (1986).

8. B.J. Kellett and F.F. Lange, "Hot-Forging Characteristics of Fine-Grained ZrO_2 and Al_2O_3/ZrO_2 Ceramics," *J. Am. Ceram. Soc.*, **69** [8] C-172-3 (1986).

9. F. Wakai, S. Sakaguchi, K. Kanayama, H. Kato and H. Onishi, "Hot Work of Yttria-Stabilized Tetragonal ZrO_2 Polycrystals," in Ceramic Materials and Components for Engines, Eds., W. Bunk and H. Hausner, Deutsch Keramische Cesellschaft, p. 315-22 (1986).

10. C. Carry and A. Mocellin, "Examples of Superplastic Forming Fine-Grained Al_2O_3 and ZrO_2 Ceramics," High Tech Ceramics, Ed. P. Vincenzini, Materials Science Monograph 38A, Elsevier Science Publishers, Amsterdam, p. 1043-52 (1987).

11. X. Wu and I-W. Chen, "Superplastic Bulging of Fine Grained Zirconia," *J. Am. Ceram. Soc.* **73** [3] (1990).

12. W.D. Kingery, H.K. Bowen and D.R. Uhlmann, "Introduction to Ceramics," p. 240, John Wiley and Sons, New York (1976).

13. T.K. Gupta, J.H. Bechtold, R.C. Kuznicki, L.H. Cadoff and B.R. Rossing, "Stabilization of Tetragonal Phase in Polycrystalline Zirconia," *J. Mater. Sci.*, **12**, 2421-2426 (1977).

14. T.K. Gupta, "Sintering of Tetragonal Zirconia and Its Characteristics," *Sci. Sintering*, **10** [3] 205-16 (1978).

15. T.K. Gupta, F.F. Lange and J.H. Bechtold, "Effect of Stress-Induced Phase Transformation on the Properties of Polycrystalline Zirconia Containing Metastable Tetragonal Phase," *J. Mater. Sci.*, **13**, 1464-70 (1978).

16. I-W. Chen, Y.H. Chiao and K. Tsuzaki, "Statistics of Martensitic Nucleation," *Acta Metall.* **33** [10] 1847-1859 (1985).

17. K. Tsukuma, Y. Kubota and T. Tsukidate, "Thermal and Mechanical Properties of Y_2O_3-Stabilized Tetragonal Zirconia Polycrystals," pp. 382-90, in Advances in Ceramics, vol. 12, *Science and Technology of Zirconia II*, Eds., N. Claussen, M. Ruhle and A. Heuer, American Ceramic Society, Columbus, OH (1983).

18. F.F. Lange, "Transformation Toughened ZrO_2: Correlations Between Grain Size and Control and Composition in the ZrO_2-Y_2O_3 System," *J. Am. Ceram. Soc.*, **69** [3] 240-2 (1986).

19. S.L. Hwang and I-W. Chen, "Grain Size Control of Tetragonal Zirconia Polycrystals Using The Space Charge Concept", submitted to *J. Am. Ceram. Soc.* (1989).

20. I.G. Lee, and I-W. Chen, "Sintering and Grain Growth in Tetragonal and Cubic Zirconia," in Sintering '87, Eds., S. Somiya, M. Shimada, M. Yoshimura and R. Watanabe, Elsevier Applied Science, London, p. 340-5 (1988).

21. C.K. Yoon and I-W. Chen, "Superplastic Flow of Two-Phase Ceramics Containing Rigid Inclusions -- Zirconia/Mullite Composites," *J. Am. Ceram. Soc.*, in press (1990).

22. C-M.J. Hwang and I-W. Chen, "Effect of a Liquid Phase on Superplasticity of 2m/o Y_2O_3-Stabilized Tetragonal Zirconia Polycrystals," *J. Am. Ceram. Soc.*, in press (1990).

23. W.A. Kaysser, M. Sprissler, C.A. Handwerker and J. Blendell, "Effect of a Liquid Phase on the Morphology of Grain Growth in Alumina," *J. Am. Ceram. Soc.*, **70** [5] 339-43 (1987).

24. C-W. Li and W.D. Kingery, "Solute Segregation at Grain Boundaries in Polycrystalline Al_2O_3," pp. 368-78, in *Structure and Properties of MgO and Al_2O_3 Ceramics*, Ed. W.D. Kingery, Advances in Ceramcis, Vol. 10, American Ceramic Society, Columbus, OH (1984).

25. T-S Yeh and M.D. Sacks, "Low-Temperature Sintering of Aluminum Oxide," *J. Am. Ceram. Soc.*, **71** [10] 841-44 (1988).

2.3 "Superplastic Ceramic Composites"

I-W. Chen, in Advanced Composite Materials

SUPERPLASTIC CERAMIC COMPOSITES*

I-Wei Chen, Department of Materials Science and Engineering, University of Michigan, Ann Arbor, Michigan 48109-2136

ABSTRACT

Ceramic composites offer the special advantage of microstructural stability during large strain superplastic deformation. They tend to have both a higher flow stress and local stress around reinforcing particles, especially when the aspect ratio of the inclusions is high. Thus, only equiaxed ceramic composites are amenable to superplastic forming at the present time.

INTRODUCTION

Superplasticity is phenomenologically defined as the ability of a material to exhibit exceptionally large tensile elongation during stretching.[1-2] It is a property commonly found in many metals and alloys when the grain size is refined below several microns and the deformation temperature is above two-thirds of the melting point.[2] At such small sizes micrograins can flow, much like sand particles in a water-saturated slip, by way of atomic diffusion along grain boundaries.[1,3-7] These materials intrinsically embody a high resistance to strain localization, or necking, in tensile deformation because necking necessarily entails a higher local strain rate and thus a higher local flow stress, which will be resisted by the rest of the body.[3,8] Several commercial processes in metal industries have taken advantage of these high ductilities to form intricate, large scale components directly into their net shape.[7,9-10]

Compared to monolithic ceramics, composites have the distinct advantage of superior microstructural stability against both static and dynamic grain growth. The as-sintered composites usually have a smaller grain size, even though they may require a higher sintering temperature than the monolithic ceramics made of either constituent. In particular, a duplex microstructure can be obtained, i.e., one in which two phases are of nearly equal volume fraction and are both multiply connected. Known for their fine grain sizes and excellent resistance against coarsening, many such microstructures have figured prominently in the

* Supported by U.S. AFOSR under Grant No. 87-0289, U.S. DOE (BES) under Grant No. DE-FG02-87ER45302, and U.S. ARO under Contract No. DAAL03-89-K0133.

historical development of superplastic metallic alloys (e.g., Pb-Sn and Zn-Al alloys, α-β brass, α-β titanium alloys, and α-γ stainless steel).[2] Duplex microstructures have also been obtained for zirconia/mullite and zirconia/alumina composites. These duplex composites can maintain their very fine microstructures even after large superplastic deformation.

In this paper, we will briefly review the current understanding of microstructural control and deformation mechanisms of superplastic ceramic composites. Our attention will be directed to ceramic composites containing two dissimilar phases, specifically, zirconia/alumina and zirconia/mullite systems. Composites made of different polymorphs of the same ceramics, such as tetragonal and cubic zirconia or α'- and β'-sialons, are not considered here.

MICROSTRUCTURAL ASPECTS

In developing superplastic ceramics, high deformation rate and high ductility are the primary objectives. Practical considerations further dictate that they should be achievable at the lowest temperature possible. The basis of materials considerations concerning a high deformation rate and a low deformation temperature lies in the constitutive equation of superplastic flow, which can be expressed in the following form:[2]

$$\dot{\varepsilon} = A\,\sigma^n/d^p \qquad (1)$$

In the above, $\dot{\varepsilon}$ is the strain rate, σ is the stress, d is the grain size, n and p are stress and grain size exponents, respectively, and A is a temperature-dependent, diffusion-related coefficient which can be expressed in an Arrhenius form. For superplastic ceramics, n and p are typically in the range between 1 and 3. Therefore, a high deformation rate and a low deformation temperature can be achieved by lowering grain size. Additional care must be taken to ensure that the fine-grained microstructure remains stable under superplastic deformation, i.e., to prevent dynamic grain growth from taking place, and to keep the grain boundaries' cohesive strength sufficient in order to sustain high ductility without fracture. Tetragonal zirconia polycrystal (TZP), which fulfills all the above requirements,[11] may be regarded as a prime example of a superplastic ceramic.

To investigate the formability of ceramics containing two dissimilar phases, composites of zirconia/alumina[12-13] and zirconia/mullite[14-15] have been studied throughout the entire range of composition. Y-TZP with up to 80 v/o of alumina or mullite are superplastic and have very good formability.[11,16] Among them, composites with a duplex microstructure (i.e. when both phases have approximately the same volume fractions) have the finest grain size and

often the lowest flow stress. Examples of the duplex microstructures of zirconia/alumina and zirconia/mullite are shown in Fig. 1. They have a grain size of 0.2 μm. Sintered in the temperature range of 1370 to 1480°C, these duplex composites can maintain their very fine microstructures even after large superplastic deformation.

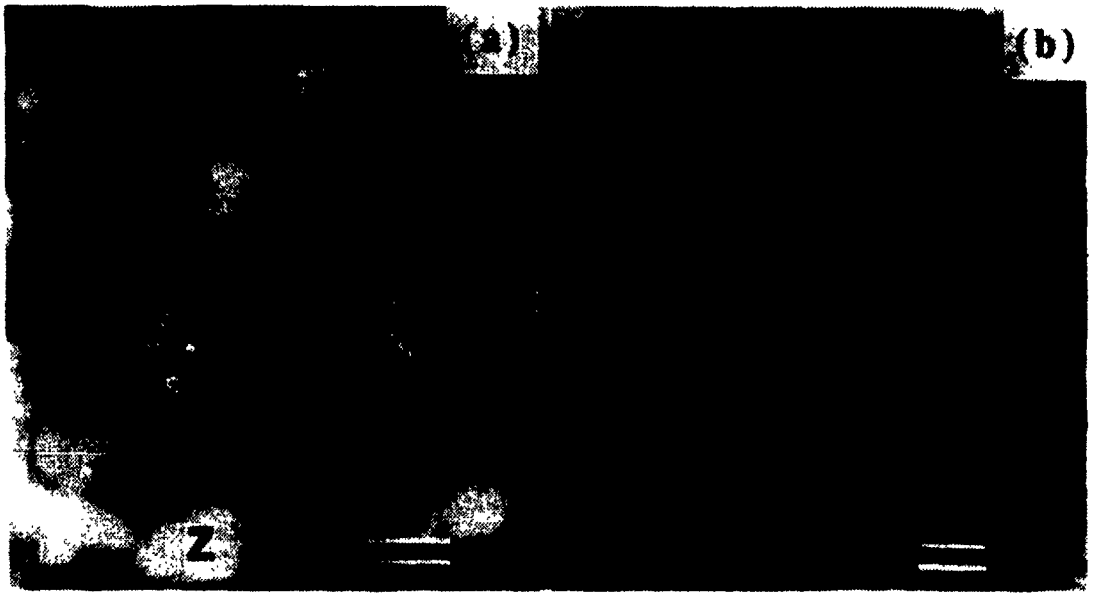

Figure 1 Microstructure of (a) Y-TZP/alumina composite and (b) Y-TZP/mullite composite. (Bar = 0.2 μm)

Considerable microstructural stability is already evident when the second phase is present at a small volume fraction, typically no more than 10%. This improvement is especially important for dynamic grain growth. A striking example is encountered in alumina with zirconia inclusions. While fine-grained pure alumina is subject to rapid dynamic grain growth, its grain size remains largely stable during superplastic deformation when 10 v/o ZrO_2 is added.

The basic issue of microstructural stability of composites was first addressed by Zener [17] and was attributed to the particle pinning effect. Superplastic ceramic composites offer an opportunity to re-examine this effect in ultrafine-grained ceramics. Let the matrix grain size be d, the particle size be r, and the volume fraction of the second phase be v. The data from fine-grained zirconia/mullite and zirconia/alumina, for a volume fraction of the second phase between 1 and 15%, are then found to follow a scaling relation, as shown in Fig. 2, given by the following equation:

$$d = \alpha\, r/v^{1/3} \qquad (2)$$

where α is about 0.75. Note that Hellman and Hiller have proposed a picture to envision the scaling relationship by assuming pinning particles residing on every grain corner.[18] Since a tetrakaidecahedral grain has 24 grain corners, and each one of them is shared by four grains, it follows that there are 6 pinning particles, on average, for every grain. The correlation of Eq (1), on the other hand, implies that only 0.4 pinning particle is appropriated for every grain. In other words, the pinning condition for real materials seems to be much less stringent than those envisioned by theorists. This is indeed encouraging from a practical point of view for developing superplastic composites.

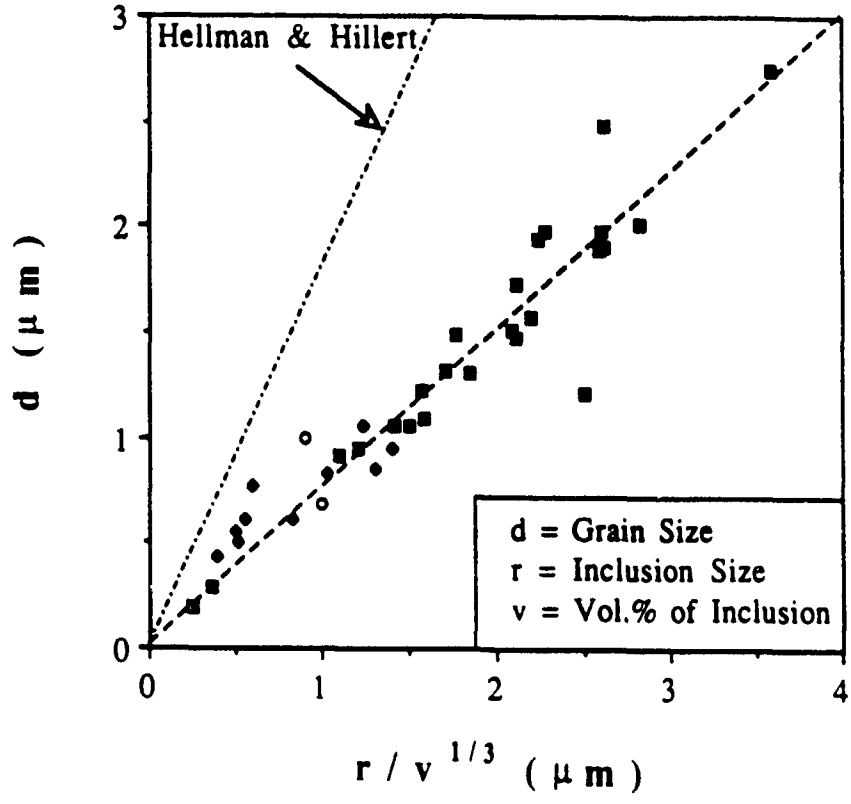

Figure 2 Grain size d as a function of inclusion size r and volume fraction of inclusion v. The symbol ♦ denotes mullite inclusion in TZP matrix; the other symbols are for zirconia inclusions in alumina matrices.

DEFORMATION CHARACTERISTICS

There is a general agreement that deformation mechanisms in superplasticity are akin to diffusional creep,[3] although modifications of the conventional description[19] are required.[4-6,20-22] The present discussion of deformation characteristics is confined to comparisons based on the phenomenological constitutive equation (Eq(1)). The effect of a second phase is rationalized based on continuum mechanics models for zirconia/mullite and zirconia/alumina

composites. In both cases, there is little mutual solubility between constituent phases at the sintering and deformation temperatures. Therefore, their deformation resistance may be determined entirely by knowing the deformation resistance of the constituent phases, after computing the appropriate stress and strain distributions in the composite.[6] The two ceramic composites considered here serve as model systems of a soft matrix (TZP) containing equiaxed and rigid inclusions (mullite and alumina).

At 1350°C, the flow stress of mullite is two orders of magnitude higher than that of 2Y-TZP of a comparable grain size.[14-15] Hence, mullite inclusions in 2Y-TZP can be considered rigid. For such a composite, a continuum model which pictures the composite flow as a non-newtonian fluid containing rigid particulates is appropriate.[6,14] The prediction of this rheological model is:

$$\dot{\varepsilon} = \dot{\varepsilon}_o \, (1-v)^{2+n/2} \tag{3}$$

where v is the volume fraction of the rigid inclusions, $\dot{\varepsilon}_o$ is the strain rate of the reference matrix, taken as the one with an identical grain size but without inclusions, and $\dot{\varepsilon}$ is the strain rate of the composite. Experimental data for 2Y-TZP containing up to 80 v/o mullite, shown in Fig. 3, are in very good agreement with this model if mullite is considered to be a rigid, included phase. Note that the model apparently remains applicable at a suprisingly high volume fraction of a second phase.

Deformation data for 3Y-TZP containing up to 70 v/o alumina, also shown in Fig. 3, are equally well described by the rigid inclusion model. This is surprising, too, since pure alumina has a deformation resistance comparable to that of 3Y-TZP. This apparent contradiction becomes explicable if we recall that even a little zirconia impurity (1000 ppm) can severely reduce the deformation rate of alumina.[22] Therefore, although pure alumina is no harder than 3Y-TZP in creep resistance, alumina in a zirconia matrix should nevertheless behave rather like rigid inclusions, consistent with the data in Fig. 3. The continuum rheological model with rigid, equiaxed inclusions has thus been verified in superplastic flow of Y-TZP with both mullite and alumina as a second phase.

The particle shape effect of non-equiaxed, hard inclusions on superplastic flow has also been considered in the literature.[14] When the alumina-to-silica ratio in mullite is decreased to 1.25 an elongated morphology for mullite with an average

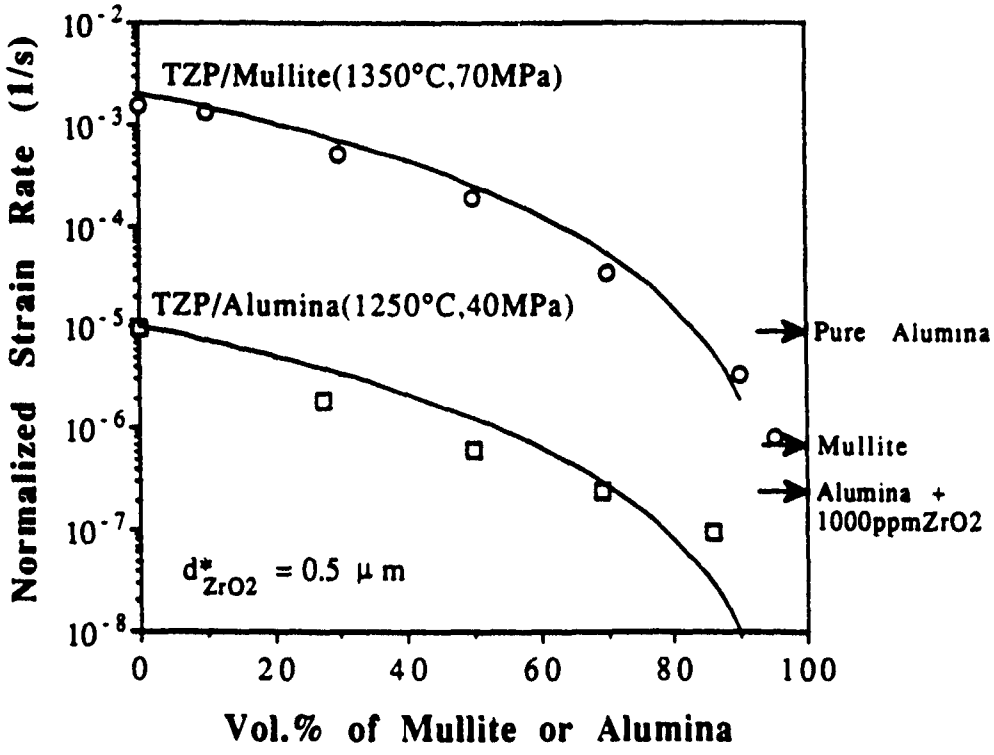

Figure 3 Strain rate as a function of volume fraction of mullite or alumina in two TZP matrices deformed at the same flow stress. Strain rate data have been normalized to account for the grain size dependence with respect to a reference matrix grain size $d^* = 0.5\ \mu m$. Also indicated on the right are the strain rate of pure alumina, mullite, and alumina with 1000 ppm zirconia, all at a comparable grain size. Two solid curves are predictions of the rheological model assuming that mullite and alumina form rigid equiaxed inclusions. Data for TZP/mullite are from Ref. 15, and for TZP/alumina from Refs. 12 and 13.

aspect ratio of 5 can be obtained in a zirconia/mullite composite. Such elongated hard inclusions act as short fibers in a soft matrix to strengthen the composite considerably. Using a shear-lag analysis, we have evaluated the strengthening effect and expressed the flow equation as

$$\dot{\varepsilon} = \dot{\varepsilon}_o (1 - v)^{1 + (1 + n/2)A} \qquad (4)$$

for parallel fibers and

$$\dot{\varepsilon} = \dot{\varepsilon}_o (1 - v)^{1 + (1 + n/2)(2/3 + A/3)} \qquad (5)$$

for random fibers. In the above, A is the fiber aspect ratio (length/radius). These predictions are plotted in Fig. 4 for various cases of interest. Experimental evidence for this fiber strengthening effect was reported elsewhere.[14] Considerable stress concentrations, which increase linearly with the aspect ratio, are also predicted by this analysis.

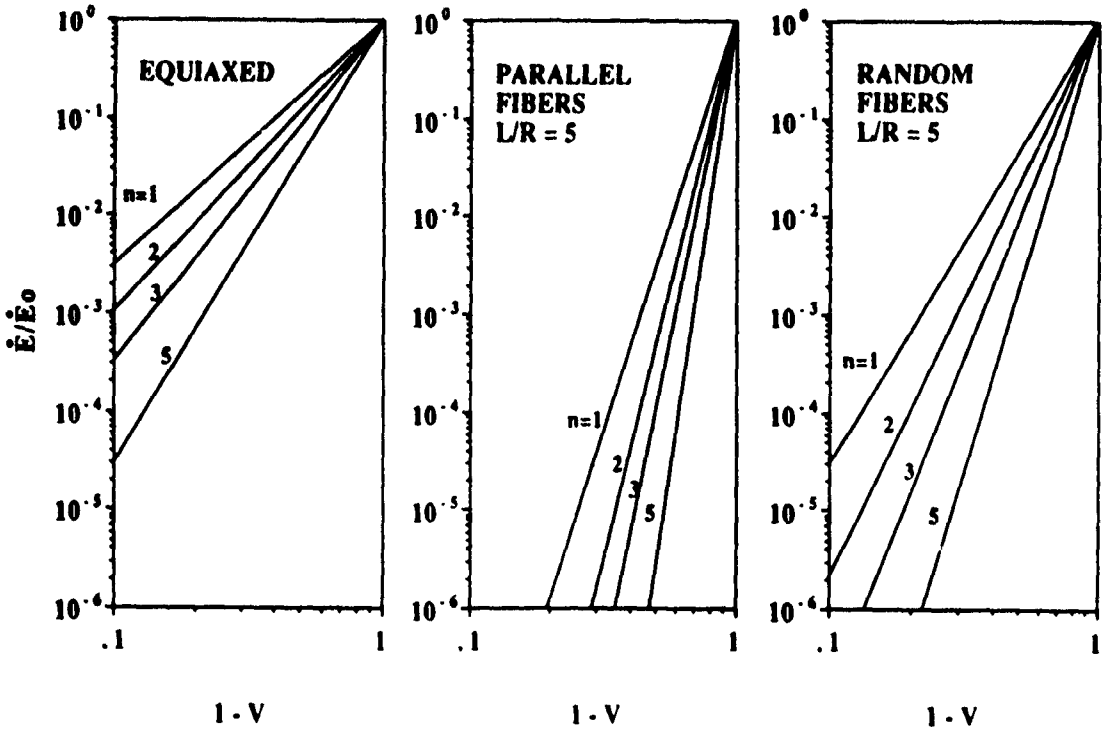

Figure 4 Strain rate reduction factor, $\dot{E}/\dot{E}_o$ as a function of volume fraction of inclusions (fibers), v.

As mentioned in the previous section, the presence of a second phase may substantially stabilize an ultrafine-grained microstructure against static and dynamic grain growth. Since less than 10 v/o of a second phase is needed for this purpose, the anticipated hardening effect according to the continuum picture of Eq (3) is rather mild. Nevertheless, a dramatic change of stress-strain curve does result from the suppression of dynamic grain growth, which would otherwise cause strain hardening. An excellent example is afforded by comparing alumina and alumina/zirconia composites, see Fig. 5. At 10 v/o zirconia addition, the dynamic grain growth and the accompanying strain hardening is entirely suppressed.

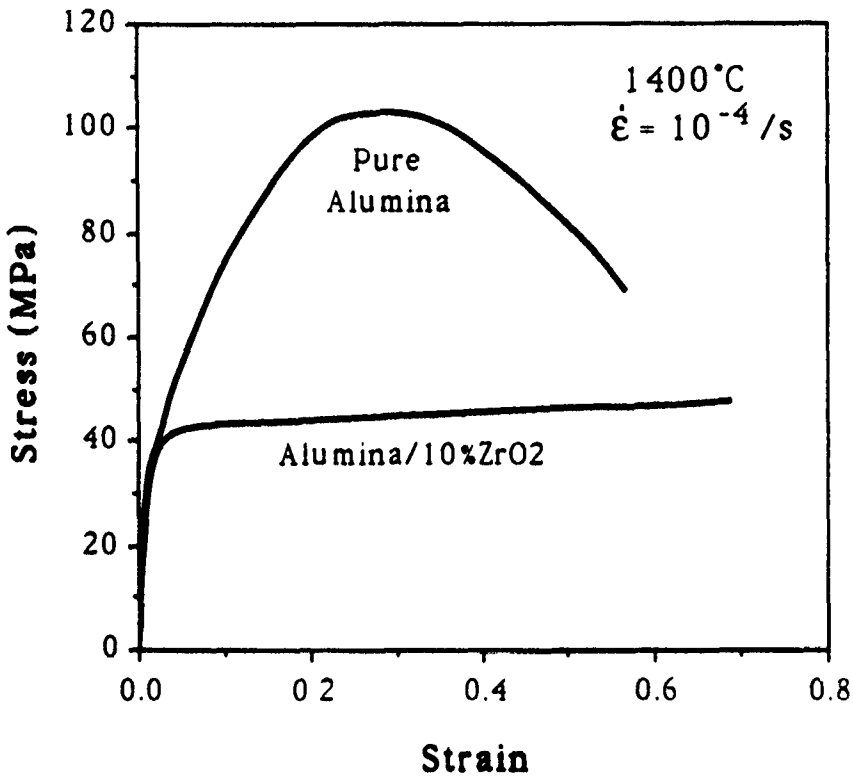

Figure 5 Stress-strain curves for alumina. Strain hardening in pure alumina is due to dynamic grain growth. The eventual decrease in stress in pure alumina is a result of cavitation.

SUPERPLASTIC FORMING

To evaluate formability of superplastic ceramics, a punch-stretching test has been developed.[24] This test was initially developed by metallurgists for evaluating sheet formability of metals at room temperature.[25] Both mechanical and practical considerations have established that such a test is more severe and informative than the conventional tensile test for the above purpose, at least for sheet forming processes.[3,25] In this test, an initially flat ceramic disk was punched at high temperature into a hat shape. The disk was supported at the rim and was stretched over a hemispherical punch of a radius of 6.5 mm. Typically, the punch was advanced until a bulged dome of a height equal to the punch radius was formed. At this point, the surface area of the dome was approximately twice that of the base, corresponding to a biaxial engineering strain of 100%. The average strain rate is simply τ^{-1}, where τ is the total forming time. For a typical forming time of 30 min. in the laboratory, the average forming strain rate is 5.5×10^{-4}/s.

Fig. 6 shows two superplastically punch-stretched zirconia/mullite, zirconia/alumina composites with their approximate forming temperatures and times indicated. Generally, the required forming time increases with lower forming temperatures. Composites with a higher alumina or mullite content require a higher forming temperature. Excellent, glossy surface finish was obtained in all the zirconia-rich composites. The surface appearance was less glossy when the zirconia content was less than 20 v/o.

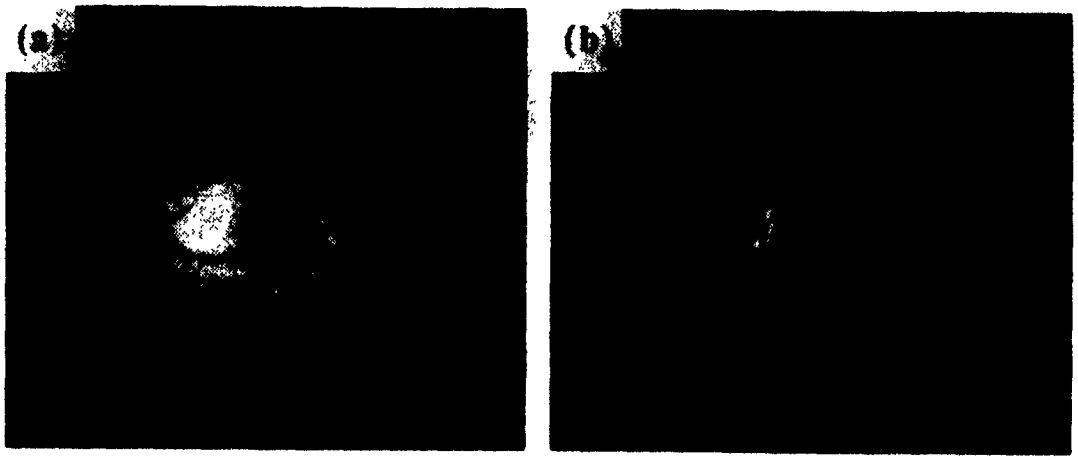

Figure 6 Punch-stretched (a) Y-TZP/alumina composite and (b) Y-TZP/mullite composite.

Wakai et al. have previously noted that, in the case of alumina/3Y-TZP composites, the average alumina grain size correlates poorly with ductility, but the size of the largest alumina grain does well.[26] This observation seems particularly explicable for alumina, which is prone to anisotropic, abnormal grain growth. Since the few large grains in an otherwise fine-grained matrix have a relatively minor influence on the average flow stress (see Eq (3)) but do cause considerable stress concentrations due to their poorer diffusional accommodation as a result of the longer diffusion distances in their vicinity, they can cause enhanced cavitation, which is detrimental to tensile ductility. Other stress-concentrating heterogeneities in ceramic composites will have a similar effect. In particular, when non-equiaxed reinforcing particulates are present, the very significant stress concentrations[14] at these particles will inevitably degrade the damage tolerance to render large tensile ductility unattainable. It is probably for this reason that no fiber, whisker, or platelet reinforced ceramic composite is superplastic to our knowledge.

CONCLUSIONS

Since the discovery of ceramic superplasticity in 1986, considerable progress in superplastic ceramics has been made in the last four years. Several ceramic composites have now been reported to be superplastic, including

zirconia/alumina, zirconia/mullite, and silicon nitride/silicon carbide. In this paper we have attempted to provide instructive examples drawn from this experience. In general, composites offer an advantage of microstructural stability against coarsening, but they tend to have a higher flow stress and local stresses around hard phases. At presentl ceramic composites containing reinforcement fibers, whiskers, or platelets are generally not amenable to superplastic forming.

ACKNOWLEDGEMENT

Unpublished data and figures, provided by S.L. Hwang, L.A. Xue and X. Wu, are gratefully acknowledged.

REFERENCES

1. C.E. Pearson, "The Viscous Properties of Extruded Eutectic Alloys of Lead-Tin and Bismuth-Tin," *J. Inst. Met.*, **54** [1] 111 (1934).

2. J.W. Edington, K.N. Melton and C.P. Cutler, "Superplasticity," *Progress in Materials Science*, **21** [2] 61-170 (1976).

3. W.A. Backofen, Deformation Processing, Addison-Wesley Publishing Company, Reading, MA, Chap.10, pp.199-226 (1972).

4. M.F. Ashby and R.A. Verrall, "Diffusion-Accommodated Flow and Superplasticity," *Acta Metall.* **21**, 149-163 (1973).

5. R.C. Gifkin, "Grain Boundary Sliding and Its Accommodation During Creep and Superplasticity,"*Metall. Trans.*,7A [8] 1225-1232 (1976).

6. I-W. Chen, "Superplastic Flow of Two-Phase Alloys," in Superplasticity, Eds. B. Baudelet and M. Suery, Centre National de la Recherche Scientifique, Paris, France, Chap. 5, pp. 5.1-5.20 (1985).

7. J. Pilling and N. Ridley, Superplasticity in Crystalline Solids, Institute of Metals, London, (1989).

8. E.W. Hart, "Theory of the Tensile Test," *Acta Metall.*, **15** [2] 351-55 (1967).

9. N.E. Paton and C.H. Hamilton, Superplastic Forming of Structural Alloys, Eds., The Metallurgical Society of AIME, Warrendale, PA, p. 257-71 (1982).

10. M. Kobayashi and F. Wakai, Superplasticity, MRS Conference Proceedings, Int'l. Mtg. on Adv. Mater. v. 7, Materials Research Society, Pittsburg, PA (1989).

11. I-W. Chen and L.A. Xue, "Development of Superplastic Structural Ceramics," *J. Am. Ceram. Soc.*, **73** [9] 2585-2609 (1990).

12. F. Wakai, Y. Koidama, S. Sakaguchi, N. Murayama, H. Kato and T. Nagano, "Superplastic Deformation of ZrO_2/Al_2O_3 Duplex Composites," in Superplasticity, MRS Int'l. Mtg. on Adv. Mater., Eds. M. Doyama, S.S. Somiya, R.P.H. Chang, M. Kobayashi and F. Wakai, Materials Research Society, Pittsburgh, PA, v. 7, pp. 259-266 (1989).

13. F. Wakai, "A Review of Superplasticity in ZrO_2-Toughened Ceramics," *Br. Ceram. Trans. J.*, **88** [6] 205-8 (1989).

14. C.K. Yoon and I-W. Chen, "Superplastic Flow of Two-Phase Ceramics Containing Rigid Inclusions—Zirconia/Mullite Composites, *J. Am. Ceram. Soc.*, **73** [6] 1555-65 (1990).

15. C.K. Yoon, "Superplastic Flow of Mullite/2Y-TZP Composites," Ph.D. Thesis, Department of Materials Science and Engineering, University of Michigan (1990).

16. X. Wu, "Deformation Processing of Ceramics," Ph.D. Thesis, Department of Materials Science and Engineering, University of Michigan (1990).

17. C. Zener, "Private Communication to the Author," see C.S. Smith, "Grains, Phases and Interfaces: an Interpretation of Microstructure," *Trans. AIME* , **175**, 15-51 (1948).

18. P. Hellman and M. Hillert, "On the Effect of Second-Phase Particles on Grain Growth," *Scand. J. Met.*, **4** [5] 211-9 (1975).

19. W.D. Kingery, H.K. Bowen and D.R. Uhlmann, Introduction to Ceramics, p. 240, John Wiley and Sons, New York (1976).

20. A. Ball and M.M. Hutchinson, "Superplasticity in the Aluminum Zinc Eutectoid," *Metal Sci. J.*, **3** [1] 1-7 (1969).

21. A.K. Mukherjee, "The Rate Controlling Mechanism in Superplasticity," *Mat. Sci. Eng.*, **8** [2] 83-89 (1971).

22. E. Arzt, M.F. Ashby and R.A. Verrall, "Interface Controlled Diffusional Creep," *Acta Metall.*, **31** [12] 1977-89 (1983).

23. F. Wakai, T. Iga and T. Nagano, "Effect of Dispersion of ZrO_2 Particles on Creep of Fine-Grained Al_2O_3," *J. Ceram. Soc. Japan*, **96** [12] 1206-9 (1988).

24. X. Wu and I-W. Chen, "Superplastic Bulging of Fine-Grained Zirconia," *J. Am. Ceram. Soc.* **73** [3] 746-9 (1990).

25. S.S. Hecker and A.K. Ghosh, "The Forming of Sheet Metal," *Scientific American*, November, 100-109 (1976).

26. T. Kuroishi, K. Uno and F. Wakai, "Characterization of Superplastic ZrO_2-Toughened Al_2O_3 Prepared by Slip Casting," in Superplasticity, Vol. 7, *MRS Int'l Mtg. on Adv. Mats.*, Eds. M. Doyama, S.S. Somiya, R.P.H. Chang, M. Kobayashi and F. Wakai, Materials Research Society, Pittsburgh, Pa, v. 7, p. 267-74 (1989).

III. TAILORING GRAIN BOUNDARY MOBILITY

Tetragonal zirconia is the first superplastic ceramic ever reported. Its grain size of 0.3 μm in Y-TZP is unusually easy to achieve by conventional sintering techniques. Moreover, this grain size is rather stable during large deformation at elevated temperatures. Such a remarkable microstructural stability has not been fully explained in fundamental terms prior to the research of this project. By a set of systematic experiments, we were able to conclude that the observation is a classic example of space-charge solute drag on grain boundary. Indeed, this provides a definitive example of solute drag in oxide ceramics. Moreover, we demonstrated that a one-to-one correspondence between the deformation behavior (e.g., stress-strain curve) and the grain boundary mobility exists (see 2.1) and that both can be tailored by switching on a certain amount of solute drag. The latter controls the grain boundary mobility and thus affects dynamic grain growth which in turn impacts the flow stress.

3.1 "Sintering and Grain Growth in Tetragonal and Cubic Zirconia"

I.G. Lee and I-W. Chen, in Sintering '87, Proceedings of 4th International Symposium on Science and Technology of Sintering

SINTERING AND GRAIN GROWTH IN TETRAGONAL AND CUBIC ZIRCONIA

I.G. Lee and I-Wei Chen
Department of Materials Science and Engineering
The University of Michigan
Ann Arbor, Michigan 48109-2136

ABSTRACT

The different sinterability of tetragonal and cubic zirconia can be attributed to their different behavior of grain growth. Growth rate of cubic grains in 8 m/o Y_2O_3-ZrO_2 was found to be 30 to 250 times faster than that of tetragonal grains in 2 m/o Y_2O_3-ZrO_2. Although grain growth in both materials follows the parabolic law, the activation energy is 105 Kcal/mole for the tetragonal zirconia and 69 kcal/mole for the cubic zirconia. Measurements of dihedral angles revealed a larger grain boundary energy in the cubic phase than in the tetragonal phase. The possible origins of their different behavior are discussed.

INTRODUCTION

In order to achieve full densification, excessive grain growth has to be suppressed in firing. Experience with zirconia systems has provided ample evidence that the grain size of the cubic phase is much larger than that of the tetragonal phase, suggesting the possibility of a lower sintered density in the cubic phase regime. Indeed, this is confirmed in many zirconia systems. As an example, Fig. 1 shows the compositional dependence of sintered densities of ZrO_2-Y_2O_3 and ZrO_2-In_2O_3 ceramics. The decreased densities in the cubic phase are quite evident for both. Examinations of the sintered microstructures revealed large cubic grains containing intragranular pores in the cubic phase regime. Thus the role of grain growth in sintering of zirconia ceramics appears to be a classical one: a faster grain growth causes pore detachment from grain boundaries, preventing full densification. To afford a better control of sintering of these ceramics, it is clearly necessary to understand the mechanistic origin of the large disparity of grain growth in the two zirconia phases. The purpose of this paper is to report on the grain growth kinetics and grain boundary characteristics for both tetragonal and cubic zirconia, and to provide a rationale for their different behavior.

EXPERIMENTAL

Coprecipitated zirconia powders containing 2 to 8 m/o Y_2O_3 were used in this study. Pellets were sintered between 1300°C and 1700°C in air for various time. Grain sizes were measured by the linear intercept method, with the reported values being 1.56

sintering. The activation energies were not determined, since they will be affected by the activation energy of densification. The latter has been reported to be around 96 Kcal/mole for CaO stabilized cubic zirconia (13 m/o CaO).[1]

DISCUSSIONS

Our results on both tetragonal and cubic zirconia demonstrate that both undergo normal grain growth in the temperature range studied. The activation energy of the tetragonal phase is higher than the cubic phase. Although there has been no systematic report on grain growth of tetragonal zirconia in the literature to the authors' knowledge, our findings on cubic zirconia are consistent with a previous study of CaO stabilized cubic zirconia (16 m/o CaO) which gave a growth exponent of 0.4 and an activation energy of 80 Kcal/mole.[2]

Two considerations of normal grain growth are (a) driving force and (b) mobility of grain boundaries. The dihedral angle measurements have established that the driving force for grain growth is the largest for cubic zirconia, intermediate for cubic or tetragonal grains in a mixed-phase matrix, and smallest for an entirely tetragonal zirconia. Although this aspect is consistent with the contrasting grain sizes of the two phases in all three types of microstructures, it can not be the sole reason for the much faster growth rate in the cubic phase. Our data indicate that a difference of up to 250 times is seen in the rate constant K, yet grain boundary energies differ by less than a factor of 2. Further explanation must be sought elsewhere to explain the grain growth behavior.

It appears that the mobility of the cubic grains is much higher than that of the tetragonal grains. One possibility is that the boundary diffusivity of the cubic grains is higher. This can be explained by referring to the theory of Borisov *et al.*[3]which couples the thermodynamic consideration to grain boundary diffusion,

$$\gamma_b = A\,RT\,\ln(D_b/D_l) \qquad (5)$$

In the above, γ_b is the boundary energy, D_b is the boundary diffusivity, D_l is the lattice diffusivity, A is a geometric constant related to the atomic area on the grain boundary and to the jump statistics, and RT has its usual meaning. This model has been verified in many metallic alloys[4] and at least in one ceramic system (i.e. yttria-doped alumina)[5]. Hence a lower boundary energy is predicted to be accompanied by a lower boundary diffusivity and a higher activation energy. This prediction is consitent with our data, if we assume a proportionality between K and boundary diffusivity.

The large difference in grain boundary energies and diffusivities in the two phases could be due to a different behavior of solute segregation in the two materials. For example, an enrichment of yttrium on the tetragonal boundary but not on the cubic boundary can generate such an effect. Indeed, for certain solutes which segregate over a longer spatial extent, it is expected that boundary mobility may be controlled by solute drag, which involves lattice diffusion. The activation energy for grain growth in tetragonal zirconia is 105 Kcal/mole, which is comparable to that of self diffusion of yttrium cations in a yttria stabilized cubic lattice (102Kcal).[6] The activation energy of boundary diffusivity in yttria stabilized cubic zirconia is 70 Kcal/mole,[6] which is closer to the activation energy for grain growth in cubic zirconia. It should also be noted that the presence of a grain boundary glassy phase in tetragonal zirconia could decrease the apparent grain boundary energy and increase the diffusion distance across the boundary.

It is recalled that both ionic conductivity[7-8] and densification rate in hot pressing[9] exhibit a strong yttria compositional dependence in the present system. That is, both cation and anion (lattice) diffusivities increase when the yttria content increases from 5 to 8 m/o. Although this phenomenon of enhanced kinetics is pronounced and probably general in all lightly doped zirconia ,[10] its magnitude is still a factor of 3 to 10 smaller than the enhancement of the rate constants K in grain growth in the same compositional range. Nevertheless, together with the consideration of grain boundary energies, it could present an alternative rationale for the observed different growth behavior.

Concerning sintering schedule, Wu and Brook[11] suggested that fast firing to higher

times the average intercept lengths. Grain growth in initial and intermediate stage sintering was investigated at 1400°C for shorter time, using rapidly heated specimens. Dihedral angles between tetragonal and cubic phases were measured using specimens containing both phases (at 4 m/o and 6 m/o Y_2O_3).

RESULTS

Data of grain size of 2 and 8 m/o Y_2O_3 as a function of sintering time are shown in Figs. 2 and 3. Between 1300°C and 1700°C, the 2 m/o Y_2O_3 samples are entirely tetragonal; while at 8 m/o Y_2O_3, they are entirely cubic. Both sets of data obey the parabolic growth law,

$$d^2 - d_o^2 = K\,(t-t_o) \qquad (1)$$

where d is the grain size at time t, d_o is the grain size at time t_o, and K is a rate constant. The rate constant for the cubic phase is 30 times to 250 times larger than that for the tetragonal phase, reflecting a ratio of grain sizes of 5 to 10. The activation energies of the rate constants are 105 Kcal/mole for the tetragonal grain growth and 69 Kcal/mole for the cubic grain growth, as shown in Fig. 4.

Grain growth in the two phase regimes are difficult to assess quantitatively, due to the lack of compositional contrast between the two phases in scanning electron microscopy and the poor statistics for grain size measurements in transmission electron microscopy. Nevertheless, qualitatively, we were able to identify the cubic grains which always grow to larger sizes than those of the tetragonal grains. This is the case both for 4 m/o Y_2O_3, when the cubic grains are mostly surrounded by the tetragonal grains, and for 6 m/o Y_2O_3, when the cubic grains form a continuous majority matrix. Dihedral angles at triple points of two cubic grains and one tetragonal grain are related to the cubic grain boundary energy γ_{cc} and the c/t phase boundary energy γ_{tc}. This can be seen in Fig. 5a. Likewise, dihedral angles at triple points of two tetragonal grains and one cubic grain are related to the tetragonal grain boundary energy γ_{tt} and γ_{tc}, as shown in Fig. 5b. The dihedral angle θ_{cc} in Fig. 5a is smaller by about 30° than the dihedral angle θ_{tt} in Fig. 5b. Using the following relationship

$$2\gamma_{tc}\cos(\theta_{tt}/2) = \gamma_{tt} \qquad (2)$$

$$2\gamma_{tc}\cos(\theta_{cc}/2) = \gamma_{cc} \qquad (3)$$

with the dihedral angles listed in Table 1, the ratios of interfacial energies were determined.

Table 1. Measured dihedral angles

	4 m/o Y_2O_3	6 m/o Y_2O_3
θ_{tt}	134±7°	131±7°
θ_{cc}	97±11°	105±10°

Their average can be represented as the following ratios

$$\gamma_{cc} : \gamma_{tc} : \gamma_{tt} = 1 : 0.76 : 0.63 \qquad (4)$$

Grain growth in the initial and intermediate stages was also investigated.These data will be published elsewhere. At 1400°C, it was found that the densification rates of 2 m/o and 8 m/o samples are essentially the same during the initial and intermediate stage of

temperature is preferrable for sintering zirconia. Their suggestion was based on the observation that the activation energy of densification [1] is higher than that for grain growth[2] in CaO stabilized cubic zirconia.[2] While this recommendation is sound for cubic zirconia, it is not likely to be useful for tetragonal zirconia in view of the much higher activation energy of grain growth reported in this study. Indeed, our experience found that slow firing at low temperatures yielded the best results for tetragonal zirconia in most cases.

ACKNOWLEDGEMENTS

This research is supported by the US Air Force Office of Scientific Research, under Grant No. AFOSR-87-0289. We are grateful to Dr. Jie Xu for providing unpublished data on In_2O_3 stabilized ZrO_2.

REFERENCES

1. P.J. Jorgensen, in *Sintering and Related Phenomena*, p. 401, eds. G.C. Kuczynski, N.A. Hooton and C.F. Gibbon, Gordon and Breach, New York (1967).
2. T.Y. Tien and E.C. Subbarao, *J. Am. Ceram. Soc.*, **46**, 10, 489-492 (1963).
3. V.T. Borisov, V.M. Golikov, and G.V. Scherbedinskiy, *Phys. Metals Metallograph*, **17**, 80 (1964).
4. D. Gupta, *Metall. Trans.* **8A**, 1431 (1977).
5. P.Nanni, C.T.H. Stoddart, and E.D. Hondros, *Mater. Chem.*, **1**, 297 (1976).
6. Y.Oishi, K. Ando, and Y. Sakka, Advances in Ceramics, Vol.7, 208-219 (1983).
7. T.M. Dixon, L.D. LaGrange, U. Merten, C.F. Miller and J.T. Porter II, *J. Electrochem. Soc.* **110**, 276 (1963).
8. D.W. Strickler and W.G. Carlson, *J. Amer. Ceram. Soc.* **47**, 122 (1964).
9. S. Wu and R.J. Brook, *Solid State Ionics*, *14*, 123 (1984).
10. T.Y, Tien and E.C. Subbarao, J. Chem, Phys. **39**, 1041 (1963).
11. S. Wu and R.J. Brook, *Advances in Ceramics*, **12**, 693 (1984).

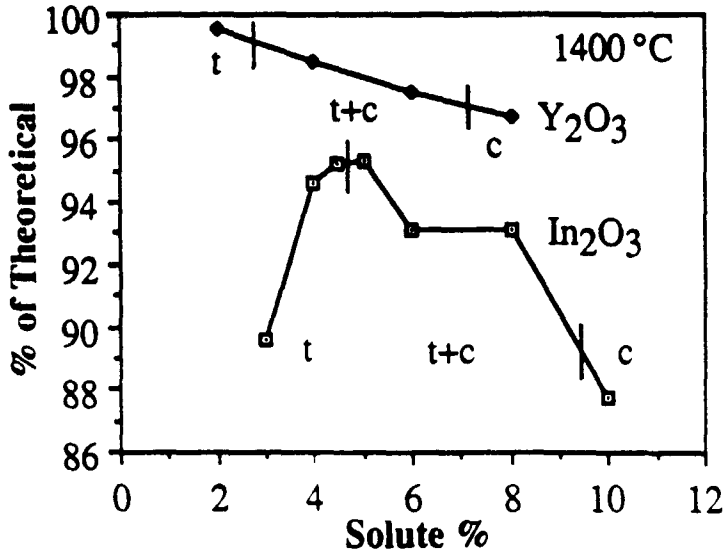

Fig. 1. Sintered density at 1400°C as a function of stabilizer content

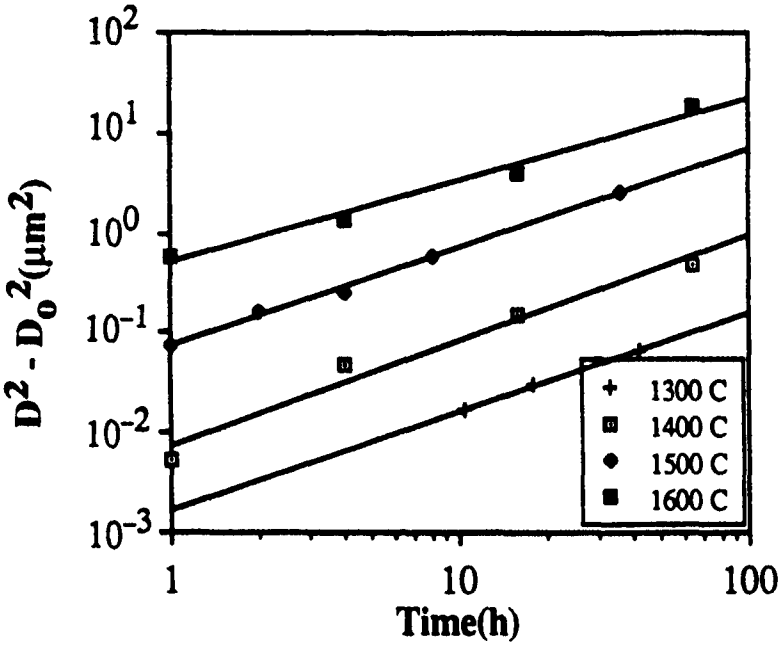

Fig. 2. Grain growth kinetic for 2 m/o Y_2O_3-ZrO_2(tetragonal)

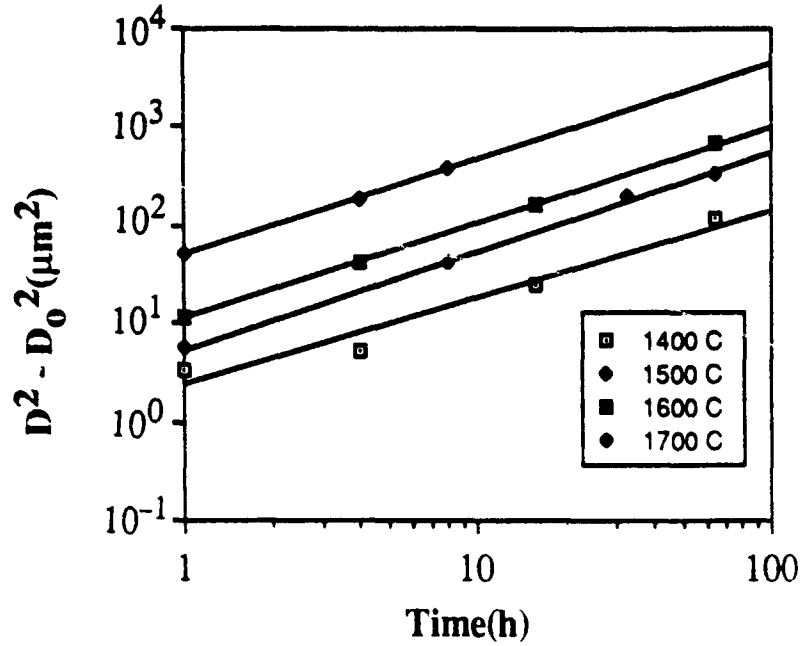

Fig. 3. Grain growth kinetics for 8 m/o Y_2O_3-ZrO_2(cubic)

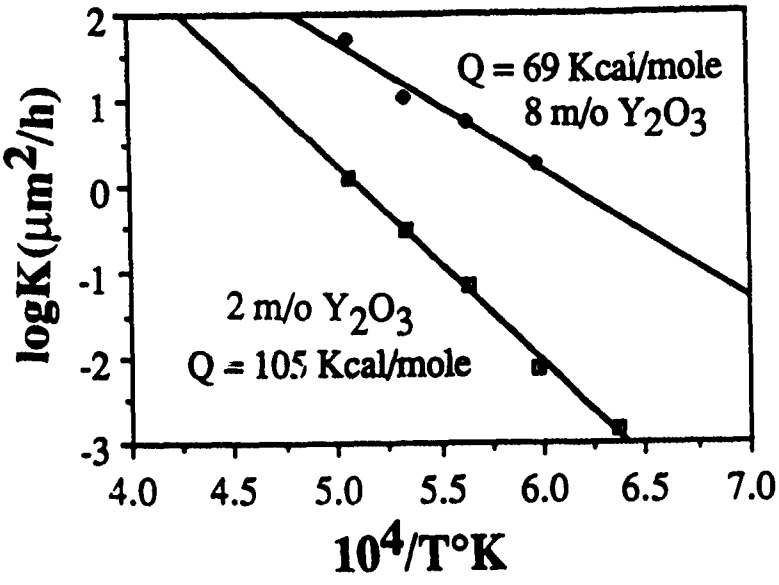

Fig. 4. Activation energies of grain growth in cubic and tetragonal zirconia

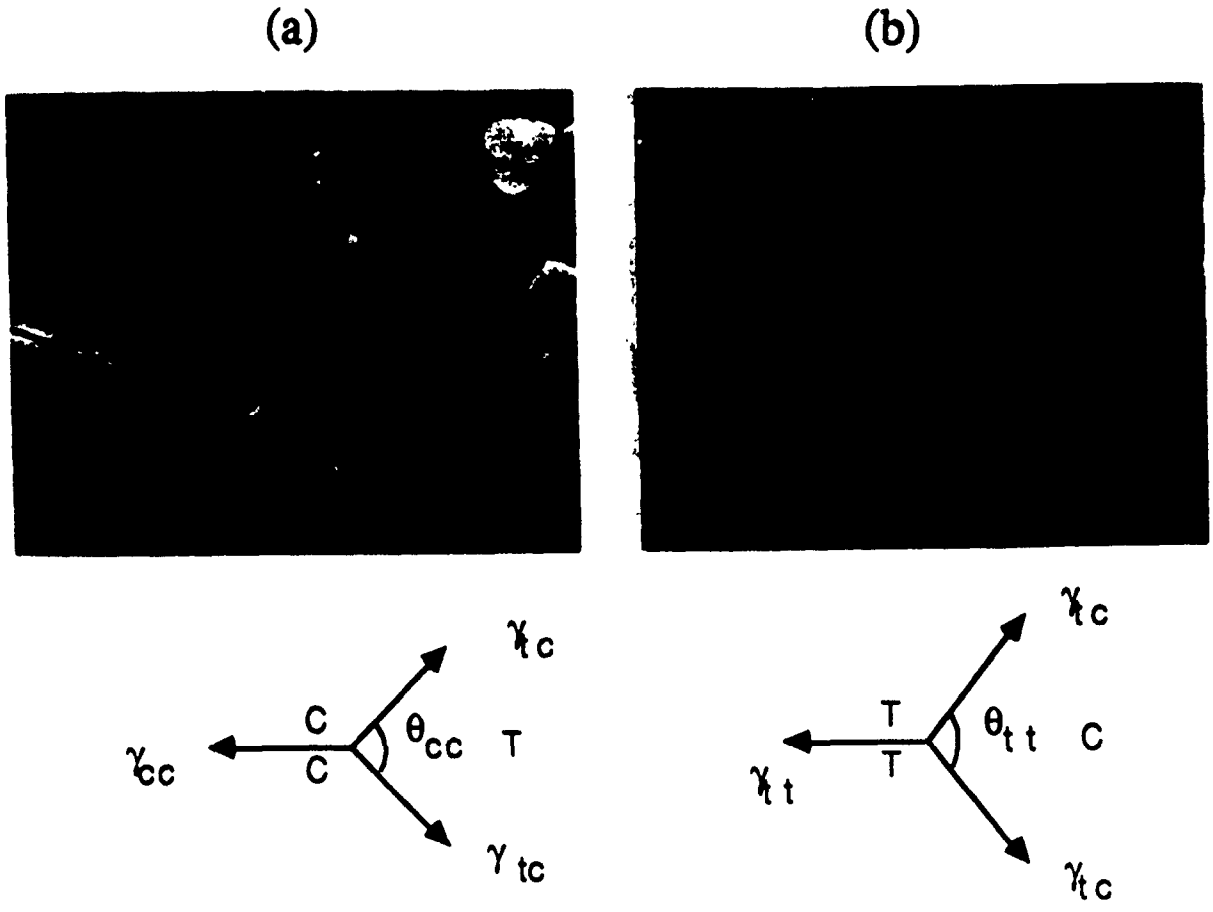

Fig. 5. Relationship between dihedral angles and interfacial energies
(a) a tetragonal grain surrounded by cubic grains in 6 m/o Y_2O_3-ZrO_2
(b) cubic grains surrounded by tetragonal grains in 4 m/o Y_2O_3-ZrO_2

3.2 "Grain Size Control of Tetragonal Zirconia Polycrystals Using the Space Charge Concept"

S.L. Hwang and I-W. Chen, *Journal of the American Ceramic Society*

Reprinted from the Journal of the American Ceramic Society, Vol 73, No 11, November 1990

journal Electronic Structure of Ceramics

J Am Ceram Soc, 73 [11] 3269-77 (1990)

Grain Size Control of Tetragonal Zirconia Polycrystals Using the Space Charge Concept

Shyh-Lung Hwang* and I-Wei Chen*

Department of Materials Science and Engineering, University of Michigan, Ann Arbor, Michigan 48109-2136

Grain growth kinetics and grain-boundary segregation of 12Ce-TZP and 2Y-TZP, containing divalent to pentavalent cationic dopants, were studied. In all cases, normal grain growth following the parabolic growth relation was observed at higher temperatures. The mobility of grain boundaries was suppressed by the addition of divalent and trivalent cations, unchanged or enhanced by the addition of tetravalent and pentavalent cations. Larger cations have a stronger effect in suppressing grain growth. From ESCA, AES, and STEM analysis of the near grain-boundary regions, it is further concluded that only divalent and trivalent cations segregate. These observations can be satisfactorily rationalized using the space charge concept and the model of impurity drag. [Key words: grain growth, tetragonal zirconia polycrystals, segregation, grain boundaries, dopants.]

I. Introduction

In the space charge theory of Frenkel,[1] later extended by Eshelby, Koehler, and their co-workers,[2,3] surfaces, grain boundaries, and dislocation cores in an ionic crystal are predicted to possess a net charge and to have a region of space charge of the opposite sign adjacent to these lattice discontinuities. While in theory the types of surface and space charges are dependent on the formation energies of point defects (vacancies and interstitials) in pure ionic crystals, it is more likely, as in almost all practical cases, that they are dictated by the effective charge of the aliovalent impurities. Physically, if dopants of a positive (negative) effective charge are present in the bulk, then the surface, in thermal equilibrium, must possess a countercharge which is negative (positive). The dopants, in turn, must segregate to the region adjacent to the surface as a space charge so that the bulk of the crystal remains essentially neutral. The role of Schottky defects is merely one which mediates the above solid "electrolyte," although any tendency toward binding between point defects and dopants to form neutral complexes can sharply reduce both the surface and the space charge.[3] Experimental evidence for the above behavior, the most definitive one being found in alkali halides, has been previously reviewed by Kingery.[4] In comparison, systematic studies of such effects in oxides have been lacking, although some limited data exist in MgO[5,6] and Al_2O_3.[7]

Tetragonal zirconia polycrystals (TZPs) are a class of distorted fluorite structure oxide ceramic which have an appreciable solubility, of the order of a few percent, for a large number of cationic dopants. The majority of such dopants are divalent and trivalent cations which also serve as tetragonal stabilizers. According to the space charge theory outlined above, they are expected to segregate to grain boundaries. If so, they may also exert a solute drag on the motion of grain boundaries. Inasmuch as grain size control is an essential tool for tailoring mechanical properties of transformation-toughened TZPs, with a direct consequence on their compressive strengths, tensile strengths, fracture toughness, superplasticity, and thermal stability, an understanding of the space charge phenomena and their relationship to grain growth is of considerable interest.

We have selected a Ce-TZP, containing 12 mol% CeO_2, as a base material and studied the effect of a number of dopants on its grain growth and segregation behavior. This base material was chosen because it remained in the single-phase tetragonal field when a small amount of dopants, ranging from divalent to pentavalent cations, were added. To gain further insight into the energetics and kinetics of the segregation and grain growth behavior, dopants of different ionic radia are contrasted. In addition, several other TZPs were studied to further verify the space charge concept.

II. Experimental Procedure

High-purity 12Ce-TZP* and oxide or carbonate powders were used as starting materials. Except where noted, dopant concentrations were fixed at 1% substitution of the total cation sites. The powder mixtures of 12Ce-TZP and the designated amount of additive oxides were attrition-milled in an alumina jar using zirconia milling media with a polyelectrolyte. The milled slurry was cast, under a pressure of up to 1 MPa, into cakes with a diameter of 47 mm, which were dried and isostatically pressed at 400 MPa. The green density after isopressing was between 60% to 65% of the theoretical density. Samples of 2Y-TZP and other TZPs were prepared similarly, except for a smaller dopant concentration of 0.6% substitution of the total cation sites when specified.

Sintering was performed in air at a constant heating rate of 10°C/min up to the desired temperatures, held there from 3 to 70 h, and then cooled in the furnace. In the case of indium additions, samples were packed in powders of the same compositions to reduce the effect of indium volatization. The density of the sintered specimen was determined by a water immersion method and the phase content was analyzed by X-ray diffractometry. For grain growth studies, only samples of a density better than 99%, and of 100% tetragonal phase, were used.

To reveal the grain boundaries, thermal etching for 5 min at 50°C below the sintering temperature was used. Grain sizes were measured on SEM micrographs by multiplying the average linear intercept of at least 500 grains by 1.5.

All the specimens could be fractured intergranularly at room temperatures. This feature allowed the use of X-ray photoelectron spectroscopy for chemical analysis (ESCA) of

D. M. Smyth—contributing editor

Manuscript No. 198024. Received October 27, 1989; approved June 15, 1990.
Supported by the Air Force Office of Scientific Research under Grant No. 87-0289.
*Member, American Ceramic Society.

*Tosoh, Tokyo, Japan, with 0.01 wt% Na_2O and 0.009 wt% SiO_2.

the grain boundaries. A Perkin-Elmer PHI 5400 ESCA† with Mg and Al targets was used. Since the ESCA signals came primarily from elements on and within a distance of 1 to 2 nm from the surface, such measurements are representative of the near grain-boundary compositions. To determine the depth distribution of the composition, argon ion beam sputtering, at 3 kV and 10 mA/mm^2, was applied to progressively remove the near grain-boundary materials. Auger electron spectroscopy (AES) was similarly performed using a JEOL JAMP 30,‡ operated at low voltages. Scanning transmission electron microanalysis (STEM) of the grain-boundary region was also performed using a JEOL 2000 FX analytical electron microscope‡ equipped with a high-angle beryllium-window XEDS detector,§ to complement the ESCA and AES analysis.

III. Results and Analysis

(1) Charge, Solubility, and Vegard's Slope

To evaluate the effect of the ionic size of dopants and the strain energy thereof, lattice constants of ZrO_2–MO_x solid solutions are required. Most data of solubilities and Vegard's slopes of the binary solid solutions in the tetragonal ZrO_2–MO_x phase field are available in the literature or from prior work in our laboratory.[10–20] When necessary, they have been checked by precision X-ray measurements in this study. These data are summarized in Table I for all the solutes studied here. The reported solubilities are for the tetragonal phase at 1300°C, and the Vegard's slopes are for the unit-cell volume at room temperature. (Despite the phase change, the unit-cell volume of both the tetragonal and the cubic phase usually follows the same correlation $\Delta V/V_0 = \alpha C$, where V_0 is the (extrapolated) volume of pure ZrO_2, C is the mole fraction of solute, and α is the Vegard's slope.[21] Thus, the data on the unit-cell volume of these two phases have been used interchangeably.) While these data may not be necessarily pertinent for phenomena occurring at other temperatures or for ternary systems, it is obvious that the solutes studied here do cover a broad range of charges, sizes, and solubilities, so that any systematic dependence of segregation and grain growth on these parameters, if it exists, should become apparent from our results. In terms of ionic sizes, among the divalent solutes, $Mg^{2+} < Ca^{2+}$; among the trivalent solutes, $Sc^{3+} < In^{3+} < Yb^{3+} < Y^{3+}$; among the tetravalent solutes, $Ti^{4+} < Zr^{4+} < Ce^{4+}$; among the pentavalent solutes, $Nb^{5+} \approx Ta^{5+}$. It is also interesting to note that both Ca^{2+} and In^{3+}, which have the smallest Vegard's slopes among aliovalent dopants, have the largest solid solubilities. On the other hand, isovalent dopants (Ti^{4+} and Ce^{4+}) all have large solubilities in ZrO_2 irrespective of sizes. Clearly, both charge and size mismatch are important considerations for tetragonal solubilities in this class of oxides. The lattice contraction in the presence of "oversized" dopants, e.g., Mg^{2+} and Sc^{3+}, is due to the oxygen vacancies they create.

(2) Grain Size and Grain Growth Kinetics

Table II illustrates the progression of grain sizes, after sintering at 1400°C for 2 h and annealing at 1420°C for 12 h, of a series of 12Ce-TZP with different dopants. Selected micrographs are shown in Fig. 1 to demonstrate the different grain sizes. The grain size increases in the following order of solutes:

$$Ca^{2+} < Mg^{2+} < Y^{3+} < Yb^{3+} < In^{3+} < Sc^{3+} < Ce^{4+}(\text{base composition}) \leq Ti^{4+} < Ta^{5+} \leq Nb^{5+}$$

A comparison of the above ranking with the data of ionic radii and charges of the solutes leads to the following observations: (a) solutes of a lower valence are correlated with smaller grain sizes; (b) solutes of a larger radius are correlated with smaller grain sizes. Within the above series, there is no exception to the above correlations.

We have obtained data of grain growth kinetics over a range of temperatures for the 12Ce-TZP doped with 1 mol% Ca^{2+}, Mg^{2+}, Y^{3+}, YB^{3+}, In^{3+}, and Sc^{3+} in order to substantiate the above observations. In addition, undoped 12Ce-TZP was also studied. We have plotted, in Fig. 2, the data of 1420°C assuming the following equation holds:

$$d^n - d_0^n = K(t - t_0) \qquad (n = 2,3) \tag{1}$$

In the above, d is the grain size, at time t, d_0 is the reference grain size at time t_0, and K is a temperature-dependent rate constant. When $n = 2$, this is the so-called normal grain growth equation. In the above we have chosen, in most cases, the reference point as the 3-h sintered one, provided the density at such time has already achieved 99%. Otherwise, a longer t_0 is chosen to ensure the same high density. On a log-log plot, a good fit to Eq. (1) should have a slope of unity. Using this criterion, we find that the parabolic law gives a better representation of the data at 1420° and 1500°C, while the cubic law seems more satisfactory at 1300°C. It is also noted that the relative order of the grain size among TZPs with different dopants remains the same throughout the temperature range studied. To make this clear, the temperature dependence of the rate constant in the parabolic law is plotted in Fig. 3, with the activation energy given next to the Arrhenius lines. A systematic decrease of the activation energy with increasing mobility is now apparent. Lastly, we note that the ranking of the solute in terms of its effect on grain size is the same as that found in Table II. For example, at 1420°C, in Fig. 2, $Ca^{2+} < Mg^{2+} < Y^{3+} < Yb^{3+} < In^{3+} < Sc^{3+} < Ce^{4+}$ (base composition).

In the theory of normal grain growth, the rate constant in Eq. (1) can be expressed as

$$K = 2M\gamma \tag{2}$$

In the above, M is the mobility of the grain boundary and γ is the grain-boundary energy. It is M, not γ, that can often be varied drastically by solute additions. Since the grain-boundary energies of these TZPs are not known, although they are not expected to vary by more than a factor of 2 to 3, we shall let $\gamma = 0.3$ J/m^2 in order to compare the mobility in doped 12Ce-TZP with data of other oxides compiled by Yan *et al.*[22] Also available are the mobility data of 2Y-TZP and 8Y cubic zirconia published recently by our group.[8] These data are shown in Fig. 4, in which T_m, the melting temperature, has been used for temperature normalization (T_m = 2700°C for ZrO_2). Clearly, the mobility of zirconia grain boundaries covers a fairly broad range at any given temperature. For example, a 12Ce-TZP doped with 1 mol% CaO has a mobility comparable to 2Y-TZP, while the 8Y cubic zirconia has a mo-

†Perkin-Elmer, Eden Prairie, MN
‡JEOL, Tokyo, Japan
§Tracor-Northern, Middleton, WI.

Table I. Ionic Radius, Volume Misfit, and Solubility of MO_x in ZrO_2

	Ionic radius* (nm)	Vegard's slope†	Solubility (mol% MO_x)	Ref
Mg^{2+}	0.089	−0.223(c)	1	11
Ca^{2+}	0.112	0.095(c)	5	12
Sc^{3+}	0.087	−0.113(t)	6	13
In^{3+}	0.092	0.012(t)	9	13
Yb^{3+}	0.099	0.067(t)	5	13
Y^{3+}	0.102	0.077(t)	5	14, 15
Ti^{4+}	0.074	−0.172(c)	15	16, 17
Ce^{4+}	0.097	0.179(t)	17	18, 19
Nb^{5+}	0.074	0.041(t)		20
Ta^{5+}	0.074	0.041(t)		20

*Reference 10. All for 8-fold coordination. Ionic radius of Zr^{4+} = 0.084 nm. †$\Delta V/V_0 = \alpha C$ (α = Vegard's slope, C = solute mole fraction, V_0 = unit-cell volume of pure ZrO_2)

Table II. Grain Sizes of 12Ce-TZP + 1 mol% MO_x

	2+		3+				4+		5+	
Solute	Ca	Mg	Y	Yb	In	Sc	Ce	Ti	Ta	Nb
Grain size (μm)	1.04	1.56	1.75	1.86	2.15	2.36	2.93	3.03	3.20	3.29

bility at least an order of magnitude higher than 12Ce-TZP. It is also clear that the mobility of zirconia is not out of line with other ceramics when compared at the same homologous temperature. The activation energies and the prefactor of mobilities are listed in Table III.

(3) Solute Segregation in Ce-TZP

Direct evidence of solute segregation at the grain boundaries of 12Ce-TZP was obtained by ESCA, AES, and STEM. Typical ESCA spectra demonstrating the above are shown in Fig. 5(A), in which both the spectrum taken from the as-fractured, intergranular surfaces and that after 3-min sputtering are compared. Using this technique, we have verified the segregation of Mg^{2+}, Sc^{3+}, In^{3+}, and Y^{3+}. The level of segregation for In^{3+} is somewhat higher than the rest of the trivalent group. This was presumably due to its volatility, which would drive In^{3+} toward grain boundaries to escape therefrom. The segregation of Ta^{5+}, Nb^{5+} and Ce^{4+} was not detected. It should also be noted that Si peaks were searched for but not found in the above experiment. However, when 0.5 mol% of SiO_2 was intentionally added to 2Y-TZP, a Si^{4+} peak was detected on the grain boundary. Lastly Ca^{2+}, Yb^{3+}, and Ti^{4+} were not detected because of their low sensitivity factor or the overlapping peaks of Zr^{4+} and these elements.

Because of the low bulk solute content, a direct determination of the enrichment factor was not possible. As an alternative, the following semiquantitative analysis was performed. We normalized the dopant peaks, P_D, at the grain boundary by the host Zr peak, P_{Zr}, with the relative elemental sensitivity factor ζ taken into account in the following way:

$$S_D = C_0(P_D/\zeta_D)/(P_{Zr}/\zeta_{Zr}) \quad (3)$$

where C_0 is the bulk solute concentration (1% in most cases). In the above, integrated peak intensity was used for P_D and P_{Zr}, and the sensitivity factors were taken from Ref. 23. The enrichment factor S_D thus defined serves as an approximate index of the extent of grain-boundary segregation. The results are shown in Table IV.

We have performed a similar analysis using AES for the Ca-doped and Yb-doped 12Ce-TZP. The enrichment of Ca^{2+} can be seen in Fig. 5(B). Using the procedure above and Eq. (3), we obtained an enrichment factor equal to 5. The low-energy peak of Yb^{3+} cannot be differentiated from Zr^{4+} peaks, unfortunately, because of peak overlap. Higher-energy peaks were not possible because of surface charging problems. The AES results are also given in Table IV.

We have examined thin foil samples of Ca-doped 12Ce-TZP using STEM. The signal of Ca^{2+} was detected readily at

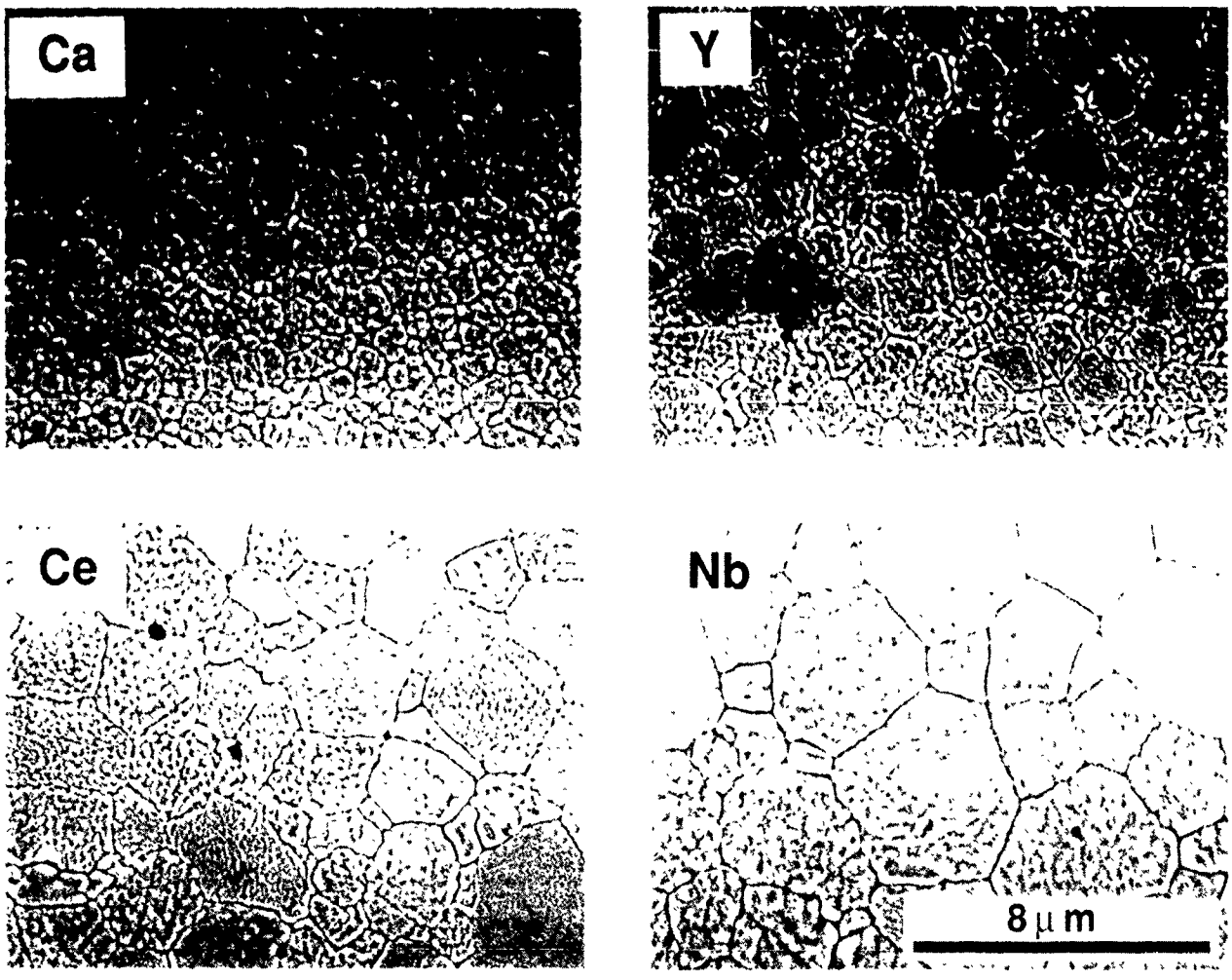

Fig. 1. Microstructure of 12Ce-TZP sintered at 1400°C for 2 h and annealed at 1420°C for 12 h, dopants indicated

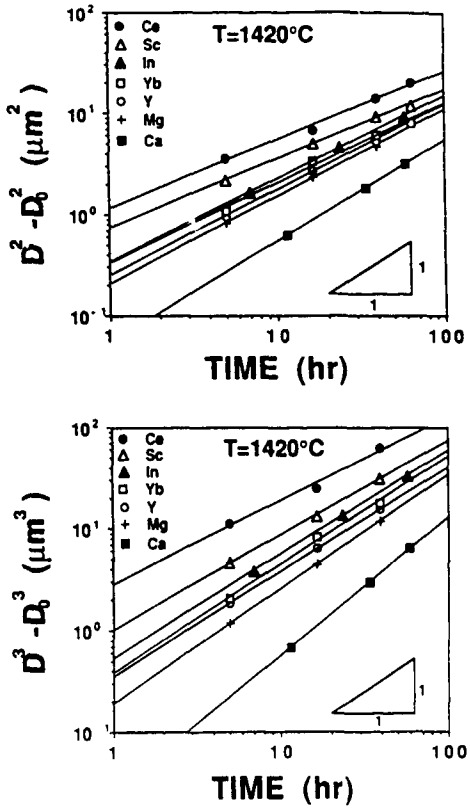

Fig. 2. Grain growth kinetics of 12Ce-TZP at 1420°C; dopants indicated.

the grain boundary, with a beam size of 5 nm, but not within the grain. It should also be noted that Si-rich pockets could sometimes be detected at the triple junctions with a 1-nm glassy layer extended into all three grain boundaries. Si peaks could be seen from microanalysis of those regions. Similar observations were made on Yb^{3+}-doped samples.

Summarizing the above data from ESCA, AES, and STEM, we find Ca^{2+}, Mg^{2+}, and In^{3+} segregate strongly, Sc^{3+} and Y^{3+} (and probably Yb^{3+}) segregate moderately, and other dopants, including Ce^{4+}, do not segregate or could not be studied. In addition, a Si-rich glassy layer exists at grain boundaries.

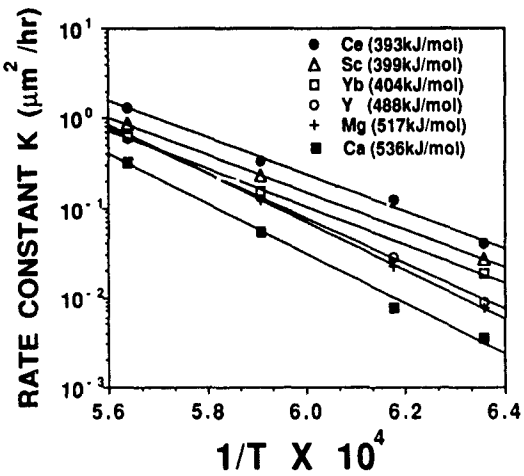

Fig. 3. Rate constant of the parabolic grain growth law against reciprocal temperature; dopants and activation energies indicated.

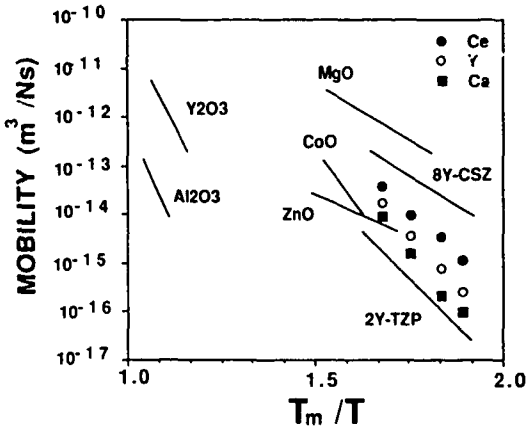

Fig. 4. Grain-boundary mobility of zirconia solid solutions and other oxides compared at the same homologous temperature. Data labeled as Ce are for 12Ce-TZP and data labeled as Y and Ca are for 12Ce-TZP with each dopant.

(4) Segregation in Other TZPs

In 2Y-TZP (containing 3.9 mol% $YO_{1.5}$), Y^{3+} was found to segregate at the grain boundary, with an enrichment ratio of 1.9 according to ESCA results. Thus, cationic dopants from divalent to pentavalent ones were added to study co-segregation of Y^{3+} and the dopants. In addition, we have studied the effect of annealing atmosphere on segregation. These results are summarized in Table V. When dopants at a concentration of 0.6% substitution of cation sites were added, we found all except Ce^{4+}, Ti^{4+}, Nb^{5+}, and Ta^{5+} segregated to the grain boundary. In the case of Ce^{4+}/Ce^{3+}, after annealing at 1300° for 1 h in argon or hydrogen, Ce^{3+} was found to segregate strongly at the grain boundary. Overall, the segregation behavior of dopants in 2Y-TZP is exactly the same as that found in 12Ce-TZP, despite the different segregation tendencies of Y^{3+} and Ce^{4+} themselves.

We have also studied two other TZPs with trivalent stabilizers. These are a Sc-TZP with 6.2 mol% $ScO_{1.5}$ and an In-TZP with 8.6 mol% $InO_{1.5}$. In both cases, segregation of the trivalent stabilizers at grain boundaries was detected by ESCA. These results are also summarized in Table V.

(5) Concentration of Dopant

Since Ca^{2+} appears to be the most potent dopant for suppressing grain growth, it is of practical interest to examine the effect of Ca^{2+} concentration. We have measured the rate constant K in Eq. (1), for $n = 2$, at 1420°C for several Ca^{2+} concentrations. As shown in Fig. 6, the rate constant decreases monotonically with Ca^{2+} concentration between 0 and

Table III. Grain-Boundary Mobility M of Zirconia Solid Solution*

Composition (solution in mol%)	M_0 (m^3/(N s))	Q (kJ/mol)
$12CeO_2$	1.34×10^{-2}	393
$12CeO_2$, $1ScO_{1.5}$	1.29×10^{-2}	399
$12CeO_2$, $1YbO_{1.5}$	1.31×10^{-2}	404
$12CeO_2$, $1YO_{1.5}$	4.19	488
$12CeO_2$, 1MgO	30.5	517
$12CeO_2$, 1CaO	51.7	536
$3.9YO_{1.5}$ (2Y-TZP)	2.24×10^{-2}	445
$14.8YO_{1.5}$ (8Y-CSZ)	3.74×10^{-5}	284

*$M = M_0 \exp(-Q/RT)$

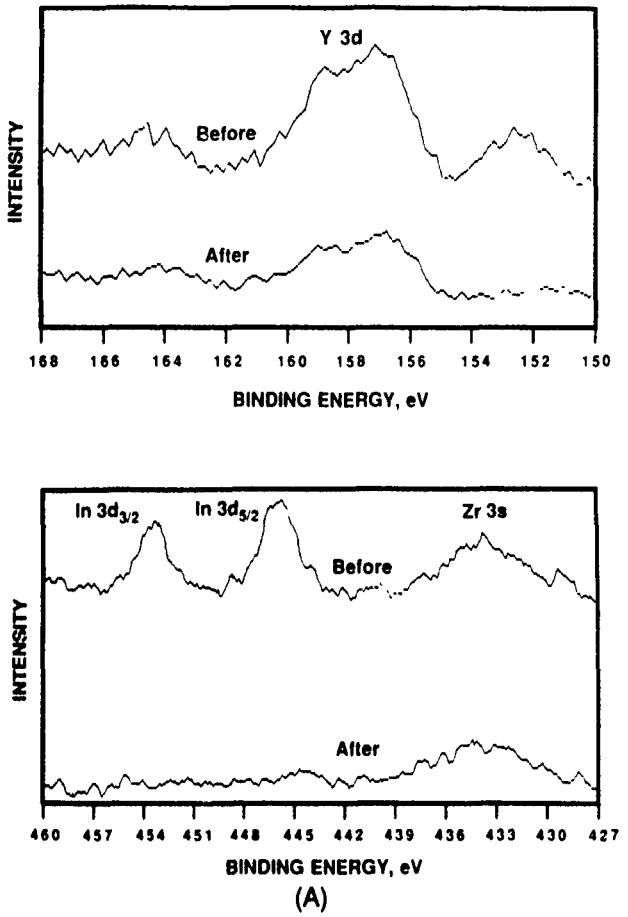

Fig. 5. (A) ESCA spectra of two intergranularly fractured 12Ce-TZP doped separately with Y and In. Spectra after argon ion sputtering also shown. (B) AES spectra of intergranularly fractured 12Ce-TZP doped with Ca. Spectrum after argon ion sputtering also shown.

Table IV. Solute Segregation at 12Ce-TZP Grain Boundaries

Solute	Enrichment factor C_{gb}/C_{bulk}	Method
Ca	5	Auger
Mg	6.5	ESCA
Y	2	ESCA
Sc	2.3	ESCA
In	7.8	ESCA

Table V. Solute Segregation at t-ZrO_2 Grain Boundaries

Solute (mol%)	Enrichment factor C_{gb}/C_{bulk}
$3.9YO_{1.5}$	1.9
$3.9YO_{1.5}$, 0.3MgO	1.9 (Y), 6.0 (Mg)
$3.9YO_{1.5}$, $0.3CeO_2$	1 (Ce)
$3.9YO_{1.5}$, $0.3CeO_{1.5}$	>10 (Ce)*
$6.2ScO_{1.5}$	2.0
$8.6InO_{1.5}$	4.5

*In hydrogen.

1 mol%. Thus, it is verified that the effect of Ca^{2+} increases with its concentration. At concentrations higher than 1 mol%, the two-phase field of tetragonal and cubic phases was entered. For example, cubic grains were observed at a volume fraction of 10% at Ca^{2+} concentration of 1.5 mol%. However, since cubic grains are relatively large and thus distant from each other, compared to tetragonal grains, they have little pinning effect on the growth of tetragonal grains, at least initially. A more detailed study of the kinetics of grain growth of the two-phase region is in progress.

IV. Theoretical Considerations

(1) Electrostatics

To theoretically predict the electrostatic potential and the charge distribution in the double layer near lattice discontinuities, knowledge of the formation energies of cation vacancies and anion vacancies, as well as binding energies between dopant and point defects, is required. For tetragonal zirconia, no quantitative information on these properties is available, although it is known that anion vacancies are the predominant point defects. This information alone is sufficient for making the qualitative prediction that pure ZrO_2 possesses a negatively charged grain boundary if we assume that the formation energy of an anion vacancy is smaller than that of a

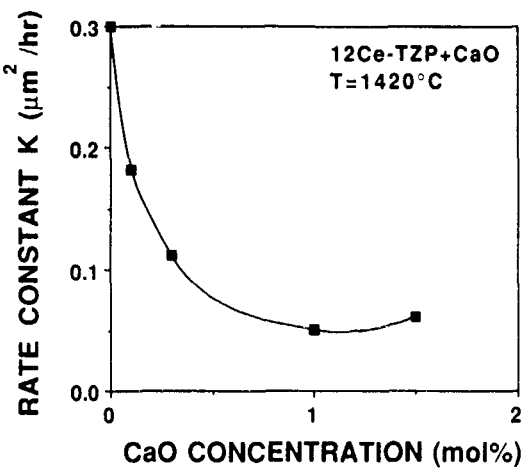

Fig. 6. Rate constant of the parabolic grain growth law of 12Ce-TZP vs dopant (CaO) concentration at 1420°C.

cation vacancy. For an illustration of the concept, we have sketched defect concentrations in Fig. 7. Note that charge balance is maintained in the bulk while thermal equilibrium is reached at the grain boundary. A negatively charged grain boundary with a negative electrostatic potential as sketched is thus necessary to fulfill the above two requirements. If divalent and trivalent cations substitute for Zr^{4+}, at a concentration higher than that of the intrinsic point defects, then the grain boundary is reversed to possess a positive charge. This is also illustrated for the case of Ca doping in Fig. 7, where similar requirements of charge neutrality in the bulk and defect equilibrium at the boundary can be fulfilled by reversing the grain-boundary charge and electrostatic potential. In between, at a special temperature–dopant concentration condition, the grain boundary remains neutral. This condition is referred to as the isoelectric point. Theoretical predictions suggest that the isoelectric temperature increases with the dopant concentration.[3]

We have estimated in the Appendix the concentration of intrinsic anion vacancies in pure ZrO_2. We find that, in order for intrinsic anion vacancies to dominate over 1% cation dopants, a temperature higher than 2400°C must be exceeded. Thus, over the temperature range studied here, the grain-boundary charge is determined by the dopants.

Our data indicate that, generally, divalent and trivalent cations segregate to the grain boundary, but tetravalent and pentavalent cations do not. These observations strongly suggest that the grain boundaries are positively charged in 12Ce-TZP, 2Y-TZP, and other TZPs stabilized by trivalent cations so that only cations with a negative effective charge are attracted to the lattice discontinuities as a space charge. These results can be understood in the following way:

(a) 2Y-TZP with a small amount of other dopants—The positive grain-boundary charge is induced by the majority aliovalent species, i.e., Y^{3+}; similar cases are encountered in Sc-TZP and In-TZP, i.e., Sc^{3+} and In^{3+}.

(b) Ce-TZP with divalent and trivalent dopants—The positive grain-boundary charge is induced by the aliovalent dopants, i.e., Mg^{2+}, Ca^{2+}, Sc^{3+}, In^{3+}, Yb^{3+}, and Y^{3+}.

(c) Ce-TZP with tetravalent dopants—It is known that some Ce^{3+} forms at high temperatures in air in CeO_2. The same undoubtedly also occurs in Ce-TZP. Ce^{3+} could thus serve as the requisite dopant that induces a positive charge on the grain boundary. By assuming that the Ce^{4+}/Ce^{3+} ratio in Ce-TZP is the same as in CeO_2, the concentration of Ce^{3+} is estimated in the Appendix and found sufficiently higher than those of intrinsic defects. Thus it should dominate the electrostatic behavior.

(d) Ce-TZP with pentavalent dopants—Nb^{5+} and Ta^{5+} are compensated by Ce^{3+} at high temperatures in CeO_2, according to the study of Naik and Tien.[24,25] The same presumably also occurs in Ce-TZP. The excess Ce^{3+} over and beyond that is then capable of inducing a positive charge on the grain boundary. To support this argument we have estimated the concentration of Ce^{3+}, with Nb^{5+} or Ta^{5+} doping, in the Appendix and found Ce^{3+} always in excess.

(e) In principle, tetragonal ZrO_2 with an appropriate amount of Nb^{5+} or Ta^{5+} dopants could possess a negatively charged grain boundary. This is not practical, however, for TZP of the composition ZrO_2–$(Nb,Ta)_2O_5$ cannot be retained at room temperature.[20] Thus, the most Nb^{5+} and Ta^{5+} can do in TZP is to shift the electrolytic condition slightly closer to the isoelectric point so that the grain boundary is less charged.

(f) Theoretically, Zr^{4+}/Zr^{3+} reduction would also be the dominant mechanism responsible for the nonstoichiometry observed in pure ZrO_2. If so, a positively charged grain boundary in pure ZrO_2 should exist. All other arguments presented above still stand.

Based on the above argument, we believe that, in effect, all the TZPs currently known to us should have a positively charged grain boundary and a negative space charge made up of lower-valence cation segregants. In view of the above, we will limit our analysis below to divalent and trivalent dopants only.

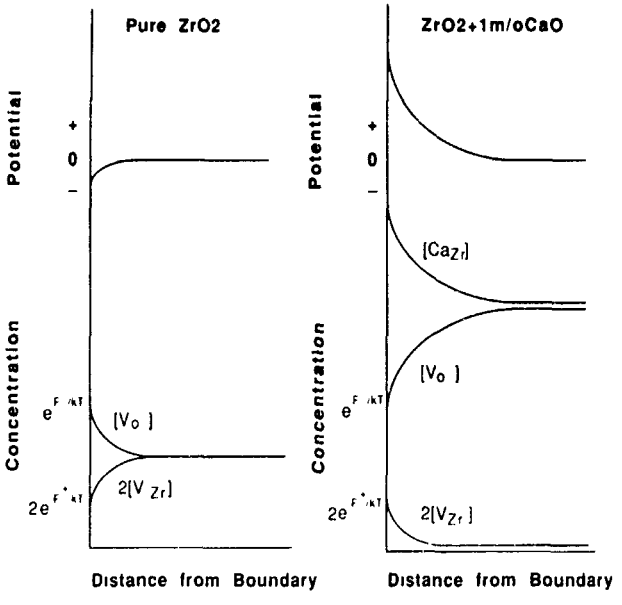

Fig. 7. Schematic variations of electrostatic potential and defect concentrations with distance from grain boundary. Opposite grain-boundary charges are developed in the intrinsic (pure ZrO_2) and in the extrinsic (ZrO_2 + 1 mol% CaO) regimes ($F^{\cdot}$ = formation energy of V_{Zr}, $F^{\cdot\cdot}$ = formation energy of $V_O^{\cdot\cdot}$)

(2) Solute Drag

Assuming the solute drag theory of Cahn[26–28] is applicable in the present case, the grain-boundary mobility can be expressed as

$$M = \frac{D}{\Delta C(kT)} \tag{4}$$

In the above, D is the diffusivity of the solute, ΔC is the excess concentration per unit grain-boundary area, and kT has its usual meaning. In ZrO_2 and its solid solutions, oxygen vacancy diffusion is much faster than cation diffusion. Thus, the main drag on the grain-boundary mobility comes from cation solutes. In the following, we will examine the dependence of D and ΔC on the size and the charge of cation solutes in order to rationalize the grain size sequence reported in Table II.

In the case of attractive interactions, most of the excess solutes are localized near the grain boundary, and the drag force is due to short-range interactions between solutes and the grain boundary.[26–28] Both elastic interactions and electrostatic interactions could be responsible for the attraction. Although its exact quantity is not known, the electrostatic potential in the double layer is probably of the order of 1 to 2 eV, in view of the calculated defect energies in fluorite structures recently reported.[29,30] The elastic interaction can be estimated from the misfit energy.[31]

$$U_0(\text{elastic}) = \frac{2}{9}\mu\Omega\left(\frac{1+\nu}{1-\nu}\right)\alpha^2 \tag{5}$$

where μ is the shear modulus (80 GPa), Ω is the formula volume (0.035 nm^3), ν is Poisson's ratio (0.3), and α is Vegard's slope for volume misfit given in Table I. The typical values of the elastic energy range from 0.02 to 0.29 eV when α increases from 0.05 to 0.20. Thus, the electrostatic interaction is much

larger than elastic interactions likely to be present in the system. The contribution due to polarization is probably also small, judging from the numerical studies on the dipole contributions to space charge by Yan *et al.*[32]

In view of the above, we believe that in tetragonal zirconia, the attractive potential, electrostatic in origin, is primarily governed by the effective charge of the dopants and secondarily by the binding energy between these dopants and oxygen vacancies but is insensitive to ionic size, polarizability, and solubility. Dopants with a larger effective charge are expected to be more strongly attracted to the grain boundary as the dominant space charge. This is consistent with our data in Section III that divalent solutes (effective charge = −2) segregate stronger (and impede grain growth more) than trivalent solutes (effective charge = −1).

Our data also indicate that smaller dopants, such as Mg^{2+} among divalent ones and Sc^{3+} among trivalent ones, result in a higher grain-boundary mobility. In the extreme case, the difference in mobilities can be an order of magnitude. Refering to Tables IV and V, we find that the variation in the enrichment factor among dopants of the same valence is not substantial. (In^{3+} was excluded from this comparison because of its high vapor pressure.) Therefore, it seems more likely that the effect of ionic size is due to the faster diffusivity of smaller cations, i.e., D rather than ΔC in Eq. (4). Although data for interdiffusion of solutes in TZP are not available, the above proposition is consistent with solute interdiffusivity in cubic zirconia[33] and with several related observations in precipitate coarsening[13] which implicates faster diffusivities of smaller ions relative to other trivalent and divalent cations.

V. Discussion

(1) Grain Growth in TZP

The solute drag mechanism was first proposed by Lee and Chen to be the cause of slower grain growth found in 2Y-TZP in comparison to that in 8Y cubic zirconia.[8] In addition to a slower growth rate, they observed a much higher activation energy and a lower grain-boundary energy in 2Y-TZP. They argued that all such observations are consistent with grain-boundary segregation and solute drag in 2Y-TZP and not in 8Y cubic zirconia. Segregation of stabilizers in tetragonal zirconia to grain boundaries has not been reported before, although segregation of Y^{3+} to the free surfaces has been known for some time through the work of Auger electron spectroscopy. Based on the latter observation, Burggraaf and co-workers had speculated that a similar trend occurred at tetragonal grain boundaries and could cause a grain growth suppression.[34] The present study, by providing direct observations of segregation and a systematic comparison of different dopants, supports and extends Lee and Chen's conclusion to other TZP systems.

Concerning activation energies of mobility shown in Fig. 3 and Table III, a correlation between a higher activation energy and a lower mobility seems to hold. The temperature dependence of the mobility arises from two sources, the excess solute ΔC and the (lattice) interdiffusion of solute D, according to Eq. (4). If we further assume that isoelectric solutes segregate similarly, as suggested by their similar enrichment ratios, then the difference in activation energies among them is due to the diffusivity. Since larger solutes are expected to have a higher activation energy for lattice diffusion (also supported by diffusivity experiments[33]), the observed trend in activation energy is consistent with the overall picture thus far provided.

To appreciate the implication of the temperature dependence of ΔC, the following preliminary estimation of segregation energy is helpful. We note the activation energies for lattice interdiffusion and self-diffusion in cubic zirconia are 423 (Ca), 293 (Mg), 423 (Y), and 391 (Zr), all in units of kJ/mol.[33] If we assume that these values are unchanged for TZP, we can then compare them with Q in Table III and attribute the difference to segregation energy. In this way, we find that the segregation energy of divalent cations (Ca^{2+}, Mg^{2+}) is consistently higher than that of the trivalent cation (Y^{3+}). Taking Ca^{2+} as an example, the segregation energy is estimated to be 113 kJ/mol or 1.22 eV. This value, though crude, seems reasonable. Presumably, it is this segregation energy which gives rise to the temperature dependence of ΔC.

(2) Strain Energy Argument

Lange[35-36] and co-workers have offered an entirely different proposition to explain the slow grain growth in stabilized TZP.[35,36] They suggest that the tetragonal phase field is much narrower at 1300° to 1500°C, at equilibrium, than generally assumed, and that a suppression of grain growth is observed only in the "two-phase" field, which approaches equilibrium by solute partitioning over a very long time. Such a picture, however, does not provide a mechanism for the slow grain growth by itself unless the cubic phase is already present and serves as the pinning phase. The latter is unlikely since the cubic grains are typically much larger than tetragonal grains and are thus relatively few in number. To provide a mechanism for suppressing grain growth, they further propose that during grain growth, solute partitioning also proceeds to give rise to a strain energy as a result of the compositional dependence of lattice parameters.[36] This rise in strain energy, according to this argument, suppresses grain growth. This latter proposal can be tested against the grain growth data reported here directly. Since In^{3+} doping causes the least misfit, according to Table I, we should observe the fastest grain growth in this material. This is not the case in Figs. 2 and 4. Likewise, since Ca^{2+} doping causes less misfit than Mg^{2+} doping, the grain growth in Mg^{2+}-doped Ce-TZP should be faster—again in contradiction to our results. Indeed, we must conclude that Lange's strain-energy argument is not borne out by the data of grain growth kinetics.

Data in Fig. 6 are similar to the observation made by Lange on the Y^{3+} concentration dependence of grain size in the ZrO_2–Y_2O_3 system, yet we believe that the data can be easily rationalized by the proportionality between ΔC and C_0, which results in an inverse dependence of M and C_0, according to Eq. (4). When a two-phase field is finally entered at higher concentrations, the mobility of tetragonal grain boundary will probably remain constant (being set by the solubility limit of the tetragonal phase) until the cubic phase fraction becomes high. This explains the shape of the curve in Fig. 6.

(3) Role of a Glassy Phase

We finally address the issue of the glassy grain-boundary phase which seems to exist ubiquitously in a zirconia system. First, we must state that the space charge should arise near any geometric discontinuity, including a phase boundary, which is a source and sink of point defects.[3] Thus, even in the presence of a glassy layer between grains, the grain-boundary movement will experience a solute drag. Second, in the very fine grain ceramics that we have studied, the thickness of the glassy layer is about 1 nm, which would be within the coherent length calculated by Clarke using a structural force model.[37] Thus, it is not surprising that adjacent grains interact in a way similar to grains across a "clean" boundary. This argument is further supported by the existence of the characteristic dihedral angle between tetragonal and cubic grains in the two-phase field.[8] Third, for such thin grain boundaries, it is probable that diffusion across the glassy layer is fast compared to solute drag which is controlled by lattice diffusion. Thus, the mobility of a grain boundary, wetted by a small amount of glass, can still be rate-limited by solute drag via the space charge mechanism. In this regard, the overall grain growth kinetics of a slightly glass-containing ceramic is not mechanistically different from that of a glass-free ceramic

VI. Conclusions

(a) In all the cases of practical interest, tetragonal zirconia possesses a positively charged grain boundary causing segregation of divalent and trivalent stabilizers to the grain boundaries, independent of ionic size and solubility.

(b) Grain-boundary mobility in TZP is primarily controlled by the space charge segregation of divalent and trivalent solutes, and secondly by the lattice diffusivities of these solutes: the largest divalent solute provides the strongest grain-boundary drag.

(c) The activation energy of grain-boundary mobility in TZP is higher than that of lattice interdiffusivity of dopants. The difference may be attributed to a segregation energy; the divalent solutes have a higher segregation energy than trivalent solutes.

(d) A sufficiently thin glassy layer has no effect on the applicability of the space charge concept. Thus, solute drag can still operate in slightly glass-containing ceramics of very fine grains.

APPENDIX

Nonstoichiometry in ZrO_2, Ce-TZP, and Nb-Doped Ce-TZP

(1) ZrO_2

Pure ZrO_2 contains anion vacancies and may be written as ZrO_{2-x}. According to the recent data of Aldebert *et al.*,[38] x varies from 0.001 at 1925°C to 0.052 at 2410°C in a helium atmosphere. Extrapolating these data to lower temperatures, the values of x are given in Fig. A1. These values are representative of the concentration of the intrinsic vacancies. Clearly, they are much smaller than the typical dopant concentrations used in this study.

(2) CeO_2 and Ce-TZP

Pure CeO_2 contains anion vacancies, compensated by concurrent reduction of Ce^{4+} to Ce^{3+}. Thus, it may be written as $Ce^{4+}_{1-2x}Ce^{3+}_{2x}O_{2-x}$. Ce^{3+} is responsible for a type of electronic conductivity, via the so-called small polaron mechanism.[22] The latter has a very small activation energy, ca. 0.15 eV, compared to that of the $[Ce^{3+}]$, ca. 2.1 eV. Thus, the nonstoichiometry and $[Ce^{3+}]$ can be determined by conductivity indirectly.[24]

Naik and Tien found a correlation between electrical conductivity σ and x of the following form:[24,25]

$$[Ce^{3+}]_{intrinsic} = 2x = 2.3 \times 10^{-2}\sigma\,(\Omega^{-1}\cdot cm^{-1}) \qquad (A\text{-}1)$$

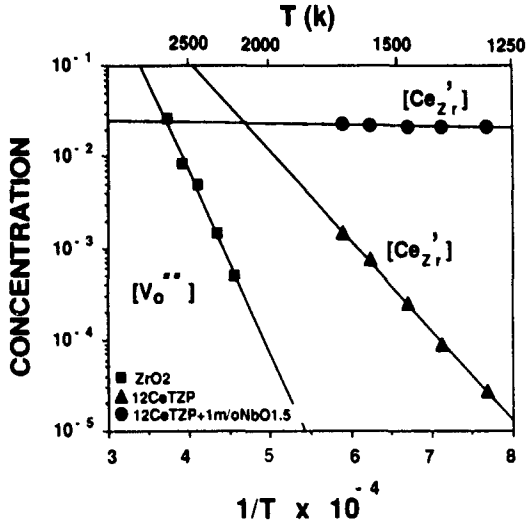

Fig. A1. Defect concentrations vs reciprocal temperature for pure ZrO_2 and its solid solutions (see text)

between 900° and 1329°C, through conductivity and thermogravimetric experiments in CeO_2. From their conductivity data at 1420°, 1329°C, and below, we can estimate $[Ce^{3+}]$ in pure CeO_2. Assuming $[Ce^{3+}]$ in 12Ce-TZP is 12% of the above, we plot the estimated $[Ce^{3+}]$ in 12Ce-TZP in Fig. A1. Clearly, in the absence of aliovalent dopants, $[Ce^{3+}]$ is sufficiently abundant between 1000° and 2000°C to be the predominant charged species.

(3) 12Ce-TZP Doped with Nb^{5+} and Ta^{5+}

Naik and Tien reported that Nb^{5+} dopants in CeO_2 at high temperatures were accommodated by replacing equal numbers of Ce^{4+} and formation of Ce^{3+}.[24,25] Thus, the Nb-doped CeO_2 may be written as $Ce^{4+}_{1-2x-y}Ce^{3+}_{2x+y}Nb^{5+}_yO_{2-x}$ to account for both the intrinsic and the extrinsic defects. Assuming the same mobility of electrons by the small polaron mechanism we have calculated $[Ce^{3+}]$ in a CeO_2–0.40 mol% Nb_2O_5 at 1029° and 1420°C, from the conductivity data of Naik and Tien.[24,25] Comparing $[Ce^{3+}]$ in the Nb^{5+}-doped (extrinsic) case and the undoped (intrinsic) case estimated in Section (2), we find the following relation being observed closely:

$$[Ce^{3+}]_{extrinsic} = [Ce^{3+}]_{intrinsic} + [Nb^{5+}] \qquad (A\text{-}2)$$

at these temperatures. This conclusion is also supported by the closeness of the thermogravimetric data of the doped and undoped CeO_2 at high temperatures.[24,25] Assuming the same mechanism of Nb^{5+}/Ce^{3+} compensation operates in 12Ce-TZP, we have calculated the total concentration of Ce^{3+} with 1% Nb^{5+} dopants and plotted it in Fig. A1.

Acknowledgments: We are grateful to Dr. T. S. Sheu for providing Sc- and In-stabilized zirconia and to Mr. T.Y. Syau for performing Auger microanalysis.

References

[1]J. Frenkel, Kinetic Theory of Liquids; p. 36. Oxford University Press, New York, 1946.

[2]J. D. Eshelby, E. Newey, P. Pyatt, and A. Lidiard, "Changed Dislocations and the Strength of Ionic Crystals," *Philos Mag.*, **3**, 75–89 (1958).

[3]K. L. Kliewer and J. S. Koehler, "Space Charge in Ionic Crystals, I. General Approach with Application to NaCl," *Phys. Rev.*, **140** [4A] A1226–40 (1965).

[4]W. D. Kingery, "Possible Concepts Necessary and Sufficient for Interpenetration of Ceramic Grain-Boundary Phenomena. I, Grain-Boundary Characteristics, Structure, and Electrostatic Potential," *J Am. Ceram. Soc*, **57** [1] 1–12 (1974); "II, Solute Segregation, Grain-Boundary Diffusion, and General Discussions," *ibid.*, **57** [2] 74–83 (1974).

[5]W. D. Kingery, T. Mitamura, J. B. Vander Sande, and E L. Hall, "Boundary Segregation of Ca, Fe, Ca, and Si in MgO," *J. Mater Sci*, **14**, 1766–67 (1979).

[6]Y. M. Chiang, A. F. Henriksen, W. D. Kingery, and D. Finello, "Characterization of Grain-Boundary Segregation in MgO," *J Am Ceram Soc.*, **64** [7] 385–89 (1981).

[7]C.-W. Li and W. D. Kingery, "Solute Segregation at Grain Boundaries in Polycrystalline Al_2O_3", pp. 368–78 in Advances in Ceramics, Vol. 10, Structure and Properties of MgO and Al_2O_3 Ceramics Edited by W. D. Kingery. American Ceramic Society, Columbus, OH, 1984.

[8]I. G Lee and I-W. Chen, "Sintering and Grain Growth in Tetragonal and Cubic Zirconia"; pp 340–45 in *Sintering '87* Edited by S Somiya, M. Shimada, M. Yoshimura, and R Watanabe. Elsevier Applied Science, London, U.K., 1988.

[9]M. Rühle, N Claussen, and A. H Heuer, "Microstructural Studies of Y_2O_3-Containing Tetragonal ZrO_2 Polycrystals (Y-TZP)", pp. 352–70 in Advances in Ceramics, Vol. 12, Science and Technology of Zirconia II. Edited by N. Claussen M. Rühle, and A. H. Heuer, American Ceramic Society, Columbus, OH, 1984

[10]R. D Shannon, "Revised Effective Ionic Radii and Systematic Studies of Interatomic Distances, Halides and Chalcogenides," *Acta Crystallogr*, **A32**, 756 (1976).

[11]S M. Sim and V S Stubican, "Phase Relations and Ordering in the System ZrO_2–MgO," *J Am. Ceram Soc*, **70** [7] 521–26 (1987).

[12]T.Y Tien and E. C Subbarao, "X-ray and Electrical Conductivity Study of Fluorite Phase in the System ZrO_2–CaO," *J Chem Phys*, **39** [4] 1041–47 (1963)

[13]T -S Sheu, "Phase Stability of Zirconia Solid Solutions", Ph D Thesis University of Michigan, Ann Arbor, MI, (1989)

[14]H. Toraya, "Effect of $YO_{1.5}$ Dopant on Unit-Cell Parameters of ZrO_2 at Low Contents of $YO_{1.5}$," *J Am Ceram Soc*. **72** [4] 662–64 (1989)

[15]H G Scott, "Phase Relationships in the Zirconia-Yttria System,"

J. Mater. Sci., **10** 1527–35 (1975).

[16]D. C. Agrawal, R. Gopalakrishnon, and D. Chakravorty, "Phase and Microstructures in Zirconia–Calcia–Titania Multiphase Ceramics," *J. Am. Ceram. Soc.*, **72** [6] 912–15 (1989).

[17]M. J. Bannister and J. M. Barnes, "Solubility of TiO_2 in ZrO_2," *J. Am. Ceram. Soc.*, **69** [11] C-269–C-271 (1986).

[18]E. Tani, M. Yoshimura, and S. Somiya, "Revised Phase Diagram of the System ZrO_2–CeO_2 below 1400°C," *J. Am. Ceram. Soc.*, **66** [7] 506–10 (1983).

[19]K. Urabe, K. Ogata, H. Ikawa, and S. Udagawa, "Phase Transformation and Lattice Constants of Zirconia Solid Solutions in the System Y_2O_3–CeO_2–ZrO_2"; pp. 147–52 in Materials Science Forum, Vol. 34-36, Ceramic Developments. Edited by C. C. Sorrell and B. Ben-Nissan. Trans Tech Publications, Aedermannsdorf, Switzerland, 1988.

[20]D. J. Kim, "The Effect of Alloying on the Transformability of Y_2O_3 Stabilized Tetragonal ZrO_2"; Ph.D. Thesis. University of Michigan, Ann Arbor, MI, 1988.

[21]M. Yoshimura, "Phase Stability of Zirconia," *Am. Ceram. Soc. Bull.*, **67** [12] 1950–55 (1988).

[22]M. F. Yan, R. M. Cannon, and H. K. Bowen. "Grain Boundary Migration in Ceramics"; pp. 276–307 in Ceramic Microstructure '76. Edited by R. M. Fulrath and J. A. Pask. Westview Press, Boulder, CO, 1977.

[23]C. P. Wagner, W. R. Riggs, L. E. Davis, J. F. Moulder, and G. E. Muilenberg, Handbook of X-ray Photoelectron Spectroscopy. Perkin-Elmer Corp., Eden Prairie, MN, 1979.

[24]I. K. Naik and T. Y. Tien, "Small Polaron Mobility in Non-Stoichiometric Cerium Dioxide," *J. Phys. Chem. Solids*, **38** [3] 311–15 (1978).

[25]I. K. Naik and T. Y. Tien, "Electrical Conduction in Nb_2O_5-Doped Cerium Oxides," *J. Electrochem. Soc.*, **126** [4] 562–66 (1979).

[26]J. W. Cahn, "The Impurity Drag Effect in Grain Boundary Motion," *Acta Metall.*, **10** [9] 789–98 (1962).

[27]K. Lücke and H. P. Stüwe, "On the Theory of Impurity Controlled Grain Boundary Motion," *Acta Metall.*, **19** [10] 1087–99 (1971).

[28]D. J. Srolovitz, R. Eykholt, D. M. Barnett, and J. P. Hirth, "Moving Discommensurations Interacting with Diffusing Impurities," *Phys. Rev. B*, **35** [12] 6107–21 (1987).

[29]W. C. Mackrodt and P. M. Woodrow, "Theoretical Estimates of Point Defect Energies in Cubic Zirconia," *J. Am. Ceram. Soc.*, **69** [3] 277–80 (1986).

[30]A. Dwivedi and A. N. Cormack, "A Computer Simulation Study of the Defect Structure of Calcia-Stabilized Zirconia," *Philos. Mag. A*, **61** [1] 1–22 (1990).

[31]J. D. Eshelby, "Determination of the Elastic Field of an Ellipsoidal Inclusion and the Related Problems," *Proc. R. Soc. London, A*, **241**, 376–96 (1957).

[32]M. F. Yan, R. M. Cannon, and H. K. Bowen, "Space Charges, Elastic Field and Dipole Contributions to Equilibrium Solute Segregation at Interfaces," *J. Appl. Phys.*, **54** [2] 764–78 (1983).

[33]Y. Oishi, K. Ando, and Y. Sakka, "Lattice and Grain-Boundary Diffusion Coefficients of Cations in Stabilized Zirconias"; pp. 208–19 in Advances in Ceramics, Vol. 7, Characterization of Grain Boundaries. Edited by M. F. Yan and A. H. Heuer. American Ceramic Society, Columbus, OH, 1983.

[34]A. J. A. Winnubst and A. J. Burggraaf, "The Aging Behavior of Ultrafine-Grained Y-TZP in Hot Water"; pp. 39–47 in Advances in Ceramics, Vol. 24A, Science and Technology of Zirconia III. Edited by S. Somiya, N. Yamamoto, and H. Hanagida. American Ceramic Society, Westerville, OH, 1988.

[35]F. F. Lange, "Transformation Toughened ZrO_2: Correlations Between Grain Size Control and Composition in the ZrO_2–Y_2O_3 System," *J. Am. Ceram. Soc.*, **69** [3] 240–42 (1986).

[36]F. F. Lange, D. B. Marshall, and J. B. Porter, "Controlling Microstructures Through Phase Partitioning from Metastable Precursors: The ZrO_2–Y_2O_3 System"; pp. 519–32 in Ultrastructure Processing of Advanced Ceramics. Edited by J. K. Mackenzie and D. R. Ulrich. Wiley, New York, 1988.

[37]D. R. Clarke, "On the Equilibrium Thickness of Intergranular Glassy Phases in Ceramic Materials," *J. Am. Ceram. Soc.*, **70** [1] 15–22 (1987).

[38]P. Aldebert and J.-P. Travers, "Structure and Ionic Mobility of Zirconia at High Temperature," *J. Am. Ceram. Soc.*, **68** [1] 34–40 (1985). □

IV. THE ROLES OF LIQUID PHASE IN SUPERPLASTIC CERAMICS

Liquid phase is ubiquitous in certain ceramic systems, e.g., zirconia and silicon nitride. Since the liquid resides at the grain boundary, it can influence the microstructural evolution. This aspect is usually viewed negatively because of the resulting degradation of properties. On the other hand, the grain boundary liquid may also confer important advantages, such as a lower flow stress in superplastic deformation. However, this must be done judiciously to maintain a satisfactory threshold against decohesion. We have systematically studied liquid additives in zirconia and in silicon nitride with the intent of understanding their roles in microstructural development and in deformation. This has led to the discovery of Cu and other patented elements as beneficial additives to Y-TZP for enhancing the formability. In the case of silicon nitride, we discovered a novel mechanism in which the colloidal interaction between grains via the liquid phase gives rise to a unique shear-thickening phenomenon in creep. The mechanisms of liquid-assisted grain growth and creep have also been elucidated.

4.1 "Anisotropic Grain Growth During Final Stage Sintering of Silicon Nitride Ceramics"

C.M. Hwang, T.Y. Tien and I-W. Chen, in Sintering '87, Proceedings of 4th International Symposium on Science and Technology of Sintering

ANISOTROPIC GRAIN GROWTH DURING FINAL STAGE SINTERING OF SILICON NITRIDE CERAMICS

C.M. Hwang, T.Y. Tien, and I-Wei Chen
Department of Materials Science and Engineering
The University of Michigan
Ann Arbor, Michigan 48109-2136
U.S.A.

ABSTRACT

The kinetics of grain growth of ß SiAlON are reported for a broad range of compositions containing YAG and cordierite additives. Anisotropic growth favoring a prismatic morphology was found in all cases. Both the length and the width of the grains follow a cubic growth law. The activation energies were determined to be between 145 and 180 Kcal/mole. High resolution TEM examination revealed a rounded growth front along the [001] direction and a sharp interface with very few ledges along the [210] direction. A growth model, which envisions continuous growth in the [001] direction and lateral ledge growth in the [210] direction, appears to provide a satisfactory explanation of these observations.

INTRODUCTION

Grain growth during the final stage of liquid phase sintering is commonly reported to follow a cubic law analogous to Ostwald ripening. Both diffusion through the liquid and interface reactions at the solid/liquid interface are possible rate-controlling mechanisms [1]. Most theoretical analyses and model experiments have been conducted for isotropic systems consisting of equiaxed grains. In silicon nitride ceramics, however, grain shapes are very anisotropic, with β-SiAlON grains growing as hexagonal prisms along the [001] direction [2]. An example of such microstructure is shown in Fig. 1. Anisotropic grain growth in liquid phase sintering of this system has not been quantitatively studied. This investigation reports on the kinetics of grain growth and on the structure of solid/liquid interfaces in ß-SiAlON with $Y_3Al_5O_{12}$ (YAG) and $Mg_2Al_4Si_5O_{18}$ (cordierite) additions. Based on these experimental observations, a model is proposed to account for the anisotropic growth behavior.

EXPERIMENTAL

SiAlON solid solutions were prepared in the system Si, Al, X/O, N, with X = Y or Mg. The ß solid solution compositions are shown in Fig. 2. The compositions were sintered in a nitrogen atomsphere between 1400° and 1800°C. The kinetics of both densification during sintering and the accompanying α to ß phase transformation were already reported in the companion paper [3]. Data for grain growth were taken after the completion of the phase transformation. High resolution electron microscopy was performed using a JOEL 2000FX microscope operating at 200KV.

Fig. 1 A typical SEM microstructure of ß-SiAlON ceramics. (bar = 5 μm)

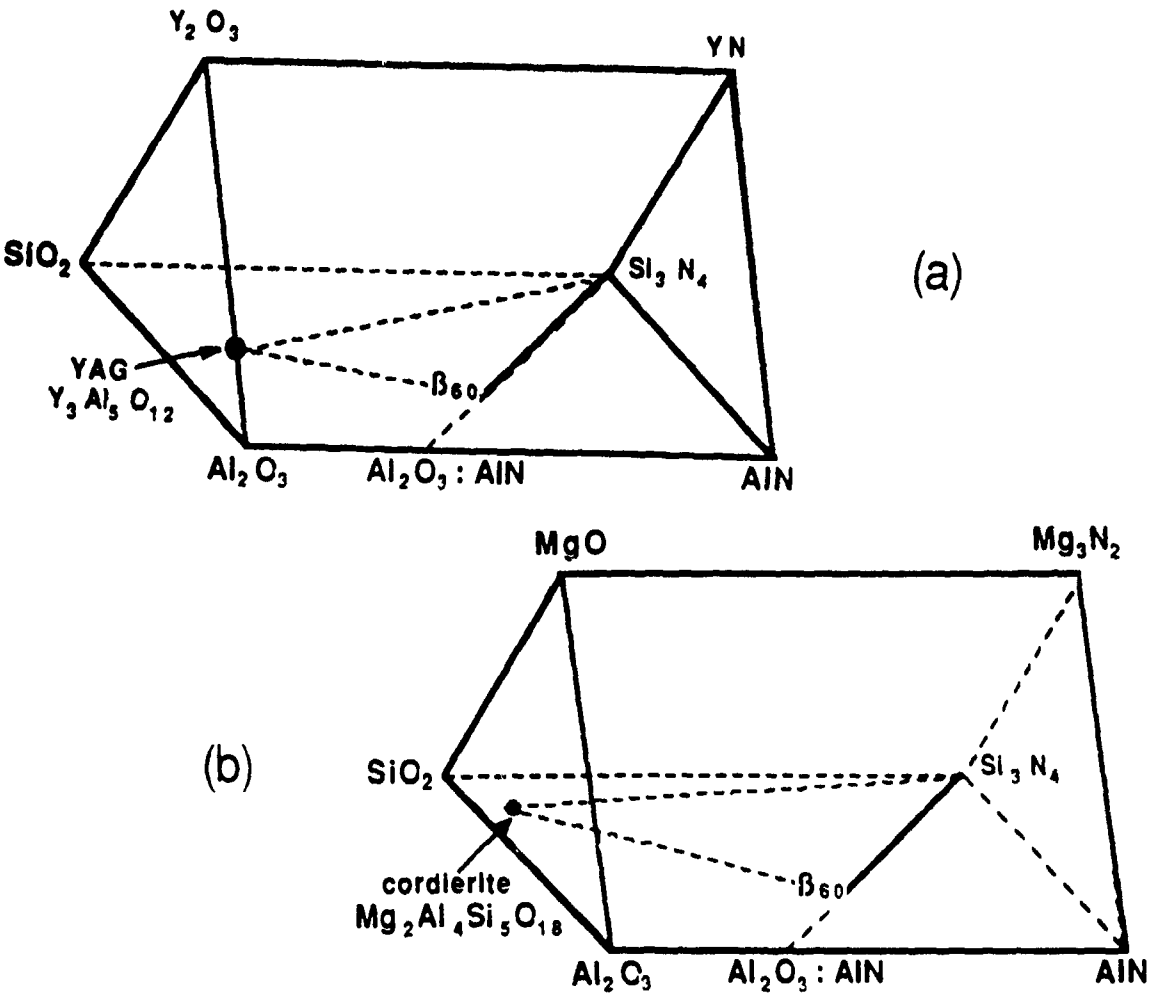

Fig. 2 The phase diagrams in the system Si, Al, X/O, N, with (a) X=Y and (b) X=Mg.

RESULTS

The growth rates of ß grains in the SiAlON-YAG system are shown in Fig. 3 for the [001] direction (length) and the [210] direction (width). The rates are highly anisotropic and can be expressed in the form:

$$d^n - d_o^n = K(t-t_o) \quad (1)$$

where d is the average grain dimension at time t, d_o is the dimension at time t_o. A cubic law, n=3, was found to be consistent with all of the growth data, in both directions and in both systems. The rate constant, K, is relatively insensitive to the amount of the liquid (Fig. 4), but very sensitive to the alumina content as shown in Fig. 5. A higher growth rate was found in the SiAlON-YAG system (Fig. 6). The activation energy of the rate constant was found to be about 160 Kcal/mole for the SiAlON-YAG system and about 170 Kcal/mole for the SiAlON-cordierite system. Similar to the difference in the kinetics of densification and phase transformation discussed in the companion paper [3], grain growth in the SiAlON-cordierite system is consistently slower than that in the SiAlON-YAG system. This is due to the difference in liquid viscosity in the two systems which results from the difference in the silica content of the liquids.

Further insight into the growth anisotropy was provided by examination of the solid/liquid interface using high resolution electron microscopy. A micrograph of a lattice image of a ß grain in the SiAlON-YAG system is shown in Fig. 7a. The structure of this grain, which is mostly enclosed in a glassy phase, was identified by diffraction analysis as shown in the figure. The semi-spherical cone in the [001] growth front is clearly shown in Fig. 7b, which indicates the presence of continuous growth steps characteristic of a diffuse interface. Along the [210] growth front, the interface is sharp except for a ledge as shown in Fig. 7c. These structures are suggestive of different growth kinetics which are in turn responsible for the anisotropic grain shape.

MODEL OF ANISOTROPIC GRAIN GROWTH

The model we propose here assumes continuous growth on the diffuse interface in the [001] direction and lateral growth by a ledge mechanism on the sharp prismatic planes in the [210] directions. The model is schematically depicted in Fig. 8. We represent the volume of the prism by

$$v = \pi l r^2 \quad (2)$$

where l is the length and r is the root mean square radius of the cross section. The growth rate is given by

$$dv/dt = \pi r^2\, dl/dt + 2\pi l r\, dr/dt \quad (3)$$

In the above, the first term is the growth rate in the [001] direction and the second term is the growth rate in the [210] directions. The normalized driving force for grain growth is taken to be

$$F = \gamma\Omega/kTr \quad (4)$$

where γ is the normalized solid/liquid energy of the prismatic planes, Ω is the molecular volume, and kT has its usual meaning.

The growth rates in the two directions are respectively given by

$$dl/dt = DcF/r \quad (5)$$

and

$$dr/dt = DcF/l \quad (6)$$

In the above, D is the solute diffusivity in the liquid which is used to relate the jump probability at the solid/liquid interface, and c is the solute concentration in the liquid. Here,

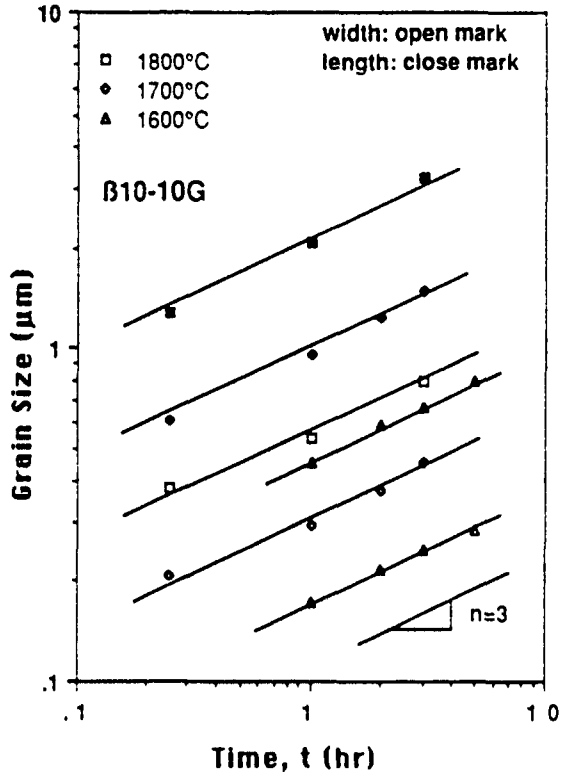

Fig. 3 Grain growth as a function of sintering temperature in the system SiAlON-YAG.

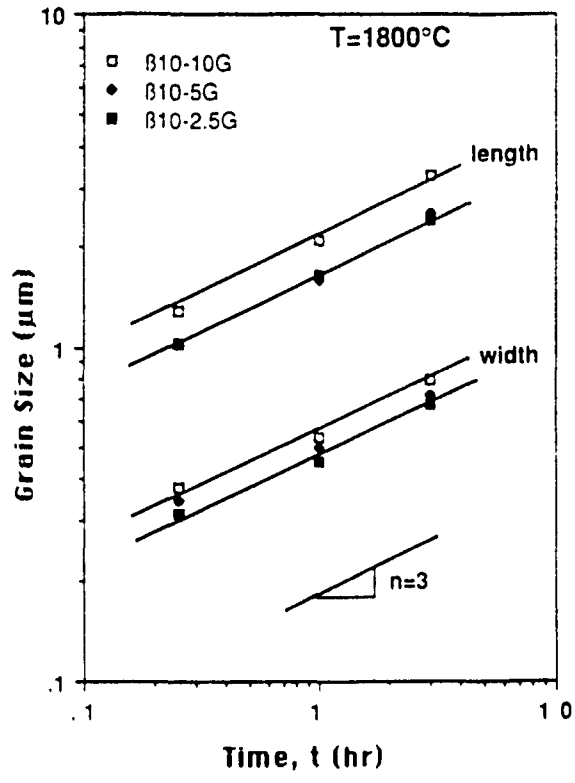

Fig. 4 Grain growth as a function of additive content in the system SiAlON-YAG.

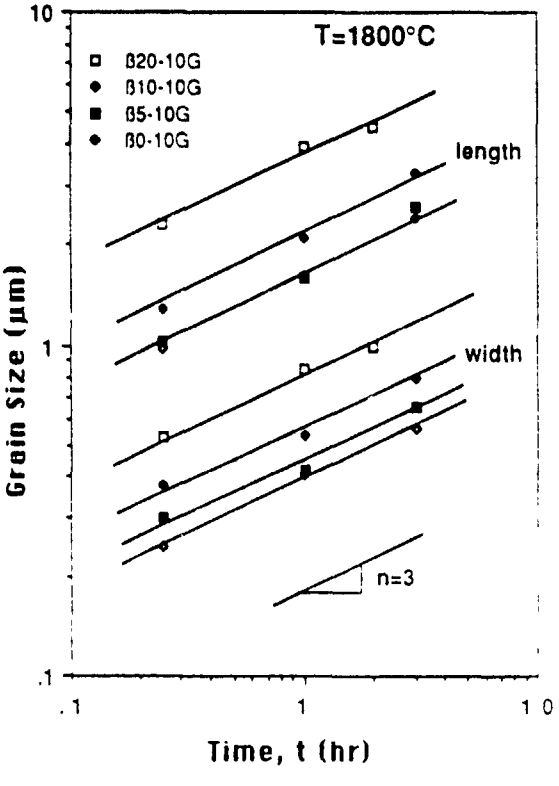

Fig. 5 Grain growth as a function of Al eq.% in the SiAlON composition in the system SiAlON-YAG.

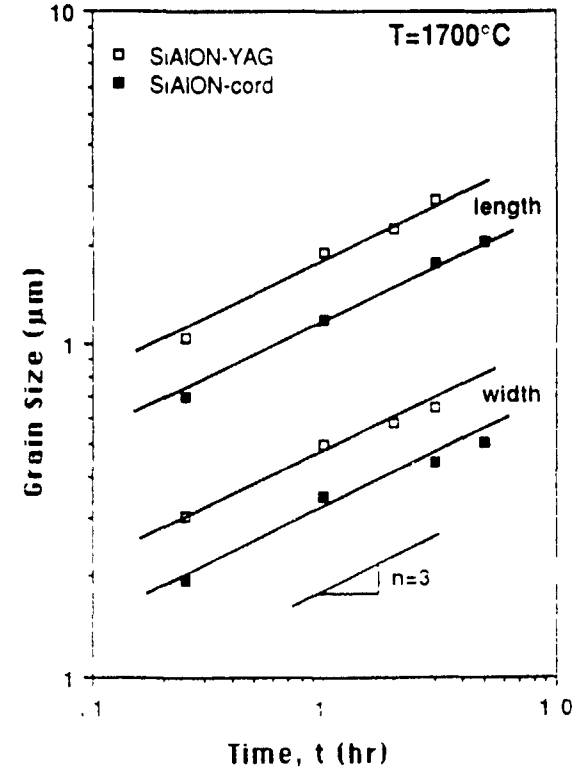

Fig. 6 Comparison of grain growth kinetics in the systems SiAlON-YAG and SiAlON-cordierite.

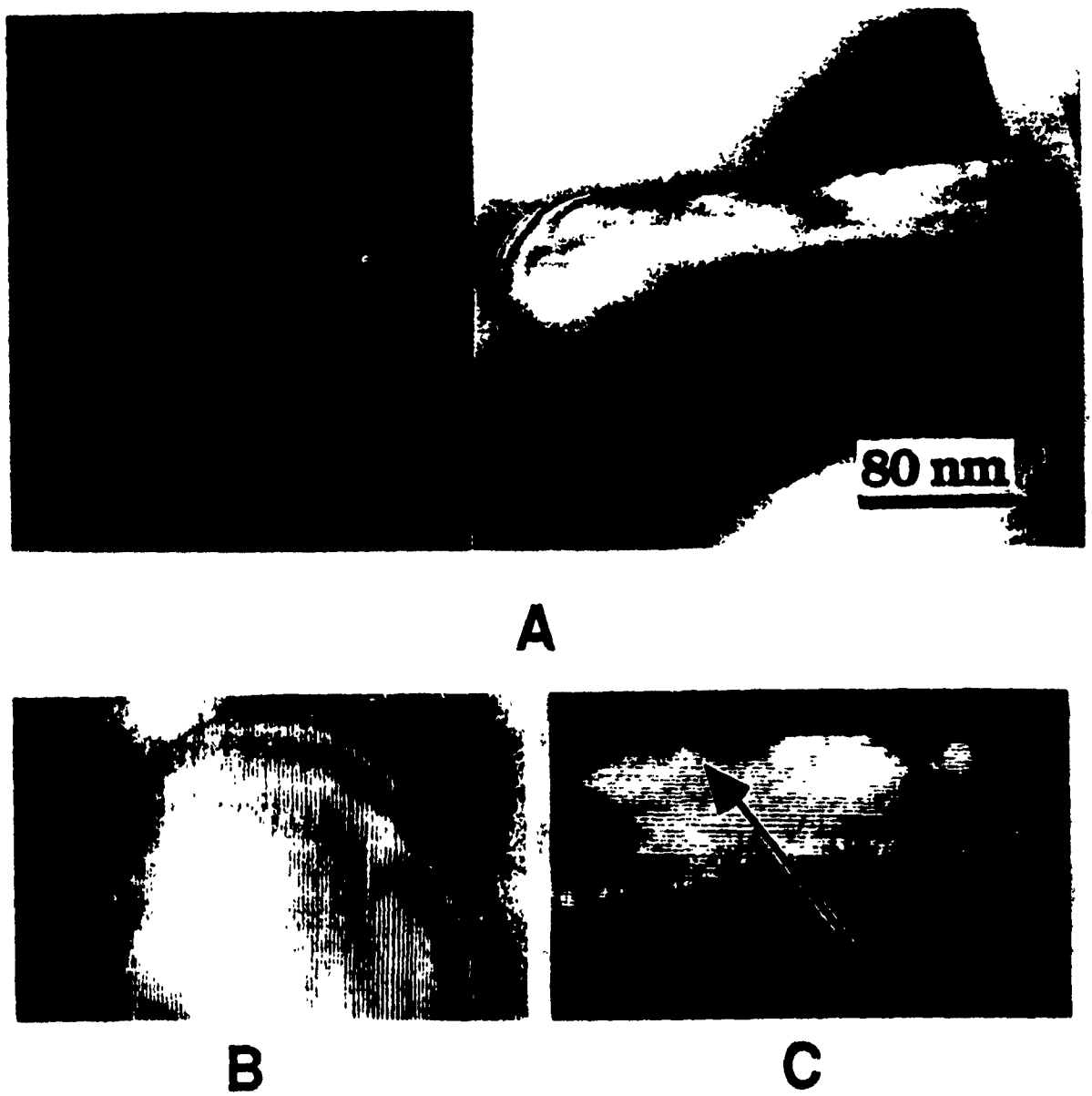

Fig. 7 a) A typical grain in SiAlON ceramics. (10•0) plane is parallel to the grain axis [001] direction. b) The enlarged view of the growth front in the [001] direction. c) The enlarged view of the growth ledge on the (10•0) plane.

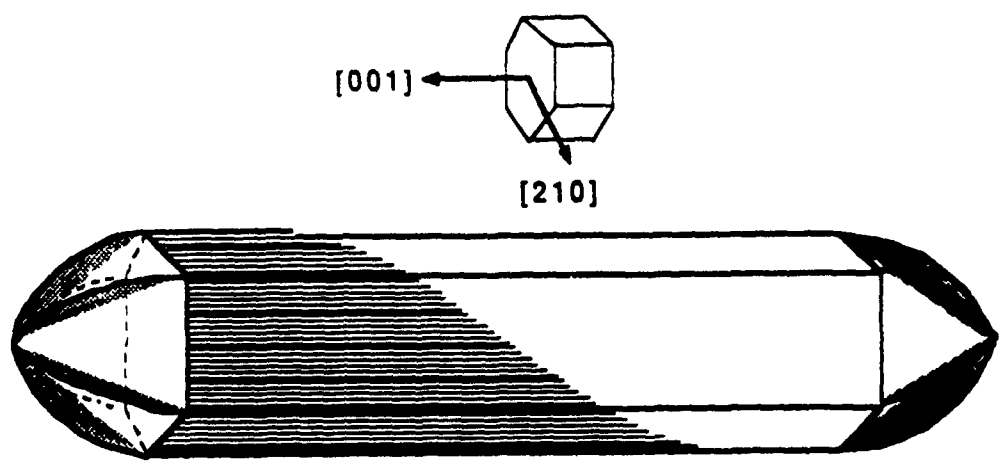

Fig. 8 A schematic illustrating the solid-liquid interface structures of a β SiAlON grain in the [001] and [210] directions during anisotropic grain growth.

we have assumed diffusion control in both cases and a perfect sink efficiency at the diffuse (00•1) interface and along the ledge on the (10•0) prismatic planes. Only lattice sites facing the [001] direction are counted. Additional geometric considerations, which will slightly affect the growth rates at low volume fractions of liquid, have been omitted in both expressions.

Because of the diffusion dependence of the growth equations given above, it is clear that the origin of the growth anisotropy for these grains lies in the disparity of available growth sites for the two types of solid/liquid interfaces. Following a simple manipulation of Eqs. 4-6, we confirm that a cubic law is followed by both l and r. As expected, their rate constants are both proportional to $Dc\gamma\Omega/kT$, but otherwise differ by a factor of $(l_0/r_0)^3$, strongly favoring growth in the length direction. Here, l_0 and r_0 are the grain length and radius, respectively, at time t_0.

DISCUSSIONS

Phenomenologically, anisotropic grain growth in the present systems seems to be consistent with the diffusion control mechanism outlined above. The key observations in support of this argument are (a) growth exponents being 3; (b) kinetics sensitive to liquid viscosity but not to liquid fractions; and (c) similar activation energies in both the sharp [210] and diffuse [001] growth directions. Note that (b) is not consistent with interface reaction control; furthermore, in contrast to (c), a higher activation energy for the sharp interface is expected for interface reactions.

The presence of a ledge on (10•0) prismatic planes can be thought of as due to a screw dislocation in the [001] direction. As a common origin providing growth steps on an atomically sharp interface, a screw dislocation normal to such a plane generates a spiral growth step which expands outward at a constant radial velocity [4]. Simple calculations pertinent to Ostwald ripening of prismatic grains have verified, however, that the critical radius of the spiral in the present case is of the order of r. Hence, only one spiral turn can fall on the six prismatic (10•0) surfaces. Indeed, in Figure 7c, only one growth step can be seen on the side surface. As this growth step sweeps over (10•0) surfaces by one turn, the prism grows in the width direction by one molecular layer.

ACKNOWLEDGEMENT

This research was supported by US Department of Energy, Office of Basic Energy Sciences, Materials Science Division, under Grant No. DE-FG02084-ER45069. One of us (I-W. C) also acknowledges the support by US Air Force, under Grant No. AFOSR-87-0289. The experimental assistance of H. Hohnke is gratefully appreciated.

REFERENCES

1. R.M. German, Liquid Phase Sintering, Plenum Press, New York (1985).
2. H. Hohnke and T.Y. Tien, Progress in Nitrogen Ceramics, Martinus Nijhoff, Netherlands (1983).
3. C.M. Hwang and T.Y. Tien, the companion paper (1987).
4. F.C. Frank, *Discussions Faraday Soc.*, 5, 46 (1949).

journal

Reprinted from the Journal of the American Ceramic Society, Vol 73, No 6, June 1990

J Am Ceram Soc., 73 [6] 1626-32 (1990)

Effect of a Liquid Phase on Superplasticity of 2-mol%-Y_2O_3-Stabilized Tetragonal Zirconia Polycrystals

Chin-Mau James Hwang*,* and I-Wei Chen*

Department of Materials Science and Engineering, University of Michigan, Ann Arbor, Michigan 48109-2136

A small addition of CuO to 2-mol%-Y_2O_3-stabilized tetragonal zirconia polycrystals significantly enhances superplasticity by forming an amorphous grain-boundary phase containing primarily Cu^+, Y^{3+}, Zr^{4+}, and O^{2-}. This phase apparently melts at around 1130°C, but it already provides a fast diffusion path even below the melting temperature. There are abrupt changes in stress exponent, activation energy, and grain size exponent across the melting temperature. Superplasticity is diffusion-controlled below the melting temperature and is interfaced-controlled above that. [Key words: yttria-stabilized tetragonal zirconia polycrystals, plasticity, liquid phase, creep, grain boundaries.]

I. Introduction

Ceramic superplasticity has been investigated in recent years by many researchers,[1-10] most notably Wakai and co-workers.[2-4] Large tensile ductilities were demonstrated in a few cases,[2-6] raising the hope that superplastic forming of crystalline ceramics may be technologically feasible someday. Presently, yttria-stabilized tetragonal zirconia polycrystals (Y-TZP) and their composites can be superplastically deformed at a strain rate of 10^{-4}/s, temperatures above 1400°C, and stress around 25 MPa, but the flow stress increases rapidly to well above 100 MPa as the temperature is lowered to 1250°C.[2-4,7,10] We believe that the prospect for superplastic forming of ceramics will become brighter if the forming temperature and the flow stress can be lowered to say, 1200°C and 50 MPa, which are comparable to hot working conditions for metallic alloys such as superalloys and molybdenum.[11,12]

We have speculated that a lower forming temperature and a lower flow stress might be realized in ceramics sintered at low temperatures. If so, then there are two obvious approaches which might be taken to achieve this goal. The first one is a processing approach, using colloidal techniques to lower the sintering temperature. A classical example of this type was given by Rhodes on a yttria-stabilized zirconia which was sinterable at 1000°C.[13] The second one is a chemical approach, using additives which lead to liquid-phase sintering.[14,15] In this study, we have explored both approaches in Y-TZP and obtained a very substantial improvement in the superplastic forming conditions.

The benefit of low-temperature sintering made possible by collodial processing should be apparent. Ceramics processed in this way are known to have smaller grains with a narrower size distribution.[13,16,17] These microstructural features can facilitate diffusional creep which is akin to superplasticity. Evidence for liquid-enhanced creep has also been documented in silicon nitride,[18,19] glass-ceramics,[20,21] other polycrystalline ceramics,[22-24] and metal.[25] In theory, for this to happen, the liquid has to wet grain boundaries fully and support a normal stress. In addition, the surrounding grains must be able to dissolve in this liquid. Under such circumstances, mass transport along and across grain boundaries will largely take place within the liquid film, which remains between grains regardless of the local stress state. This is the so-called solution-reprecipitation mechanism.

Without a liquid phase, diffusional creep via grain boundary is described by the Coble equation[26]

$$\dot{\varepsilon} = A_1\sigma\Omega\delta_{gb}D_{gb}/kTd^3 \quad (1)$$

In the above, $\dot{\varepsilon}$ is the strain rate, A_1 is a constant, σ is the stress, Ω is the atomic volume, δ_{gb} is the effective thickness of the grain boundary, D_{gb} is grain-boundary diffusivity, k is the Boltzmann constant, T is the temperature, and d is the grain size. The presence of a liquid phase at the grain boundary can alter the above equation in several ways. The following two cases are of special interest to the present study.[20,21,27,28]

(A) Diffusion control: If the mass transport through and across the grain boundary is rate-controlling, then Eq. (1) is modified by substituting $C_l\delta_l D_l$ for $\delta_{gb}D_{gb}$. Here C_l and D_l are the solubility and the diffusivity, respectively, of the rate-controlling species in the liquid film, and δ_l is the liquid film thickness. Since δ_l is proportional to the volume fraction of the liquid, V_l, and the grain size, the following rate equation obtains:

$$\dot{\varepsilon} = A_2\sigma\Omega V_l C_l D_l/kTd^2 \quad (2)$$

In the above, we have introduced a new constant A_2.

(B) Interface control: If the solute diffusion rate far exceeds the interface reaction rate required for atom attachment and detachment, then diffusional creep is controlled by the latter and the strain rate is proportional to the rate of the interface reaction. Quite commonly, such reactions have a nonlinear, threshold type of dependence on the driving force, which is $\sigma\Omega$ in our case (for example, if nucleation of a surface step is required).[29] The average strain per grain, from the deposition and removal of materials at its grain boundary, is inversely proportional to the grain size. Taking these considerations into account, the following rate equation obtains:

$$\dot{\varepsilon} = A_3(\sigma\Omega)^n/kTd \quad (3)$$

In the above, we have introduced a new stress exponent $n > 1$ and another constant A_3.

It should be obvious that the presence of an amorphous, and, indeed, any low-melting-point grain-boundary phase, has an effect similar to using liquid. This statement is supported by reports of enhanced kinetics sometimes observed below the melting (eutectic) temperature of the grain-boundary phase.[15] We believe the above mechanistic picture leading to Eqs. (2) and (3) for liquid-enhanced creep is applicable below

R. Raj—contributing editor

Manuscript No. 198254. Received July 13, 1989; approved December 1, 1989.

Presented at the 91st Annual Meeting of the American Ceramic Society, Indianapolis, IN, April 23-27, 1989 (Basic Science Division, Paper No. 121-B-89).

Supported by the U S. Air Force Office of Scientific Research under Grant No. 87-0289.

*Member, American Ceramic Society

*Now at Dow Chemical Central Research, Advanced Ceramic Laboratory, Midland MI 48674

the eutectic temperature as well, if we simply envision the grain-boundary phase as a short-circuit diffusion path. However, considering the different physical properties of grain-boundary phases above and below the eutectic temperature, we may still anticipate a transition in the enhanced Coble creep behavior near the eutectic temperature.

In this study we report sintering, grain growth, and superplasticity of Y-TZP's, with and without addition of a small amount of a low-melting phase. We wish to demonstrate that a drastic improvement of the superplastic forming conditions can be achieved by such an addition. A better understanding of such practice will be afforded by an examination of the evidence for mechanism changes attributable to the presence of amorphous and liquid grain-boundary phases.

II. Experimental Procedure

(1) Materials

The two systems selected in this study were single-phase zirconia containing 2 mol% Y_2O_3, designated as 2Y-TZP, and 2Y-TZP containing CuO. Unlike 3Y-TZP (ZrO_2 with 3 mol% Y_2O_3) which typically contains both the tetragonal and the cubic phase, 2Y-TZP is a single-phase tetragonal polycrystal. The eutectic melting temperature of CuO/Cu_2O–ZrO_2 is conveniently located at 1130° and 1090°C in air and in 1 atm (10^5 Pa) of oxygen, respectively.[30] The above temperatures are within the range of low-temperature superplasticity for 2Y-TZP. Since the solubility of Cu in zirconia is negligible, Cu is not expected to alter TZP's deformation behaviors by solid solution. To keep the amount of the liquid phase small, only 0.3 and 1 mol% CuO were added to 2Y-TZP.

Highly pure commercial 2Y-TZP† and CuO‡ powders were used as starting materials. The powder mixtures of 2Y-TZP and the designated amount of CuO were attrition-milled in an alumina jar using zirconia milling media with a surfactant. The milled slurry was cast, under a pressure of up to 0.7 MPa, into cakes with a diameter of 47 mm, which were dried and isostatically pressed at 400 MPa. The green density after isopressing was between 60% and 65% of the theoretical density.

Sintering studies were performed in air using a sintering dilatometer, at a constant heating rate of 7.5°C/min. For deformation studies, samples were sintered at 1250°C for 1.5 h. The density of the sintered specimen was determined by a water immersion method, and the phase content was analyzed by X-ray diffractometry. Only those specimens with more than 98% of the theoretical density and 100% tetragonal phase were accepted for this study. Annealing at various temperatures and times was also performed to coarsen the grain size when necessary.

(2) Testing

Square bar compression specimens with a height/width ratio of 2.3 were prepared by grinding. Deformation was conducted in uniaxial compression to minimize the effect of cavitation on the constitutive behavior. All tests were conducted in air, between 1000° and 1250°C, with strain rates from 10^{-6} to 10^{-2}/s, in a platinum furnace. The actual specimen temperature during the test was monitored by a thermocouple immediately adjacent to the specimen surface. An alumina hemispherical seat and a set of SiC plattens were used in the loading train. With this arrangement, little evidence of end friction was detectable even at very high strain rates. Specimens were allowed to stabilize at the test temperature for 10 to 15 min before the tests began. Deformation was continuously monitored during the test using an extensometer. Most tests were run using a constant displacement rate, and the load and displacement readings were converted into true stress and true strain rate data reported below. Since steady-state deformation could be reached with strains of the order of a few percent, a single specimen was often used for flow stress determinations at two to three increasing displacement rates. Typically, a test lasted no longer than one-half hour at the test temperature, and testing was terminated after reaching a height reduction of 50%. Under these conditions, very little, if any, grain growth was found in the deformed specimens.

Microstructures and microchemistry of the studied specimens were characterized by electron spectroscopy for chemical analysis (ESCA), SEM, and TEM. The grain size reported was obtained by multiplying the average linear intercept of at least 500 grains by 1.56. Additional micromechanical measurements of hardness and indentation toughness were made by using a Vickers indenter operated at a load over the range of 15 and 40 kg.

III. Experimental Results and Analysis

(1) Sintering and Grain Growth

CuO (0.3 mol%) greatly affected the densification behavior of 2Y-TZP, as evidenced by a shift of the shrinkage curves toward a lower temperature. The maximum shrinkage rate of CuO-containing 2Y-TZP (denoted as 2YZ–0.3 Cu) occurred at 1120°C. Unlike the shrinkage curve of 2Y-TZP, which appears symmetric with respect to the inflection point, at 1165°C, the shrinkage of CuO-containing specimen was much faster above the inflection point. Since the eutectic temperature in the air is 1130°C in the system CuO/Cu_2O–ZrO_2, we may attribute the enhanced sintering to the formation of a liquid phase. This kind of nonsymmetrical shrinkage behavior in sintering has been reported before in other materials when a liquid is generated during heating.[15]

We found it possible to obtain specimens with ≥98% theoretical density in 2Y-TZP by sintering at 1200°C, and in 0.3% CuO-added 2Y-TZP at 1150°C. Higher densities could be routinely obtained by raising the sintering temperature. For deformation studies described below, samples sintered at 1250°C for 1.5 h were used.

The addition of CuO enhanced grain growth as well, as evident from the micrographs in Fig. 1, after sintering at 1250°C for 1.5 h. Linear intercept measurement of the two micrographs in Fig. 1 gave a grain size of 0.21 and 0.35 μm for single-phase and CuO-containing 2Y-TZP, respectively. Despite their different sizes, grains in both TZP's remained equiaxed. Thus, we may compare their deformation behaviors without regard to grain morphology.

(2) Superplasticity of 2Y-TZP

The flow behavior of 2Y-TZP of a grain size of 0.21 μm is summarized in Figs. 2 and 3. Figure 2 demonstrates that a strain rate sensitivity m, defined as the slope in the log strain rate–log stress plot, of 0.67 ± 0.05 is obeyed at all temperatures except at the highest stresses. A high strain rate sensitivity is characteristic of superplastic flow. Above 800 MPa (i.e., 1% of the shear modulus) at lower temperatures, the strain rate sensitivity is lower, below 0.1, indicating a change of deformation behavior from superplasticity into obstacle or lattice resistance–limited dislocation glide. The stress exponent n, defined as the reciprocal of m, is 1.6 in the superplastic regime in this material and it increases to over 10 above 800 MPa. Previously reported values of strain rate sensitivity in 3Y-TZP range from 0.33 to 1, all at higher temperatures.[2–6,31]

The temperature dependence of the superplastic flow is shown in Fig. 3, giving a single activation energy Q of 630 kJ/mol between 1100° and 1250°C. The value is on the high end of the range of activation energies, from 360 to 655 kJ/mol, reported for creep and superplasticity of Y_2O_3-stabilized tetragonal and cubic zirconia.[2–6,31–34]

The grain size dependence of superplastic flow of 2Y-TZP during superplastic deformation at 1175°C is shown in Fig. 4,

†Tosoh, Tokyo, Japan
‡Alfa Products, Danvers, MA

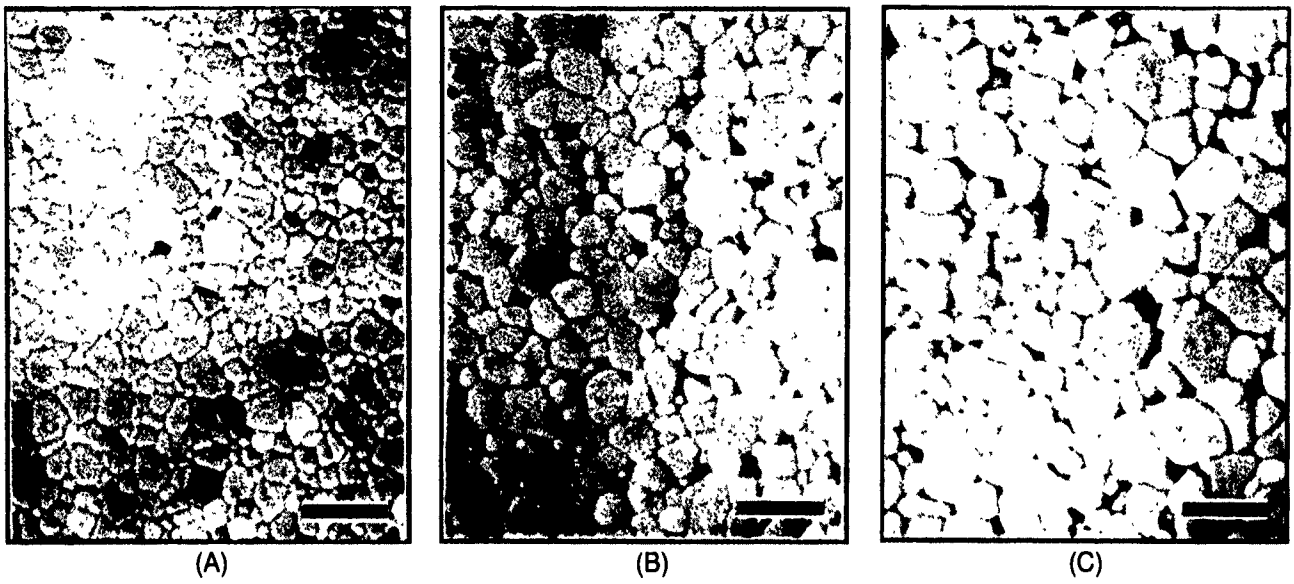

Fig. 1. As-sintered microstructures of three 2Y-TZP's: (A) without additive, (B) with 0.3 mol% CuO, and (C) with 1 mol% CuO; bar = 1 μm.

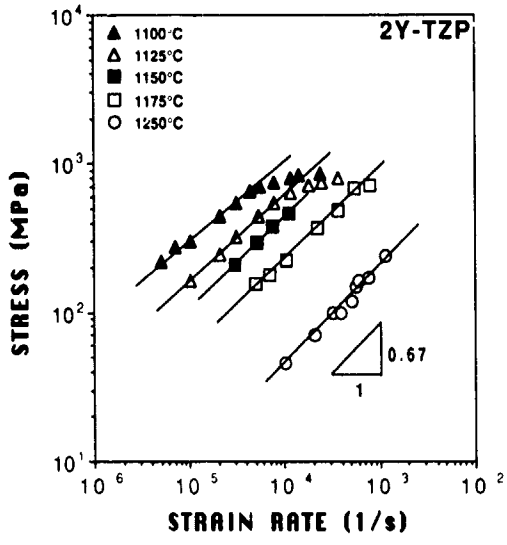

Fig. 2. True stress–strain rate relationships for 2Y-TZP at various temperatures.

where the strain rate at a constant stress is plotted versus the grain size in logarithmic scale. The result yielded a grain size exponent p, defined as the negative of the slope in Fig. 4, of 2.7 ± 0.2. Previously, 2Y-TZP has been studied by Wakai for one grain size only, over the temperature range of 1250° to 1450°C, and by Yoon and Chen in our laboratory for a range of grain sizes over the temperature range of 1250° to 1400°C.[10] Using the activation energy and the grain size exponent reported above, we can compare our data with those of the two previous studies at 1250°C, for a reference grain size of 0.33 μm. As shown in Fig. 5, these data are reasonably close to each other.

(3) Superplasticity of CuO-Containing 2Y-TZP

Flow behaviors of two CuO-containing 2Y-TZP's, one with 0.3 mol% CuO and a grain size of 0.35 μm and the other with 1 mol% CuO and a grain size of 0.41 μm, are summarized in Figs. 6 to 9. Comparing Figs. 2 and 6, it is obvious that in all cases deformation in the CuO-containing 2Y-TZP's is much faster than that in the single-phase 2Y-TZP, by several orders of magnitude, even though the single-phase 2Y-TZP has the smallest grain size, 0.21 μm.

The strain rate sensitivities of the CuO-containing 2Y-TZP's are high, between 0.5 and 0.8, as evident from Figs. 6(A) and (B). This feature is still characteristic of superplastic flow. However, unlike their counterpart without CuO addition, the

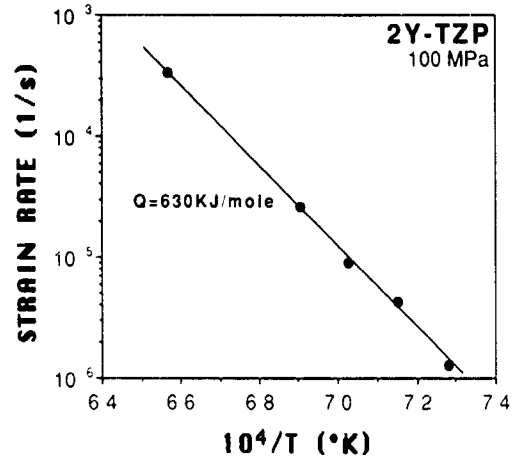

Fig. 3. Temperature dependence of strain rate of 2Y-TZP at 100 MPa

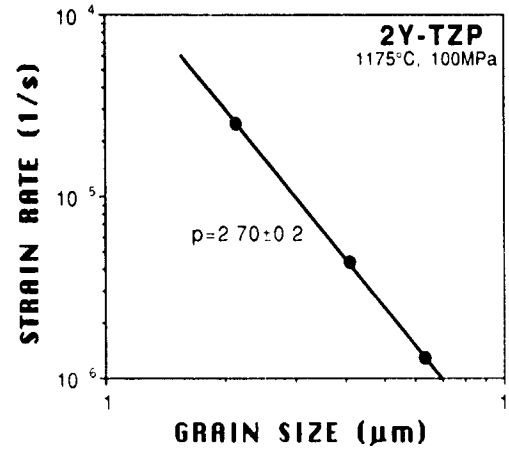

Fig. 4. Grain size dependence of strain rate of 2Y-TZP at 100 MPa and 1175°C

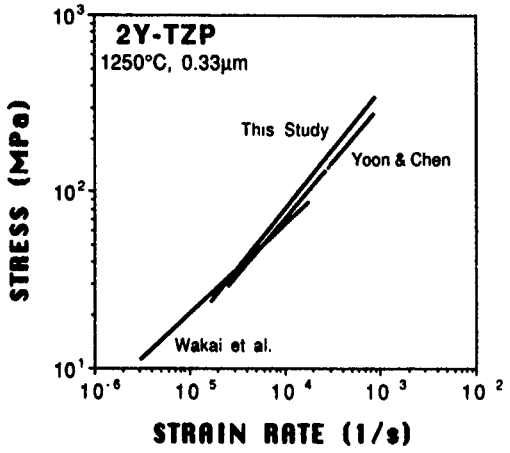

Fig. 5. Superplasticity data of 2Y-TZP by different investigators at 1250°C.

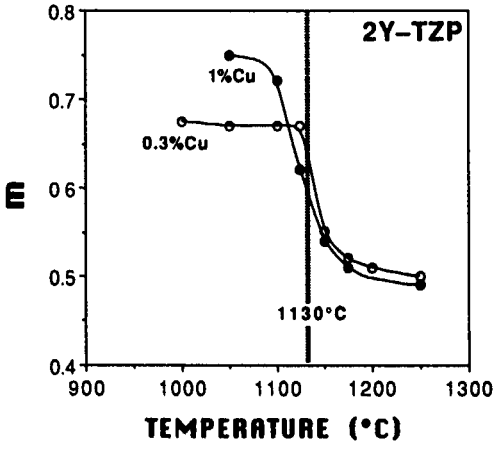

Fig. 7. Temperature dependence of strain rate sensitivity, m, in two CuO-containing 2Y-TZP's.

strain rate sensitivities of both TZP's decrease gradually as the temperature increases and then go through a somewhat abrupt transition at the eutectic temperature, as highlighted in Fig. 7.

The temperature dependence of superplastic flow of these materials undergoes a corresponding transition at the eutectic temperature, becoming lower at higher temperatures as shown in Fig. 8. This effect is more evident for the higher CuO content. For example, the activation energy decreased from 445 to 415 kJ/mol in 0.3%-CuO-added 2Y-TZP, and from 405 to 233 kJ/mol in 1%-CuO-added 2Y-TZP. In both cases, the activation energy below the eutectic temperature is already lower than that of 2Y-TZP without CuO addition.

The grain size dependence of 0.3%-CuO-added 2Y-TZP is shown in Fig. 9 for two temperatures, one above and the other below the eutectic temperature. In both cases, the grain size exponents are much lower than that in single-phase 2Y-TZP. In addition, this exponent is higher at a lower temperature, i.e., 1.64 ± 0.15 at 1000°C and 1.23 ± 0.1 at 1175°C.

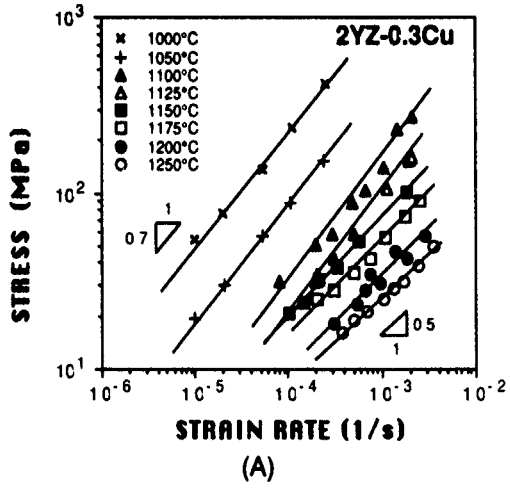

(A)

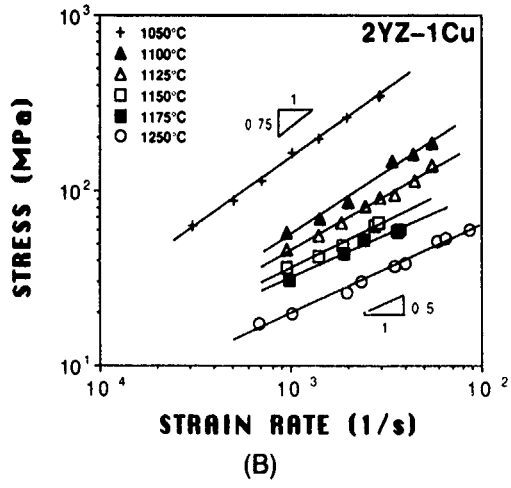

(B)

Fig. 6. True stress-strain rate relationships for 2Y-TZP with (A) 0.3 mol% and (B) 1 mol% CuO.

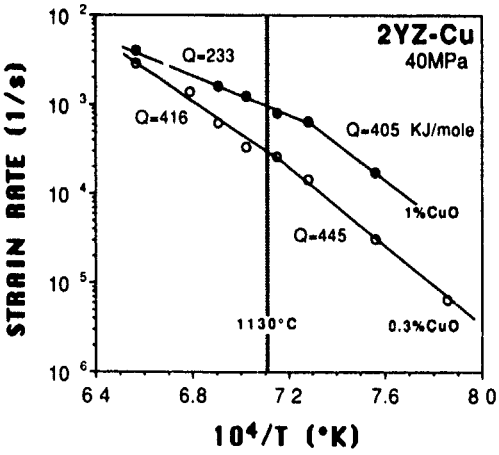

Fig. 8. Temperature dependence of strain rate of two CuO-containing 2Y-TZP's at 40 MPa.

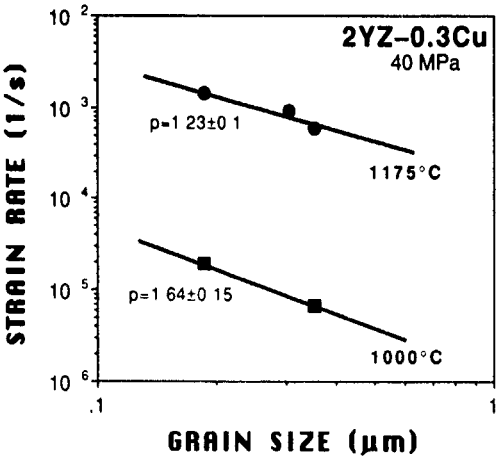

Fig. 9. Grain size dependence of strain rate of two CuO-containing 2Y-TZP's at 40 MPa below and above the eutectic temperature

Apparently, the transition behaviors noted previously in strain rate sensitivity and in activation energy also occurred in the grain size exponent at the eutectic temperature. Taken in toto, these results demonstrate clearly that the deformation mechanisms in CuO-containing 2Y-TZP, at both above and below the eutectic temperature, are different from that of pure 2Y-TZP.

Lastly, to make clear the effect of the amount of CuO addition on deformation, we plot in Fig. 10 the ratio of the strain rates, at 40 MPa, of the two CuO-containing 2Y-TZP's for the entire temperature range studied. It is clear from Fig. 10 that, below the eutectic temperature, the strain rate increases rapidly with an increasing CuO addition. Above the eutectic temperature, however, the effect of the CuO amount is much less. Indeed, the strain rate seems to be independent of the CuO amount at temperatures approaching 1300°C. The implication of this and other observations on deformation mechanisms will be discussed further in a later section.

(4) Grain-Boundary Phase

Direct evidence of the presence of a Cu-rich grain-boundary layer was obtained by ESCA and TEM. We found that all the 2Y-TZP's could be fractured nearly intergranularly at room temperature. In the CuO-containing specimens, the fracture surface, according to the ESCA analysis, contained Cu^{+}, Y^{3+}, Zr^{4+} and O^{2-}. Since the ESCA signals came primarily from elements on and within a distance of 1 to 2 nm from the surface, to determine the depth distribution of the above species, ion beam sputtering was applied to progressively remove the near-grain-boundary material. This then resulted in a rapid, monotonic decrease of the Cu concentration with the sputtering time, its signal falling below detectability after 3 min. This indicated that Cu was present only within a thin layer at the grain boundary. It should also be noted that Si peaks were searched for but not found in the above experiment. However, when 0.5 mol% of SiO_2 was intentionally added to 2Y-TZP, a Si^{4+} peak was detected on the grain boundary.

A TEM micrograph shown in Fig. 11(A) of the same material sintered at 1250°C revealed this Cu-rich layer to be amorphous. The amorphous layer was of the order of 1 to 2 nm and was distributed relatively uniformly along the grain boundary. The amount of the amorphous phase was too low to give a diffuse scattering halo in the selected area diffraction pattern. An accumulation of the amorphous phase at the triple point was found in a few cases, such as the one shown in Fig. 11(B). In contrast, we found that in single-phase 2Y-TZP, the glassy phase was too limited to be detectable in TEM in most cases.

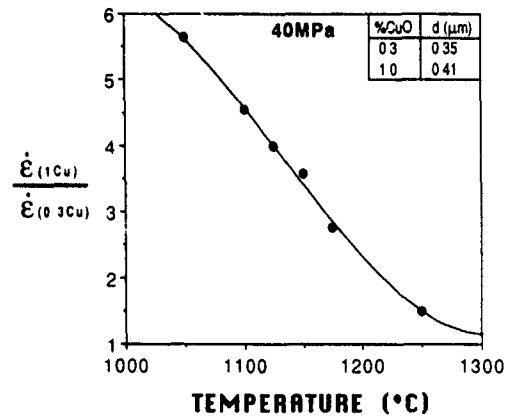

Fig. 10. Ratio of strain rate of two CuO-containing 2Y-TZP's with 1 and 0 3 mol% CuO

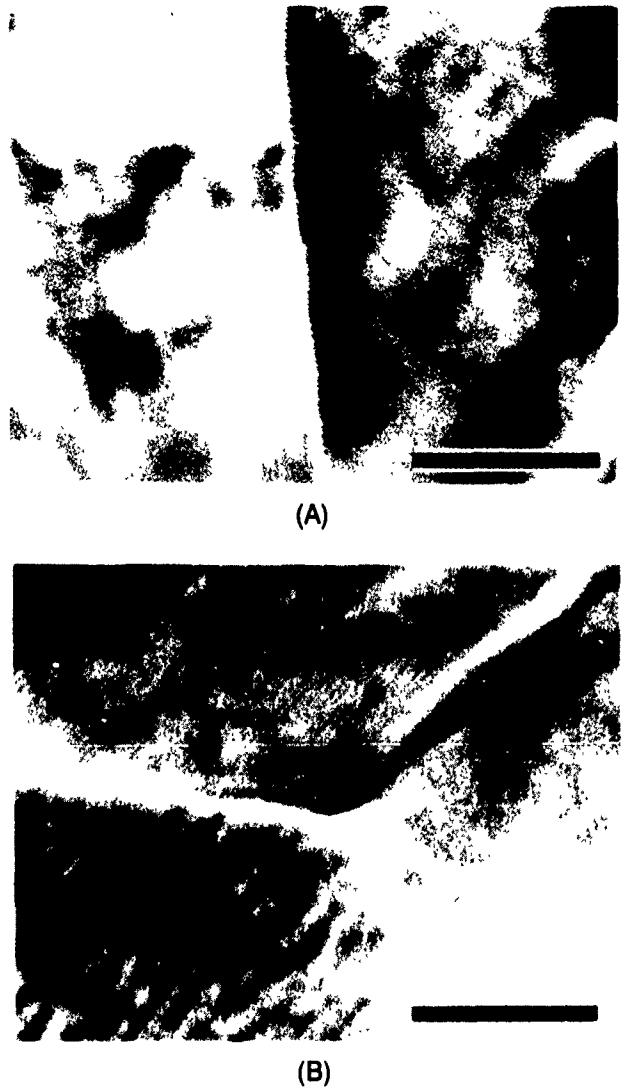

Fig. 11. TEM micrographs revealing a thin layer of amorphous phase at the (A) grain boundary and (B) triple point of CuO-containing 2Y-TZP; bar = 20 nm.

(5) Microstructural and Micromechanical Observations

Micromechanical properties, including hardness and indentation toughness of 2Y-TZP's with and without CuO additions, are presented in Table I. In comparing these data, it should be noted that the grain sizes of the two materials are not the same and they have not been optimized for best room-temperature properties. It is evident, however, that the CuO addition of a small amount has a negligible effect on mechanical properties at room temperatures.

Deformed microstructures of 2Y-TZP's with and without CuO addition were examined by SEM and TEM. In all cases, no significant cavitation damage or change in grain shape and grain size was found after the compression test was performed, regardless of the temperature, stress, strain rate, total strain, or additive amount. Further examination by TEM of a 0.3%-CuO-added specimen, at a strain of 85%, again showed no sign of cavitation. The lack of cavitation was finally confirmed by the density measurement.

Table I. Mechanical Properties of 2Y-TZP's with and without an Additive

Material	Toughness ($MPa\ m^{1/2}$)	Hardness (GPa)
2YZ	4.34 ± 0.30	11 9
2YZ–0.3% Cu	5.98 ± 0.24	10.6

IV. Discussion

(1) Superplastic Forming Conditions

The flow stress of CuO-containing 2Y-TZP at 1200°C was much lower than those reported previously for 3Y-TZP.[2-7,31] This is illustrated in Fig. 12, in which all the reported 3Y-TZP strain rate data at 40 MPa are plotted against the reciprocal temperature. The strain rates of this study, also shown in the graph, are significantly higher than the rest. Clearly, then, the addition of a low-melting phase is an effective way to facilitate ceramic superplasticity. Although a uniaxial tensile test was not performed in the present study, our group has reported biaxial shell stretching of the same ceramic, at a strain rate approaching 10^{-3}/s at 1150°C, to large strains.[35] We found no acceleration of cavitation in those tests and verified that the microstructure remained stable during deformation. Inasmuch as such an experiment is commonly regarded as the most severe formability test in the sheet metal forming field, it has provided, in our view, the most encouraging indication to date that superplastic forming of ceramics would be technologically feasible. It is also important to note that the low-temperature mechanical properties were not significantly affected by the addition of a small amount of low-melting phase.

(2) Grain-Boundary Phase in CuO-Added 2Y-TZP

As confirmed by the TEM and ESCA analyses, there was a low-melting (1130°C), probably amorphous, continuous phase along the grain boundaries of CuO-containing 2Y-TZP. This phase contained Cu,[‡] Y, Zr, and O, and it apparently facilitated sintering, grain growth, grain-boundary sliding, and creep. Two prerequisites for such effects are (1) the grain-boundary phase must cover or wet the entire grain boundaries, and (2) the surrounding grains must be able to dissolve in this phase. As evidenced from the TEM and ESCA results, these requirements were apparently satisfied by the Cu-rich grain-boundary phase.

Heating above the eutectic temperature poses an additional requirement for the grain-boundary phase; i.e., it has to support a normal stress in order to be effective in diffusional creep. Otherwise, the liquid would be squeezed out totally by compression and would not be able to promote creep. A thin intergranular liquid phase can fully support a normal stress if its thickness does not exceed the equilibrium thickness determined by the balance of a dispersion attraction between adjoining grains and a repulsion due to the structure of the intergranular liquid. (A thicker liquid layer will be squeezed around a bit until a thin film of the above equilibrium thickness is left to support the normal stress.) As both of these interactions are of short range (<10 nm), it is a natural consequence that the equilibrium thickness is of the order of 1 nm.[36] This seems to be the case in the present system of CuO-containing 2Y-TZP. Unfortunately, little is known about the structure of the liquid and the dielectric properties of the adjoining grains to allow a quantitative prediction of the equilibrium thickness. However, at the concentrations of CuO that we used, the thickness of the grain-boundary layer is estimated to be 0.3 and 1.0 nm. In the above estimation we have assumed a grain diameter of 0.3 nm and the volume fraction of the liquid to be 0.003 and 0.01, respectively. Since these values are probably smaller than the equilibrium thickness, we believe the grain-boundary liquid in our study can support a normal stress.

[‡]Although CuO was added initially, the more stable state of Cu at high temperatures (above 1000°C) in air is Cu^+ (Ref. 29). This was confirmed by the ESCA analysis in the sintered materials.

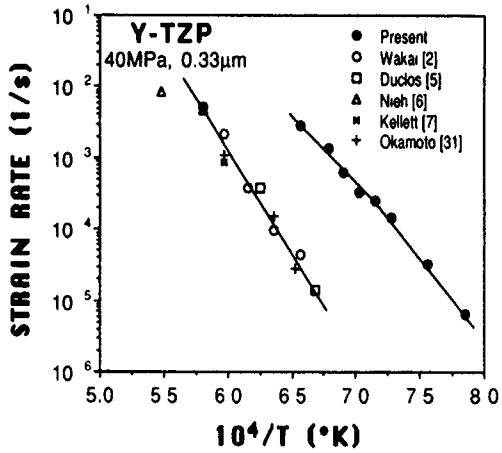

Fig. 12. Comparison of temperature dependence of strain rate of 3Y-TZP from Refs. 2, 5–7, and 31 with 2Y-TZP (this study) at a reference stress of 40 MPa and a reference grain size of 0.33 μm. Except for Ref. 6, all tests were performed in air.

(3) Mechanisms of Superplasticity in CuO-Containing 2Y-TZP

The main effects of CuO on the constitutive behavior of 2Y-TZP are summarized in Table II. We now attempt to rationalize these results in terms of the three mechanisms listed in the Introduction, Eqs. (1) to (3). In doing so, we first acknowledge that we still lack a satisfactory micromechanical model which accounts for the stress exponent and other aspects of superplasticity, despite many such attempts in the past two decades.[37,38] However, there is a general agreement that superplasticity is akin to diffusional creep and involves grain-boundary sliding and grain-boundary migration, but it somehow proceeds at a much faster rate. In the absence of a definitive model, it is difficult for us to make quantitative and absolute predictions of the stress and grain size exponents, etc. at this time. Instead, we have arrived at our rationalization based on the comparison of the qualitative trends in constitutive parameters by invoking the general parallelism between diffusional creep and superplasticity.

We believe that the deformation mechanism in single-phase 2Y-TZP is similar to that of Coble creep, as described by Eq. (1). When CuO is added, below 1130°C, creep is enhanced and controlled by a faster diffusion in the grain boundary, as described by Eq. (2). Above 1130°C, as a liquid phase forms, diffusion is so fast that creep is controlled by interface reactions, as described in Eq. (3). The above picture is consistent with our observations in the following ways.

(1) The stress exponent should remain the same but the grain size exponent should decrease by one as the mechanism changes from Eq. (1) to (2), which was exactly the case with 2Y-TZP and CuO-containing 2Y-TZP below the eutectic temperature.

(2) The stress exponent should increase and the grain size exponent should decrease as the mechanism changes from Eq. (2) to (3), which was exactly the case with CuO-containing 2Y-TZP when the eutectic temperature was crossed.

(3) The diffusion-controlled, grain-boundary-phase-enhanced creep should depend on the amount of the grain-boundary phase, while the interface-controlled, liquid-enhanced creep should not, which was exactly the case observed below and above 1130°C in our experiment, respectively.

(4) Whether it is diffusion control or interface control is dependent on the rates of the two mechanisms. The slower one should be the controlling mechanism. Therefore, the Arrhenius plot of the strain rate should have a concave downward curvature giving a lower activation energy at higher temperatures, which was exactly the case observed below and above 1130°C in our experiment.

Further interpretation of the data of activation energies is difficult at this time for the following reasons. First, even if Coble creep operated in 2Y-TZP, superplasticity would likely

Table II. Summary of Parameters in the Constitutive Equation for Superplasticity ($\dot{\varepsilon} = A\sigma^n d^{-p} \exp[-Q/kT]$)

Material	Grain-boundary phase	n	Q (kJ/mol)	p	A
2Y-TZP	None	1.5 ± 0.15	630	2.70 ± 0.2	
2Y-TZP/0.3% CuO (below 1130°C)	Amorphous solid	1.3 ± 0.1	445	1.64 ± 0.15	Proportional to %CuO
2Y-TZP/0.3% CuO (above 1130°C)	Liquid	2.0 ± 0.1	416	1.23 ± 0.1	Independent of %CuO

involve grain-boundary migration which could be controlled by short-range lattice diffusion if solute segregation occurred. (Direct evidence of solute segregation in a wide range of tetragonal zirconia has been reported by our group recently.)[39,40] The relatively high activation energy of 630 kJ/mol in 2Y-TZP was probably a result of the above. Second, activation energy in Eq. (2) involves both diffusivity and solubility; thus the activation energy of 445 kJ/mol below the eutectic temperature cannot be attributed to a single process. Third, activation energy of the interface process is not well documented; thus it is difficult to judge whether or not the activation energy of 416 kJ/mol above the eutectic temperature was reasonable.

V. Conclusions

(1) The addition of CuO enhances both densification and grain growth because of the formation of a liquid phase. The liquid-forming temperature is consistent with the eutectic temperature, 1130°C, in the system Cu_2O/CuO–ZrO_2. Direct evidence of the grain-boundary phase is provided by TEM and ESCA analyses. The grain-boundary phase contains Cu^+, Y^{3+}, Zr^{4+}, and O^{2+}, and it apparently wets the grain boundary.

(2) The addition of a suitable, low-melting, grain-boundary phase is an effective means to facilitate superplasticity. In 2Y-TZP it has resulted in a substantial decrease in the flow stress, activation energy, and grain size exponent, while retaining damage tolerance, hardness, and toughness. Based on the present results, it is suggested that superplasticity below 1200°C and 50 MPa can be easily achieved in Y-TZP.

(3) A transition in superplastic flow behavior occurs in the vicinity of the eutectic temperature. Decreases in strain rate sensitivity, activation energy, and grain size exponent have been observed as the grain-boundary liquid phase formed. Coble creep, grain-boundary-phase-enhanced diffusional creep, and liquid-enhanced interface creep are proposed as the dominant deformation mechanisms in 2Y-TZP and in CuO-containing 2Y-TZP below and above the eutectic temperature, respectively.

Acknowledgment: We are grateful to Mr. S. L. Hwang for the TEM and ESCA analyses

References

[1]C. Carry and A. Mocellin, "High Ductilities in Fine-Grained Ceramic"; pp. 16.1–16.19 in Superplasticity. Edited by B. Baudelet and M. Suery. Centre National de la Recherche Scientifique, Paris, France, 1985.

[2]F. Wakai, S. Sakaguchi, and Y. Matsuno, "Superplasticity of Yttria-Stabilized Tetragonal ZrO_2 Polycrystals," *Adv. Ceram. Mater.*, **1** [3] 259–63 (1986).

[3]F. Wakai, N. Murayama, S Sakaguchi, H. Kato, and K. Kuroda, "Deformation of Superplastic Tetragonal ZrO_2 Polycrystals", pp. 583–93 in Advances in Ceramics, Vol. 24, Science and Technology of Zirconia III. Edited by S. Somiya, N. Yamamoto, and H. Yanagida. American Ceramic Society, Westerville, OH, 1988.

[4]F. Wakai and H Kato, "Superplasticity of TZP/Al_2O_3 Composite," *Adv Ceram. Mater*, **3** [1] 71–76 (1988).

[5]R. Duclos, J. Crampson, and B. Amana, "Structural and Topological Study of Superplasticity in Zirconia Polycrystals," *Acta Metall*, **37** [3] 877–83 (1989).

[6]T. G. Nieh, C M McNally, and J. Wadsworth, "Superplastic Properties of a Fine-Grained Yttria-Stabilized Tetragonal Polycrystal of Zirconia," *Scr. Metall* **22**, 1297–1300 (1988)

[7]B J Kellett and F F Lange, "Hot-Forging Characteristics of Fine-Grained ZrO_2 and Al_2O_3/ZrO_2 Ceramics," *J Am Ceram Soc*, **69** [8] C-172–C-173 (1986)

[8]K R. Venkatachari and R Raj, "Superplastic Flow in Fine-Grained Alumina," *J Am Ceram Soc*, **69** [2] 135–38 (1986).

[9]C. Carry and A Mocellin, "Superplastic Creep of Fine-Grained $BaTiO_3$ in a Reducing Environment," *J Am Ceram Soc*, **69** [9] C-215–C-216 (1986)

[10]C. K. Yoon and I-W. Chen, "Superplastic Flow of Mullite–Zirconia Composites"; to be published in Advances in Ceramics.

[11]Superalloys; p. 16.5 in Metal Handbook, desk edition. Edited by H. E. Boyer and T. L. Gall. American Society for Metals, Metals Park, OH, 1985.

[12]Properties of Molybdenum; p. 1216 in Metal Handbook, Vol. 1. Edited by T. Lyman. American Society for Metals, Metals Park, OH, 1961.

[13]W. H. Rhodes, "Agglomerate and Particle Size Effects on Sintering Yttria-Stabilized Zirconia," *J. Am. Ceram. Soc*, **64** [1] 19–22 (1981).

[14]W. D. Kingery, "Densification During Sintering in the Presence of a Liquid Phase, I. Theory," *J. Appl. Phys.*, **30** [3] 301–306 (1959).

[15]R. M. German, Liquid Phase Sintering. Plenum Press, New York, 1985.

[16]I. A. Aksay, "Microstructure Control Through Colloidal Consolidation"; pp. 94–104 in Advances in Ceramics, Vol. 9, Forming of Ceramics. Edited by J. A. Mangels and G. L. Messing. American Ceramic Society, Columbus, OH, 1984.

[17]M. F. Yan, "Effects of Physical, Chemical, and Kinetic Factors on Ceramic Sintering"; p. 21 in Advances in Ceramics, Vol. 21, Ceramic Powder Science. Edited by G. L. Messing, K. S. Mazdiyasni, J.W. McCauley, and R. A. Haber. American Ceramic Society, Westerville, OH, 1987.

[18]A. Tsuge, K. Nishida, and M. Komatsu, "Effect of Crystallizing the Grain-Boundary Phase on the High-Temperature Strength of Hot-Pressed Si_3N_4 Containing Y_2O_3," *J. Am. Ceram. Soc.*, **58** [7–8] 323–26 (1975).

[19]C. F. Chen and T.Y. Tien. "High-Temperature Mechanical Properties of SiALON Ceramics: Microstructural Effect," *Ceram. Eng. Sci Proc.*, **8** [7–8] 778–95 (1987).

[20]R. Raj and C. K. Chyung, "Solution-Precipitation Creep in Glass Ceramics," *Acta Metall.*, **29** [1] 159–66 (1981).

[21]J-G. Wang and R. Raj, "Mechanism of Superplastic Flow in a Fine-Grained Ceramic Containing Some Liquid Phase," *J. Am. Ceram. Soc.*, **67** [6] 399–409 (1984).

[22]D.W. Durney, "Solution-Transfer, an Important Geological Deformation Mechanism," *Nature (London)*, **235** [2] 315–17 (1972).

[23]G. M. Pharr and M. F. Ashby, "On Creep Enhanced by a Liquid Phase," *Acta Metall.*, **31** [1] 129–38 (1983).

[24]R. Sheikh and G. M. Pharr, "Further Observations on Creep Enhanced by a Liquid Phase in Porous Potassium Chloride," *Acta Metall.*, **33** [2] 231–38 (1985).

[25]G. M. Pharr, P. S. Godavarti, and B. L. Vaandrager, "Effects of Wetting on the Compression Creep Behavior of Metals Containing Low Melting Intergranular Phases," *J. Mater. Sci.*, **24**, 784–792 (1989).

[26]R. L. Coble, "A Model for Boundary Diffusion Controlled Creep in Polycrystalline Materials," *J. Appl. Phys.*, **34** [6] 1679–84 (1963).

[27]R. A. Stocker and M. F. Ashby, "On the Rheology of the Upper Mantle," *Rev. Geophys. Space Phys.*, **11**, 391–426 (1973).

[28]E. H. Rutter, "The Kinetics of Rock Deformation by Pressure Solution," *Philos. Trans. R. Soc. London, A*, **283**, 203–19 (1976).

[29]J. W. Cahn, "Theory of Crystal Growth and Interface Motion in Crystalline Materials," *Acta Metall.*, **8** [8] 554–62 (1960).

[30]A. M. M. Gadalla and J. White, p. 33 in Phase Diagram for Ceramics, 1969 Supplement. Edited by E. M. Levin, C. R. Robbins, and H. F. McMurdie. American Ceramic Society, Columbus, OH; Figs. 2145 and 2146.

[31]Y. Okomoto, J. Ieuji, Y. Yamada, K. Hayashi, and T. Nishikawa, "Creep Deformation of Yttria-Stabilized Tetragonal Zirconia (Y-TZP)"; pp. 565–72 in Advances in Ceramics, Vol. 24, Science and Technology of Zirconia III. Edited by S. Somiya, N. Yamamoto, and H. Yanagida. American Ceramic Society, Westerville, OH, 1988.

[32]P. E. Evans, "Creep in Yttria- and Scandia-Stabilized Zirconia," *J. Am. Ceram. Soc.*, **53** [7] 365–69 (1970).

[33]M. S. Seltzer and P. K. Talty, "High-Temperature Creep of Y_2O_3-Stabilized ZrO_2," *J. Am. Ceram. Soc.*, **58** [3–4] 124–30 (1975).

[34]F. Wakai and T. Nagona, "The Role of Interface-Controlled Diffusion Creep on Superplasticity of Yttria-Stabilized Tetragonal ZrO_2 Polycrystals," *J. Mater. Sci. Lett.*, **7**, 607–609 (1988).

[35]X. Wu and I-W. Chen, "Superplastic Forming of Fine-Grained Ceramics"; presented at the 91st Annual Meeting of the American Ceramic Society, Indianapolis, IN, 1989 (Basic Science Division, Paper No. 125-B-89).

[36]D. R. Clarke, "On the Equilibrium Thickness of Intergranular Glassy Phases in Ceramic Materials," *J. Am. Ceram Soc*, **70** [1] 15–22 (1987).

[37]J.W. Edington, K. N. Melton, and C. P. Cutler, "Superplasticity," *Prog Mater. Sci.*, **21** [2] 61–170 (1976).

[38]I-W. Chen, "Superplastic Flow of Two-Phase Alloys", pp 5 1–5 20 in Superplasticity. Edited by B. Baudelet and M. Suery Centre National de la Recherche Scientifique, Paris, France, 1985.

[39]I. G. Lee and I-W. Chen, "Sintering and Grain Growth in Tetragonal and Cubic Zirconia"; pp. 340–45 in Sintering '87 Edited by S Somiya, M Shimada, M Yoshimura, and R Watanabe Elsevier Scientific, Amsterdam, Netherlands, 1988

[40]S L. Hwang and I-W Chen, "Grain Size Control of Tetragonal Zirconia Polycrystals using the Space Charge Concept", unpublished work □

SHEAR THICKENING CREEP IN SUPERPLASTIC SILICON NITRIDE[†]

I-Wei Chen and Shyh-Lung Hwang

Department of Materials Science and Engineering
University of Michigan
Ann Arbor, MI 48109-2136

ABSTRACT

A novel shear thickening phenomenon has been observed in superplastic silicon nitrides compression tested between 1500 and 1600°C. Liquid enhanced creep of sialons undergoes a transition from Newtonian behavior to shear-thickening behavior at a characteristic stress, with the strain rate sensitivity increasing from unity to around two. The transition stress is always around 20 MPa even though the Newtonian flow stress is very sensitive to temperature, grain size, and phase compositon. Rheopexic hysteresis, manifested as a slow stress relaxation to a steady state value after a strain rate decrease, was also observed in the shear thickening regime. We attribute the cause for shear thickening to a repulsive force between initially wetted sialon grains, which form a "dry" and "rigid" bridge in between when pressed above a characteristic stress, possibly due to the contact of the residue Stern layers on the opposing grain/liquid interfaces. A micromechanical model, which takes into account the stress variation among differently oriented grain boundaries, has been formulated to assess the effect of "rigid" grain boundaries. A continual stochastic rearrangement of grain configurations and a relatively thick Stern layer are suggested as the necessary pre-requisites for shear thickening in liquid enhanced creep.

[†] Supported by U.S. Air Force Office of Scientific Research under Grant No. 87-0289.

Key Words: Silicon nitride, creep, superplastic, grain boundary, glass

I. INTRODUCTION

Creep including superplastic flow of ceramic materials and metals is commonly described by a power law

$$\dot{\varepsilon} = \alpha \sigma^n \tag{1}$$

where $\dot{\varepsilon}$ is the creep rate, σ is the flow stress, α is a material constant, and n is a non-dimensional material constant. When the creep mechanism is that of diffusional plating of grain boundaries, n equal to one is often found and such flow behavior is formally analogous to Newtonian flow in fluid mechanics. On the other hand, a higher n value can arise when deformation is at least partially attributed to dislocations or cavitation, or is somehow limited by interface reactions. A stress exponent lower than unity has never been reported in these materials to the best of our knowledge.[1-2]

Deformation of slurries, colloids, and polymeric liquids can be similarly described by Eq (1). However, both $n > 1$ and $n < 1$ are commonly observed depending on the materials. Expressed in terms of viscosity, $\eta = \sigma/\dot{\varepsilon}$, shear thinning corresponds to $n > 1$ for a decreasing viscosity at a higher strain rate, while shear thickening corresponds to $n < 1$ for an increasing viscosity at a higher strain rate.[3] Quantitative models have been proposed for shear thickening in polymeric melts, drawing on the special features of molecular configurations that evolve with shear rate.[4-5] In colloids it has also been linked to either the formation of an extended gel-like superstructure between particles[6-7] or to the breakdown of easy-slip patterns.[8-9] On the other hand, shear thickening in slurries and granular materials, such as wet sand and soil, is generally attributed to dilatant flow involving particles rolling over each other with dewetted liquid trapped in intersticies.[10-11] In the latter two classes of materials (colloids and slurries), rheological studies are mostly limited to solid volume fractions of no more than 75%.

Superplastic sialons of very fine microstructures which exhibit tensile ductilities in excess of several hundred percent have been recently discovered.[12] Sialons are solid solutions based on Si_3N_4. When the tetrahedral Si-N network is modified by substitution of Al for Si and O for N, β'-sialon isomorphic with β-Si_3N_4 forms with a general formula of $Si_{6-x}Al_xO_xN_{8-x}$.[13] When additional metal ion interstitials are added to the network, the formula is altered to become $M_{z/n}Si_{6-x-z}Al_{x+2}O_xN_{8-x}$, and the crystalline structure is converted to one isomorphic with α-Si_3N_4. This is termed α'-sialon.[14] In most cases, some amount of glassy phase ranging from 5 to 20 vol% coexists with α' and β' sialons.[15] It is in this class of ceramics that we have observed a novel Newtonian to shear thickening transition which occurs at a characteristic stress, ca. 20 MPa in compression between 1500 and 1600°C. The main experimental observation of this highly unusual phenomenon is reported in the present paper along with a theoretical model that rationalizes the transition. Further details of the materials development, their microstructures and their constitutive behavior will be reported elsewhere.[15]

II. EXPERIMENTAL

2.1 Materials

Sialons used in this study were prepared by mixing proper amounts of Si_3N_4, AlN, Al_2O_3 and Y_2O_3 powders. The starting powders were very fine and, in the case of Si_3N_4, contain a very high α phase content. They were attrition milled in isopropol alcohol for 2 h with porcelin or high purity alumina milling media. The milled slurry was stirred and dried under heat to obtain a uniform powder mixture. Fully dense ceramic blanks were then prepared by hot pressing under 28 MPa for 20 min. at 1550°C using a graphite die operating in nitrogen. Some materials were also hot pressed or annealed for a longer time in an attempt to vary the microstructure. The phase compositions were analyzed by x-ray diffraction. For a summary of the preparation conditions and the phase assemblage, see Table 1, in which the materials designation will be used in the rest of this paper. Finally, some typical micrographs of the microstructure are shown in Fig. 1. Note that

in the micrograph to the right, grains almost always overlap because of their very small sizes compared to the thickness of the TEM sample. Additional information on the processing, microstructure, and phase equilibrium will be reported elsewhere.[15]

2.2 Testing

Specimens for compression tests were cut from blanks and ground into 3 mm x 3 mm x 6 mm bars. Other dimensions and height-to-width ratios were also tested to evaluate the effect of friction on compression experiments. The specimens were placed between two SiC plattens. A piece of graphite foil was inserted between the specimen and the platten to further reduce friction. Testing was conducted in a vacuum furnace, with tungsten mesh heating elements, between 1500°C and 1575°C in high purity nitrogen. The load frame used was an MTS operated under servohydraulic control to provide a constant true strain rate during the compression test. In general, a test was terminated after reaching a true strain of -0.5. Under the above operating conditions, we found little barrelling of the specimen after testing. In addition, the flow stress was independent of the height-to-width ratio used when the latter exceeded 2. Thus, friction was probably negligible in these experiments.

III. RESULTS

A typical set of stress-strain curves at various strain rates in compression is shown in Fig. 2. All data shown here and below are in true stress, true strain, and true strain rate. Except at the lower strain rates, the flow stress is essentially constant over a large range of strain. Thus, a steady state is no doubt reached in those cases. The strain hardening observed at the lower strain rates is a result of microstructural coarsening. Such a phenomenon is common among fine-grained materials that deform via diffusional creep, superplasticity, or solutional reprecipitation creep, which is believed to be operational here. The initial transient reflects some elastic deformation of the specimen, the compliance of the loading train, and mostly plastic deformation during the

evolution of the initial microstructure. The nominal strain of the transient varies from 3 to 15% increasing with strain rate.

Comparing the flow stresses at the four strain rates in Fig. 2 at the same amount of time, say 500 s after the start of deformation, we find that the ratio of the two lowest flow stresses (2.0) is the same as that of the corresponding strain rates, but the ratio of the two highest flow stresses (1.9) is much higher than that of the corresponding strain rates (1.4). In rheological terms, then, deformation at the two lower strain rates is Newtonian, but deformation at the higher strain rates is shear thickening. If the flow stress data are read at the same strain, say 0.15, then we still find shear thickening at the higher strain rates, but shear thinning instead at the lower strain rates.

Data of flow stress and strain rate have been collected over a wide range of deformation conditions for a large number of superplastic sialon materials. (In the case of continuous strain hardening, the flow stress data are ones obtained at 500 s after deformation. Otherwise, the steady state flow stress data are used.) Some representative ones are shown in Fig. 3. The data shown in this figure were obtained at one test temperature, 1550°C, and are expressed in stress versus strain rate, both in logarithmic scale. They all have a rather abrupt change in the slope, which is the same as the reciprocal stress exponent, 1/n (also commonly termed strain rate sensitivity, m, $m = \frac{\partial \ln \sigma}{\partial \ln \dot{\varepsilon}}$, especially in the superplasticity literature). It has a value of unity below the transition transition stress, and greater than unity above that. This corresponds to n = 1 below the transition and n ~ 0.5 above the transition. It is important to note that, despite the wide range of strain rate covered, the transition stress always lies near 20 MPa. Data of one material at different temperatures from 1500 to 1575°C are shown in Fig. 4. A similar transition, occurring at approximately the same stress, is seen in every case. Moreover, the slopes at below and above the transition are the same as those found in Fig. 3. In short, flow in uniaxial compression at stresses higher than the transition stress, now termed σ^*, is much more sensitive to strain rate compared to Newtonian flow, requiring a much higher flow stress.

Transient deformation experiments involving a rate increase or rate decrease have also been performed. The rate increase in equal increments was programmed to occur at equal strain increments up to a maximum strain rate and then similarly decreased again to zero. The recorded flow stress just prior to the step increase/decrease is shown as a data point in Fig. 5, and the trajectory that connects all the data points forms a stress-strain-rate loop. In this plot we found a hysteresis (in the counter-clockwise sense) in the shear-thickening regime, which is absent in the Newtonian regime. The latter hysteresis indicates that, after a strain rate decrease, it requires considerable time (strain) to fully relax the flow stress to the steady state value. Despite the hysteresis, the transition is, nevertheless, reversible in either direction. This kind of transient, termed rheopexy, is common among fluids which are shear thickening.[3,16] For shear-thinning fluids, the loop is of the opposite nature (clockwise).[3,16] (For solids undergoing dislocation creep, a similar transient reflecting the evolution of internal stresses has also been observed, even though $n > 1$ in this case.[17])

Lastly, we have tried, but failed, to verify a similar Newtonian shear thickening transition in tensile deformation. Although very large elongation can be obtained at lower stresses in many sialon materials studied here, none has a steady state tensile flow stress high enough in comparison with compression deformation in the shear thickening regime. A more complete report of the constitutive relation of superplastic flow of these sialons, along with microstructural studies, will be provided elsewhere.[15]

IV. A MODEL FOR NEWTONIAN—SHEAR THICKENING TRANSITION

Let us now summarize our observations regarding the Newtonian-shear thickening transition. The transition occurs at a characteristic stress, of the order of 20 MPa, which is independent of temperature and phase composition. The transition is reversible and strain independent, but has a hysteresis in the shear thickening regime. Although the data are not presented here, we have also found that creep in the Newtonian regime is grain size dependent, which is responsible

for the strain hardening seen in Fig. 2 at the lowest strain rate.[15] Indeed, it must be operated by a diffusion-related mechanism, such as diffusional creep (most likely enhanced by the liquid phase) or solution/reprecipitation creep,[18-22] in conjunction with grain boundary sliding, rotation, and switching events which continually stimulate the evolution of the grain/grain configurations to sustain large strain deformation. The latter are evidently needed for steady-state superplastic flow.[23]

We now formulate a continuum mechanics description to model the above transition. We first postulate that, in the sialon materials, a micromechanical transition from a deformable Newtonian state to a non-deformable rigid state can occur within isolated volume elements at stresses above σ^*. Let the volume fraction of the rigid state "phase" be v_f, and the creep rate of the Newtonian state phase be $\dot{\varepsilon}_0$, then

$$\dot{\varepsilon}_0 = \sigma/\eta \tag{2}$$

where η is an apparent viscosity which is dependent on temperature, grain size, phase composition, and liquid content. The creep rate of the "composite" of the two "phases" is given by

$$\dot{\varepsilon} = (1-v_f)^{2.5}\, \dot{\varepsilon}_0 \tag{3}$$

In the above, the result of a recent study by Yoon and Chen on a superplastic flow of a two-phase composite containing rigid inclusions in a soft matrix was used to obtain the prefactor on the right hand side.[24] If we further envision that v_f increases with stress above σ^*, then the transition from Newtonian flow to shear thickening flow can be rationalized.

To develop the model further, we next associate the unit of volume element to a small region containing one grain boundary only. We also propose that, when the normal pressure on the grain boundary exceeds a certain critical stress σ_c, the associated volume element becomes rigid. Thus, the volume fraction of the rigid "phase" v_f is simply the fraction of grain boundaries that support a normal pressure in excess of σ_c.

The average normal pressure on grain boundaries can be estimated approximately using a two-dimensional picture. Grain boundaries are pictured, as in Fig. 6, to be randomly oriented spatially, but with a locally equilibriated configuration containing segments intersecting at 120° with each other. The average normal pressure on any such boundary of any orientation can be computed approximately by referring to a periodic array of hexagonal grains of the same orientation. This seems to be a reasonable approximation which, in effect, replaces the actual boundary condition by a periodic one at some distance from the grain boundary of interest. As shown in the Appendix, the average normal pressure $\bar{\sigma}$ thus computed may be represented as

$$\bar{\sigma} = \sigma \left(\frac{1}{2} + \cos 2\theta\right) \tag{4}$$

where θ is the angle between grain boundary normal and the external stress direction. It should be noted that the maximum normal pressure occurs at $\theta = 0$, where $\bar{\sigma} = 1.5\ \sigma$. For $90° \geq \theta \geq 60°$, a negative normal pressure, i.e. tension, should prevail. In the following, we will assume that the above stress estimate for hexagonal grains is also applicable in the three-dimensional case for evaluating rigid grain boundaries.

As the applied stress in uniaxial compression increases to reach $\frac{2}{3}\sigma_c$, grain boundaries which are normal to the stress axis ($\theta = 0$) first become rigid. As the stress increases further, some grain boundaries with a non-zero θ angle also become rigid. The fraction of such rigid grain boundaries is found by evaluating the solid angle of all the boundaries in three dimensions up to an azimuthal angle θ from the pole, normalized by 4π

$$v_f = \frac{1}{4\pi} \int_0^{2\pi} \int_0^{\frac{1}{2}\cos^{-1}\left(\frac{\sigma_c}{\sigma} - \frac{1}{2}\right)} 2 \sin\theta \ d\theta \ d\phi \qquad \left(\sigma \geq \frac{2}{3}\sigma_c\right) \tag{5}$$

In the above, the factor 2 in the integrand is introduced to account for symmetry (between θ and $180° - \theta$), and the upper integration limit for θ is set to coincide with $\bar{\sigma} = \sigma_c$. Evaluating the integration and after some trigonometric manipulation, we obtain

$$v_f = 1 - \sqrt{\frac{1}{4} + \frac{\sigma_c}{2\sigma}} \qquad \left(\sigma \geq \frac{2}{3}\sigma_c\right) \tag{6}$$

Note that v_f is always no higher than 0.5 since grain boundaries with $90° \geq \theta \geq 60°$ are not in compression. Combining Eq (6) and Eq (3), this yields, finally, the strain rate

$$\dot{\varepsilon} = \begin{cases} \sigma/\eta & \left(\sigma < \frac{2}{3}\sigma_c\right) \\ \left(\frac{1}{4} + \frac{\sigma_c}{2\sigma}\right)^{1.25} \frac{\sigma}{\eta} & \left(\sigma \geq \frac{2}{3}\sigma_c\right) \end{cases} \tag{7}$$

The above results are plotted in Fig. 7 in log σ - log $\dot{\varepsilon}$ to compare with the experimental data shown in Figs. 3 and 4. If we identify σ^* with $\frac{2}{3}\sigma_c$, then the shape of the predicted σ-$\dot{\varepsilon}$ plot, including its slope in the two regimes, is similar to the one observed. The reason that the predicted transition looks sharper is because we have assumed an abrupt transition at the critical stress σ_c. It could have been smoothed out by allowing some distribution in grain size, grain shape, etc. Overall, then, the mechanical model seems to capture the basic characteristics of the Newtonian/shear thickening transition.

The physical origin of the critical stress, σ_c, which is responsible locally for the transition, remains to be identified. This will be discussed in the next section.

V. DISCUSSION

5.1 Grain/Liquid/Grain Interaction

It is now well-known that almost all grain boundaries in silicon nitrides and sialons are wetted by a thin glassy phase.[25] Clarke has argued that an equilibrium thickness (denoted as Δ_0) of this phase should be maintained because the van der Waal attraction between grains is counterbalanced by a repulsive interaction due to the structure of the liquid.[26] His model predicts an interaction

potential similar to that given by the Dejaguin-Landau-Verwey-Overbeek (DLVO) theory of colloidal stability where a balance is maintained between attractive van der Waal forces and repulsive electrostatic forces.[27] Plotting this potential as a function of grain/grain separation, h, a primary minimum at small h with a very high potential barrier outside and a shallow secondary minimum further beyond that is the common feature predicted by this model. Thus, a stress-free grain boundary should maintain an intergranular glassy phase of an equilibrium thickness Δ_0, located at the secondary minimum, while a stressed grain boundary will become slightly depressed toward the potential barrier but otherwise able to support a normal pressure, provided the potential barrier outside the primary minimum is not exceeded.

Our experimental results are consistent with the idea that a repulsive force between grains exists: at pressures above σ_c, grain boundaries seem to be able to support a large normal pressure without much further deformation. On the other hand, since the Newtonian/shear thickening transition is reversible, it may be further concluded that the potential barrier is quite high, enough to support several hundred MPa's as seen from Figs. 2-3 so that the primary minimum where reversibility would have been lost is not accessible in our experiments.

One unsatisfactory aspect of the above model is that it leaves the significance of σ_c, and the appearance of a sharp transition stress σ^*, unclarified. In our opinion, this can be readily improved by incorporating the concept of a Stern layer at the liquid/grain interface, again in analogy to the theory of colloidal stability.[27] As shown in Fig. 8, if a Stern layer of compactly packed liquid molecules forms on the interface, then the grain/grain interaction given by Clarke's model is truncated at twice the distance of one Stern layer thickness $2\Delta_S$, and the grain to grain distance should be limited to the same. For the same potential between "bare" grains, the truncated potential at $2\Delta_S$ decreases with increasing Δ_S. Using the above picture, we interpret that, in the sialon ceramics studied here, the Stern layer is sufficiently thick to render only a relatively low repulsion remaining at $\Delta_0 \geq h \geq 2\Delta_S$. Thus, the flow behavior is virtually unaffected by the grain/liquid/grain interaction until the normal pressure is sufficient to squeeze out the liquid so that only the Stern layers remain. This would occur at $\sigma^* = 20$ MPa, or through our model which

established its relation to σ_c, at a repulsive force of 30 MPa or so. The latter stress is then the repulsion at $h = 2\Delta_s$ in the sialon system. In view of the compactness of the Stern layer structure compared to a normal liquid, we further suggest that, at stresses above σ_c, with the grain boundary liquid entirely squeezed out except for the Stern layers, both grain boundary sliding and grain boundary diffusion would be much retarded. It is in this sense that the grain boundary has become "rigid" and "dry," and the micromechanical transition envisioned in Section IV is realized.

A rough calculation is now made to estimate the critical stress σ_c using Clarke's model. At a distance greater than $2\Delta_s$, the normal stress between grains separated by a liquid can be expressed as

$$F = \frac{H}{6\pi h^3} \cdot 1.6 \times 10^9 \ (J/m^2)\ \eta_o^2 \exp\left(\frac{-h}{\xi}\right) \qquad (8)$$

(At a distance smaller than $2\Delta_s$, the Stern layers are in touch and we expect the repulsion to increase rapidly beyond that given by Eq (8).) In the above, H is the Hamaker constant, η_o is the ordering parameter ($o \leq \eta_o \leq 1$), and ξ is the correlation length for the liquid. Following Clarke, we choose $\xi = 0.3$ nm which is the molecular size of the SiO_4 tetrahedral unit representative of the grain boundary liquid, and $H = 7.6 \times 10^{-20}$ J for $(Si_3N_4)_s$ - $(SiO_2)_l$ - $(Si_3N_4)_s$ solid-liquid-solid combination. If we further assume that the thickness of the Stern layer is the same as ξ, then the estimated stress at $h = 2\Delta_s = 2\xi$ is 35 MPa (for $\eta_o = 0.5$), which is very close, perhaps fortuitously, to our measured σ_c value of 30 MPa.

5.2 Shear Thickening Models and Observations

Several other interpretations of shear thickening phenomenon in slurries, colloids and molecular melts or solutions were mentioned in the Introduction. The models proposed for polymeric melts and solutions[3-5,28-29] envision flow-induced association, entanglement, or crystallization of molecules, due to enhanced collisions, chain alignment, or chain stretching. These ideas are quite specific to polymeric molecular structures and generally not applicable to the

other cases, although the notion that two or more molecules can form "quasi-aggregates"[30-31] which have a higher viscosity than the unassociated polymeric solutions is certainly analogous to our micromechanical picture of "rigid" inclusions. The idea of network formation under enhanced collision kinetics can be extended to colloids in which a gel-like behavior with some dilatancy prior to a steep viscosity increase has been observed.[3] In this case, the initial state contains colloidal particles that are separated by repulsion which, under the flow action, are brought into contact (i.e., falling into the primary minimum). Such a gel-like transition, however, is often irreversible, as manifested by a permanent increase in the sedimentation volume. This is in contrast to the reversible transition described in the previous section. It has also been established for colloids that, under a shear stress, colloidal particles are organized into closely packed layers by hydrodynamic action to minimize the resistance to shear, in a manner not unlike the slip pattern in crystalline solids.[8-9] At a certain shear stress, flow instability occurs when particles fall in between layers, resulting in a flow "jam" and a rapid increase of viscosity. This instability stress has been found to be highly sensitive to the size and volume fraction of the particles, as well as their size and shape distribution.[8] This latter feature is contradictory to our observation of a constant characteristic stress at the transition.

Besides the above interpretations, there is the classical model for shear thickening based on the observation in sand and soil. Essentially, in a closely packed slurry, such as wet sand, particle rolling will inevitably cause a volumetric dilation that draws in liquid, as originally commented on by Reynolds.[10] If there is just enough liquid present initially to wet all the closely packed particles, any disturbance of this configuration is likely to generate some open pores. The shear-thickening transition may then be associated with the liquid break-up (i.e., cavitation) that produces locallized dewetted regions adjacent to liquid-filled pores, with local drying being responsible for the increase in flow resistance.[11] Such a transition is expected to be dictated by the capillarity force of the pores which must scale, by similitude, with reciprocal particle size. This prediction is again contradictory to our observation of a constant transition stress over the varied microstructural length scales investigated. We should acknowledge, of course, that our model also envisions a

liquid redistribution and some "drying" (albeit with the Stern layer remaining) even though no actual dewetting/cavitation is expected.

Finally, it should be emphasized that shear-thickening reported for the above systems were all obtained at a much higher strain rate, a much lower particle fraction, a much larger particle size (except perhaps in polymeric solutions), a much lower temperature, and probably with little shape accommodation of the particle itself by elastic-plastic deformation or diffusion.[3,9,16] This distinction makes the present observation rather unique among the large variety of shear-thickening reports found in the literature. In this respect, it is not surprising to find these previous models inconsistent with our observation.

5.3 Concurrent and Competing Flow Mechanisms

The flow phenomena described in this work occurred in steady-state deformation at large strains. A continual evolution of grain/grain configurations and the interchange of mechanical states are essential for any large strain, steady-state, two-phase flow process, especially if one of the constituent phases is non-deformable. Thus, the grain boundaries which become rigid do so only for a certain time, and they are eventually relieved from pressure and separated; meanwhile, grains at other locations are compressed to become rigid. Presumably, these changes are driven by stochastic grain boundary sliding and grain rotation events.[32] Without this evolution and interchange of states, grains subject to a high normal pressure would have been locked and the creep process would have been stopped. Indeed, such an exhausting creep process involving depletion of a viscous liquid on highly pressed grain boundaries has been recently described by several investigators.[33-34] If maximal strains before exhaustion in such a process are of the order of the liquid fraction, which is much less than the superplastic strain achieved in our experiments, it is clear that shear-thickening is not directly related to the latter mechanism. On the other hand, the transient behavior described in Section III, which is probably due to the squeezing out or replenishing of the liquid as the compressed grain boundaries adjust their liquid thickness between Δ_0 and $2\Delta_s$, can be understood using similar viscous flow models.[33-35]

While superplastic sialons may not be the only ceramics which exhibit a shear-thickening transition, such a transition could be masked by other concurrent mechanisms operating in creep. For example, creep deformation of ceramics is frequently interrrupted by cavitation at grain boundaries, even in compression, due to the tensile stress concentration at triple points where incompatibility from grain boundary sliding is most severe.[36] In silicon nitride, for example, a cavitation-related transition from n = 1 to n = 2 has been reported.[37] Similar observations in glass ceramics are also well-documented.[38] Such a transition is of the opposite type of shear-thickening transition and can obscure the latter if occurring at the same time. Since the magnitude of the local tensile stress rises with the grain size in diffusional creep and the like (superplasticity and liquid enhanced dissolution/reprecipitation), a fine-grained microstructure which has a higher ductility and lower flow stress is probably needed for avoiding cavitation and for observing shear-thickening in ceramics. Shear-thickening transitions in certain systems may also be unimportant if the transition stress is too high. For example, if our proposed model proves correct, then the structure and thickness of the liquid absorption on the grain/liquid interface will dictate the transition stress, which could vary over several orders of magnitude in different systems because of the short-ranged nature of the repulsion at the scale of the coherent length.[26] While further studies are required to provide a better understanding of this aspect, it seems noteworthy that shear-thickening was not observed in other superplastic ceramics (zirconia,[12,18,24] alumina,[12,39] mullite,[40] and glass ceramics[20]). If so, it may well be a unique flow behavior of sialons.

APPENDIX

Average Normal Stress on an Inclined Grain Boundary

The average normal stress on any inclined grain boundary in a periodic hexagonal array can be obtained from equilibrium consideration, provided no shear traction is transmitted by grain boundaries. Consider the periodic array shown in Fig. A1 and draw the free-body diagram as outlined by the dashed lines and the two adjacent grain boundaries. The average normal stresses on the two grain boundaries are denoted by $\bar{\sigma}_1$ and $\bar{\sigma}_2$. Their force balance in the applied stress direction gives

$$\bar{\sigma}_1 \cos\theta + \bar{\sigma}_2 \cos(60° + \theta) = \sigma (\cos\theta + \cos(60° + \theta)) \tag{A1}$$

Similarly, force balance in the orthorgonal direction, where there is no external stress, gives

$$\bar{\sigma}_1 \sin\theta + \bar{\sigma}_2 \sin(60° + \theta) = 0 \tag{A2}$$

Solving the above set of simultaneous equations and simplifying the solution by trigonometric manipulation, we obtain the following result

$$\bar{\sigma}_1/\sigma = \tfrac{1}{2} + \cos 2\theta \tag{A3}$$

and

$$\bar{\sigma}_2 / \bar{\sigma}_1 = - \sin\theta / \sin(60° + \theta) \tag{A4}$$

Of course, Eq (A4) can be shown to be the same as Eq (A3) following a transformation from θ to $60° + \theta$. Thus, only Eq (A3) is quoted in the text as Eq (4).

The above solution is exact and independent of the actual mechanism of deformation operating in the material. The assumption of zero boundary shear traction is reasonable as long as grain boundary sliding is not impeded.

TABLE 1: COMPOSITONS*, HEAT TREATMENTS, AND PHASE ASSEMBLAGES OF SIALONS

Designation**	Si_3N_4	AlN	Al_2O_3	Y_2O_3	Phase Assemblage
S0610	83.73	7.77	3.73	3.70	30% α' + 70% β'
H0610	83.73	7.77	3.73	3.70	100% β'
S1510	73.71	15.42	1.01	8.91	90% ($\alpha + \alpha'$) + 10% β' + YAG
H1510	73.71	15.42	1.01	8.91	>95% α' + YAG
S1010	79.19	11.24	2.50	6.06	60% ($\alpha + \alpha'$) + 40% β' + YAG
S1025	68.50	14.69	10.70	6.09	35% ($\alpha + \alpha'$) + 65% β' + YAG
S0633	65.73	13.13	16.56	3.73	>95% β' + YAG

* Composition expressed in wt%

** S—Hot pressed at 1550°C for 20 min.
H—Hot pressed at 1550°C for 20 min. followed by annealing at 1550°C for 100 min.

REFERENCES

1. W.R. Cannon and T.G. Langdon, "Review—Creep of Ceramics, Part 1. Mechanical Characterization," *J. Mater. Sci.*, **18**, 1-50 (1983).

2. W.R. Cannon and T.G. Langdon, "Review—Creep of Ceramics, Part 2. An Examination of Flow Mechanisms," *J. Mater. Sci.*, **23**, 1-20 (1988).

3. W.H. Bauer and E.A. Collins, "Thixotropy and Dilatancy," Chap. 8 in Rheology, Theory and Applications, Vol. 4, Eds. F.R. Eirich, Academic Press, New York, p. 423-59 (1967).

4. E.P. Vrahopoulou and A.J. McHugh, "Shear-induced Association of Polymer Molecules," *Chem. Eng. Comm.*, **57**, 289-95 (1987).

5. E.P. Vrahopoulou and A.J. McHugh, "A Consideration of the Yamamoto Network Theory with Non-Gaussian Chain Segments," *J. Rheology*, **31** [5] 371-84 (1987).

6. J.Th.G. Overbeek, "Rheology of Lyophobic Systems," Chap. 9, p. 342-68 in Colloid Science, Ed. H.R. Kruyt, Elsevier Publishing Co., Amsterdam (1952).

7. H. van Olphen, Clay Colloid Chemistry, 2nd Ed., J. Wiley & Sons, Inc., New York (1977).

8. R.L. Hoffman, "Discontinuous and Dilatant Viscosity Behavior in Concentrated Suspensions, II. Theory and Experimental Tests," *J. Colloid and Interface Science*, **46** [3] 491-506 (1974).

9. R.L. Hoffman, "Discontinuous and Dilatant Viscosity Behavior in Concentrated Suspensions, III. Necessary Conditions for their Occurrence in Viscometric Flows," *Adv. in Colloids and Interface Sci.*, **17**, 161-84 (1982).

10. O. Reynolds, "On the Dilatancy of Media Composed of Rigid Particles in Contact," *Phil. Mag.*, **20** [127] 469-81 (1985).

11. H. Freundlich and H.L. Roder, "Dilatancy and Its Relation to Thixotropy," *Trans. Fraday Soc.*, **34** [127] 308-16 (1938).

12. I-W. Chen and L.A. Xue, "Development of Superplastic Structural Ceramics," *J. Amer. Ceram. Soc.*, **73** [9] 2585-2609 (1990).

13. L.J. Gauckler, H.L. Lukas and T.Y. Tien, "Crystal Chemistry of β-Si_3N_4 Solid Solutions Containing Metal Oxides," *Mater. Res. Bull.*, **11** [5] 503-12 (1976).

14. S. Hampshire, H.K. Park, D.P. Thompson and K.H. Jack, "α'-Sialon Ceramics," *Nature*, **274** [5674] 880-2 (1978).

15. S.L. Hwang and I-W. Chen, "Transient-Liquid Aided Superplastic Forming of Silicon Nitrides," paper 7-JXI-91 presented at the 93rd Annual Meeting of the American Ceramic Society, Cincinnati, OH, April 28-May 2, 1991.

16. H.A. Barnes, "Shear-Thickening ("Dilatancy") in Suspensions of Nonaggregating Solid Particles Dispersed in Newtonian Liquids," *J. Rheology*, **33** [2] 329-66 (1989).

17. S. Takeuchi and A.S. Argon, "Review—Steady-State Creep of Single-Phase Crystalline Matter at High Temperatures," *J. Mater. Sci.*, **11**, 1542-66 (1976).

18. C-M.J. Hwang and I-W. Chen, "Effect of a Liquid Phase on Superplasticity of 2 mol% Y_2O_3-Stabilized Tetragonal Zirconia Polycrystals," *J. Amer. Ceram. Soc.*, **73** [6] 1626-32 (1990).

19. R. Raj and C.K. Chyung, "Solution-Precipitation Creep in Glass Ceramics," *Acta Metall.*, **29** [1] 159-66 (1981).

20. J.-G. Wang and R. Raj, "Mechanisms of Superplastic Flow in a Fine-Grained Ceramic Containing Some Liquid Phase," *J. Amer. Ceram. Soc.*, **67** [6] 399-409 (1984).

21. A. Tsuge, K. Nishida and M. Tomatsu, "Effect of Crystallizing the Grain Boundary Phase on the High-Temperature Strength of Hot-Pressed Si_3N_4 Containing Y_2O_3," *J. Amer. Ceram. Soc.*, **58** [7-8] 323-26 (1975).

22. C.F. Chen and T.Y. Tien, "High-Temperature Mechanical Properties of SiAlON Ceramics: Microstructural Effect," *Ceram. Eng. Sci. Proc.*, **8** [7-8] 778-95 (1987).

23. M.F. Ashby and R.A. Verrall, "Diffusion-Accommodated Flow and Superplasticity," *Acta Metall.*, **21**, 149-63 (1973).

24. C.K. Yoon and I-W. Chen, "Superplastic Flow of Two-Phase Ceramics Containing Rigid Inclusions—Zirconia/Mullite Composites," *J. Amer. Ceram. Soc.*, **73** [6] 1655-65 (1990).

25. D.R. Clarke and G. Thomas, "Grain Boundary Phases in a Hot-Pressed MgO Fluxed Silicon Nitride," *J. Amer. Ceram. Soc.*, **60** [11-12] 491-95 (1977).

26. D.R. Clarke, "On the Equilibrium Thickness of Intergranular Glass Phases in Ceramic Materials," *J. Amer. Ceram. Soc.*, **70** [1] 15-22 (1987).

27. A.W. Adamson, Physical Chemistry of Surfaces, 4th ed., J. Wiley & Sons, Inc., New York, 1982.

28. O. Quadrat, "Negative Thixotropy in Polymer Solutions," *Adv. Colloid and Interf. Sci.*, **24**, 45-75 (1985).

29. E.P. Vrahopoulou and A.J. McHugh, "Shear-Thickening and Structure Formation in Polymer Solutions," *J. Non-Newtonian Fluid Mechanics*, **25**, 157-175 (1987).

30. R. Simha, "Effect of Concentration on the Viscosity of Dilute Solutions," *J. Res. Nat. Bur. Stds.*, **42**, 409-18 (1949).

31. S.G. Weissburg, R.Simha and S. Rothman, "Viscosity of Dilute and Moderately Concentrated Polymer Solutions," *J. Res. Nat. Bur. Stds.*, **47**, 298-314 (1951).

32. I-W. Chen and A.S. Argon, "Creep Cavitation of 304 Stainless Steel," *Acta Metall.*, **29**, 1321-33 (1981).

33. J.R. Dryden, D. Kucerousky, D.S. Wilkinson and D.F. Watt, "Creep deformation Due to a Viscous Grain Boundary Phase," *Acta Metall.*, **37** [7] 2007-2015 (1989).

34. K.D. Debschutz, R. Danzer and G. Petzow, "Finite Element Modelling of Ceramic Materials with a Viscous Grain Boundary Phase," Ceramic Today, Tomorrow's Ceramics, Ed. P. Vincenzini, p. 727-36, Elsevier Sci. Publishing (1991).

35. D.C. Drucker, "Engineering and Continuum Aspects of High Strength Materials," Chap. 27 in High-Strength Materials, Ed. V.F. Zackay, pp. 795-833, J. Wiley & Sons, Inc., New York (1965).

36. A.S. Argon, I-W. Chen and C.W. Lau, "Intergranular Cavitation in Creep—Theory and Experiment," in Creep-Fatigue-Environment Interactions, Eds. R.M.N. Pelloor and N.S. Stolloff, pp. 46-85, The Metallurgical Society of AIME, New York (1980).

37. F.F. Lange, B.I. Davis and D.R. Clarke, "Compressive Creep of Si_3N_4/MgO Alloys Part I. Effect of Composites," *J. Mater. Sci.*, **15** [3] 601-10 (1980).

38. R. Morrell and K.H.G. Ashbee, "High Temperature Creep of Lithium Zinc Silicate Glass Ceramics," *J. Mater. Sci.*, **8**, 1253-70 (1973).

39. L.A. Xue and I-W. Chen, "Superplastic Alumina Ceramics with Grain Growth Inhibitors," *J. Amer. Ceram. Soc.*, **74** [4] 842-45 (1991).

40. L.A. Xue and I-W. Chen, "Superplastic Mullite by Transient-Phase Processing," submitted to *J. Amer. Ceram. Soc.*, (1991).

FIGURE CAPTIONS

Fig. 1. Microstructure of superplastic sialon S0610 (left SEM, right TEM).

Fig. 2. Compressive stress-strain curves at various strain rates of sialon S0610 at 1550°C.

Fig. 3. Stress versus strain rate at 1550°C for several superplastic sialons in compression. $\left(m = \text{slope} = \frac{\partial \ln \sigma}{\partial \ln \dot{\varepsilon}}\right)$

Fig. 4. Stress versus strain rate for S0610 sialon at various temperatures in compression. $\left(m = \text{slope} = \frac{\partial \ln \sigma}{\partial \ln \dot{\varepsilon}}\right)$

Fig. 5. A transient stress-strain rate loop of S1025 sialon tested at 1550°C in compression.

Fig. 6. A polycrystal with wetted grain boundaries at various orientations.

Fig. 7. Predicted stress-strain rate curve based on a two-phase model.

Fig. 8. Interaction ϕ between grains at a separation h, with two Stern layers on the grain/liquid interfaces.

Fig. A1. A hexagonal grain in a periodic array loaded by a distant uniaxial tensile stress and locally by normal stresses on the grain boundaries.

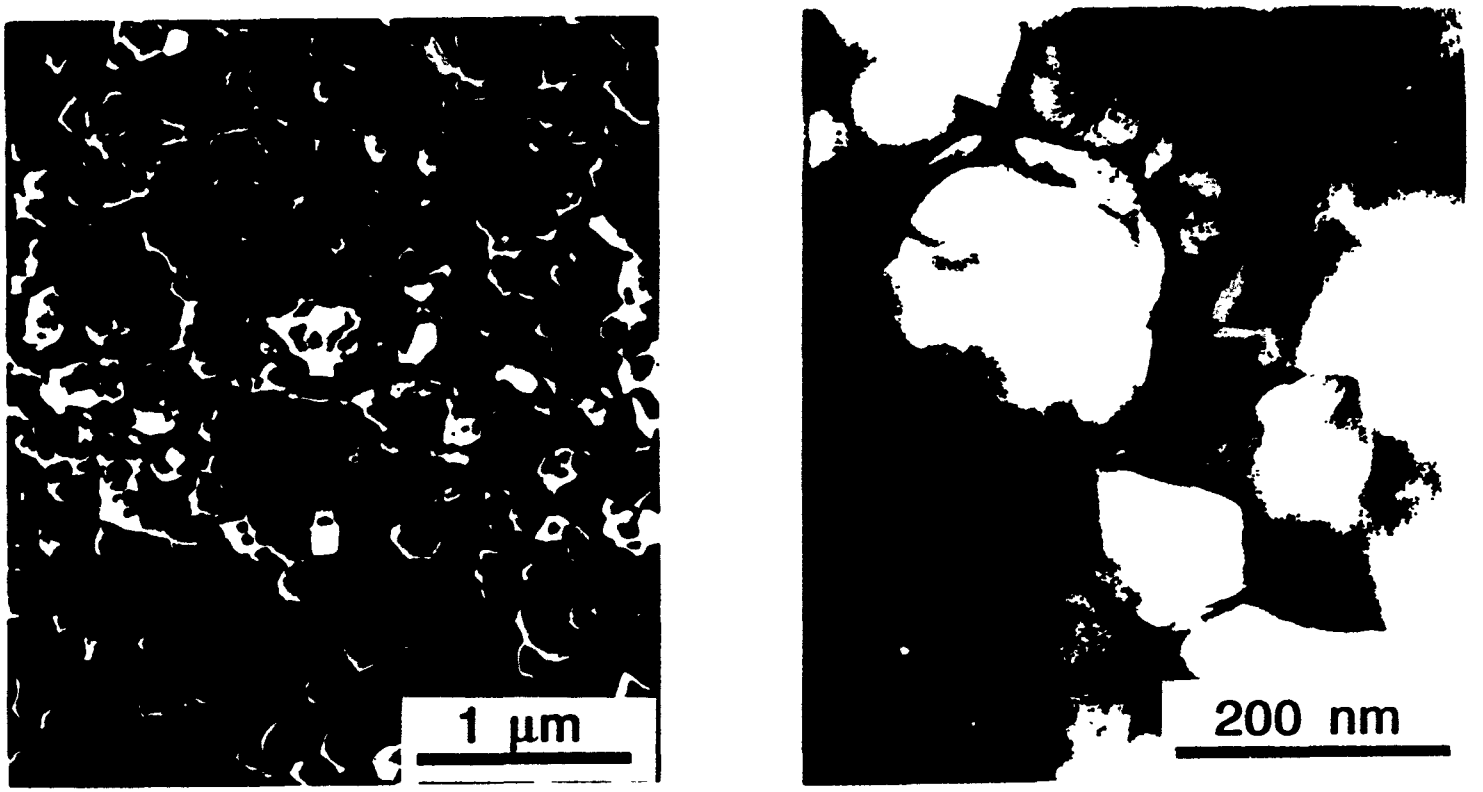

Fig. 1. Microstructure of superplastic sialon S0610 (left SEM, right TEM).

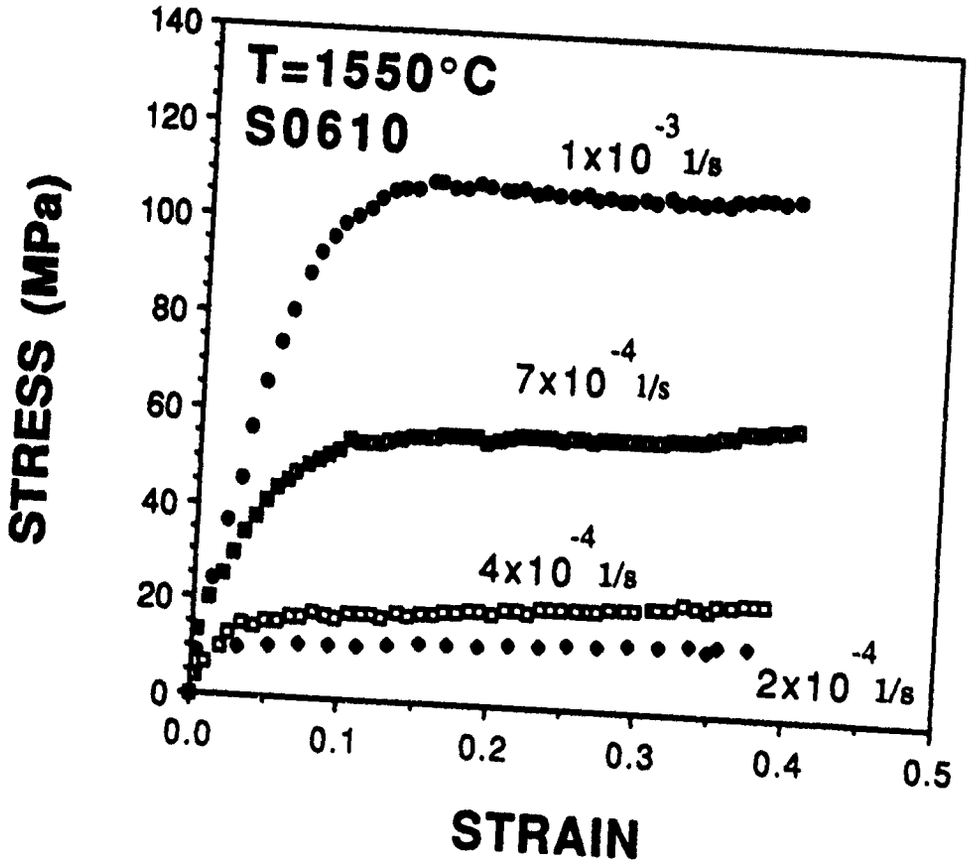

Fig. 2. Compressive stress-strain curves at various strain rates of sialon S0610 at 1550°C.

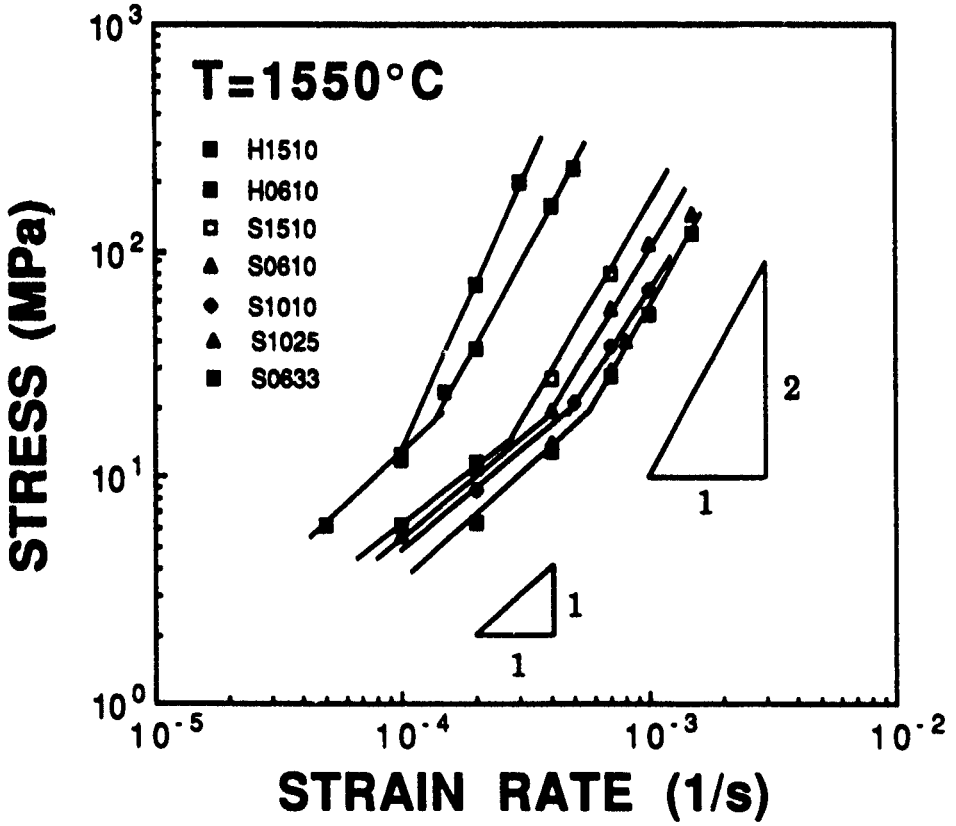

Fig. 3. Stress versus strain rate at 1550°C for several superplastic sialons in compression. $\left(m = \text{slope} = \frac{\partial \ln \sigma}{\partial \ln \dot{\varepsilon}}\right)$

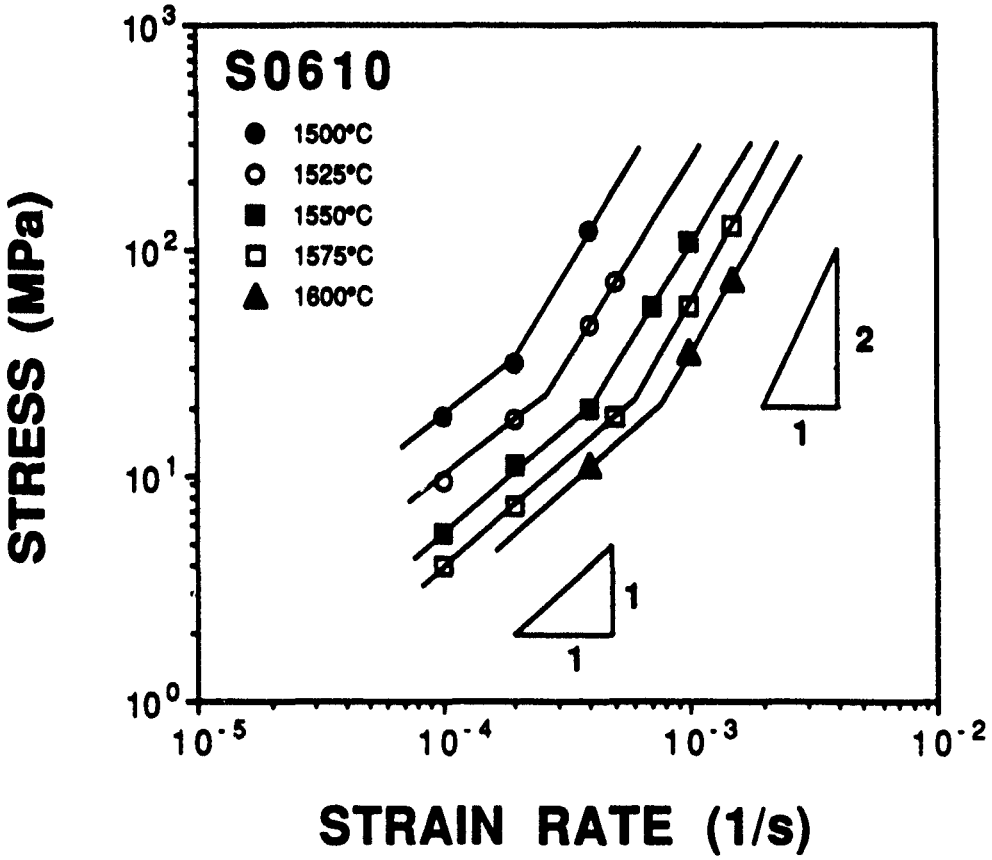

Fig. 4. Stress versus strain rate for S0610 sialon at various temperatures in compression. $\left(m = \text{slope} = \frac{\partial \ln \sigma}{\partial \ln \dot{\varepsilon}}\right)$

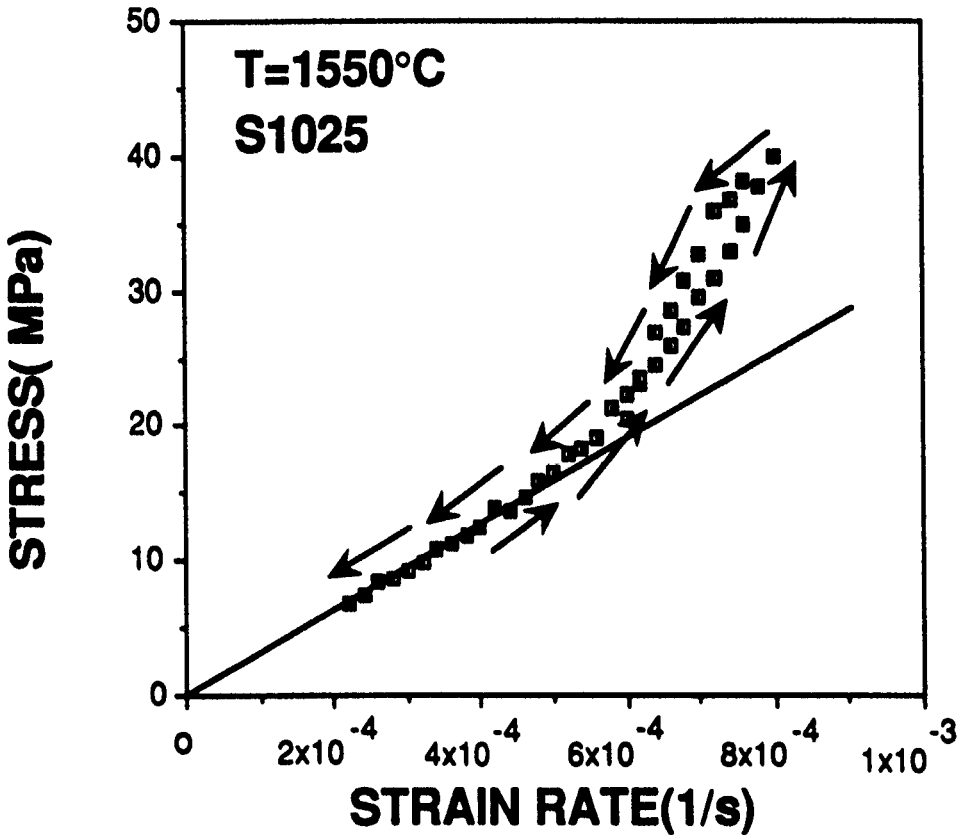

Fig. 5. A transient stress-strain rate loop of S1025 sialon tested at 1550°C in compression.

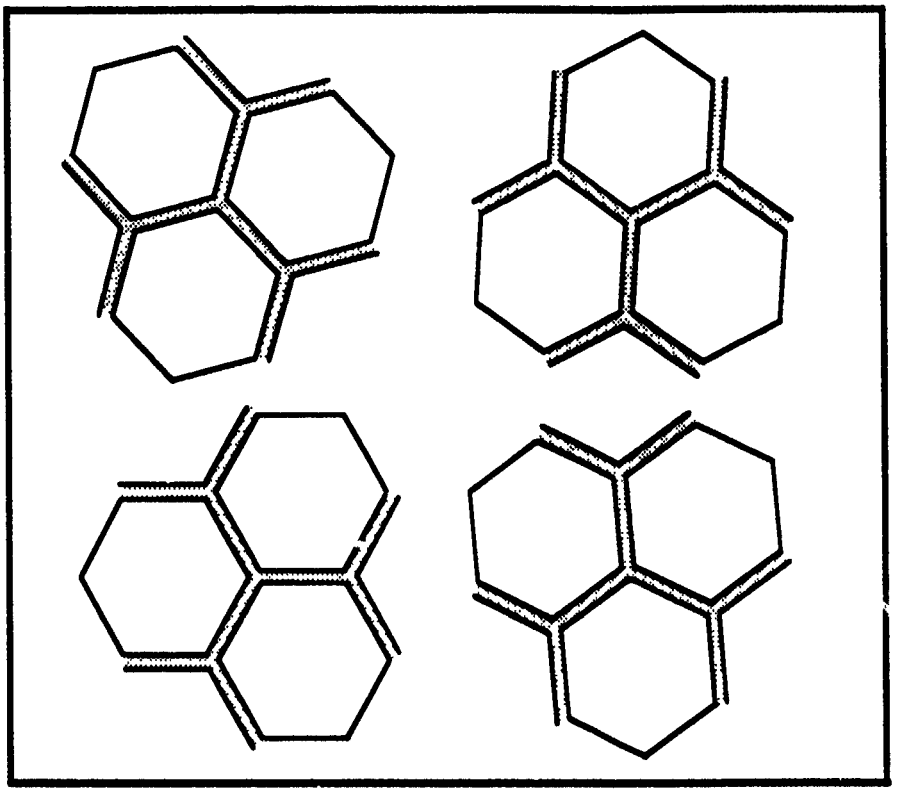

Fig. 6. A polycrystal with wetted grain boundaries at various orientations.

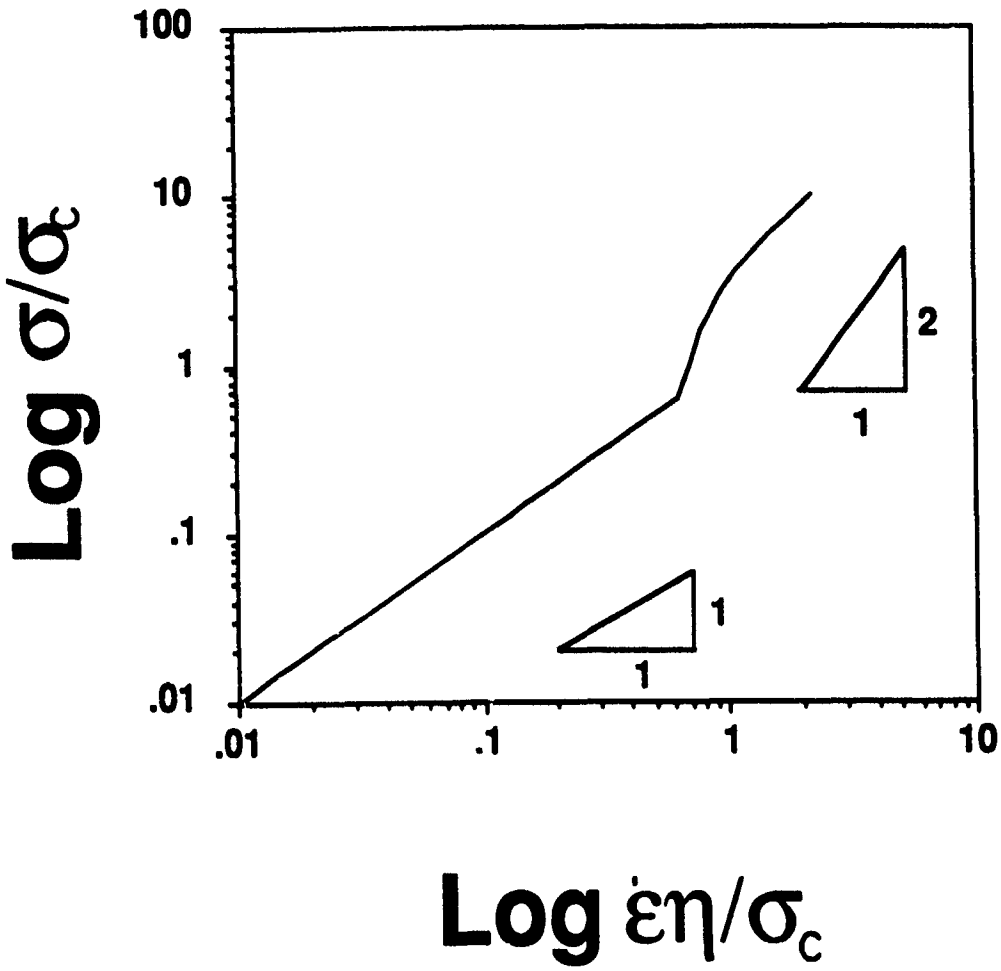

Fig. 7. Predicted stress-strain rate curve based on a two-phase model.

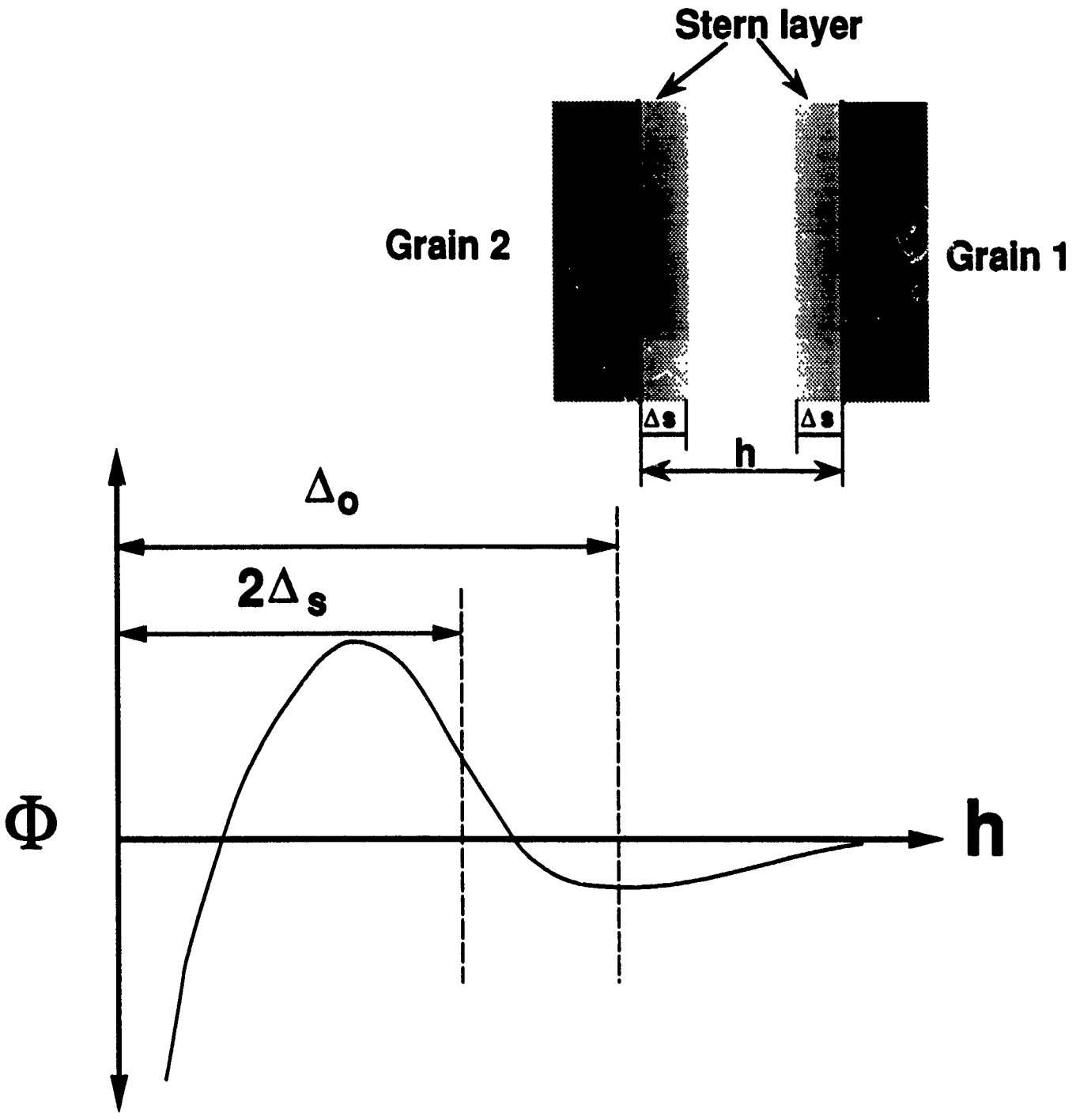

Fig. 8. Interaction ϕ between grains at a separation h, with two Stern layers on the grain/liquid interfaces.

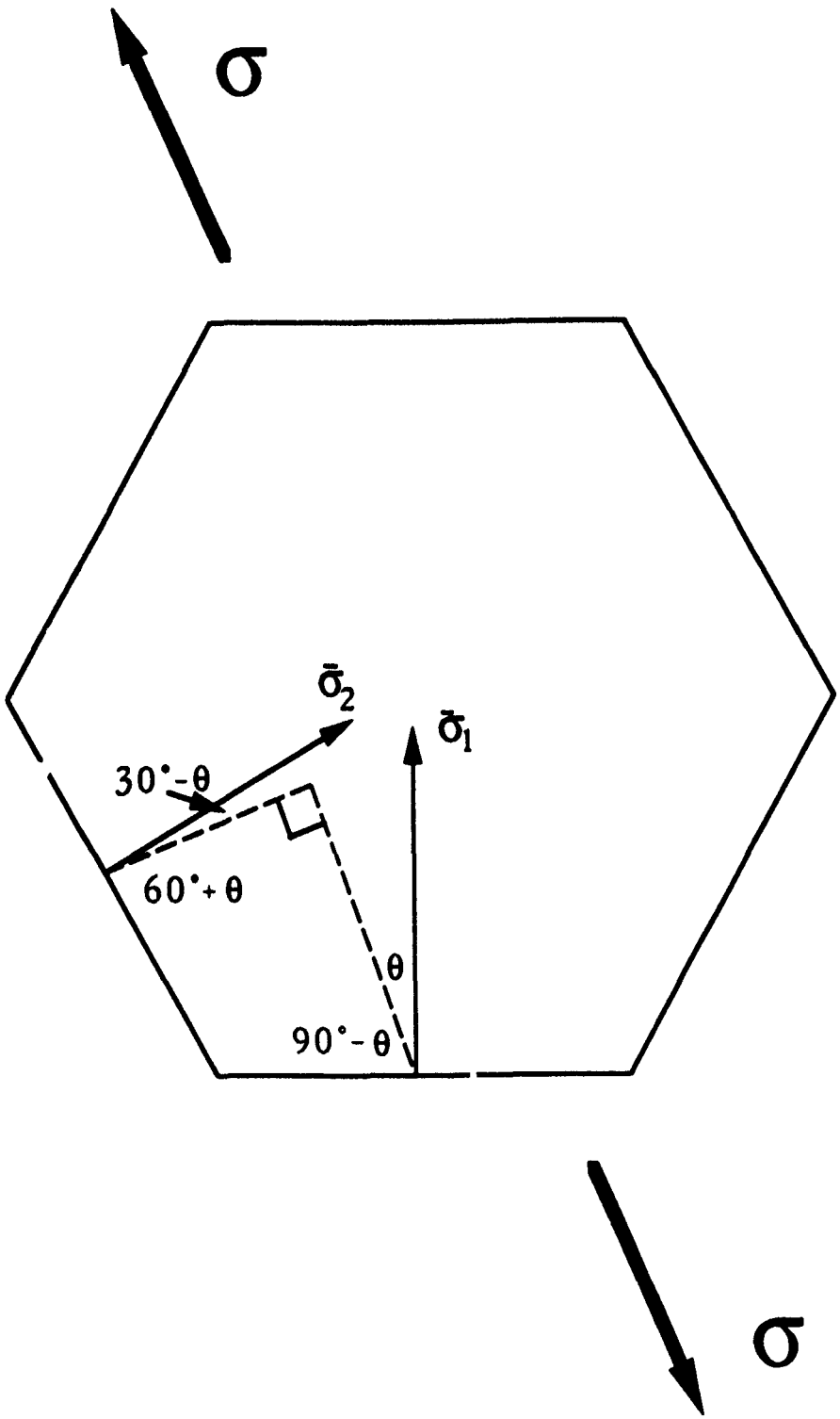

Fig. A1. A hexagonal grain in a periodic array loaded by a distant uniaxial tensile stress and locally by normal stresses on the grain boundaries.

V. PUNCH-STRETCHING—A BIAXIAL FORMABILITY TEST

The punch-stretching test is a standard sheet-metal formability test used in the metal industry. The adaptation of such a test to ceramics was attempted in the current research to provide a visually apparent and mechanically demanding demonstration of the formability of superplastic ceramics. In a typical test, the stretching strain is of the order of 100%, and the stress-state is biaxial tensile. To complement the experimental work, a new analysis using a clamped shell model for the tests was also obtained which recognized the importance of rate-sensitivity of the deformation appropriate for superplastic forming. The analysis further provides a physically transparent and quantitatively adequate estimate of the forming load which can be used for process optimization by minimizing the forming load. The initial success of this methodology was demonstrated with a Y-TZP containing liquid additive (see Sec. 4.1) and is described in the following paper. The test has also been successfully performed for other superplastic ceramics, as summarized graphically in Sec. 2.1.

journal

Reprinted from the Journal of the American Ceramic Society, Vol 73, No 3, 1990

J. Am. Ceram. Soc., 73 [3] 746–49 (1990)

Superplastic Bulging of Fine-Grained Zirconia

Xin Wu* and I-Wei Chen*

Department of Materials Science and Engineering, University of Michigan, Ann Arbor, Michigan 48109-2136

A tetragonal zirconia containing 2 mol% Y_2O_3, with 0.3 mol% CuO addition as a grain-boundary phase, was superplastically stretched at 1150°C using a hemispherical punch. Mechanical analyses were performed to establish that a biaxial tensile stress/strain state was achieved in the process with a maximal strain of 0.5 in the thinned hemispherical shell. The material was damage tolerant up to a critical strain rate, approximately 10^{-3} s^{-1}. [Key words: mechanical properties, zirconia: yttria stabilized tetragonal polycrystals, grain boundaries, plasticity.]

I. Introduction

Superplastic forming of zirconia ceramics by forging,[1,2] direct and inverse extrusion,[3] and bar and sheet bending[4] has been reported by several groups. None of the above attempts was conducted under a biaxial tension. In the shell-forming experiment reported by Carry and Mocellin,[3] although a hemispherical shape was obtained, it nevertheless involved mostly balanced compression and tension (i.e., pure shear). Even the uniaxial tensile tests, widely reported by many investigators,[5–7] are not as severe as the biaxial tensile tests for the purpose of assessing formability.[8] In addition, the typical forming time was long (from 30 min to several hours), and the forming temperature was high (between 1300° and 1500°C). For technological applications, it would be much more desirable if biaxial forming at a higher speed and a lower temperature could be practiced. This would permit more shaping flexibility, higher productivity, lower energy consumption, and less capital and tooling costs. The work reported here is a feasibility study of biaxial forming using tetragonal zirconia polycrystals (TZP) expressly processed for low-temperature superplasticity.

II. Experimental Procedures

The TZP selected in this study has a base composition of 98 mol% ZrO_2 and 2 mol% Y_2O_3, which is a single-phase (tetragonal) fine-grain ceramic. To this composition, 0.3 mol% CuO was added to form a grain-boundary phase, which has a eutectic temperature estimated as 1130°C. The powders were colloidally processed and sintered to full density at 1250°C. The grain size, taken as the linear intercept between grain boundaries multiplied by 1.5, was 0.35 μm. The grain-boundary phase was examined by electron spectroscopy for chemical analysis (ESCA) and transmission electron microscopy (TEM) and found to contain Cu^+, Y^{3+}, Zr^{4+}, and O^{2-} in a continuous amorphous layer of a thickness of 1 to 2 nm. Deformation of this material was studied in compression over a temperature range from 1000° to 1250°C and found to be superplastic. At 1150°C, the constitutive equation may be represented by

$$Y = k\dot{\varepsilon}^{0.55} \quad (1)$$

where Y is the flow stress (MPa), $\dot{\varepsilon}$ is the strain rate (s^{-1}), and $k = 2 \times 10^3$ MPa·$s^{0.55}$. Further details of the processing, characterization, and mechanical properties have been reported elsewhere.[9]

For superplastic forming, circular disks of a thickness of 1 mm and a diameter of 32 mm were prepared by grinding with diamond wheels. The surface roughness after grinding was measured by a surface roughness analyzer, and found to be of the order of 1 μm, primarily in the form of long grinding troughs and ridges. During forming, a disk was placed between a hemispherical punch and a circular die, both made of hot-pressed SiC. The punch had a radius of 6 mm and the die inner diameter was 15.875 mm with a rounded edge. The edge of the disk was not clamped. After heating to 1150° or 1200°C in air, the punch was advanced at a programmed displacement–time profile actuated by a servohydraulic mechanical tester.* Both constant displacement rate tests and constant strain rate tests, to be described later, were performed in this study. A typical experiment, forming a hat-shaped article with a hemispherical dome, as shown in Fig. 1, was completed within 10 min. The object had excellent surface finish and showed no wrinkling at the rim.

III. Results and Discussion

Load versus punch displacement curves for three runs are shown in Fig. 2, for 1150° and 1200°C, and for the constant punch speeds of 0.3 and 0.6 mm/min (corresponding to a total forming time of 20 and 10 min, respectively). The variation in the load can be qualitatively understood by the temperature and strain rate dependence of the flow stress and will be further analyzed later.

For a direct measurement of strains in the deformed region, several sets of Knoop indentation marks of various orientations were made on the outer surface before forming. These marks had a length of a few micrometers and a spacing of 250 μm. After forming, their locations were again measured from scanning electron microscopy (SEM) photographs and compared with the original sites. When combining these data with the profile of the deformed shell, we can calculate all the strain components, including radial strain ε_r, hoop strain ε_ϕ, thickness strain ε_t, and effective strain ε_e, which is $[(2/3)(\varepsilon_r^2 + \varepsilon_\phi^2 + \varepsilon_t^2)]^{1/2}$. These results are shown in Fig. 3. Two features of the strain distribution are notable. First, the punch contact region has a higher strain than that outside. Second, the maximum strain in the contact region is not located at the pole, but at 2 mm away from it. We also note that the flange was not deformed appreciably, as evidenced by the small decrease of the outer diameter after forming and its nearly unchanged thickness.

These results can be rationalized by the following picture of the stress states, schematically depicted in Fig. 4. In the

R. Raj—contributing editor

Manuscript No. 198025. Received October 27, 1989; approved November 27, 1989.

Presented at 91st Annual Meeting of the American Ceramic Society, Indianapolis, IN, April 23–27, 1989 (Basic Science Division, Paper No. 124-B-89).

Supported by the U.S. Air Force Office of Scientific Research under Grant No. 87-0289.

*Member, American Ceramic Society.

*MTS Systems Corp., Minneapolis, MN.

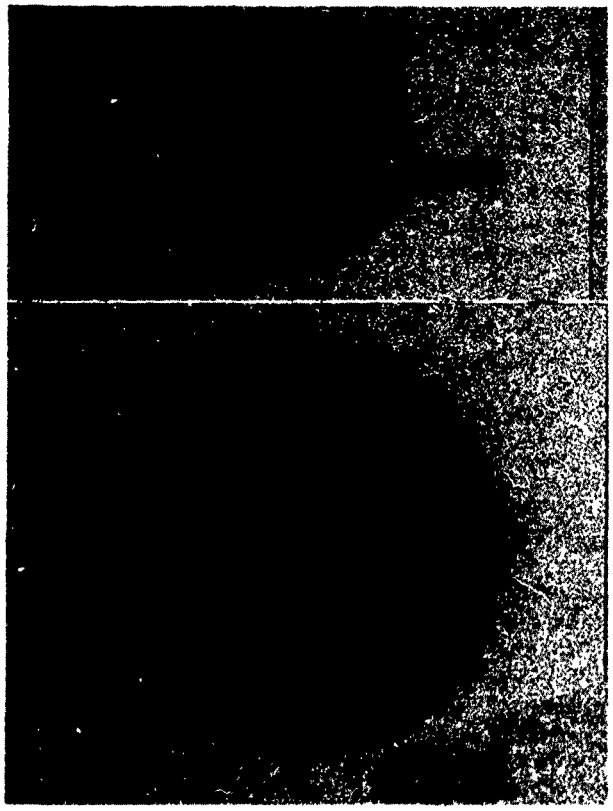

Fig. 1. ZrO_2 sample after forming at 1150°C for 10 min, with a constant punch velocity of 0.6 mm/min (shown in top and side view, with the punch).

contact region, the stresses on the shell include a normal pressure from the die, a contact friction, and a biaxial tension in the shell. The above stress state causes a biaxial stretching of the shell, which also thins simultaneously. The friction reduces the biaxial tension, thus reducing the deformation at the pole. (This is commonly called the "friction hill" effect.[10]) Outside the contact region, the shell is deformed by a progressively smaller radial and hoop stress. Because of the lack of the normal pressure, the strain rate is now much lower, and a nearly stepwise drop in the strain rate is experienced at the edge of the punch contact region. Further outward, the hoop stress continues to decrease and eventually becomes compressive. Such compressive stress is mechanically required to support the net load of the punch. To be kinematically consistent, the hoop strain also becomes negative, made possible by the inward flow of the material from the region near

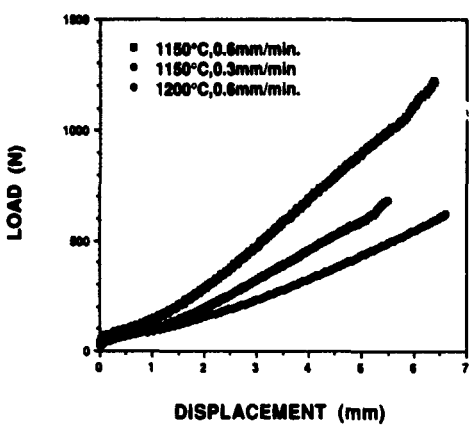

Fig. 2. Load-displacement curves for punch stretching at temperatures of 1150° and 1200°C, and at punch speeds of 0.3 and 0.6 mm/min.

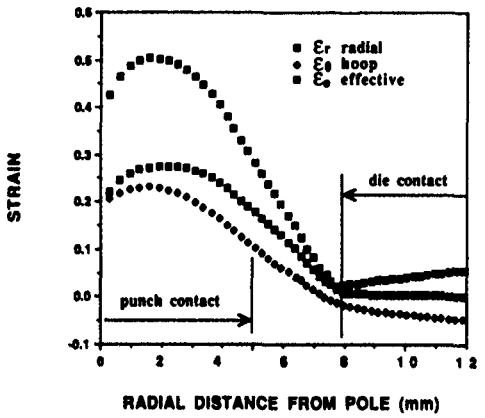

Fig. 3. Distribution of strains ε_r, ε_θ, ε_t over radial distance from pole.

the flange. It is now clear that in the present experiment, large strain biaxial tensile stretching, in a way quite similar to pressure bulging of a thin shell, has been achieved.

It is interesting to note that, although the present experiment has a configuration similar to deep drawing,[10] in which the flange is under a minimum constraint, its mechanics actually resemble more that of punch stretching,[10] in which the flange is clamped. In deep drawing, the thickness of the flange remains the same, but its diameter decreases so that the material is drawn inward toward the deepening wall; meanwhile, the base is not deformed. Thus the wall is under plane strain tension, but the flange is under plane strain shear.[10] In the present experiment, however, owing to the lack of strain hardening in the superplastic regime, the material in contact with the punch, as well as the outer annulus in the dome, does not harden enough to transmit the requisite stress to draw in the flange. Rather, stretching and thinning

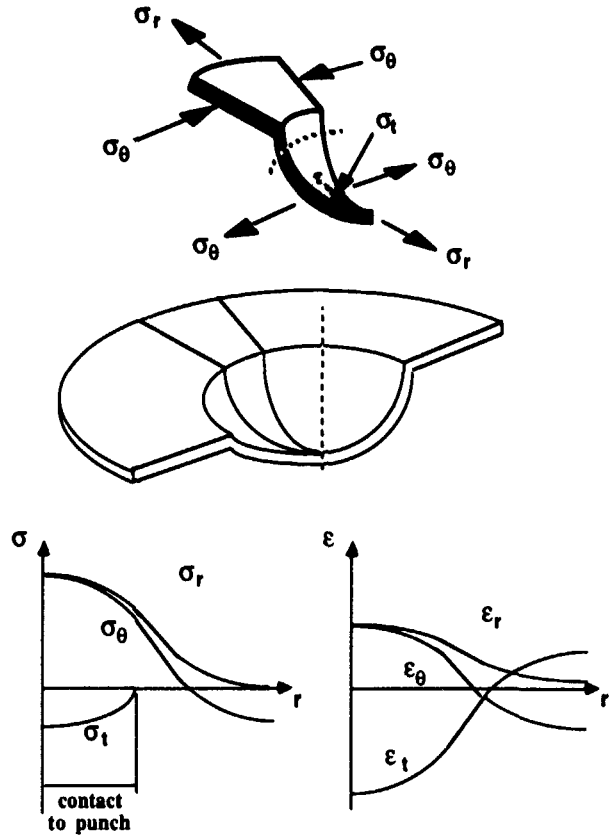

Fig. 4. Schematic of stress-strain states in punch stretching.

are confined to the dome region inside the die lip in a way similar to punch stretching even though no hold-down is applied.[10] In this connection it is important to note that, just like punch stretching, the present test of biaxial tensile stretching is much more severe than uniaxial tension.[8] Thus, the large forming strains achieved by the present experiment is most assuring from a practical viewpoint concerning sheet ceramic forming.

At higher displacement rates or lower temperatures, fracture of the disk sometimes occurred when the punch displacement approached the end displacement of 6.5 mm, as shown in Fig. 2. To determine the maximum strain rate reached prior to fracture, we have performed a simplified (upper bound) stress analysis assuming that the strain is uniform in the entire bulged region. From geometry, it can be shown that the area of the bulge (A) is

$$A = 2\pi R^2(1 - \cos\beta) + \pi(a^2 - R^2\sin^2\beta)/\cos\beta \quad (2)$$

where R is the radius of the punch, a is the inner radius of the die, and β is the half angle subtended by the punch contact to the center of the punch. The height of the dome (h) is given by

$$h = R(1 - \cos\beta - \sin\beta\tan\beta) + a\tan\beta \quad (3)$$

Using the Tresca yield criterion, we find that the pressure required to deform the shell (p) is

$$p = 2Y\ln(1 + t/R) \quad (4)$$

where t is the thickness of the shell. Then the total load on the punch (P) is

$$P = \pi R^2 p\sin^2\beta \quad (5)$$

where the friction component has been ignored. Lastly, the strain rate is given by

$$\dot{\varepsilon} = (dA/d\beta)(d\beta/dh)(dh/dt)/A \quad (6)$$

where dh/dt is the punch velocity. The above equations can be numerically evaluated to provide the load–displacement curves and the strain rate–displacement curves. These are shown in Fig. 5 for the deformation conditions given in Fig. 2. It is clear by comparing Figs. 2 and 5 that the predicted load–displacement curves are quite satisfactory, reproducing both qualitatively and quantitatively major features of the experimental results. It is seen that at a velocity of 0.6 mm/min, the strain rate has exceeded 10^{-3} s^{-1} when h exceeded 5.5 mm.

It is possible to avoid the strain rate maximum without lengthening the forming time by using a higher displacement rate initially and a lower one later. Indeed, the displacement

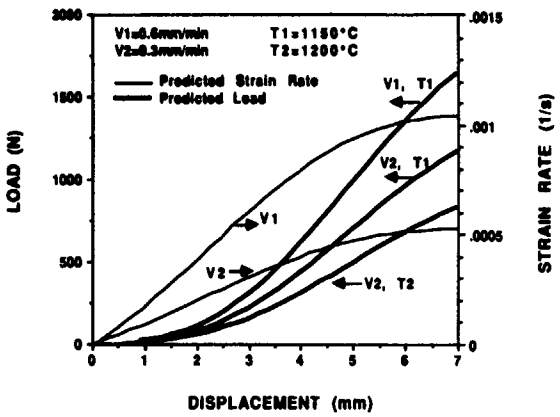

Fig. 5. Predicted load–displacement curves and strain rate–displacement curves for the experimental conditions in Fig. 2. The material flow properties taken from Hwang and Chen.[9]

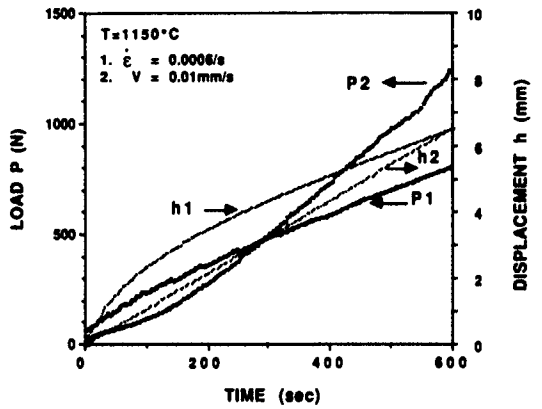

Fig. 6. Comparison of load and displacement in two forming schedules: (1) constant punch speed of 0.6 mm/min; (2) constant strain rate of 6×10^{-3}, with the same final shape at 10 min.

rate can be programmed so that the average strain rate, given by Eq. (6), is a constant throughout the experiment. In one such displacement rate program, we used a constant strain rate of 6×10^{-4} s^{-1} for a total forming time of 10 min, which is the same as the total time if a constant displacement rate of 0.6 mm/min is used. The recorded load and displacement curves of these two experiments are compared in Fig. 6. It is clear that the peak load is lower in the constant strain rate test than in the constant displacement test. Also, fracture was never encountered in the constant strain rate test at 1150°C when the forming time was 10 min. Micrographic examinations of these specimens revealed a much better surface quality in all cases.

Surface damages were examined using SEM and found to accentuate at a distance of approximately 2 mm from the pole, in close agreement with the location of the maximum radial strain shown in Fig. 3. In cases where indentation marks were made, crack opening was always observed regardless of the orientation of the mark. This observation has provided a further confirmation of the biaxial tensile nature of the stresses in the contact region. Despite the opening, however, the indentation cracks did not seem to propagate. Instead, the continuous grinding marks tended to cause more severe cracking during forming and were responsible for shell fracture when it did take place. Some examples of surface cracking are shown in Fig. 7. These observations attest to the

Fig. 7. Surface cracking after forming at 1150°C at 0.6 mm/min; the sample was ground and marked by Knoop indentation before forming.

excellent damage tolerance of the superplastic TZP studied here. The higher propensity for damage development from long-dimension surface perturbations has been recognized in sheet-metal forming and analyzed previously.[11-12] We also found that when the surface was prepolished using 1-mm diamond paste before forming, the population of surface cracking was greatly reduced.

IV. Conclusion

We have demonstrated that superplastic forming in biaxial tension to large strains can be achieved in a fine-grained tetragonal zirconia, at 1150°C, at a strain rate approaching 10^{-3} s^{-1}. Mechanical analyses have been applied to rationalize the observed forming load, strain distribution and damages, and to suggest process modifications to improve forming condition. Given the excellent formability of this material, we believe that superplastic forming now provides an attractive alternative for near-net-shape forming of zirconia ceramics.

References

[1]B. J. Kellett and F. F. Lange, "Hot-Forging Characteristics of Fine-Grained ZrO_2 and Al_2O_3/ZrO_2 Ceramics," *J. Am. Ceram. Soc.*, **69** [8] 172–73 (1986).

[2]F. Wakai, S. Sakaguchi, and H. Kato, "Compressive Deformation Properties and Microstructures in the Superplastic Y-TZP," *J. Ceram. Soc. Jpn.*, **94** [8] 721–25 (1986).

[3]C. Carry and A. Mocellin, "Examples of Superplastic Forming Fine-Grained Al_2O_3 and ZrO_2 Ceramics"; pp. 1043–52 in High Tech Ceramics, Materials Science Monograph 38A. Edited by P. Vincenzini, Elsevier, Amsterdam, Netherlands, 1987.

[4]F. Wakai, S. Sakaguchi, K. Kanayama, H. Kato, and H. Onishi, "Hot Work of Yttria-Stabilized Tetragonal ZrO_2 Polycrystals"; pp. 315–22 in Ceramic Materials and Components for Engines. Edited by W. Bunk and H. Hausner. Deutsch Keramische Gesellschaft, 1986.

[5]F. Wakai, S. Sakaguchi, and Y. Matsuro, "Superplasticity of Yttria-Stabilized Tetragonal ZrO_2 Polycrystals," *Adv. Ceram. Mater.*, **1** [3] 259–63 (1986).

[6]F. Wakai and H. Kato, "Superplasticity of TZP/Al_2O_3 Composite," *Adv. Ceram. Mater.*, **3** [1] 71–76 (1988).

[7]T. G. Nieh, C. M. McNally, and J. Wadsworth, "Superplastic Properties of a Fine-Grained Yttria-Stabilized Tetragonal Polycrystal of Zirconia," *Scr. Metall.*, **22** [8] 1297–1300 (1988).

[8]G. LeRoy and J. D. Embury, "The Utilization of Failure Maps to Compare the Fracture Modes Occurring in Aluminum Alloys"; pp. 183–207 in Formability. Edited by S. S. Hecker, A. F. Ghosh, and H. C. Gezel. The Metallurgical Society, AIME, New York, 1978.

[9]C. M. J. Hwang and I-W. Chen, "Effect of a Liquid Phase of Superplasticity of 2 mol% Y_2O_3-Stabilized Tetragonal Zirconia Polycrystals"; to be published in *J. Am. Ceram. Soc.*

[10]W. A. Backofen, Deformation Processing; pp. 162–68. Addison-Wesley, Reading, MA, 1972.

[11]Z. Marciniak and K. Kuczynski, "Limit Strains in the Process of Stretch-Forming Sheet Metal," *Int. J. Mech. Sci.*, **9**, 609–20 (1967).

[12]K. Neglo, E. Chater, and K.W. Neale, "Effects of the Shape of a Geometric Defect and of Interactions Between Defects of Limit Strains for Biaxially Stretched Sheets," *Int. J. Mech. Sci.*, **29** [12] 807–20 (1987). □

VI. PERSONNEL ASSOCIATED WITH THE RESEARCH

6.1 Professional Personnel

I-Wei Chen, Principal Investigator	(1987-1991)
J.M. Huang, Research Fellow	(1987-1989)
L.A. Xue, Senior Research Fellow	(1989-1991)

6.2 Graduate Students

I-G. Lee, Masters Student	(1987-1988)
X. Wu, Doctoral Student	(1989-1991)
S.L. Hwang, Doctoral Student	(1988-1991)

VII. PUBLICATIONS (in chronological order)

1. I.G. Lee and I-W. Chen, "Sintering and Grain Growth in Tetragonal and Cubic Zirconia," Sintering '87, Proceedings of 4th International Symposium on Science and Technology of Sintering, November 4-7, 1987, Tokyo, Japan, Eds. S. Somiya, M. Shimada, M. Yoshimura and R. Watanabe, **1**, 340-345 (1988).

2. C.M. Hwang, T.Y. Tien and I-W. Chen, "Anisotropic Grain Growth During Final Stage Sintering of Silicon Nitride Ceramics," Sintering '87, Proceedings of 4th International Symposium on Science and Technology of Sintering, November 4-7, 1987, Tokyo, Japan, Eds. S. Somiya, M. Shimada, M. Yoshimura and R. Watanabe, **2**, 1034-1039 (1988).

3. X. Wu and I-W. Chen, "Superplastic Bulging of Fine-Grained Zirconia," *J. of American Ceramic Society*, **73** [3] 146-9 (1990).

4. C.M. Hwang and I-W. Chen, "Effect of a Liquid Phase on Superplasticity of 2-mol% Y_2O_3-Stabilized Tetragonal Zirconia Polycrystals," *J. of American Ceramic Society*, **73** [6] 1626-32 (1990).
5. I-W. Chen and L.A. Xue, "Development of Superplastic Structural Ceramics," *J. of American Ceramic Society*, **73** [9] 2585-2609 (1990).

6. S.L. Hwang and I-W. Chen, "Grain Size Control of Tetragonal Zirconia Polycrystals Using the Space Charge Concept," *J. of American Ceramic Society*, **73** [11] 3269-77(1990).

7. I-W. Chen, "Superplastic Ceramics," in Ceramic Powder III: Ceramic Transactions, V. 12, Proceedings of 3rd International Symposium on the Science of Processing, Eds. E. Messing and S-I. Hirano, American Ceramic Society, p. 607-17 (1990).

8. I-W. Chen, "Superplastic Ceramic Composites," in Advanced Composite Materials, Ed. M. Sacks, *Ceramic Transactions*, **19**, 695-706 (1991).

9. S-L. Hwang and I-W. Chen, "Shear Thickening Creep in Superplastic Silicon Nitride," accepted for publication in *J. of American Ceramic Society* (1991).

VIII. PATENT

I-W. Chen and C.M. Hwang, "Method of Superplastically Deforming Zirconia Materials," approval by U.S. Patent Office expected in Spring, 1992.